JSCSEN 87(5)545–667(2022)

ISSN 1820-7421(Online)

Journal of the Serbian Chemical Society

Electronic version

VOLUME 87

No 5

BELGRADE 2022

Serbian Chemical Society 125 ANNIVERSARY

Available on line at

CXII 1897

www.shd.org.rs/JSCS/

The **Journal of the Serbian Chemical Society** (formerly Glasnik Hemijskog društva Beograd), one volume (12 issues) per year, publishes articles from the fields of chemistry. The **Journal** is financially supported by the **Ministry of Education, Science and Technological Development of the Republic of Serbia.**

Articles published in the **Journal** are indexed in **Clarivate Analytics products: Science Citation Index-Expanded™** – accessed *via* **Web of Science®** and **Journal Citation Reports®**.

Impact Factor announced 2021: **1.240; 5-year Impact Factor**: **1.144**.

Articles appearing in the **Journal** are also abstracted by: **Scopus, Chemical Abstracts Plus (CAplus℠), Directory of Open Access Journals, Referativnii Zhurnal (VINITI), RSC Analytical Abstracts, EuroPub, Pro Quest** and **Asian Digital Library.**

Publisher:	**Serbian Chemical Society**, Karnegijeva 4/III, P. O. Box 36, 1120 Belgrade 35, Serbia tel./fax: +381–11–3370–467, E-mails: **Society** – shd@shd.org.rs; **Journal** – jscs@shd.org.rs Home Pages: **Society** – http://www.shd.org.rs/, **Journal** – http://www.shd.org.rs/JSCS/
Internet Service:	Contents, Abstracts and full papers (from Vol 64, No. 1, 1999) are available in the electronic form at the Web Site of the **Journal** (http://www.shd.org.rs/JSCS/).
Former Editors:	**Nikola A. Pušin** (1930–1947), **Aleksandar M. Leko** (1948–1954), **Panta S. Tutundžić** (1955–1961), **Miloš K. Mladenović** (1962–1964), **Đorđe M. Dimitrijević** (1965–1969), **Aleksandar R. Despić** (1969–1975), **Slobodan V. Ribnikar** (1975–1985), **Dragutin M. Dražić** (1986–2006).
Editor-in-Chief:	BRANISLAV Ž. **NIKOLIĆ**, Serbian Chemical Society (E-mail: jscs-ed@shd.org.rs)
Deputy Editor:	DUŠAN **SLADIĆ**, Faculty of Chemistry, University of Belgrade
Sub editors:	
Organic Chemistry	DEJAN **OPSENICA**, Institute of Chemistry, Technology and Metallurgy, University of Belgrade JÁNOS **CSANÁDI**, Faculty of Science, University of Novi Sad
Biochemistry and Biotechnology	OLGICA **NEDIĆ**, INEP – Institute for the Application of Nuclear Energy, University of Belgrade
Inorganic Chemistry	MILOŠ **ĐURAN**, Serbian Chemical Society
Theoretical Chemistry	IVAN **JURANIĆ**, Serbian Chemical Society
Physical Chemistry	LJILJANA **DAMJANOVIĆ-VASILIĆ**, Faculty of Physical Chemistry, University of Belgrade
Electrochemistry	SNEŽANA **GOJKOVIĆ**, Faculty of Technology and Metallurgy, University of Belgrade
Analytical Chemistry	SLAVICA **RAŽIĆ**, Faculty of Pharmacy, University of Belgrade
Polymers	BRANKO **DUNJIĆ**, Faculty of Technology and Metallurgy, University of Belgrade
Thermodynamics	MIRJANA **KIJEVČANIN**, Faculty of Technology and Metallurgy, University of Belgrade
Chemical Engineering	TATJANA **KALUĐEROVIĆ RADOIČIĆ**, Faculty of Technology and Metallurgy, University of Belgrade
Materials	RADA **PETROVIĆ**, Faculty of Technology and Metallurgy, University of Belgrade
Metallic Materials and Metallurgy	ANA **KOSTOV**, Mining and Metallurgy Institute Bor, University of Belgrade
Environmental and Geochemistry	VESNA **ANTIĆ**, Faculty of Agriculture, University of Belgrade
History of and Education in Chemistry	DRAGICA **TRIVIĆ**, Faculty of Chemistry, University of Belgrade
English Language Editors:	LYNNE **KATSIKAS**, Serbian Chemical Society VLATKA **VAJS**, Serbian Chemical Society JASMINA **NIKOLIĆ**, Faculty of Technology and Metallurgy, University of Belgrade
Technical Editors:	VLADIMIR **PANIĆ**, ALEKSANDAR **DEKANSKI**, VUK **FILIPOVIĆ**, Institute of Chemistry, Technology and Metallurgy, University of Belgrade
Journal Manager & Web Master:	ALEKSANDAR **DEKANSKI,** Institute of Chemistry, Technology and Metallurgy, University of Belgrade
Office:	VERA **ĆUŠIĆ**, Serbian Chemical Society

Subscription: The annual subscription rate is **150.00 €** including postage (surface mail) and handling. For Society members from abroad rate is **50.00 €**. For the proforma invoice with the instruction for bank payment contact the Society Office (E-mail: shd@shd.org.rs) or see JSCS Web Site: http://www.shd.org.rs/JSCS/, option Subscription.

Godišnja pretplata: Za članove SHD: **2.500,00 RSD**, za penzionere i studente: **1000,00 RSD**, a za ostale: **3.500,00 RSD**:za organizacije i ustanove: **16.000,00 RSD**. Uplate se vrše na tekući račun Društva: **205-13815-62**, poziv na broj **320**, sa naznakom "pretplata za JSCS".

Nota: Radovi čiji su svi autori članovi SHD prioritetno se publikuju.

Odlukom Odbora za hemiju Republičkog fonda za nauku Srbije, br. 66788/1 od 22.11.1990. godine, koja je kasnije potvrđena odlukom Saveta Fonda, časopis je uvršten u kategoriju međunarodnih časopisa (**M-23**). Takođe, aktom Ministarstva za nauku i tehnologiju Republike Srbije, 413-00-247/2000-01 od 15.06.2000. godine, ovaj časopis je proglašen za publikaciju od posebnog interesa za nauku. **Impact Factor** časopisa objavljen 2021. godine iznosi **1,240**, a petogodišnji **Impact Factor 1,144**.

The **Journal of the Serbian Chemical Society** (formerly Glasnik Hemijskog društva Beograd), one volume (12 issues) per year, publishes articles from the fields of chemistry. The **Journal** is financially supported by the **Ministry of Education, Science and Technological Development of the Republic of Serbia.**

Articles published in the **Journal** are indexed in **Clarivate Analytics products: Science Citation Index-Expanded™** – accessed *via* **Web of Science®** and **Journal Citation Reports®**.

Impact Factor announced 2020: **1.097; 5-year Impact Factor**: **1.023**.

Articles appearing in the **Journal** are also abstracted by: **Scopus, Chemical Abstracts Plus (CAplus℠), Directory of Open Access Journals, Referativnii Zhurnal (VINITI), RSC Analytical Abstracts, EuroPub, Pro Quest** and **Asian Digital Library.**

Publisher:	**Serbian Chemical Society**, Karnegijeva 4/III, P. O. Box 36, 1120 Belgrade 35, Serbia tel./fax: +381–11–3370–467, E-mails: **Society** – shd@shd.org.rs; **Journal** – jscs@shd.org.rs Home Pages: **Society** – http://www.shd.org.rs/, **Journal** – http://www.shd.org.rs/JSCS/
Internet Service:	Contents, Abstracts and full papers (from Vol 64, No. 1, 1999) are available in the electronic form at the Web Site of the **Journal** (http://www.shd.org.rs/JSCS/).
Former Editors:	**Nikola A. Pušin** (1930–1947), **Aleksandar M. Leko** (1948–1954), **Panta S. Tutundžić** (1955**–**1961), **Miloš K. Mladenović** (1962–1964), **Đorđe M. Dimitrijević** (1965–1969), **Aleksandar R. Despić** (1969–1975), **Slobodan V. Ribnikar** (1975–1985), **Dragutin M. Dražić** (1986–2006).
Editor-in-Chief:	BRANISLAV Ž. **NIKOLIĆ**, Serbian Chemical Society (E-mail: jscs-ed@shd.org.rs)
Deputy Editor:	DUŠAN **SLADIĆ**, Faculty of Chemistry, University of Belgrade
Sub editors:	
Organic Chemistry	DEJAN **OPSENICA**, Institute of Chemistry, Technology and Metallurgy, University of Belgrade JÁNOS **CSANÁDI**, Faculty of Science, University of Novi Sad
Biochemistry and Biotechnology	OLGICA **NEDIĆ**, INEP – Institute for the Application of Nuclear Energy, University of Belgrade
Inorganic Chemistry	MILOŠ **ĐURAN**, Serbian Chemical Society
Theoretical Chemistry	IVAN **JURANIĆ**, Serbian Chemical Society
Physical Chemistry	LJILJANA **DAMJANOVIĆ-VASILIĆ**, Faculty of Physical Chemistry, University of Belgrade
Electrochemistry	SNEŽANA **GOJKOVIĆ**, Faculty of Technology and Metallurgy, University of Belgrade
Analytical Chemistry	SLAVICA **RAŽIĆ**, Faculty of Pharmacy, University of Belgrade
Polymers	BRANKO **DUNJIĆ**, Faculty of Technology and Metallurgy, University of Belgrade
Thermodynamics	MIRJANA **KIJEVČANIN**, Faculty of Technology and Metallurgy, University of Belgrade
Chemical Engineering	TATJANA **KALUĐEROVIĆ RADOIČIĆ**, Faculty of Technology and Metallurgy, University of Belgrade
Materials	RADA **PETROVIĆ**, Faculty of Technology and Metallurgy, University of Belgrade
Metallic Materials and Metallurgy	NENAD **RADOVIĆ**, Faculty of Technology and Metallurgy, University of Belgrade
Environmental and Geochemistry	VESNA **ANTIĆ**, Faculty of Agriculture, University of Belgrade
History of and Education in Chemistry	DRAGICA **TRIVIĆ**, Faculty of Chemistry, University of Belgrade
English Language Editors:	LYNNE **KATSIKAS**, Serbian Chemical Society VLATKA **VAJS**, Serbian Chemical Society JASMINA **NIKOLIĆ**, Faculty of Technology and Metallurgy, University of Belgrade
Technical Editors:	VLADIMIR **PANIĆ**, ALEKSANDAR **DEKANSKI**, VUK **FILIPOVIĆ**, Institute of Chemistry, Technology and Metallurgy, University of Belgrade
Journal Manager & Web Master:	ALEKSANDAR **DEKANSKI,** Institute of Chemistry, Technology and Metallurgy, University of Belgrade
Office:	VERA **ĆUŠIĆ**, Serbian Chemical Society

Editorial Board

From abroad: **R. Adžić**, Brookhaven National Laboratory (USA); **A. Casini**, University of Groningen (The Netherlands); **G. Cobb**, Baylor University (USA); **D. Douglas**, University of British Columbia (Canada); **G. Inzelt**, Etvos Lorand University (Hungary); **N. Katsaros**, NCSR "Demokritos", Institute of Physical Chemistry (Greece); **J. Kenny**, University of Perugia (Italy); **Ya. I. Korenman**, Voronezh Academy of Technology (Russian Federation); **M. D. Lechner**, University of Osnabrueck (Germany); **S. Macura**, Mayo Clinic (USA); **M. Spiteller**, INFU, Technical University Dortmund (Germany); **M. Stratakis**, University of Crete (Grecce); **M. Swart**, University de Girona (Cataluna, Spain); **G. Vunjak-Novaković**, Columbia University (USA); **P. Worsfold**, University of Plymouth (UK); **J. Zagal**, Universidad de Santiago de Chile (Chile).

From Serbia: **B. Abramović**, **V. Antić, V. Beškoski**, **J. Csanadi**, **Lj. Damjanović-Vasilić**, **A. Dekanski**, **V. Dondur**, **B. Dunjić**, **M. Đuran, S. Gojković**, **I. Gutman**, **B. Jovančićević**, **I. Juranić**, **L. Katsikas**, **M. Kijevčanin**, **V. Leovac**, **S. Milonjić**, **V.B. Mišković-Stanković, O. Nedić**, **B. Nikolić**, **J. Nikolić, D. Opsenica**, **V. Panić**, **M. Petkovska**, **R. Petrović**, **I. Popović**, **B. Radak**, T. **Kaluđerović Radiočić, N. Radović**, **S. Ražić**, **D. Sladić**, **S. Sovilj**, **S. Šerbanović**, **B. Šolaja**, **Ž. Tešić**, **D. Trivić, V. Vajs**.

Subscription: The annual subscription rate is **150.00 €** including postage (surface mail) and handling. For Society members from abroad rate is **50.00 €**. For the proforma invoice with the instruction for bank payment contact the Society Office (E-mail: shd@shd.org.rs) or see JSCS Web Site: http://www.shd.org.rs/JSCS/, option Subscription.

Godišnja pretplata: Za članove SHD: **2.500,00 RSD**, za penzionere i studente: **1000,00 RSD**, a za ostale: **3.500,00 RSD**:za organizacije i ustanove: **16.000,00 RSD**. Uplate se vrše na tekući račun Društva: **205-13815-62**, poziv na broj **320**, sa naznakom "pretplata za JSCS".

Nota: Radovi čiji su svi autori članovi SHD prioritetno se publikuju.

Odlukom Odbora za hemiju Republičkog fonda za nauku Srbije, br. 66788/1 od 22.11.1990. godine, koja je kasnije potvrđena odlukom Saveta Fonda, časopis je uvršten u kategoriju međunarodnih časopisa (**M-23**). Takođe, aktom Ministarstva za nauku i tehnologiju Republike Srbije, 413-00-247/2000-01 od 15.06.2000. godine, ovaj časopis je proglašen za publikaciju od posebnog interesa za nauku. **Impact Factor** časopisa objavljen 2020. godine iznosi **1,097**, a petogodišnji **Impact Factor 1,023**.

INSTRUCTIONS FOR AUTHORS (2021)

GENERAL

The *Journal of the Serbian Chemical Society* (the *Journal* in further text) is an international journal publishing papers from all fields of chemistry and related disciplines. Twelve issues are published annually. The Editorial Board expects the editors, reviewers, and authors to respect the well-known standard of professional ethics.

Types of Contributions

Original scientific papers	(up to 15 typewritten pages, including Figures, Tables and References) report original research which must not have been previously published.
Short communications	(up to 8 pages) report unpublished preliminary results of sufficient importance to merit rapid publication.
Notes	(up to 5 pages) report unpublished results of short, but complete, original research
Authors' reviews	(up to 40 pages) present an overview of the author's current research with comparison to data of other scientists working in the field
Reviews[a]	(up to 40 pages) present a concise and critical survey of a specific research area. Generally, these are prepared at the invitation of the Editor
Surveys	(about 25 pages) communicate a short review of a specific research area.
Book and Web site reviews	(1 - 2 pages)
Extended abstracts	(about 4 pages) of Lectures given at meetings of the Serbian Chemical Society Divisions
Letters to the Editor	report miscellaneous topics directed directly to the Editor

[a]Generally, Authors' reviews, Reviews and Surveys are prepared at the invitation of the Editor.

Submission of manuscripts

Manuscripts should be submitted using the **OnLine Submission Form**, available on the JSCS Web Site (**http://www.shd-pub.org.rs/index.php/JSCS**). The manuscript must be uploaded as a Word.doc or .rtf file, with tables and figures (including the corresponding captions – above Tables and below Figures), placed within the text to follow the paragraph in which they were mentioned for the first time.

Please note that **Full Names (**First Name, Last Name), **Full Affiliation** and **Country** (from drop down menu) of **ALL OF AUTHORS** (written in accordance with English spelling rules - the first letter capitalized) must be entered in the manuscript Submission Form (Step 3). Manuscript Title, authors' names and affiliations, as well as the Abstract, **WILL APPEAR** in the article listing, as well as in **BIBLIOGRAPHIC DATABASES (WoS, SCOPUS...)**, in the form and in the order entered in the author details

Graphical abstract

Graphical abstract is a one-image file containing the main depiction of the authors work and/or conclusion and must be supplied along with the manuscript. It must enable readers to quickly gain the main message of the paper and to encourage browsing, help readers identify which papers are most relevant to their research interests. Authors must provide an image that clearly represents the research described in the paper. The most relevant figure from the work, which summarizes the content, can also be submitted. The image should be submitted as a separate file in **Online Submission Form - Step 2**.

Specifications: The graphical abstract should have a clear start and end, reading from top to bottom or left to right. Please omit unnecessary distractions as much as possible.

- **Image size:** minimum of 500×800 pixels (W×H) and a minimum resolution of 300 dpi. If a larger image is sent, then please use the same ratio: 16 wide × 9 high. Please note that your image will be scaled proportionally to fit in the available window in TOC; a 150x240 pixel rectangle. Please be sure that the quality of an image cannot be increased by changing the resolution from lower to higher, but only by rescanning or exporting the image with a higher resolution, which can be set in usual "settings" option.
- **Font:** Please use Calibri and Symbol font with a large enough font size, so it is readable even from the image of a smaller size (150 × 240 px) in TOC.
- **File type:** JPG and PNG only.

No additional text, outline or synopsis should be included. Please do not use white space or any heading within the image.

Cover Letter

Manuscripts must be accompanied by a cover letter (strictly uploaded in **Online Submission Step 2**) in which the type of the submitted manuscript and a warranty as given below are given. The Author(s) has(have) to warranty that the manuscript submitted to the *Journal* for review is original, has been written by the stated author(s) and has not been published elsewhere; is currently not being considered for publication by any other journal and will not be submitted for such a review while under review by the *Journal*; the manuscript contains no libellous or other unlawful statements and does not contain any materials that violate any personal or proprietary rights of any other person or entity. All manuscripts will be acknowledged on receipt (by e-mail).

Illustrations

Illustrations (Figs, schemes, photos…) in TIF or EPS format (JPG format is acceptable for colour and greyscale photos, only), must be additionally uploaded (Online Submission Step 2) as a separate file or one archived (.zip, .rar or .arj) file. Figures and/or Schemes should be prepared according to the **Artwork Instructions -** http://www.shd.org.rs/JSCS/jscs-pdf/Artwork_Instructions.pdf!

For any difficulties and questions related to **OnLine Submission Form -** https://www.shd-pub.org.rs/index.php/JSCS/submission/wizard, please refer to **User Guide -** https://openjournal-systems.com/ojs-3-user-guide/ , Chapter **Submitting an Article -** https://openjournalsystems.com/ojs-3-user-guide/submitting-an-article/. If difficulties still persist, please contact JSCS Editorial Office at **JSCS@shd.org.rs**

A manuscript not prepared according to these instructions will be returned for resubmission without being assigned a reference number.

Conflict-of-Interest Statement*: Public trust in the peer review process and the credibility of published articles depend in part on how well a conflict of interest is handled during writing, peer review, and editorial decision making. A conflict of interest exists when an author (or the author's institution), reviewer, or editor has financial or personal relationships that inappropriately influence (bias) his or her actions (such relationships are also known as dual commitments, competing interests, or competing loyalties). These relationships vary from those with negligible potential to those with great potential to influence judgment, and not all relationships represent true conflict of interest. The potential for a conflict of interest can exist whether or not an individual believes that the relationship affects his or her scientific judgment. Financial relationships (such as employment, consultancies, stock ownership, honoraria, paid expert testimony) are the most easily identifiable conflicts of interest and the most likely to undermine the credibility of the journal, the authors, and of science itself. However, conflicts can occur for other reasons, such as personal relationships, academic competition, and intellectual passion.

Informed Consent Statement*: Patients have a right to privacy that should not be infringed without informed consent. Identifying information, including patients' names, initials, or hospital numbers, should not be published in written descriptions, photographs, and pedigrees unless the information is essential for scientific purposes and the patient (or parent or guardian) gives written informed consent for publication. Informed consent for this purpose requires that a patient who is identifiable be shown the manuscript to be published. Authors should identify Individuals who provide writing assistance and disclose the funding source for this assistance. Identifying details should be omitted if they are not essential. Complete anonymity is difficult to achieve, however, and informed consent should be obtained if there is any doubt. For example, masking the eye region in photographs of patients is inadequate protection of anonymity. If identifying characteristics are altered to protect anonymity, such as in genetic pedigrees, authors should provide assurance that alterations do not distort scientific meaning and editors should so note. The requirement for informed consent should be included in the journal's instructions for authors. When informed consent has been obtained it should be indicated in the published article.

Human and Animal Rights Statement* When reporting experiments on human subjects, authors should indicate whether the procedures followed were in accordance with the ethical standards of the responsible committee on human experimentation (institutional and national) and with the Helsinki Declaration of 1975, as revised in 2000 (5). If doubt exists whether the research was conducted in accordance with the Helsinki Declaration, the authors must explain the rationale for their approach, and demonstrate that the institutional review body explicitly approved the doubtful aspects of the study. When reporting experiments on animals, authors should be asked to indicate whether the institutional and national guide for the care and use of laboratory animals was followed.

---

*International Committee of Medical Journal Editors ("Uniform Requirements for Manuscripts Submitted to Biomedical Journals"), February 2006

PROCEDURE

All contributions will be peer reviewed and only those deemed worthy and suitable will be accepted for publication. The Editor has the final decision. To facilitate the reviewing process, authors are encouraged to suggest up to three persons competent to review their manuscript. Such suggestions will be taken into consideration but not always accepted. If authors would prefer a specific person not be a reviewer, this should be announced. The Cover Letter must be accompanied by these suggestions. Manuscripts requiring revision should be returned according to the requirement of the Editor, within 60 days upon reception of the reviewing comments by e-mail.

The *Journal* maintains its policy and takes the liberty of correcting the English as well as false content of manuscripts **provisionally accepted** for publication in the first stage of reviewing process. In this second stage of manuscript preparation by JSCS Editorial Office, the author(s) may be required to supply some **additional clarifications and corrections**. This procedure will be executed during copyediting actions, with a demand to author(s) to perform corrections of unclear parts before the manuscript would be published OnLine as **finally accepted manuscript (OLF Section of the JSCS website)**. Please note that the manuscript can receive the status of **final rejection** if the author's corrections would not be satisfactory.

When finally accepted manuscript is ready for printing, the corresponding author will receive a request for proof reading, which should be performed within 2 days. Failure to do so will be taken as the authors agree with any alteration which may have occurred during the preparation of the manuscript for printing.

Accepted manuscripts of active members of the Serbian Chemical Society (all authors) have publishing priority.

MANUSCRIPT PRESENTATION

Manuscripts should be typed in English (either standard British or American English, but consistent throughout) with 1.5 spacing (12 points Times New Roman; Greek letters in the character font Symbol) in A4 format leaving 2.5 cm for margins. For Regional specific, non-standard characters that may appear in the text, save documents with Embed fonts Word option: *Save as -> (Tools) -> Save Options… -> Embed fonts in the text.*

The authors are requested to seek the assistance of competent English language expert, if necessary, to ensure their English is of a reasonable standard. The Serbian Chemical Society can provide this service in advance of submission of the manuscript. If this service is required, please contact the office of the Society by e-mail (jscs-info@shd.org.rs).

Tables, figures and/or schemes must be embedded in the main text of the manuscript and should follow the paragraph in which they are mentioned for the first time. **Tables** must be prepared with the aid of the **WORD table function**, without vertical lines. The minimum size of the font in the tables should be **10 pt**. Table columns must not be formatted using multiple spaces. Table rows must not be formatted using any returns (enter key; ↵ key) and are **limited to 12 cm width**. Tables should not be incorporated as graphical objects. **Footnotes to Tables** should follow them and are to be indicated consequently (in a single line) in superscript letters and separated by semi-column.

Table caption must be placed above corresponding Table, while **Captions of the Illustrations** (Figs. Schemes...) must follow the corresponding item. **The captions, either for Tables or Illustrations**, should make the items comprehensible without reading of the main text (but clearly referenced in), must follow numerical order (Roman for Tables, Arabic for Illustrations), and should not be provided on separate sheets or as separate files.

High resolution Illustrations (named as Fig. 1, Fig. 2… and/or Scheme 1, Scheme 2…) in **TIF or EPS format** (JPG format is acceptable for photos, only) **must be additionally uploaded as a separate files or one archived (.zip, .rar) file.**

Illustrations should be prepared according to the ARTWORK INSTRUCTIONS - http://www.shd.org.rs/JSCS/jscs-pdf/Artwork_Instructions.pdf. **!**

All pages of the manuscript must be numbered continuously.

DESIGNATION OF PHYSICAL QUANTITIES AND UNITS

IUPAC recommendations for the naming of compounds should be followed. SI units, or other permissible units, should be employed. The designation of physical quantities must be in italic throughout the text (including figures, tables and equations), whereas the units and indexes (except for indexes having the meaning of physical quantities) are in upright letters. They should be in Times New Roman font. In graphs and tables, a slash should be used to separate the designation of a physical quantity from the unit

(example: p / kPa, j / mA cm^{-2}, t / °C, T_0 / K, τ / h, ln (j / mA cm^{-2})…). Designations such as: p (kPa), t [min]…, are not acceptable. However, if the full name of a physical quantity is unavoidable, it should be given in upright letters and separated from the unit by a comma (example: Pressure, kPa; Temperature, K; Current density, mA cm^{-2}…). Please do not use the axes of graphs for additional explanations; these should be mentioned in the figure captions and/or the manuscript (example: "pressure at the inlet of the system, kPa" should be avoided). The axis name should follow the direction of the axis (the name of y-axis should be rotated by 90°). Top and right axes should be avoided in diagrams, unless they are absolutely necessary.

Latin words, as well as the names of species, should be in *italic*, as for example: *i.e.*, *e.g.*, *in vivo*, *ibid*, *Calendula officinalis* L., *etc*. The branching of organic compound should also be indicated in *italic*, for example, *n*-butanol, *tert*-butanol, *etc*.

Decimal numbers must have decimal points and not commas in the text (except in the Serbian abstract), tables and axis labels in graphical presentations of results. Thousands are separated, if at all, by a comma and not a point.

Mathematical and chemical equations should be given in separate lines and must be numbered, Arabic numbers, consecutively in parenthesis at the end of the line. All equations should be embedded in the text Complex equations (fractions, integrals, matrix…) should be prepared with the aid of the **Microsoft Equation 3.0** (or higher) or **MathType** (Do not use them to create simple equations and labels). **Using the Insert -> Equation option, integrated in MS Office 2010 and MS Office 2013, as well as insertion of equation objects within paragraph text IS NOT ALLOWED.**

ARTICLE STRUCTURE

- TITLE PAGE;
- MAIN TEXT – including Tables and Illustrations with corresponding captions;
- SUPPLEMENTARY MATERIAL (optional**)**

Title page

- **Title** in bold letters, should be clear and concise, preferably 12 words or less. The use of non-standard abbreviations, symbols and formulae is discouraged.
- AUTHORS' NAMES in capital letters with the full first name, initials of further names separated by a space and surname. Commas should separate the author's names except for the last two names when 'and' is to be used. In multi-affiliation manuscripts, the author's affiliation should be indicated by an Arabic number placed in superscript after the name and before the affiliation. Use * to denote the corresponding author(s).
- *Affiliations* should be written in italic. The e-mail address of the corresponding author should be given after the affiliation(s).
- *Abstract:* A one-paragraph abstract written of 150 – 200 words in an impersonal form indicating the aims of the work, the main results and conclusions should be given and clearly set off from the text. Domestic authors should also submit, on a separate page, an Abstract - Izvod, the author's name(s) and affiliation(s) in Serbian (Cyrillic letters). (Домаћи аутори морају доставити Извод (укључујући имена аутора и афилијацију) на српском језику, исписане ћирилицом, иза Захвалнице, а пре списка референци.) For authors outside Serbia, the Editorial Board will provide a Serbian translation of their English abstract.
- *Keywords:* Up to 6 keywords should be given. Do not use words appearing in the manuscript title
- RUNNING TITLE: A one line (maximum five words) short title in capital letters should be provided.

Main text – should have the form:

- **INTRODUCTION,**
- **EXPERIMENTAL (RESULTS AND DISCUSSION),**
- **RESULTS AND DISCUSSION (EXPERIMENTAL),**
- **CONCLUSIONS,**
- **NOMENCLATURE (optional) and**
- ***Acknowledgements*: If any.**
- REFERENCES (Citation of recent papers published in chemistry journals that highlight the significance of work to the general readership is encouraged.)

The sections should be arranged in a sequence generally accepted for publication in the respective fields. They subtitles should be in capital letters, centred and NOT numbered.

- The INTRODUCTION should include the aim of the research and a concise description of background information and related studies directly connected to the paper.
- The EXPERIMENTAL section should give the purity and source of all employed materials, as well as details of the instruments used. The employed methods should be described in sufficient detail to enable experienced persons to repeat them. Standard procedures should be referenced and only modifications described in detail. On no account should results be included in the experimental section.

Chemistry

Detailed information about instruments and general experimental techniques should be given in all necessary details. If special treatment for solvents or chemical purification were applied that must be emphasized.

Example: Melting points were determined on a Boetius PMHK or a Mel-Temp apparatus and were not corrected. Optical rotations were measured on a Rudolph Research Analytical automatic polarimeter, Autopol IV in dichloromethane (DCM) or methanol (MeOH) as solvent. IR spectra were recorded on a Perkin-Elmer spectrophotometer FT-IR 1725X. ^{1}H and ^{13}C NMR spectra were recorded on a Varian Gemini-200 spectrometer (at 200 and 50 MHz, respectively), and on a Bruker Ultrashield Advance III spectrometer (at 500 and 125 MHz, respectively) employing indicated solvents (*vide infra*) using TMS as the internal standard. Chemical shifts are expressed in ppm (δ / ppm) values and coupling constants in Hz (J / Hz). ESI-MS spectra were recorded on Agilent Technologies 6210 Time-Of-Flight LC-MS instrument in positive ion mode with CH_3CN/H_2O 1/1 with 0.2 % HCOOH as the carrying solvent solution. Samples were dissolved in CH_3CN or MeOH (HPLC grade purity). The selected values were as follows: capillary voltage = 4 kV, gas temperature = 350 °C, drying gas flow 12 L min^{-1}, nebulizer pressure = 310 kPa, fragmentator voltage = 70 V.The elemental analysis was performed on the Vario EL III- C,H,N,S/O Elemental Analyzer (Elementar Analysensysteme GmbH, Hanau-Germany). Thin-layer chromatography (TLC) was performed on precoated Merck silica gel 60 F254 and RP-18 F254 plates. Column chromatography was performed on Lobar LichroPrep Si 60 (40-63 μm), RP-18 (40-63 μm) columns coupled to a Waters RI 401 detector, and on Biotage SP1 system with UV detector and FLASH 12+, FLASH 25+ or FLASH 40+ columns pre packed with KP-SIL [40-63 μm, pore diameter 6 nm (60 Å)], KP-C18-HS (40-63 μm, pore diameter 9 nm (90 Å) or KP-NH [40-63 μm, pore diameter 10 nm (100 Å)] as adsorbent. Compounds were analyzed for purity (HPLC) using a Waters 1525 HPLC dual pump system equipped with an Alltech, Select degasser system, and dual λ 2487 UV-VIS detector. For data processing, Empower software was used (methods A and B). Methods C and D: Agylent Technologies 1260 Liquid Chromatograph equipped with Quat Pump (G1311B), Injector (G1329B) 1260 ALS, TCC 1260 (G1316A) and Detector 1260 DAD VL+ (G1315C). For data processing, LC OpenLab CDS ChemStation software was used. For details, see Supporting Information.

1. Synthesis experiments

Each paragraph describing a synthesis experiment should begin with the name of the product and any structure number assigned to the compound in the Results and Discussions section. Thereafter, the compound should be identified by its structure number. Use of standard abbreviations or unambiguous molecular formulas for reagents and solvents, and of structure numbers rather than chemical names to identify starting materials and intermediates, is encouraged.

When a new or improved synthetic method is described, the yields reported in key experimental examples, and yields used for comparison with existing methods, should represent amounts of isolated and purified products, rather than chromategraphically or spectroscopically determined yields. Reactant quantities should be reported in weight and molar units and for product yields should be reported in weight units; percentage yields should only be reported for materials of demonstrated purity. When chromatography is used for product purification, both the support and solvent should be identified.

2. Microwave experiments

Reports of syntheses conducted in microwave reactors must clearly indicate whether sealed or open reaction vessels were used and must document the manufacturer and model of the reactor, the method of monitoring the reaction mixture temperature, and the temperature-time profile. Reporting a wattage rating or power setting is not an acceptable alternative to providing temperature data. Manuscripts describing work done with domestic (kitchen) microwave ovens will not be accepted except for studies where the unit is used for heating reaction mixtures at atmospheric pressure.

3. Compound characterization

The Journal upholds a high standard for compound characterization to ensure that substances being added to the chemical literature have been correctly identified and can be synthesized in known yield and purity by the reported preparation and isolation methods. For **all new** compounds, evidence adequate to establish both **identity** and **degree of purity** (homogeneity) must be provided.

Identity *- Melting point.* All homogeneous solid products (*e.g.* not mixtures of isomers) should be characterized by melting or decomposition points. The colors and morphologies of the products should also be noted.

Specific rotations. Specific rotations based on the equation $[\alpha]^t; D = (100\ \alpha) / (l\ c)$ should be reported as unitless numbers as in the following example: $[\alpha]^{20}$; D = -25.4 (c 1.93, $CHCl_3$), where c / g mL^{-1} is concentration and l / dm is path length. The units of the specific rotation, (deg mL) / (g dm), are implicit and are not included with the reported value.

Spectra/*Spectral Data.* Important IR adsorptions should be given.

For all new diamagnetic substances, NMR data should be reported (^1H, ^{13}C, and relevant heteronuclei). ^1H NMR chemical shifts should be given with two digits after the decimal point. Include the number of protons represented by the signal, signal multiplicity, and coupling constants as needed (*J* italicized, reported with up to one digit after the decimal). The number of bonds through which the coupling is operative, ^xJ, may be specified by the author if known with a high degree of certainty. ^{13}C NMR signal shifts should be rounded to the nearest 0.01 ppm unless greater precision is needed to distinguish closely spaced signals. Field strength should be noted for each spectrum, not as a comment in the general experimental section. Hydrogen multiplicity (C, CH, CH_2, CH_3) information obtained from routine DEPT spectra should be included. If detailed signal assignments are made, the type of NOESY or COSY methods used to establish atom connectivity and spatial relationships should be identified in the Supporting Information. Copies of spectra should also be included where structure assignments of complex molecules depend heavily on NMR interpretation. Numbering system used for assignments of signals should be given in the Supporting Information with corresponding general structural formula of named derivative.

HPLC/LCMS can be substituted for biochemistry papers where the main focus is not on compound synthesis.

HRMS/*elemental analysis.* To support the molecular formula assignment, HRMS data accurate within 5 ppm, or combustion elemental analysis [carbon and hydrogen (and nitrogen, if present)] data accurate within 0.5 %, should be reported for new compounds. HRMS data should be given in format as is usually given for combustion analysis: calculated mass for given formula following with observed mass: (+)ESI-HRMS *m*/*z*: [molecular formula + H]$^+$ calculated mass, observed mass. Example: (+)ESI-HRMS *m*/*z*: calculated for [$C_{13}H_8BrCl_2N + H^+$] 327.92899, observed 327.92792.

NOTE: in certain cases, a crystal structure may be an acceptable substitute for HRMS/elemental analysis.

Biomacromolecules. The structures of biomacromolecules may be established by providing evidence about sequence and mass. Sequences may be inferred from the experimental order of amino acid, saccharide, or nucleotide coupling, from known sequences of templates in enzyme-mediated syntheses, or through standard sequencing techniques. Typically, a sequence will be accompanied by MS data that establish the molecular weight.

Example: Product was isolated upon column chromatography [dry flash (SiO_2, eluent EA, EA/MeOH gradient 95/5 → 9/1, EA/MeOH/NH_3 gradient 18/0.5/0.5 → 9/1/1, and flash chromatography (Biotage SP1, RP column, eluent MeOH/H_2O gradient 75/25 → 95/5, N-H column, eluent EA/Hex gradient 6/3 → EA). was obtained after flash column chromatography (Biotage SP NH column, eluent hexane/EA 4:6 → 2:6). Yield 968.4 mg (95 %). Colorless foam softens at 96-101 °C. $[\alpha]^{20}$; D = +0,163 (c =2.0×10^{-3} g/mL, CH_2Cl_2). IR (ATR): 3376w, 2949m, 2868w, 2802w, 1731s, 1611w, 1581s, 1528m, 1452m, 1374s, 1331w, 1246s, 1171m, 1063w, 1023m, 965w, 940w, 881w, 850w, 807w, cm^{-1}. ^1H NMR (500 MHz, $CDCl_3$, δ): 8.46 (*d*, 1H, J = 5.4, H-2'), 7.89 (*s*, 1H, J = 2.0, H-8'), 7.71 (*d*, 1H, J = 8.9, H-5'), 7.30 (*dd*, 1H, J_1 = 8.8, J_2 = 2.1, H-6'), 6.33 (*d*, 1H, J = 5.4, H-3'), 6.07 (*s*, HN-Boc, exchangeable with D_2O), 5.06 (*s*, 1H, H-12), 4.92-4.88 (*m*, 1H, H-7), 4.42 (*bs*, H-3), 3.45 (*s*,CH_3-N), 3.33 (*bs*, H-9'), 3.05-2.95 (*m*, 2H, H-11'), 2.70-2.43 (*m*, 2H, H-24) and HN, exchangeable with D_2O), 2.07 (*s*, CH_3COO), 2.04 (*s*, CH_3COO), 1.42 (*s*, 9H, $(CH_3)_3$C-N(Boc)), 0.88 (*s*, 3H, CH_3-10), 0.79 (*d*, 3H,J = 6.6, CH_3-20), 0.68 (*s*, 3H, CH_3-13). ^{13}C NMR (125 MHz, $CDCl_3$, δ): 170.34, 170.27, 151.80, 149.92, 148.87, 134.77, 128.36, 125.11, 121.43, 117.29, 99.98, 75.41, 70.82, 50.43, 49.66, 47.60, 47.33, 44.97, 43.30, 41.83, 41.48, 37.65, 36.35, 35.44, 34.89,

34.19, 33.23, 31.24, 28.79, 28.35, 27.25, 26.45, 25.45, 22.74, 22.63, 21.57, 21.31, 17.85, 12.15. (+)ESI-HRMS (*m/z*): calculated for $[C_{45}H_{67}ClN_4O_6 + H]^+$ 795.48219, observed 795.48185. Combustion analysis for $C_{45}H_{67}ClN_4O_6$: Calculated. C 67.94, H 8.49, N 7.04; found C 67.72, H 8.63, N 6.75. HPLC purity: method A: RT 1.994, area 99.12 %; method C: RT 9.936, area 98.20 %.

Purity **-** Evidence for documenting compound purity should include one or more of the following:

a) Well-resolved high field 1D ^{1}H NMR spectrum showing at most only trace peaks not attributable to the assigned structure and a standard 1D proton-decoupled ^{13}C NMR spectrum. Copies of the spectra should be included as figures in the Supporting Information.
b) Quantitative gas chromatographic analytical data for distilled or vacuum-transferred samples, or quantitative HPLC analytical data for materials isolated by column chromatography or separation from a solid support. HPLC analyses should be performed in two diverse systems. The stationary phase, solvents (HPLC), detector type, and percentage of total chromatogram integration should be reported; a copy of the chromatograms may be included as a figure in the Supporting Information.
c) Electrophoretic analytical data obtained under conditions that permit observing impurities present at the 5 % level.

HRMS data may be used to support a molecular formula assignment **but cannot be used as a criterion of purity**.

4. Biological Data

Quantitative biological data are required for all tested compounds. Biological test methods must be referenced or described in sufficient detail to permit the experiments to be repeated by others. Detailed descriptions of biological methods should be placed in the experimental section. Standard compounds or established drugs should be tested in the same system for comparison. Data may be presented as numerical expressions or in graphical form; biological data for extensive series of compounds should be presented in tabular form. Tables consisting primarily of negative data will not usually be accepted; however, for purposes of documentation they may be submitted as supporting information. Active compounds obtained from combinatorial syntheses should be resynthesized and retested to verify that the biology conforms to the initial observation.

Statistical limits (statistical significance) for the biological data are usually required. If statistical limits cannot be provided, the number of determinations and some indication of the variability and reliability of the results should be given. References to statistical methods of calculation should be included. Doses and concentrations should be expressed as molar quantities (*e.g.*, mol/kg, μmol/kg, M, mM). The routes of administration of test compounds and vehicles used should be indicated, and any salt forms used (hydrochlorides, sulfates, *etc.*) should be noted. The physical state of the compound dosed (crystalline, amorphous; solution, suspension) and the formulation for dosing (micronized, jet-milled, nanoparticles) should be indicated. For those compounds found to be inactive, the highest concentration (*in vitro*) or dose level (*in vivo*) tested should be indicated.

- The RESULTS AND DISCUSSION should include concisely presented results and there significance discussed and compared to relevant literature data. The results and discussion may be combined or kept separate.
- The inclusion of a CONCLUSION section, which briefly summarizes the principal conclusions, is recommended.
- NOMENCLATURE is optional but, if the authors wish, a list of employed symbols may be included.
- REFERENCES should be numbered sequentially as they appear in the text. Please note that any reference numbers appearing in the Illustrations and/or Tables and corresponding captions must follow the numbering sequence of the paragraph in which they appear for the first time. When cited, the reference number should be superscripted in Font 12, following any punctuation mark. In the reference list, they should be in normal position followed by a full stop. Reference entry must not be formatted using Carriage returns (enter key; ↵ key) or multiple space key. The formatting of references to published work should follow the *Journal'*s style as follows:

Journals[a]:	A. B. Surname1, C. D. Surname2, *J. Serb. Chem. Soc.* **Vol** (Year) first page Number (https://doi.org/doi)[b]
Books:	A. B. Surname1, C. D. Surname2, *Name of Book*, Publisher, City, Year, pp. 100-101 (https://doi.org/doi)[b]
Compilations:	A. B. Surname1, C. D. Surname2, in *Name of Compilation*, A. Editor1, C. Editor2, Ed(s)., Publisher, City, Year, p. 100 (https://doi.org/doi)[b]
Proceedings:	A. B. Surname1, C. D. Surname2, in *Proceedings of Name of the Conference or Symposium*, (Year), Place of the Conference, Country, *Title of the Proceeding*, Publisher, City, Year, p. or Abstract No. 100
Patents:	A. B. Inventor1, C. D. Inventor2, (Holder), Country Code and patent number (registration year)
Chemical Abstracts:	A. B. Surname1, C. D. Surname2, *Chem. Abstr*. CA 234 567a; For non-readily available literature, the Chemical Abstracts reference should be given in square brackets: [C.A. 139/2003 357348t] after the reference
Standards:	EN ISO 250: *Name of the Standard* (Year)
Websites:	Title of the website, URL in full (date accessed)

[a] When citing Journals, the International Library Journal abbreviation is required. Please consult, *e.g.*, https://images.webofknowledge.com/WOK46/help/WOS/A_abrvjt.html

[b] doi should be replaced by doi number of the Article, for example: http://dx.doi.org/10.2298/JSC161212085B (as active link). If doi do not exist, provide the link to the online version of the publication.

Only the last entry in the reference list should end with a full stop.

The names of all authors should be given in the list of references; the abbreviation *et al.* may only be used in the text. The original journal title is to be retained in the case of publications published in any language other than English (please denote the language in parenthesis after the reference). Titles of publications in non-Latin alphabets should be transliterated. Russian references are to be transliterated using the following transcriptions:

ж→zh, х→kh, ц→ts, ч→ch, ш→sh, щ→shch, ы→y, ю→yu, я→ya, э→e, й→i, ь→’.

Supplementary material

Authors are encouraged to presentthe information and results non-essential to the understanding of their paper as SUPPLEMENTARY MATERIAL (can be uploaded inStep 4 of Online Submission). This material may include as a rule, but is not limited to, the presentation of analytical and spectral data demonstrating the identity and purity of synthesized compounds, tables containing raw data on which calculations were based, series of figures where one example would remain in the main text, etc. The Editorial Board retain the right to assign such information and results to the Supplementary material when deemed fit. Supplementary material does not appear in printed form but can be downloaded from the web site of the JSCS.

Mathematical and chemical equations should be given in separate lines and must be numbered, Arabic numbers, consecutively in parenthesis at the end of the line. All equations should be embedded in the text Complex equations (fractions, integrals, matrix…) should be prepared with the aid of the Microsoft Equation 3.0 (or higher) or MathType (Do not use them to create simple equations and labels). Using the Insert -> Equation option, integrated in MS Office 2010 and MS Office 2013, as well as insertion of equation objects within paragraph text IS NOT ALLOWED.

Deposition of crystallographic data

Prior to submission, the crystallographic data included in a manuscript presenting such data should be deposited at the appropriate database. Crystallographic data associated with organic and metal-organic structures should be deposited at the Cambridge Crystallographic Data Centre (CCDC) by e-mail to **deposit@ccdc.cam.ac.uk**

Crystallographic data associated with inorganic structures should be deposited with the Fachinformationszentrum Karlsruhe (FIZ) by e-mail to **crysdata@fiz-karlsruhe.de**. A deposition number will then be provided, which should be added to the reference section of the manuscript.

For detailed instructions please visit the JSCS website:
https://www.shd-pub.org.rs/index.php/JSCS/Instructions

ARTWORK INSTRUCTIONS

JSCS accepts only **TIFF** or **EPS** formats, as well as **JPEG** format (only for colour and greyscale photographs) for electronic artwork and graphic files. **MS files** (Word, PowerPoint, Excel, Visio) **NOT acceptable**. Generally, scanned instrument data sheets should be avoided. Authors are responsible for the quality of their submitted artwork. Every single Figure or Scheme, as well as any part of the Figure (A, B, C…) should be prepared according to following instructions (every part of the figure, A, B, C…, must be submitted as an independent single graphic file):

TIFF

Virtually all common artwork and graphic creation software is capable of saving files in TIFF format. This 'option' can normally be found under 'the 'Save As...' or 'Export...' commands in the 'File' menu.

TIFF (Tagged Image File Format) is the recommended file format for bitmap, greyscale and colour images.

- Colour images should be in the RGB mode
- When supplying TIFF files, please ensure that the files are supplied at the correct resolution:
    1. Line artwork: minimum of 1000 dpi
    2. RGB image: minimum of 300 dpi
    3. Greyscale image: minimum of 300 dpi
    4. Combination artwork (line/greyscale/RGB): minimum of 500 dpi
- Images should be tightly cropped, without frame and any caption.
- If applicable please re-label artwork with a font supported by JSCS (Arial, Helvetica, Times, Symbol) and ensure it is of an appropriate font size.
- Save an image in TIFF format with LZW compression applied.
- It is recommended to remove Alpha channels before submitting TIFF files.
- It is recommended to flatten layers before submitting TIFF files.

Please be sure that quality of an image cannot be increased by changing the resolution from lower to higher, but only by rescanning or exporting the image with higher resolution, which can be set in usual "settings" facilities.

EPS

Virtually all common artwork creation software, such as Canvas, ChemDraw, CorelDraw, SigmaPlot, Origin Lab…, are capable of saving files in EPS format. This 'option' can normally be found under the 'Save As...' or 'Export...' commands in the 'File' menu.

For vector graphics, EPS (Encapsulated PostScript) files are the preferred format as long as they are provided in accordance with the following conditions:

- when they contain bitmap images, the bitmaps should be of good resolution (see instructions for TIFF files)
- when colour is involved, it should be encoded as RGB
- an 8-bit preview/header at a resolution of 72 dpi should always be included
- embed fonts should always included and only the following fonts should be used in artwork: Arial, Helvetica, Times, Symbol
- the vertical space between the parts of an illustration should be limited to the bare necessity for visual clarity
- no data should be present outside the actual illustration area
- line weights should range from 0.35 pt to 1.5 pt
- when using layers, they should be reduced to one layer before saving the image (Flatten Artwork)

JPEG

Virtually all common artwork and graphic creation software is capable of saving files in JPEG format. This 'option' can normally be found under 'the 'Save As...' or 'Export...' commands in the 'File' menu.

JPEG (Joint Photographic Experts Group) is the acceptable file format **only for colour and greyscale photographs**. JPEG can be created with respect to photo quality (low, medium, high; from 1 to 10), ensuring file sizes are kept to a minimum to aid easy file transfer. Images should have a minimum resolution of 300 dpi. Image width: minimum 3.0 cm; maximum 12.0 cm.

Please be sure that quality of an image cannot be increased by changing the resolution from lower to higher, but only by rescanning or exporting the image with higher resolution, which can be set in usual "settings" facilities.

SIZING OF ARTWORK

- JSCS aspires to have a uniform look for all artwork contained in a single article. Hence, it is important to be aware of the style of the journal.
- Figures should be submitted in black and white or, if required, colour (charged). If coloured figures or photographs are required, this must be stated in the cover letter and arrangements made for payment through the office of the Serbian Chemical Society.
- As a general rule, the lettering on an artwork should have a finished, printed size of 11 pt for normal text and no smaller than 7 pt for subscript and superscript characters. Smaller lettering will yield a text that is barely legible. This is a rule-of-thumb rather than a strict rule. There are instances where other factors in the artwork, (for example, tints and shadings) dictate a finished size of perhaps 10 pt. Lines should be of at least 1 pt thickness.
- When deciding on the size of a line art graphic, in addition to the lettering, there are several other factors to address. These all have a bearing on the reproducibility/readability of the final artwork. Tints and shadings have to be printable at the finished size. All relevant detail in the illustration, the graph symbols (squares, triangles, circles, *etc*.) and a key to the diagram (to explain the explanation of the graph symbols used) must be discernible.
- The sizing of halftones (photographs, micrographs,...) normally causes more problems than line art. It is sometimes difficult to know what an author is trying to emphasize on a photograph, so you can help us by identifying the important parts of the image, perhaps by highlighting the relevant areas on a photocopy. The best advice that can be given to graphics suppliers is not to over-reduce halftones. Attention should also be paid to magnification factors or scale bars on the artwork and they should be compared with the details inside. If a set of artwork contains more than one halftone, again please ensure that there is consistency in size between similar diagrams.

General sizing of illustrations which can be used for the Journal of the Serbian Chemical Society:

- Minimum fig. size: 30 mm width
- Small fig. size - 60 mm width
- Large fig. size - 90 mm width
- Maximum fig. size - 120 mm width

Pixel requirements (width) per print size and resolution for bitmap images:

	Image width	A	B	C
Minimal size	30 mm	**354**	**591**	**1181**
Small size	60 mm	**709**	**1181**	**2362**
Large size	90 mm	**1063**	**1772**	**3543**
Maximal size	120 mm	**1417**	**2362**	**4724**

A: 300 dpi > RGB or Greyscale image
B: 500 dpi > Combination artwork (line/greyscale/RGB)
C: 1000 dpi> Line artwork

The designation of physical quantities and graphs formatting

The designation of physical quantities on figures must be in italic, whereas the units are in upright letters. They should be in Times New Roman font. In graphs a slash should be used to separate the designation of a physical quantity from the unit (example: p / kPa, t °C, T_0 / K, τ / h, ln (j / mA cm^{-2})…). Designations such as: p (kPa), t [min]…, are not acceptable. However, if the full name of a physical quantity is unavoiable, it should be given in upright letters and separated from the unit by a comma (example: Pressure, kPa, Temperature, K…). Please do not use the axes of graphs for additional explanations; these should be mentioned in the figure captions and/or the manuscript (example: "pressure at the inlet of the system, kPa" should be avoided). The axis name should follow the direction of the axis (the name of y-axis should be rotated by 90°). Top and right axes should be avoided in diagrams, unless they are absolutely necessary. Decimal numbers must have decimal points and not commas in the axis labels in graphical presentations of results. Thousands are separated, if at all, by a comma and not a point.

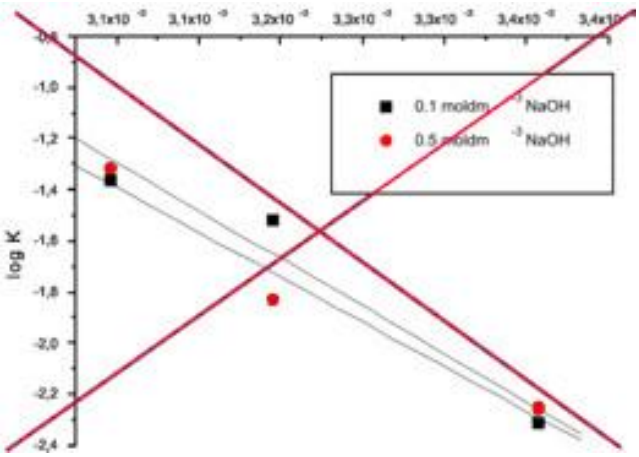

INCORRECT

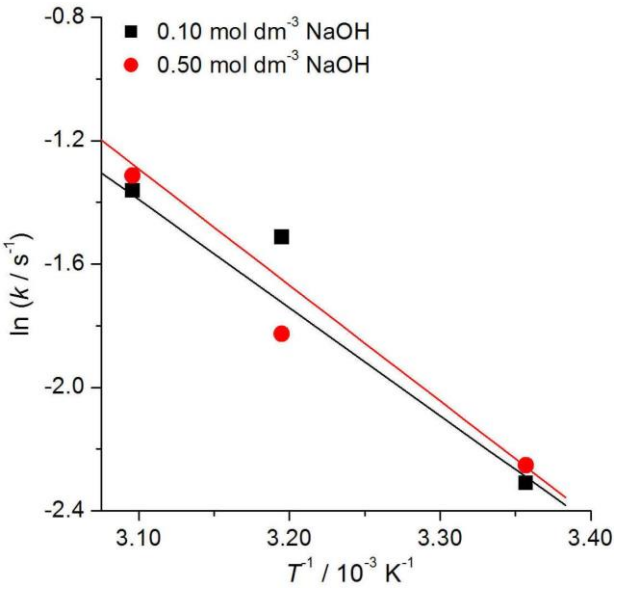

CORRECT

Journal of the Serbian Chemical Society
JSCS-info@shd.org.rs • www.shd.org.rs/JSCS

J. Serb. Chem. Soc. Vol. 87, No. 5 (2022)

CONTENTS*

Published by the Serbian Chemical Society
Karnegijeva 4/III, P.O. Box 36, 11120 Belgrade, Serbia
Printed by the Faculty of Technology and Metallurgy
Karnegijeva 4, P.O. Box 35-03, 11120 Belgrade, Serbia

* For colored figures in this issue please see electronic version at the Journal Home Page: http://www.shd.org.rs/JSCS/

Journal of the Serbian Chemical Society
JSCS@tmf.bg.ac.rs • www.shd.org.rs/JSCS

J. Serb. Chem. Soc. *87* (5) 545–559 (2022)
JSCS–5540

Original scientific paper
Published 18 February 2022

Structural, biological and computational study of oxamide derivative

IGNJAT P. FILIPOVIĆ[1#], EMINA M. MRKALIĆ[2], GIORGIO PELOSI[3], VESNA KOJIĆ[4], DIMITAR JAKIMOV[4], DEJAN BASKIĆ[5] and ZORAN D. MATOVIĆ[1]*

[1]*University of Kragujevac, Faculty of Science, Department of Chemistry, Radoja Domanovića 12, 34000 Kragujevac, Serbia,* [2]*University of Kragujevac, Institute for Information Technologies, Department of Science, Jovana Cvijića bb, Kragujevac 34000, Serbia,* [3]*Department of Chemistry, Life Sciences and Environmental Sustainability, University of Parma, 43123 Parma, Italy,* [4]*Institute of Oncology Sremska Kamenica, Novi Sad, Institutski put 4, 21204 Sremska Kamenica, Serbia and* [5]*University of Kragujevac, Faculty of Medicinal Science, S. Markovića 69, 34000 Kragujevac, Serbia*

(Received 4 December, revised 28 December, accepted 29 December 2021)

Abstract: A dicarboxylato-diamide-type compound 2,2'-[(1,2-dioxoethane-1,2--diyl)diimino]dibenzoic acid (H_4obbz) (**1**) was synthesized and characterized. The crystal structure of K_2H_2obbz·$2H_2O$ (**2**) was determined by X-ray diffraction analysis. The cytotoxic activities of the compounds were tested against four different cancer cell lines MCF-7, A549, HT-29, HeLa and a human normal cell line MRC-5. The results indicate reasonable dose-dependent cytotoxicity of the ligands that show selectivity against the tested carcinoma and healthy cell lines. Flow cytometric analysis and fluorescence microscopy showed that the most active compound, H_4obbz, induced apoptosis and G0/G1 cell cycle arrest, indicating blockage of DNA synthesis as a possible mechanism that triggers apoptosis. Docking and molecular dynamics simulations gave similar responses regarding interactions (binding) between their ligands and chaperon Grp78. The MMGBSA determined ΔG binding energies were in the range from –104 to –140 kJ mol^{-1}.

Keywords: oxamides; crystal structure; apoptosis; docking; molecular dynamics.

INTRODUCTION

Very recently, a mechanism of the drug action adopting interactions of heat shock proteins (HSP) chaperons was proposed. The IC_{50} value of the tested compound appears to be comparable with those of commercial drugs that are in clin-

* Corresponding author. E-mail: zmatovic@kg.ac.rs
# Serbian Chemical Society member.
https://doi.org/10.2298/JSC211204114F

ical use.[1,2] Between the chosen macromolecules to which the compounds were computationally simulated, the group of chaperon proteins (Grp78 from endoplasmic reticulum (ER) and Hsc70 from cytosol) were evidenced as better hosts than oligonucleotides (DNA). Furthermore, it was found that the different substituents on oxamide nitrogens resulted in the difference in cytotoxicity of the compounds. Interactions of anthranilic acid oxamidate-derivative with the membrane layer, membrane protein channels and components within cytosol (DNA, peptides/proteins) were much more suitable than that of other derivatives. Antiproliferative activity of the drug may also result from its cytostatic (effect on cell cycle) or cytotoxic effects (*e.g.*, apoptosis induction). The anti-apoptotic protein Bcl-2 plays a key role in apoptosis. Its suppressive activity in the apoptotic process may contribute to the drug resistance of tumor cells.[3–6] Intermolecular interactions, and modes of binding in the active site of an enzyme, can be determined by molecular docking. For example, targeting Grp78, and comparing binding modes of ATP and potential inhibitor can provide important insights about the cytotoxicity of a compound towards both cancerous and healthy cells.[7] At the same time, a molecular dynamics (MD) study may give an answer about the conformational and energetic change of the *holo*-protein during the time of the production run. In this paper, how the addition of an aromatic group on the arm chains of an oxamide might improve their biological activity is reported. Also, qualitative and quantitative tests on treated cells using techniques such as flow-cytometry and western-blot analysis are reported. Quantum mechanics, docking, and MD were used to further support the biological results on the interaction of the compound with malignant cells.

EXPERIMENTAL

Materials and measurements

All other chemicals of analytical reagent grade were commercially purchased and used without further purification. Elemental microanalyses for C, H, N were performed at the Microanalytical Laboratory, Faculty of Chemistry, University of Belgrade, Serbia. IR spectra were obtained in KBr pellets using a Perkin–Elmer FT-IR Spectrum One spectrophotometer. The positions of the absorbance bands are expressed in cm^{-1} and the intensities are labelled as *w* (weak), *m* (medium) or *s* (strong). Only the most significant absorption bands are reported. ^{1}H- and ^{13}C-NMR spectra were recorded on a Varian Gemini 2000 spectrometer (200 MHz). Chemical shifts are expressed as δ values (ppm) relative to 3-trimethylsilylpropionic acid-*d*4 sodium salt (TSP) as internal standard. Coupling constants *J* are given in Hz. Melting points were determined using Stuart digital melting point apparatus with accuracy ± 1 °C. The chemicals and solvents used were commercially available.

Analytical and spectral data are given in Supplementary material to this paper.

*Synthesis of 2,2'-[(1,2-dioxoethane-1,2-diyl)diimino] dibenzoic acid, H_4obbz (**1**)*[8]

To a stirred solution of anthranilic acid (3.0 g, 2.2×10^{-2} mol) in THF (50 mL) was added dropwise a solution of oxalyl chloride (1.3 g, 10^{-2} mol). The solution was stirred for 1 h. The

acid that precipitated as a white powder was filtered off under vacuum, washed with THF and air-dried. Yield: 2.50 g (74.40 %).

*Synthesis of $K_2H_2obbz·2H_2O$ (**2**)*

To a stirred solution of H_4obbz (**1**, 0.328 g, 1×10^{-3} mol) a solution of potassium hydroxide (0.112 g, 2×10^{-3} mol) was added dropwise. The solution was left in a refrigerator for a few days. The formed crystals were isolated. Yield: 0.26 g (59.6 %).

X-Ray structure determinations

Suitable crystals of **2** were grown by slow evaporation from a water solution at room temperature. X-ray diffraction data were collected using a SMART APEX diffractometer equipped with CCD detector, MoKα radiation (λ = 0.71069 Å) and corrected for absorption effects following the SADABS[9] procedure. The phase problem was solved by direct methods and the structures were refined by full-matrix least-squares on all F^2 using SHELXL97[10], as implemented in WINGX.[11] Analytical expressions of the scattering factors of neutral atoms were taken from the International Tables for X-Ray Crystallography.[12] The structure drawing was obtained using ORTEPIII.[13] Data are given in Table I.

TABLE I. Crystal structure and refinement data for compound **2**

Compound reference	K_2H_2obbz	Temperature, K	293(2)
Chemical formula	$C_8H_5KNO_4$	Space group	$R\bar{3}$
Formula Mass	218.23	No. of formula units per unit cell	18
Crystal system	Trigonal	No. of reflections measured	10544
a / Å	28.145(4)	No. of independent reflections	2281
b / Å	28.145(4)	R_{int}	0.0898
c / Å	6.484(1)	Final R_1 ($I > 2\sigma(I)$)	0.0781
α / °	90.00	Final wRF^2 ($I > 2\sigma(I)$)	0.2312
β / °	90.00	Final R_1 (all data)	0.1740
γ / °	120.00	Final wRF^2 (all data)	0.3043
Unit cell volume, Å^3	4448(2)	CCDC number	1412205

Quantum-mechanical method

Density functional theory (DFT) calculations were performed by the Gaussian 09 suite.[14] The Becke three-parameter exchange functional, in conjunction with the Lee-Yang-Parr correlation functional (B3LYP),[15-17] with the Ahlrich triple valence basis set (TZVP)[18] was used. All calculated structures were verified to be local minima (all positive eigenvalues) for ground state structures.

Docking method

Molecular docking of ligands (ATP, H_2obbz^{2-} and H_4obbz) was simulated to the three-dimensional X-ray structure of Grp78 (ref. code 3LDL[19]). This protein is Hsc70 isoform and originates from ER.[19] Docking processes were performed using AutoDock 4.2 (AD4)[20] and AutoDock Vina (Vina)[21] software equipped with a graphical user interface (GUI) AutoDock Tools 1.5.6rc3 (ADT). Full description of the methods used can be found in the Supplementary material.

MM/MD simulations

The Amber20 program[22] was used to parametrize protein complexes. The ff19SB force field, [22] TIP4P OPC water model,[23,24] and Na^+ and Cl^- parameters from Li *et al.*[25] were used

to model the protein monomer, water molecules in the solvation box, and Na^+ and Cl^-, respectively. Grp78 monomer was obtained from 3LDL X-ray PDB structure. For parametrization, ATP, H_2obbz^{2-} and H_4obbz were taken from DFT optimized structures. The best scored docking structures were used for the simulation runs. AmberTools21[22] was used for the structural modeling and data analyses while pmemd.cuda[26-28] in AMBER20[22] was employed in the MD simulation. The three ligands and corresponding Grp78-[L] complexes were modeled, simulated (MM/MM regime) and ΔG (MMGBSA method) determined in the way as described in detail in the Supplementary material.

Cell lines

The cell lines used in the study were MCF-7 (human breast adenocarcinoma), A549 (human lung carcinoma), HT-29 (human colon adenocarcinoma), HeLa (human cervix adenocarcinoma) and MRC-5 (human fetal lung fibroblasts). The cells were grown in Dulbecco's modified Eagle's medium (DMEM) with 4.5 % of glucose, supplemented with 10 % of fetal bovine serum (FBS, Sigma) and antibiotics and antimicotics solution (Sigma). All cell lines were cultivated at 37 °C in an atmosphere of 5 % CO_2 and absolute humidity.

Assays and analysis

Details for MTT assay, Annexin V-FITC/7-AAD assay for determination of apoptosis and necrosis by flow cytometry, Western blot analysis, and Cell cycle Analysis by flow cytometry are given in the cited works[29-31] and in the Supplementary material.

RESULTS AND DISCUSSION

Preparative work and spectral analysis

The syntheses of H_4obbz (**1**) and K_2obbz (**2**) are outlined in Scheme 1.

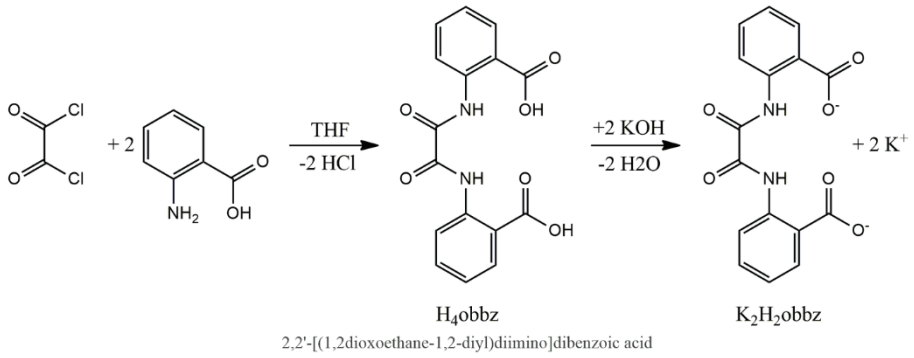

Scheme 1. Preparative path of compounds **1** and **2**.

Infrared spectra of the ligands show the characteristic absorptions of the corresponding amido-carboxylate groups, a strong and sharp ν(NH) and ν(COOH) vibration in the range observed for the compounds (**1**: 3268, 1701 cm^{-1}, **2**: 3322, 1712 cm^{-1}, Fig. S-4 of the Supplementary material). The ^1H- and ^{13}C-NMR spectra of the investigated compounds were recorded. The ^{13}C-NMR spectra showed all the carbon signals on the expected position, which further provides

support for their structures. The ^{1}H-NMR spectraum of the compound **1** consists of phenyl group signals in the δ range 6.2–8.4 ppm.

Structure

The molecular structure and crystal packing of compound **2** $K_2H_2obbz{\cdot}2H_2O$, are depicted in Fig. 1. The coordination sphere of potassium in **2** is shown in Fig. S-5 of the Supplementary material.

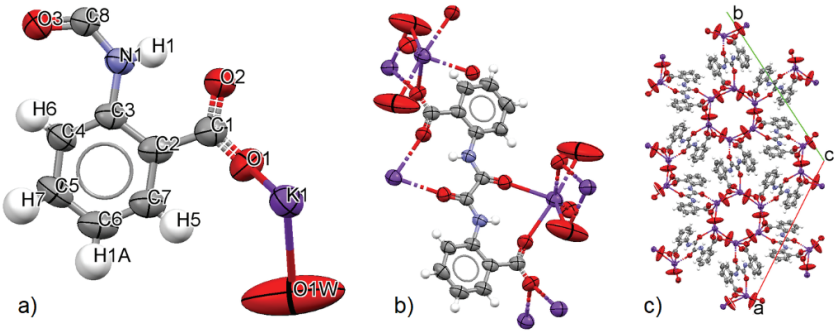

Fig. 1. Ortep diagram of $K_2H_2obbz{\cdot}2H_2O$ (**2**) structure: a) asymmetric unit with labeled atoms; b) molecular structure; c) crystal packing view along the *c* axis.

Selected bond lengths and bond angles for this compound are gathered in Table II (complete data are in Tables S-II–S-IV of the Supplementary material). Compound **2** crystallized as a dipotassium salt of compound **1**, in which the potassium ion coordinated to the carboxylic oxygen atom O2 and the amide oxygen O3 atom. This compound crystallizes as the more stable *trans* conformer in the trigonal crystal system with $R\bar{3}$ space group. The independent asymmetric unit of **2** comprises a half molecule of the anionic ligand of Cs symmetry. The asymmetric units associated with potassium atoms and water molecules form hexagonal cavities. Bonds C8−O3 and C8−N1 have lengths typical for peptide bonds. Hydrogen bonds are formed by N(1)···O(2), 2.630(8) Å, and O1(W)···O2, 2.855 Å.

TABLE II. Selected bond lengths, angles, and torsions for compound **2**

Bond lengths (A1–A2)				Bond angles (A1–A2–A3)				Bond torsions (A1–A2–A3–A4)				
A1	A2	Type	Length, Å	A1	A2	A3	Angle, °	A1	A2	A3	A4	Torsion, °
C1	C2	Single	1.49(1)	C2	C1	O1	118.2(6)	O1	C1	C2	C3	177.8(6)
C1	O1	Delocalized	1.249(8)	O1	C1	O2	121.9(7)	C1	C2	C3	N1	–1.5(8)
C2	C3	Aromatic	1.421(7)	C2	C3	N1	117.7(5)	C2	C3	N1	C8	–176.5(6)
C3	N1	Single	1.410(7)	C3	N1	C8	129.8(5)	O3	C8	N1	C3	–1(1)
C8	N1	Single	1.332(7)	N1	C8	O3	127.4(6)	O3	C8	C8	O3	–180.0(6)
C8	O3	Double	1.23(1)									
C8	C8	Single	1.53(1)									

MTT Assay

The H_nobbz^{n-4} compounds were evaluated for their *in vitro* cytotoxic activity against a panel of human malignant and normal cell lines. Cytotoxic activity was evaluated using the standard MTT assay, after exposure of cells to the tested compounds for 48 h. The commercial antitumor agent doxorubicin (DOX) was used as a reference compound. HT29 and HeLa cells are particularly sensitive to **1**, evidenced by inhibited growth of the HT29 cell line, that is similar to the reference compound, and 2 times stronger cytotoxicity to HeLa. The results are given in Table III.

TABLE III. Cytotoxicity (IC_{50} / μM) of the ligand and complexes i*n vitro*

Compound	Cell line				
	MCF-7	A549	HT29	HeLa	MRC-5
Cisplatin	1.5	36.12	22.05	2.02	–
Doxorubicin (B)	0.75	7.86	0.32	1.17	0.12
H_4obbz (C)	>100	>100	**0.36**	**0.63**	>100
K_2H_2obbz (D)	>100	>100	>100	61.86	>100

*Effect of compound **1** on apoptosis in the HeLa cell line*

In order to explore how the modality of H_4obbz induced a decrease in the viability of HeLa cells, the nature of cell death was evaluated by the Annexin V/7-AAD staining assay. As H_4obbz (**1**) showed notable cytotoxicity towards the investigated cell lines, this compound was selected for further testing. HeLa cells were treated with IC_{50} concentrations of **1** or media alone (control) for 48 h. Flow cytometric analysis revealed that the primary mode of cell death in HeLa cells induced by **1** was apoptosis, with a negligible proportion of necrotic cells. Compound **1** significantly increased the proportion of apoptotic HeLa cells, the majority of them being early apoptotic, whereas necrotic cells, although in low percent, were noticeable only in the control cells (Fig. 2).

G_0/G_1 cell cycle arrest in HeLa cell line

To further reveal the mechanisms underlying the cytotoxic activity of **1** on cell cycle, the distribution of HeLa cells was determined by flow cytometry (Fig. 3).

A 48-h treatment with **1** almost completely arrested DNA synthesis as the S phase had nearly disappeared (0.6 %). The percentage of HeLa cells accumulated in the G0/G1 phase increased from 74.9 % (control) to 79.6 % when treated with **1**. HeLa cells show no changes in cell cycle profile of G2/M cells. The disappearance of the S phase and arrest at the G0/G1 phase, induced by **(1)**, points to the blockade of DNA synthesis as a possible mechanism that triggers apoptosis.

Apoptosis and cell cycle progression are connected. Cell cycle machinery has numerous regulatory molecules that monitor and regulate the advancement of the cell cycle. These regulatory molecules are activated after DNA damage, and

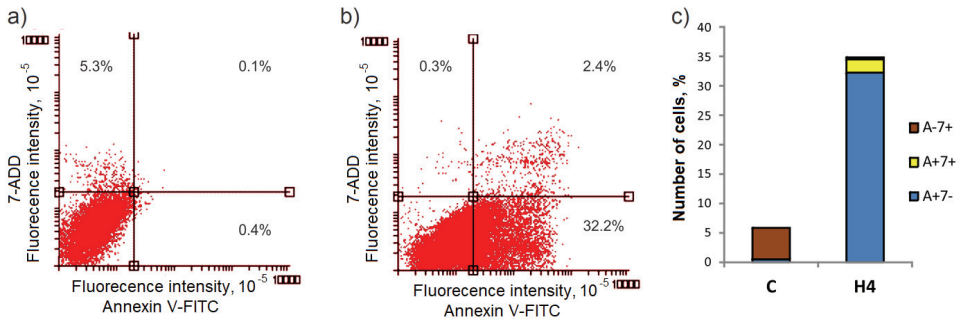

Fig. 2. Annexin V-FITC/7-AAD detection of apoptosis by flow cytometry. Dot plots illustrate distribution of viable, early apoptotic, late apoptotic and necrotic HeLa cells in untreated control (C) and treated with H_4obbz (H4). Lower left quadrant corresponds to viable cells (A– 7–), lower right to early apoptotic (A+ 7–), upper right to late apoptotic (A+ 7+) and upper left to necrotic cells (A– 7+). a) Control; b) H_4obbz; c) percentage of apoptotic and necrotic cells.

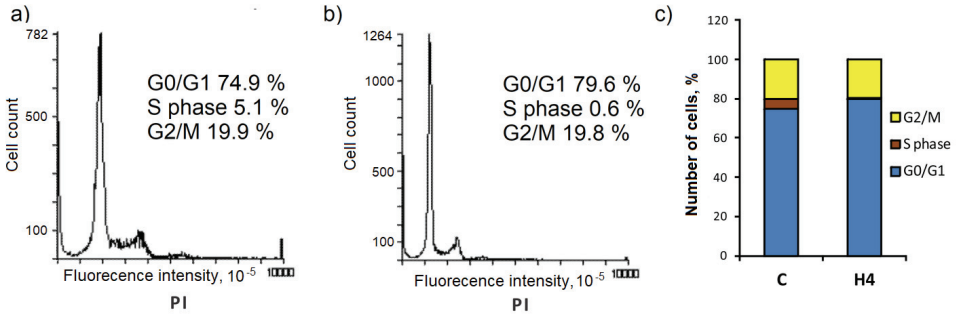

Fig. 3. Cell cycle analysis. a) Control; b) H_4obbz; c) the histograms demonstrate the cell cycle distribution of untreated HeLa cells in control sample (C) and cells treated with H_4obbz (H4).

they inhibit cell cycle progression allowing the cell to recover and repair the defect. If the damage cannot be fixed, programmed cell death launches and the cell is eliminated by apoptosis. On the other hand, genes that are supervising apoptosis are also implicated in the progression of the cell cycle. Either antiapoptotic (Bcl-2) or proapoptotic (Bax) regulatory proteins, aside from controlling the life and death of the cell, can inhibit cell cycle progression. Both molecules are transcriptional targets for p53, a tumor suppressor protein that either induces cell cycle arrest or apoptosis. Coordinated action of these molecules is pivotal for controlling cell fate.[32]

Apoptosis and cell cycle progression are connected. Cell cycle machinery has numerous regulatory molecules that monitor and regulate the advancement of the cell cycle. These regulatory molecules are activated after DNA damage, and they inhibit cell cycle progression, allowing the cell to recover and repair the defect. If the damage cannot be fixed, programmed cell death launches and the

cell is eliminated by apoptosis. On the other hand, genes that are supervising apoptosis are also implicated in the cell cycle progression. Either antiapoptotic (Bcl-2) or proapoptotic (Bax) regulatory proteins, besides controlling the life and death of the cell, can inhibit cell cycle progression. Both molecules are transcriptional targets for p53, a tumor suppressor protein that either induces cell cycle arrest or apoptosis. Coordinated action of these molecules is pivotal for controlling cell fate.[32]

Western blot (WB)

WB analysis of the effects of doxorubicin and **1** (Fig. 4) indicates that these compounds slightly modulate the total amount of the Bcl-2 protein compared to the control. When treated with **1**, in comparison with doxorubicin, the expression of Bcl-2 was lower, the expression of Bax was higher, and the expression of caspase-3 was slightly higher. Western blot analysis also demonstrated comparable but relatively low proteolytic cleavage of PARP in HeLa cells following treatment with the tested substances. The majority of chemotherapeutics induce apoptosis that is characterized by a significant expression of the Bax protein although, it was confirmed that apoptosis in various human solid tumors can be induced in the absence of any change in the level of the Bax protein.[33] In the present experiments, the analyzed compounds did not show high influence on the expression of the Bax protein. Caspases, a family of aspartate-specific cysteine proteases, play a critical role in the programmed cell death.

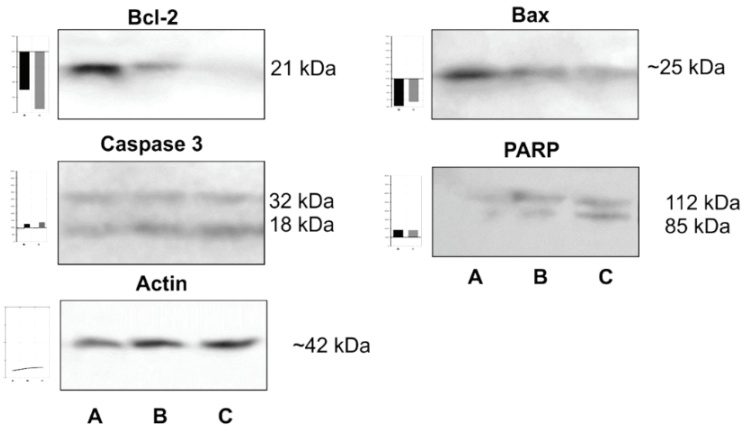

Fig. 4. Left: graphical presentation of densitometry data of protein expression obtained by Western blot analysis and processed with the ImageJ image computer program. A – control; B – doxorubicin; C – H_4obbz; right: the expression of apoptotic proteins investigated by Western blot analysis.

Caspases are important mediators in the initiation and execution of apoptotic signals.[3] The morphology of an apoptotic cell may be induced not only by cas-

pase activity, but also by the action of other families of proteases. Antitumor agents may induce cell death by apoptosis in a caspase-dependent or caspase--independent manner.[33,34] This means that apoptosis can be initiated without caspase activation, and caspase activation does not always result in cell death.[35] Doxorubicin and **1** both inhibit the growth of HeLa cells, and the degree of inhibition depends on the concentration of the test substance. The response type for the tested compounds were the same for all tested times. It was found that H_4obbz (**1**) shows a high antiproliferative effect (Table III).

It was proposed in a very recent work[2] that ER stress could be the mechanism that explains the action of the candidate drug. However, beside very probable L-protein (ER Chaperons) adduct, the possibility that the candidates interact with DNA could not be excluded. WB finding of Bcl2 expression and cleavage of PARP are in accordance with the present assumption. Roseti *et al*. showed that a novel ER stress-triggered caspase cascade, initiated by caspase-4 and involving caspase-8 and caspase-3, plays an important role in spontaneous B-cl2 cell apoptosis.[36] They also claim that ER stress triggers survival signals in B-cl2 cells by increasing GRP78 expression show that ER triggers an essential pathway for apoptosis of B-cl2 cell, and suggest that genetic and pharmacologic manipulation of ER signaling could represent an important therapeutic strategy. We do believe that the present compound fits well with the above findings and further support an ER stress mechanism as a real option with computational methods.

Docking

The structure of the target protein was downloaded directly from the RSCB PDB site (PDB entry 3LDL) and prepared as described in the Supplementary material. Co-crystalized ATP molecule was used to validate the docking method. Partial charges for all the docked structures were derived from B3LYP/TZVP QM calculations. The results of docking with both AD4 and Vina are presented in Table IV. Both programs managed to replicate the modes of binding of co--crystalized ATP. The structures of obtained results, overlaid with the crystal structure, are shown in Fig. S-1. Vina replicated crystal structure with objectively higher success.

TABLE IV. Binding energies derived from different docking software; E – estimated free energy of binding, K_i – estimated inhibition constant

Compound	AD4		Vina
	E / kJ mol^{-1}	K_i / μM	E / kJ mol^{-1}
ATP	–33.89	1.16	–47.28
H_2obbz^{2-}	–32.30	2.18	–41.84
H_4obbz	–30.17	5.22	–40.17

The binding location was defined using ATP groups as references. Phosphate groups interact with LYS296 and backbone amide nitrogens of THR37, THR38 and TYR39; Hydroxy groups of ribose interact with GLU293 and LYS296; aromatic rings of adenine interact *via* π-electrons with ARG297 and ARG367. Among others, these crucial interactions are pictured in Fig. 5.

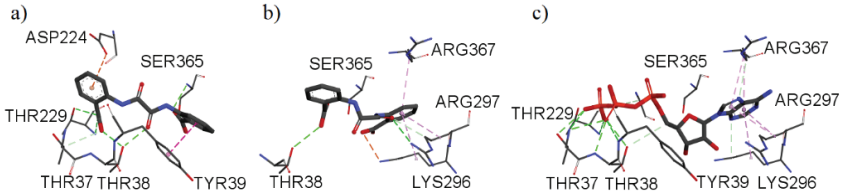

Fig. 5. Crucial actualized interactions of docking results towards Grp78: a) H_2obbz^{2-}, best score from Vina; b) H_2obbz^{2-}, best score from AD4; c) ATP, best score from Vina.

Relative energies obtained from the docking of H_2obbz^{2-} and H_4obbz in different programs agree, both slightly favoring the ionized form. AD4 and Vina seem to favor different binding modes, but both programs give almost identical solutions for the ionized and neutral form. AD4 tends to favor interactions of aromatic π-electrons of a benzoic acid moiety with ARG297 and ARG367. Instead, Vina tends to favor interactions of the carboxyl group of the benzoic acid moiety with backbone amide nitrogen of THR37 and THR38. Tested molecules are not large enough to reach both points of interest. Since both programs give solutions that interact with SER365, this residue can be considered the central point of interest. Each identified binding mode can be responsible for deactivation of Grp78 since hydrolysis of ATP at this site is crucial for the function of the protein.

Molecular dynamics

The efficacy of obbz ligands is restricted by the ability to interact with cell components. Therefore, the possible studies on the mechanism of the ligands reflected in their interaction with the either DNA or cell proteins responsible for the normal function of the cell. As mentioned above and in earlier papers the ER and cytosolic stress mechanisms as the results of docking to chaperons Grp78 and Hsc70 are predictive for more potent inhibitors, such as obbz compounds (Fig. 6).

Recent studies show that some ligands with O-donor atoms can be expected to induce ER stress and nucleus-independent apoptotic signaling. Wang *et al.*[37] were led to the conclusion that overexpression of CHOP proteins induced by the N,O ligands leads to apoptosis the cancer cell. However, Macias *et al.*[19] stated that Grp78 overexpression in tumor cells appears necessary to survive oncogenic stress. Elevated glucose metabolism leads to glucose starvation, low pH, and severe hypoxia, which are conditions under which cancer cells must survive, and are all factors that induce ER stress and activation of the Grp78 promoter. Hence,

according to these authors, successful inhibition of Grp78 from ER or cytosolic HSP70 heat shock proteins may alter the cancer cell survey.

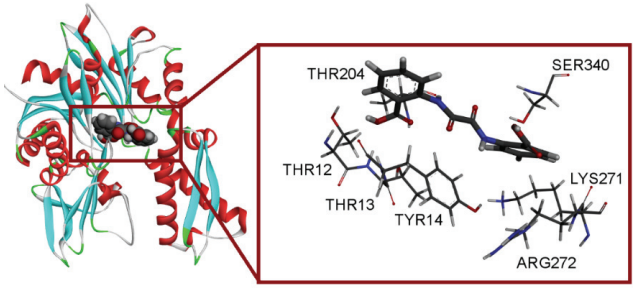

Fig. 6. MD system consisting of Grp78 monomer and the H_4obbz ligand.

Thus, it was decided to investigate the dynamics between the ligands (H_4obbz, H_2obbz^{2-} and ATP^{4-} found in 3LDL structure) and apo-Grp78 monomer, to determine how powerfully the Grp78 binds these agents comparing [L]-Grp78 free binding energies. RMSD plots of heavy atoms of the ligands and backbone N, CA, and C atoms in the Grp78 monomer along 5 trajectories (for each complex there are 5 independent samplings) are shown in Fig. 7. Usually, it is consider that small *RMSD* values along the trajectory indicate a stable state of the molecular system. Generally it can be seen see that the *RMSD* values of complexes are small (≈0.5 Å) with some exceptions due to the conformational change of the ligand. Similarly, the *RMSD* of the whole system have average values of 2 Å (Fig. 7); Some sudden jumps between small and large *RMSD* values of the protein backbone atoms are due to a periodic boundary issue.

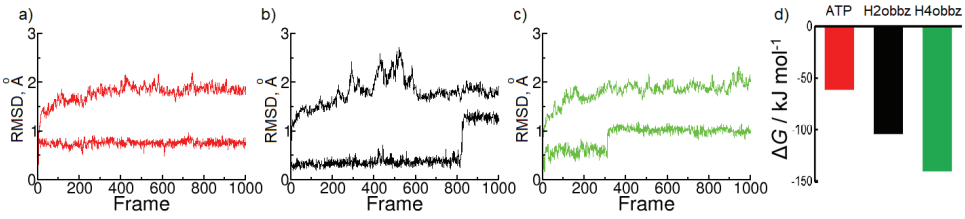

Fig. 7. *RMSD* values during MD simulation runs of Grp78 with: a) ATP; b) H_2obbz^{2-}; c) H_4obbz; higher values of *RMSD* are for protein-ligand complex while lower values are calculated only for atoms belonging to ligand; d) relative Δ*G* binding energies.

It was found that the ligands remained bound to the protein. The average distance between the center of the ligands and the surroundings residues at the binding pocket remain less than 8 Å (LYS271, THR12, THR13 and TYR14; GLU268 and LYS271; ARG272, ARG347 and SER275 – residue numeration differs by –25 from original PDB due to renumbering by Amber). In all trajectories, the

ligands were kept bound to the protein during the simulation runs. A further investigation[22] suggests that MMGBSA results serve better when used for comparison between similar molecules bonded at the same protein pocket. The results of MMGBSA analyses are in accordance with the expectations ΔG: –139.9992, –104.0201 and –61.1207 kJ mol^{-1} for H_4obbz, H_2obbz^{2-} and ATP, respectively (shown in Fig. 7 and given in Table S-I). Domain movement during the MD simulations was investigated using the online tool DynDom.[38] No domain movements during each of the simulations were found. Interactions of ligands with the most important residues in Grp78 are shown in the 2D diagram in Fig. S-3. After a thorough inspection of all trajectories in case of each [L]-Grp78 unit, i the following should be pointed out: a) The [L]-Grp78 unit behaves similarly and shows no tendency for separation from protein or their movement from the binding pocket; b) the oxamide (**1**) interacts with the THR13, TYR14 and GLY339 residues by strong hydrogen bonds and GLY339 and ARG271 residues by π-stacked and π-alkyl attraction; c) the secondary structure of the protein units were almost conserved; d) there were no domain movements of investigated protein during any of the simulations.

CONCLUSIONS

In this work 2,2'-[(1,2-dioxoethane-1,2-diyl)diimino]dibenzoic acid, H_4obbz (**1**) and its K^+ salt K_2H_2obbz (**2**) were synthetized and characterized by the spectroscopic and structural methods. The crystal structure of **2** was determined by X-ray analysis. Compound **2** crystallizes as a dipotassium salt of **1**. Compound **1** inhibited the growth of HeLa cell line similarly to the reference compound and expressed 4 times stronger cytotoxicity to HT29. Additionally, **1** exerted no toxic effects towards the healthy line (>100 μM). Flow cytometric analysis revealed that the primary mode of cell death in HeLa cells, induced by **1** was apoptosis, with a negligible proportion of necrotic cells. Treatment with **1** almost completely arrested DNA synthesis as the S phase had nearly disappeared. Western Blot and computational experiments further support the ER stress mechanism as a real option. Both docking and MD are indicative for tight binding between H_4obbz and the Grp78 chaperon. Vina and AD4 favor different binding modes in the active spot but both give comparable relative energies. Concerning MD simulations, the compounds were kept bound to the protein during the NPT production run. There were no domain movements of the investigated protein during any of the simulations. The results of MMGBSA analyses were in accordance with expectation ΔG: –139.9992, –104.0201 and –61.1207 kJ mol^{-1} for H_4obbz, H_2obbz^{2-} and ATP, respectively.

Acknowledgement. This work was supported by the Ministry of Education, Science and Technological Development of Serbia (Agreement No. 451-03-9/2021-14/200122).

ИЗВОД

СТРУКТУРНА, БИОЛОШКА И РАЧУНСКА ИПИТИВАЊА ДЕРИВАТА ОКСАМИДА

ИГЊАТ П. ФИЛИПОВИЋ[1], ЕМИНА М. МРКАЛИЋ[2], GIORGIO PELOSI[3], ВЕСНА КОЈИЋ[4], ДМИТАР ЈАКИМОВ[4], ДЕЈАН БАСКИЋ[5] и ЗОРАН Д. МАТОВИЋ[1]

[1]Универзитет у Крагујевцу, Природно–математички факултет, Институт за хемију, 34000 Крагујевац, [2]Универзитет у Крагујевцу, Институт за информационе технологије Крагујевац, 34000 Крагујевац, [3]Department of Chemistry, Life Sciences and Environmental Sustainability, University of Parma, 43123 Parma, Italy, [4]Институт за онкологију Војводине, Сремска Каменица, Нови Сад, Индустријски пут 4, 21204, Сремска Каменица и [5]Универзитет у Крагујевцу, Факултет медицинских наука, 34000 Крагујевац

Једињење 2,2'-[(1,2-диоксоетан-1,2-диил)диимино]дибензоева киселина (1, H_4obbz), и дикалијумова со овог једињења (**2**, K_2H_2obbz) су синтетисана и окарактерисана. Кристална структура једињења **2** је утврђена помоћу дифракције рендгенских зрака. Утврђена је цитотоксична активност према четири различита типа малигних ћелијских линија (MCF-7, A549, HT-29, HeLa), и према једној здравој ћелијској линији (MRC-5). Резултати указују разумну цитотоксичност која зависи од дозе, код једињења која показују селективност према малигним ћелијама у односу на здраве. Проточном цитометријом и флуоросцентном микроскопијом показано је да H_4obbz доводи до апоптозе и заустављања G0/G1 ћелијског циклуса, што указује на блокаду ДНК синтезе као могућ механизам дејства. Симулације молекулског доковања и молекулске динамике дају сличне одговоре на питање интеракција нашег једињења са хапероном Grp78. Слободне енергије везивања одређене MMGBS методом су у распону од –104 до –140 kJ mol^{-1}.

(Примљено 4. децембра, ревидирано 28 децембра, прихваћено 29. децембра 2021)

REFERENCES

1. Z. D. Matović, E. Mrkalić, G. Bogdanović, V. Kojić, A. Meetsma, R. Jelić, *J. Inorg. Biochem.* **121** (2013) 134 (https://doi.org/10.1016/j.jinorgbio.2013.01.006)
2. E. M. Mrkalić, R. M. Jelić, O. R. Klisurić, Z. D. Matović, *J. Chem. Soc. Dalt. Trans.* **43** (2014) 15126 (https://doi.org/10.1039/c3dt53384k)
3. S. Kumar, *Cell Death Differ.* **14** (2007) 32 (https://doi.org/10.1038/sj.cdd.4402060)
4. C. M. Palermo, C. A. Bennett, A. C. Winters, C. S. Hemenway, *Leuk. Res.* **32** (2008) 633 (https://doi.org/10.1016/j.leukres.2007.08.002)
5. C. Assunção Guimarães, R. Linden, *Eur. J. Biochem.* **271** (2004) 1638 (https://doi.org/10.1111/j.1432-1033.2004.04084.x)
6. L. Galluzzi, O. Kepp, G. Kroemer, *Oncogene* **31** (2012) 2805 (https://doi.org/10.1038/onc.2011.459)
7. Y. Qiao, C. Dsouza, A. A. Matthews, Y. Jin, W. He, J. Bao, F. Jiang, R. Chandna, R. Ge, L. Fu, *Eur. J. Med. Chem.* **193** (2020) 112228 (https://doi.org/10.1016/j.ejmech.2020.112228)
8. K. Nakatani, J. Y. Carriat, Y. Journaux, O. Kahn, F. Lloret, J. P. Renard, Y. Pei, J. Sletten, M. Verdaguer, *J. Am. Chem. Soc.* **111** (1989) 5739 (https://doi.org/10.1021/ja00197a036)
9. G.M. Sheldrick, *SADABS, Siemens Area Detector Absorption Correction Software*, University of Göttingen, Göttingen, 1996
10. G.M. Sheldrick, *SHELXL97, Program for Structure Refinement*, University of Göttingen, Göttingen, 1997

11. L. J. Farrugia, *J. Appl. Crystallogr.* **32** (1999) 837 (https://doi.org/10.1107/S0021889899006020)
12. W. Schmitz, *Krist. Und Tech.* **10** (1975) K120 (https://doi.org/10.1002/crat.19750101116)
13. M. N. Burnett, C. K. Johnson, *ORTEP-III: Oak Ridge Thermal Ellipsoid Plot Program for crystal structure illustrations*, Oak Ridge, TN, 1996 (https://doi.org/10.2172/369685)
14. *Gaussian 09, Revision A.02,* Gaussian, Inc., Wallingford CT, 2016
15. A. D. Becke, *Phys. Rev., A* **38** (1988) 3098 (https://doi.org/10.1103/PhysRevA.38.3098)
16. C. Lee, W. Yang, R. G. Parr, *Phys. Rev. B* **37** (1988) 785 (https://doi.org/10.1103/PhysRevB.37.785)
17. A. D. Becke, *J. Chem. Phys.* **98** (1993) 5648 (https://doi.org/10.1063/1.464913)
18. M. F. Peintinger, D. V. Oliveira, T. Bredow, *J. Comput. Chem.* **34** (2013) 451 (https://doi.org/10.1002/jcc.23153)
19. A. T. Macias, D. S. Williamson, N. Allen, J. Borgognoni, A. Clay, Z. Daniels, P. Dokurno, M. J. Drysdale, G. L. Francis, C. J. Graham, R. Howes, N. Matassova, J. B. Murray, R. Parsons, T. Shaw, A. E. Surgenor, L. Terry, Y. Wang, M. Wood, A. J. Massey, *J. Med. Chem.* **54** (2011) 4034 (https://doi.org/10.1021/jm101625x)
20. G. Jones, P. Willett, R. C. Glen, A. R. Leach, R. Taylor, *J. Mol. Biol.* **267** (1997) 727 (https://doi.org/10.1006/jmbi.1996.0897)
21. O. Trott, A. J. Olson, *J. Comput. Chem.* **31** (2010) 455 (https://doi.org/10.1002/jcc.21334)
22. *Amber 2021*, University of California, San Francisco, CA, 2021
23. W. L. Jorgensen, J. Chandrasekhar, J. D. Madura, R. W. Impey, M. L. Klein, *J. Chem. Phys.* **79** (1983) 926 (https://doi.org/10.1063/1.445869)
24. W. L. Jorgensen, J. D. Madura, *Mol. Phys.* **56** (1985) 1381 (https://doi.org/10.1080/00268978500103111)
25. P. Li, L. F. Song, K. M. Merz, *J. Chem. Theory Comput.* **11** (2015) 1645 (https://doi.org/10.1021/ct500918t)
26. A. W. Götz, M. J. Williamson, D. Xu, D. Poole, S. Le Grand, R. C. Walker, *J. Chem. Theory Comput.* **8** (2012) 1542 (https://doi.org/10.1021/ct200909j)
27. R. Salomon-Ferrer, A. W. Götz, D. Poole, S. Le Grand, R. C. Walker, *J. Chem. Theory Comput.* **9** (2013) 3878 (https://doi.org/10.1021/ct400314y)
28. S. Le Grand, A. W. Götz, R. C. Walker, *Comput. Phys. Commun.* **184** (2013) 374 (https://doi.org/10.1016/j.cpc.2012.09.022)
29. M. S. Jeremić, H. Wadepohl, V. V. Kojić, D. S. Jakimov, R. Jelić, S. Popović, Z. D. Matović, P. Comba, *RSC Adv.* **7** (2017) 5282 (https://doi.org/10.1039/C6RA26199J)
30. T. Mosmann, *J. Immunol. Methods* **65** (1983) 55 (https://doi.org/10.1016/0022-1759(83)90303-4)
31. N. Khanna, H. Jayaram, N. Singh, *Life Sci.* **75** (2004) 179 (https://doi.org/10.1016/j.lfs.2003.11.026)
32. S. Zinkel, A. Gross, E. Yang, *Cell Death Differ.* **13** (2006) 1351 (https://doi.org/10.1038/sj.cdd.4401987)
33. R. Kim, M. Emi, K. Tanabe, Y. Uchida, K. Arihiro, *Eur. J. Surg. Oncol.* **32** (2006) 269 (https://doi.org/10.1016/j.ejso.2005.12.006)
34. G. Kroemer, S. J. Martin, *Nat. Med.* **11** (2005) 725 (https://doi.org/10.1038/nm1263)
35. J. Peng, X. Chen, Q. Hu, M. Yang, H. Liu, W. Wei, S. Liu, H. Wang, *Mol. Med. Rep.* **10** (2014) 2271 (https://doi.org/10.3892/mmr.2014.2489)

36. E. Rosati, R. Sabatini, G. Rampino, F. De Falco, M. Di Ianni, F. Falzetti, K. Fettucciari, A. Bartoli, I. Screpanti, P. Marconi, *Blood* **116** (2010) 2713 (https://doi.org/10.1182/blood-2010-03-275628)
37. Y. Wang, J. Hu, Y. Cai, S. Xu, B. Weng, K. Peng, X. Wei, T. Wei, H. Zhou, X. Li, and Guang Liang, *J. Med. Chem* **56** (2013) 9601 (https://doi.org/10.1021/jm4016312)
38. C. Girdlestone, S. Hayward, *J. Comput. Biol.* **23** (2016) 21 (https://doi.org/10.1089/cmb.2015.0143).

Journal of the Serbian Chemical Society
JSCS@tmf.bg.ac.rs • www.shd.org.rs/JSCS
J. Serb. Chem. Soc. *87* (5) S104–S116 (2022) *Supplementary material*

SUPPLEMENTARY MATERIAL TO

Structural, biological and computational study of oxamide derivative

IGNJAT P. FILIPOVIĆ[1], EMINA M. MRKALIĆ[2], GIORGIO PELOSI[3], VESNA KOJIĆ[4], DIMITAR JAKIMOV[4], DEJAN BASKIĆ[5] and ZORAN D. MATOVIĆ[1]*

[1]*University of Kragujevac, Faculty of Science, Department of Chemistry, Radoja Domanovića 12, 34000 Kragujevac, Serbia,* [2]*University of Kragujevac, Institute for Information Technologies, Department of Science, Jovana Cvijića bb, Kragujevac 34000, Serbia,* [3]*Department of Chemistry, Life Sciences and Environmental Sustainability, University of Parma, 43123 Parma, Italy,* [4]*Institute of Oncology Sremska Kamenica, Novi Sad, Institutski put 4, 21204 Sremska Kamenica, Serbia and* [5]*University of Kragujevac, Faculty of Medicinal Science, S. Markovića 69, 34000 Kragujevac, Serbia*

J. Serb. Chem. Soc. *87* (5) (2022) 545–559

Docking

The protein target was prepared from the file in PDB format downloaded directly from the RSCB PDB site (PDB entry 3LDL) using AutoDock Tools. Because 3LDL is dimer, monomers were separated and only the A chain was used in further preparation. The co-crystalized ligand and water molecules were removed. Hydrogen atoms were added, Gasteiger charges were calculated, non-polar hydrogen atoms were merged and AD4 atom types were assigned to all atoms. The co-crystalized ATP molecule was used to validate the docking method after B3LYP/TZVP QM calculations from which partial charges for its atoms were obtained. Partial charges for atoms in H_2obbz^{2-} and H_4obbz structures were obtained using the same method. Non-polar hydrogens were merged, and all torsional rotations were enabled except for torsions in the amide bonds (H-N-C-O) as per default preparation options. Averaged coordinates of co-crystalized ATP were used as the center for the grid box.

Lamarckian algorithm (genetic algorithm (GA) - local search (LS) hybrid) was used for all experiments with AutoDock4. To increase the chance of finding the best solution, the number of GA-LS runs in each experiment was set to 20, the number of individuals in each generation was set to 300, the maximum number of energy evaluations per run was set to 25 million, and all other settings were set to default. Docking with Vina was done with most of the parameters at

* Corresponding author. E-mail: zmatovic@kg.ac.rs

default values, except exhaustiveness that was set to 16 to increase precision. Both Vina and AD4 managed to replicate the mode of binding between Grp-78 and ATP found in the crystal structure. This is shown in Fig. S-1.

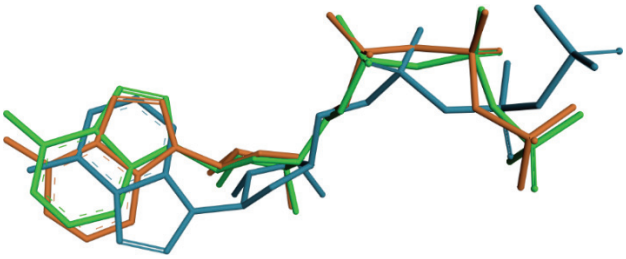

Fig. S-1. Comparison of ATP structure derived from crystal with structures from best docking solutions. Green - crystal; Orange - Vina; Blue - AD4.

Molecular dynamics

Ligand Gaussian09 Rev E.01[1] was used for the QM calculation for parameterization. AmberTools21[2] was used for the structural modeling and data analyses while pmemd.cuda[3,4] in AMBER20[2] was employed in the MD simulation. The three ligands were modeled as described below. The structure of each ligand was optimized based on the B3LYP[5-7]/TZVP[8] level of theory. Antechamber[9] in AmberTools21 was used for performing the RESP charge fitting for the three ligands. The bond, angle and torsion parameters about the ligands were based on general amber force field (GAFF,[10] version 1.8) while the protein system was modeled by the ff19SB force field. To test the quality of the developed force field for the ligands, RMSD calculation was performed between the QM optimized and MM minimized structures. The MM minimization was performedmby using the nucleic acid builder (NAB) module in AmberTools21: the first minimization was performed employing the conjugated minimization algorithm with a convergence criteria of energy gradient as $2.1 \cdot 10^{-4}$ kJ mol^{-1} Å^{-1} and maximum 20000 steps, afterwards another minimization was performed using the Newton-Raphson algorithm with treating the convergence criteria of energy gradient as $8.3 \cdot 10^{-12}$ kJ mol^{-1} Å^{-1} and a maximum of 50 steps. The *RMSD* values of MM minimized structures of ATP, H_2obbz^{2-} and H_4obbz ligands are 0.53, 0.56 and 0.23 Å, respectively, when comparing to the QM optimized ones. To further validate the parameterization, normal mode analyses were performed based on the MM level and compared to the QM calculated results. The R^2 values of the linear fittings between MM and QM calculated normal mode frequencies (aligned based on the frequency values) about ATP, H_2obbz^{2-} and H_4obbz compounds are 0.9961, 0.9815 and 0.9873, respectively. The *RMSD* values for different ligands are given in Fig. S-2. Based on these

parameterizations, modeling, minimization, MD simulations and MMPBSA/ /MMGBSA analyses were started.

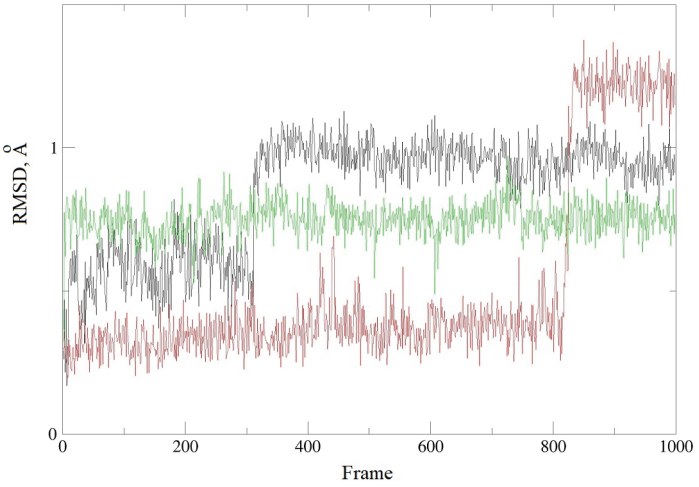

Fig. S-2. *RMSD* values of minimized solvated ligands.

Protein. The original structures of the protein-ligand complexes were prepared using the best hit from AutoDock4[11] run performed on selected target (PDB code 3LDL[12]). Afterwards these structures were adjusted based on the amino acid library in AMBER force field. A rectangular TIP4 OPC[13] water box (~75×72×50 Å) was used to solvate the system with all the water molecules are at least 1.5 Å away from the protein. Then Na+ ions were added to neutralize the negative charged system (3LD-ATP (-6), 3LDL-H_2obbz (-4) and 3LDL-H_4obbz (-2)) with their van der Waals parameters were from Li *et al.*[14] Afterwards 4 stages of minimization were carried out to optimize geometry of the solvated protein-ligand complex system. 1000 steps of steepest descend minimization plus 1000 steps of conjugated minimization were performed for each of the first three stages. 47.8 mol J^{-1} $Å^{-2}$ restraints were added to the all the atoms in the protein-ligand complex in the first stage, heavy atoms in the protein-ligand complex in the second stage while backbone C, CA and N atoms in the protein and non-metallic heavy atoms in the ligand for the third stage, respectively. The fourth stage of minimization was performed by 2000 steps of steepest descend minimization and afterwards 3000 steps of conjugated minimization with 4.78 mol kJ^{-1} $Å^{-2}$ restraints on the backbone N, CA and C atoms as well as non-metallic heavy atoms in the ligand. After that 1 ns MD simulation was performed in NVT ensemble to heat the system from 0 to 303.15 K followed by 1 ns MD simulation of equilibration carried out at 303.15 K in NVT ensemble. Afterwards 1 ns MD simulation was performed under 303.15 K and 1 atmosphere in NPT

ensemble to correct the density and further equilibrate the system. All above MD simulations were performed with 42 mol kJ^{-1} Å^{-2} restraints on the backbone N, CA and C atoms as well as the non-metallic heavy atoms in the ligand, referencing from the initial structure of each running. In the end 20 ns MD simulation of sampling was performed under 303.15 K in NPT ensemble without any restraints. Snapshots were saved for each 20 ps with totally 1000 snapshots were collected for the further analysis. Former research showed that multiple independent samplings could offer better results.[17] Here we ran 5 independent runs for each complex, totally there are 10000 snapshots along 100 ns sampling was collected for each complex. Particle mesh Ewald (PME) approach,[15-17] periodic boundary condition and 12 Å cut off were used during all the simulation. SHAKE[18] was used to constrain the bond lengths of heavy atoms and hydrogen atoms with a tolerance as 10^{-5} Å, while a three-point algorithm was used for water molecules.[19] Temperature was controlled by Langevin algorithm with collision frequency as 1.0 ps^{-1} in all the MD simulations. Pressure was controlled by using Berendsen barostat[20] with pressure relaxation time as 1.0 ps in the NPT production step.

To calculate the binding free energies between 3LDL monomer and each ligand, MMGBSA and MMPBSA analyses were carried out by using MMPBSA.py[21] in AmberTools21. GB model from Hawkins *et al.*[22,23] was used for the MMGBSA analyses by using the parameters from Tsui and Case[24] with treating salt concentration as 0.15 M. MMPBSA analyses were performed with 0.15 M ionic strength, 0.021 kJ mol^{-1}·Å^{-2} surface tension and without correction of free energy contribution from non-polar interaction. Normal mode analyses (NMA) were performed with 0.1 M ionic strength at 298.15 K by using the same GB model used in the MMGBSA analyses.

TABLE S-I. Δ*G* binding energies obtained by MMGBSA method (Energy differences are averaged over simulation run)

Energy components[a]	Average energy, kJ mol^{-1}		
	ATP	H_2obbz^{2-}	H_4obbz
VDWAALS	-207.93	-153.99	-191.51
EEL	-445.48	-320.76	-206.54
EGB	619.41	392.97	283.37
ESURF	-27.12	-22.24	-25.32
Δ*G* gas	-653.42	-474.75	-398.06
Δ*G* solv	592.29	370.73	258.06
Δ*G* binding	**-61.12**	**-104.02**	**-140.00**

[a]*VDWAALS* - van der Waals energy; *EEL* - electrostatic energy; *EGB* - polar solvation energy; *ESURF* - solvent-accessible surface area term; Δ*G* gas - Total free energy in gas phase; Δ*G* solv - Total free energy in solvent; Δ*G* binding - Estimated binding free energy calculated form the terms above.

Crucial interactions with amino-acid residues from frames with the lowest binding energy are shown in Fig. S-3.

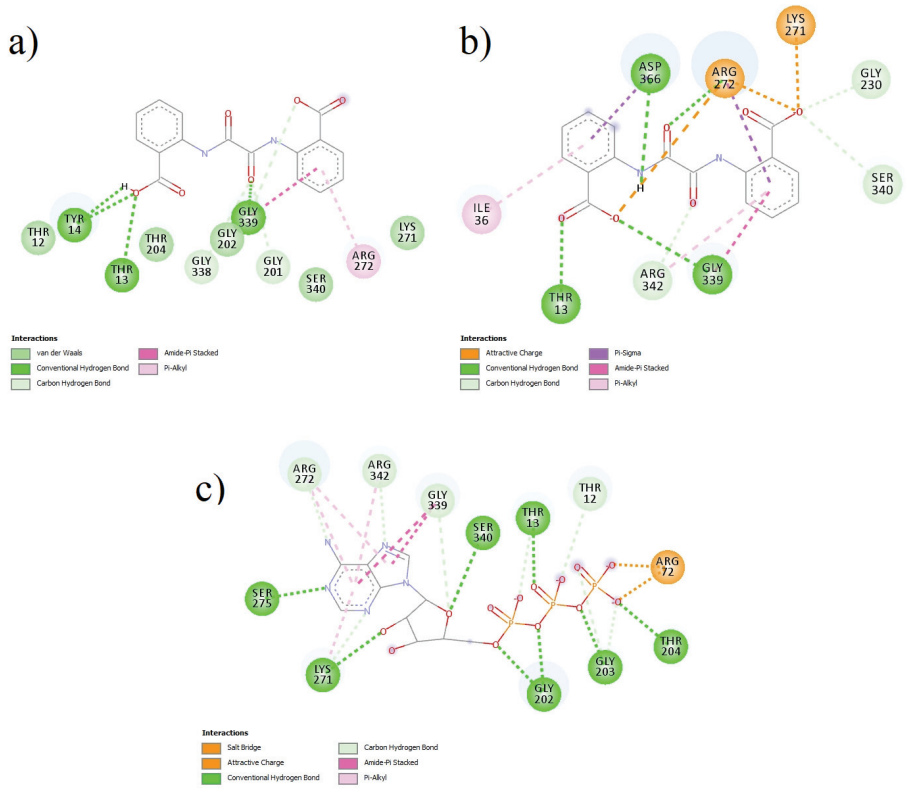

Fig. S-3. Crucial interactions of ligands with Grp78 during MD simulations. a) H_4obbz; b) H_2obbz^{2-}; c) ATP.

Biology

Cell lines: The cell lines used in the study were MCF-7 (human breast adenocarcinoma), A549 (human lung carcinoma), HT-29 (human colon adenocarcinoma), HeLa (human cervix adenocarcinoma) and MRC-5 (human foetal lung fibroblasts). The cells were grown in Dulbecco's modified Eagle's medium (DMEM) with 4.5 % of glucose, supplemented with 10 % of fetal bovine serum (FBS, Sigma) and antibiotics and antimicotics solution (Sigma). All cell lines were cultivated at 37 °C in an atmosphere of 5 % CO_2 and absolute humidity.

MTT assay: Growth inhibition was evaluated by tetrazolium colorimetric MTT assay (SIGMA). Exponentially growing cells were harvested and plated into 96-well microtiter plates (Costar) at optimal seeding density of 10^4 cells per well. Tested substances, at tenfold the required final concentration, were added

(10 µl/well) to all wells except to the control ones and microplates were incubated for 48 h. Three hours before the end of incubation period, 10 µl of MTT (5mg/ml) solution was added to all wells. Acid-isopropanol (100 µl of 0.04 M HCl in isopropanol) was added to all wells and mixed thoroughly to dissolve the dark blue crystals. After a few minutes at room temperature, to ensure that all crystals were dissolved, the plates were read on a spectrophotometer plate reader (Multiscan MCC340, Labsystems) at 540/690 nm. The inhibition of growth was expressed as a percent of a control and cytotoxicity was calculated according to the formula: $((1 - A_{test})/A_{control})100$. Two independent experiments were set out with quadruplicate wells for each concentration of the compound. The IC_{50} of compounds was determined by Median effect analysis.[25]

Annexin V-FITC/7-AAD assay for determination of apoptosis and necrosis by flow cytometry: Staining was performed according to manufacturer's protocol (Beckman Coulter, USA). Briefly, HeLa cells were treated with **(1)** in concentration equivalent to IC50 value, or media alone (control). After treatment (48 h, 37 ºC, 5 % CO_2, absolute humidity) cells were collected, washed in PBS and finally cell pellet was resuspended in ice cold binding buffer. Cell suspension ($1 \cdot 10^5$ cells) was stained with Annexin V-FITC and 7-AAD following the manufacturer's instruction. Samples were evaluated using flow cytometer (Cytomics FC500, Beckman Coulter, USA). The percentage of viable cells (AnnV-/7AAD-), early apoptotic (AnnV+/7AAD-), late apoptotic (AnnV+/7-AAD+) and necrotic cells (AnnV-/7-AAD+) was determined by Flowing Software (http://www.flowingsoftware.com/) and results were presented as dot plots.

Western blot analysis: Cells were seeded in 6-well plates at a concentration of $5 \cdot 10^5$ cells/well and treated with doxorubicin and tested compounds or media alone (control) for 48 h. The protein concentration in cell lysate was determined by Bradford protein assay in a 96-well microtiter plate (ThermoLab Systems, Multiscan Accent spectrophotometer) using bovine serum albumin as the standard. Molecular mass markers for proteins were obtained from Amersham Biosciences. For the Western blot, 50 µg of proteins per sample were separated by electrophoresis and electro-transferred to a polyvinylidene difluoride (PVDF) membrane Hybond-P (Amersham Biosciences, Arlington Heights, IL) and then blotted with primary antibodies (Bcl-2, PARP, Caspase-3, and Actin). Monoclonal antibodies against human Bcl-2 and Caspase 3 were obtained from R&D Systems (Minneapolis, MN). Anti- poly (ADP-ribose) polymerase (PARP) was purchased from Santa Cruz Biotechnology (Santa Cruz, CA). Antibody against α-actin, β-actin or γ-actin was purchased from Sigma Chemical (St. Louis, MO). Proteins were detected by an enhanced chemiluminescence (ECL Plus) kit (Amersham Biosciences), that includes peroxidase-labeled donkey anti-

rabbit and sheep anti-mouse secondary antibodies. Blots were developed with an ECL Plus detection system and recorded on Hyperfilm (Amersham Biosciences).

Cell cycle Analysis by flow cytometry: Cell cycle analysis was performed as described previously.[26] HeLa cells were incubated with media alone (control) or with **(1)** in concentration corresponding to IC50 value, for 48 h at 37 °C in 5 % CO_2. Treated cells were harvested, washed in PBS and finally fixed overnight in ice cold 70 % ethanol. After fixation, cells were washed, resuspended in PBS containing 500 μg mL^{-1} RNAseA and incubated 30 minutes at 37 °C in the dark. Staining was performed with 5 μL of propidium iodide (10mg/mL). After 15 minutes of incubation in the dark, cells were immediately analyzed by Cytomics FC500 flow cytometer (Beckman Coulter, USA). DNA content was defined by Flowing Software (http://www.flowingsoftware.com/) and cell cycle distribution was illustrated as histograms.

Infrared spectra

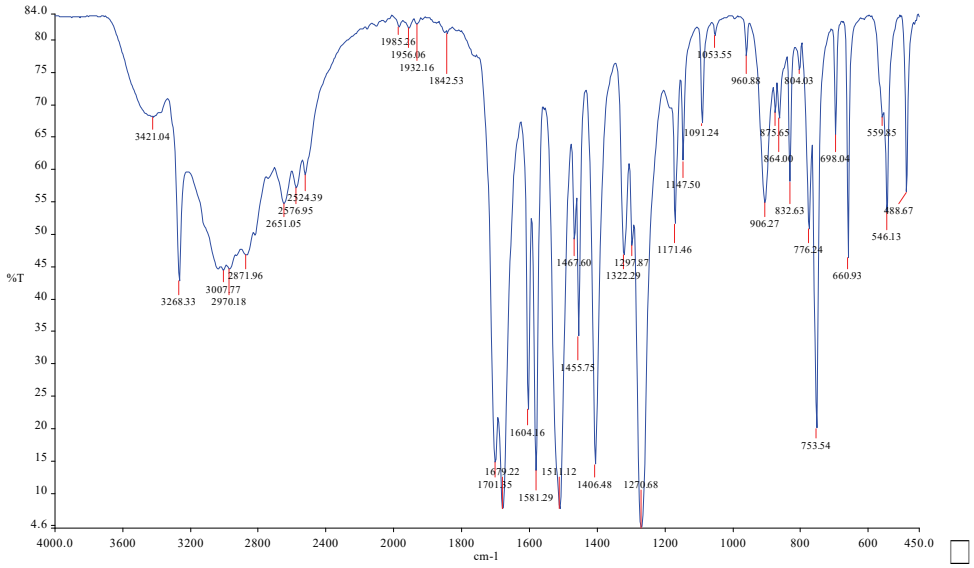

Fig. S-4. IR spectrum of H_4obbz ligand.

Crystal structure

TABLE S-II. Bond lengths in compound **(2)**

Atom 1	Atom 2	Type	Length, Å
C1	C2	Single	1.49(1)
C1	O1	Delocalised	1.249(8)
C1	O2	Delocalised	1.258(9)
C2	C3	Aromatic	1.421(7)
C2	C7	Aromatic	1.382(8)
C3	C4	Aromatic	1.37(1)
C3	N1	Single	1.410(7)
C4	H6	Single	0.930
C4	C5	Aromatic	1.39(1)
C5	H7	Single	0.930
C5	C6	Aromatic	1.384(9)
C6	H1A	Single	0.931
C6	C7	Aromatic	1.38(1)
C7	H5	Single	0.930
C8	N1	Single	1.332(7)
C8	O3	Double	1.23(1)
C8	C8	Single	1.53(1)
N1	H1	Single	0.861
C1	C2	Single	1.49(1)
C1	O1	Delocalised	1.249(8)
C1	O2	Delocalised	1.258(9)
C2	C3	Aromatic	1.421(7)
C2	C7	Aromatic	1.382(8)
C3	C4	Aromatic	1.37(1)
C3	N1	Single	1.410(7)
C4	H6	Single	0.930
C4	C5	Aromatic	1.39(1)
C5	H7	Single	0.930
C5	C6	Aromatic	1.384(9)
C6	H1A	Single	0.931
C6	C7	Aromatic	1.38(1)
C7	H5	Single	0.930
C8	N1	Single	1.332(7)
C8	O3	Double	1.23(1)
N1	H1	Single	0.861

TABLE S-III. Angles in compound **(2)**

Atom 1	Atom 2	Atom 3	Angle, °
C2	C1	O1	118.2(6)
C2	C1	O2	119.9(6)
O1	C1	O2	121.9(7)
C1	C2	C3	124.5(5)
C1	C2	C7	117.3(5)
C3	C2	C7	118.2(5)
C2	C3	C4	120.1(5)

Atom 1	Atom 2	Atom 3	Angle, °
C2	C3	N1	117.7(5)
C4	C3	N1	122.2(5)
C3	C4	H6	119.8
C3	C4	C5	120.2(6)
H6	C4	C5	120.0
C4	C5	H7	119.7
C4	C5	C6	120.6(7)
H7	C5	C6	119.7
C5	C6	H1A	120.5
C5	C6	C7	118.9(7)
H1A	C6	C7	120.5
C2	C7	C6	122.0(6)
C2	C7	H5	118.9
C6	C7	H5	119.1
N1	C8	O3	127.4(6)
N1	C8	C8	111.5(5)
O3	C8	C8	121.0(6)
C3	N1	C8	129.8(5)
C3	N1	H1	115.1
C8	N1	H1	115.2
C2	C1	O1	118.2(6)
C2	C1	O2	119.9(6)
O1	C1	O2	121.9(7)
C1	C2	C3	124.5(5)
C1	C2	C7	117.3(5)
C3	C2	C7	118.2(5)
C2	C3	C4	120.1(5)
C2	C3	N1	117.7(5)
C4	C3	N1	122.2(5)
C3	C4	H6	119.8
C3	C4	C5	120.2(6)
H6	C4	C5	120.0
C4	C5	H7	119.7
C4	C5	C6	120.6(7)
H7	C5	C6	119.7
C5	C6	H1A	120.5
C5	C6	C7	118.9(7)
H1A	C6	C7	120.5
C2	C7	C6	122.0(6)
C2	C7	H5	118.9
C6	C7	H5	119.1
C8	C8	N1	111.5(5)
C8	C8	O3	121.0(6)
N1	C8	O3	127.4(6)
C3	N1	C8	129.8(5)
C3	N1	H1	115.1
C8	N1	H1	115.2

TABLE S-IV. Torsions in compound **(2)**

Atom 1	Atom 2	Atom 3	Atom 4	Torsion, °
O1	C1	C2	C3	177.8(6)
O1	C1	C2	C7	-2.7(9)
O2	C1	C2	C3	-3(1)
O2	C1	C2	C7	176.6(6)
C1	C2	C3	C4	178.9(6)
C1	C2	C3	N1	-1.5(8)
C7	C2	C3	C4	-0.6(8)
C7	C2	C3	N1	179.0(5)
C1	C2	C7	C6	-178.1(6)
C1	C2	C7	H5	2
C3	C2	C7	C6	1.4(9)
C3	C2	C7	H5	-178.3
C2	C3	C4	H6	-179.6
C2	C3	C4	C5	0.5(9)
N1	C3	C4	H6	1
N1	C3	C4	C5	-179.1(6)
C2	C3	N1	C8	-176.5(6)
C2	C3	N1	H1	3.5
C4	C3	N1	C8	3.1(9)
C4	C3	N1	H1	-176.9
C3	C4	C5	H7	178.9
C3	C4	C5	C6	-1(1)
H6	C4	C5	H7	-1
H6	C4	C5	C6	178.9
C4	C5	C6	H1A	-177.9
C4	C5	C6	C7	2(1)
H7	C5	C6	H1A	2
H7	C5	C6	C7	-178.2
C5	C6	C7	C2	-2(1)
C5	C6	C7	H5	177.6
H1A	C6	C7	C2	177.7
H1A	C6	C7	H5	-3
O3	C8	N1	C3	-1(1)
O3	C8	N1	H1	179.2
C8	C8	N1	C3	178.6(5)
C8	C8	N1	H1	-1.4
N1	C8	C8	N1	180.0(5)
N1	C8	C8	O3	0.6(9)
O3	C8	C8	N1	-0.6(9)
O3	C8	C8	O3	-180.0(6)
O1	C1	C2	C3	-177.8(6)
O1	C1	C2	C7	2.7(9)
O2	C1	C2	C3	3(1)
O2	C1	C2	C7	-176.6(6)
C1	C2	C3	C4	-178.9(6)
C1	C2	C3	N1	1.5(8)
C7	C2	C3	C4	0.6(8)

Atom 1	Atom 2	Atom 3	Atom 4	Torsion, °
C7	C2	C3	N1	-179.0(5)
C1	C2	C7	C6	178.1(6)
C1	C2	C7	H5	-2
C3	C2	C7	C6	-1.4(9)
C3	C2	C7	H5	178.3
C2	C3	C4	H6	179.6
C2	C3	C4	C5	-0.5(9)
N1	C3	C4	H6	-1
N1	C3	C4	C5	179.1(6)
C2	C3	N1	C8	176.5(6)
C2	C3	N1	H1	-3.5
C4	C3	N1	C8	-3.1(9)
C4	C3	N1	H1	176.9
C3	C4	C5	H7	-178.9
C3	C4	C5	C6	1(1)
H6	C4	C5	H7	1
H6	C4	C5	C6	-178.9
C4	C5	C6	H1A	177.9
C4	C5	C6	C7	-2(1)
H7	C5	C6	H1A	-2
H7	C5	C6	C7	178.2
C5	C6	C7	C2	2(1)
C5	C6	C7	H5	-177.6
H1A	C6	C7	C2	-177.7
H1A	C6	C7	H5	3
C8	C8	N1	C3	-178.6(5)
C8	C8	N1	H1	1.4
O3	C8	N1	C3	1(1)
O3	C8	N1	H1	-179.2

Coordination sphere of potassium in $K_2H_2obbz \times 2H_2O$ is shown in Fig. S-5.

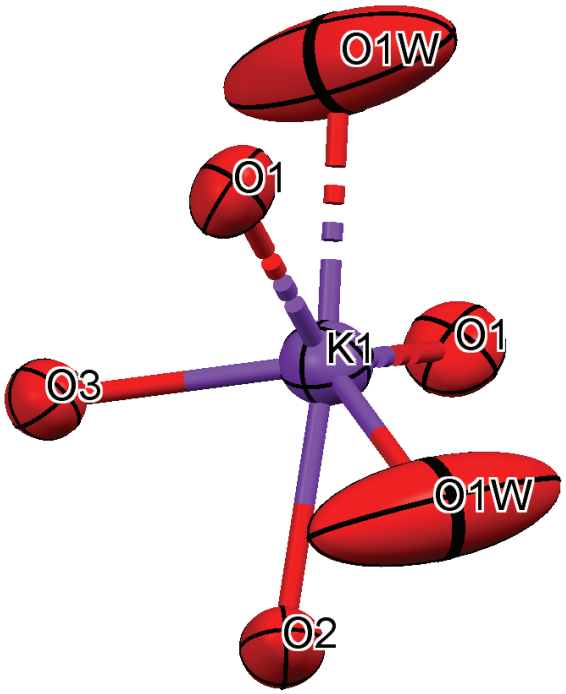

Fig. S-5 Coordination sphere of $K_2H_2obbz \times 2H_2O$.

*2,2'-[(1,2-dioxoethane-1,2-diyl)diimino] dibenzoic acid, H_4obbz (**1**)*[27]

Anal. Calcd. for $C_{16}H_{12}N_2O_6$: C, 58.54; H, 3.68; N, 8.53 %. Found: C, 57.86; H, 3.52; N, 8.49 %. Melting point: 205 °C.

*$K_2H_2obbz{\cdot}2H_2O$ (**2**)*

Anal. Calcd. for $C_{16}H_{10}K_2N_2O_8$: C, 44.03; H, 2.31; N, 6.42 %. Found: C, 43.90; H, 2.28; N, 6.40 %. ^{1}H-NMR (200 MHz, D_2O, δ / ppm): 7.20-7.36 (2H, *m*, ArH), 7.48-7.59 (2H, *m*, ArH), 7.86-7.96 (2H, *m*, ArH), 8.28-8.39 (2H, *m*, ArH). ^{13}C-NMR (50 MHz, D_2O, δ / ppm): 178.8, 150.5, 134.8, 133.8, 127.1, 123.0, 120.6, 120.4. IR (KBr, pellet ν / cm^{-1}): 3268.33m, 1701.35s, 1679.22s, 1581.29s, 1511.12s, 1455.75m, 1406.48s, 1270.68s, 1171.46m, 1147.50m, 1091.24w, 753.54s. Melting point: 217 °C.

REFERENCES

1. *Gaussian 09, Revision A.02,* Gaussian, Inc., Wallingford CT, 2016
2. *Amber 2021*, University of California, San Francisco, CA, 2021
3. A. W. Götz, M. J. Williamson, D. Xu, D. Poole, S. Le Grand, R. C. Walker, *J. Chem. Theory Comput.* **8** (2012) 1542 (https://doi.org/10.1021/ct200909j)
4. R. Salomon-Ferrer, A. W. Götz, D. Poole, S. Le Grand, R. C. Walker, *J. Chem. Theory Comput.* **9** (2013) 3878 (https://doi.org/10.1021/ct400314y)

5. A. D. Becke, *Phys. Rev. A* **38** (1988) 3098 (https://doi.org/10.1103/PhysRevA.38.3098)
6. C. Lee, W. Yang, R. G. Parr, *Phys. Rev. B* **37** (1988) 785 (https://doi.org/10.1103/PhysRevB.37.785)
7. A. D. Becke, *J. Chem. Phys.* **98** (1993) 5648 (https://doi.org/10.1063/1.464913)
8. M. F. Peintinger, D. V. Oliveira, T. Bredow, *J. Comput. Chem.* **34** (2013) 451 (https://doi.org/10.1002/jcc.23153)
9. J. Wang, W. Wang, P. A. Kollman, D. A. Case, *J. Mol. Graph. Model.* **25** (2006) 247 (https://doi.org/10.1016/j.jmgm.2005.12.005)
10. J. Wang, R. M. Wolf, J. W. Caldwell, P. A. Kollman, D. A. Case, *J. Comput. Chem.* **25** (2004) 1157 (https://doi.org/10.1002/jcc.20035)
11. G. M. Morris, R. Huey, W. Lindstrom, M. F. Sanner, R. K. Belew, D. S. Goodsell, A. J. Olson, *J. Comput. Chem.* **30** (2009) 2785 (https://doi.org/10.1002/jcc.21256)
12. A. T. Macias, D. S. Williamson, N. Allen, J. Borgognoni, A. Clay, Z. Daniels, P. Dokurno, M. J. Drysdale, G. L. Francis, C. J. Graham, R. Howes, N. Matassova, J. B. Murray, R. Parsons, T. Shaw, A. E. Surgenor, L. Terry, Y. Wang, M. Wood, A. J. Massey, *J. Med. Chem.* **54** (2011) 4034 (https://doi.org/10.1021/jm101625x)
13. W. L. Jorgensen, J. Chandrasekhar, J. D. Madura, R. W. Impey, M. L. Klein, *J. Chem. Phys.* **79** (1983) 926 (https://doi.org/10.1063/1.445869)
14. P. Li, L. F. Song, K. M. Merz, *J. Chem. Theory Comput.* **11** (2015) 1645 (https://doi.org/10.1021/ct500918t)
15. T. Darden, D. York, L. Pedersen, *J. Chem. Phys.* **98** (1993) 10089 (https://doi.org/10.1063/1.464397)
16. T. E. I. Cheatham, J. L. Miller, T. Fox, T. A. Darden, P. A. Kollman, *J. Am. Chem. Soc.* **117** (1995) 4193 (https://doi.org/10.1021/ja00119a045)
17. H. G. Petersen, *J. Chem. Phys.* **103** (1995) 3668 (https://doi.org/10.1063/1.470043)
18. J.-P. Ryckaert, G. Ciccotti, H. J. . Berendsen, *J. Comput. Phys.* **23** (1977) 327 (https://doi.org/10.1016/0021-9991(77)90098-5)
19. S. Miyamoto, P. A. Kollman, *J. Comput. Chem.* **13** (1992) 952 (https://doi.org/10.1002/jcc.540130805)
20. H. J. C. Berendsen, J. P. M. Postma, W. F. van Gunsteren, A. DiNola, J. R. Haak, *J. Chem. Phys.* **81** (1984) 3684 (https://doi.org/10.1063/1.448118)
21. B. R. Miller, T. D. McGee, J. M. Swails, N. Homeyer, H. Gohlke, A. E. Roitberg, *J. Chem. Theory Comput.* **8** (2012) 3314 (https://doi.org/10.1021/ct300418h)
22. G. D. Hawkins, C. J. Cramer, D. G. Truhlar, *Chem. Phys. Lett.* **246** (1995) 122 (https://doi.org/10.1016/0009-2614(95)01082-K)
23. G. D. Hawkins, C. J. Cramer, D. G. Truhlar, *J. Phys. Chem.* **100** (1996) 19824 (https://doi.org/10.1021/JP961710N)
24. V. Tsui, D. A. Case, *Biopolymers* **56** (2000) 275 (https://doi.org/10.1002/1097-0282(2000)56:4%3C275::aid-bip10024%3E3.0.co;2-e)
25. T. Mosmann, *J. Immunol. Methods* **65** (1983) 55 (https://doi.org/10.1016/0022-1759(83)90303-4)
26. N. Khanna, H. Jayaram, N. Singh, *Life Sci.* **75** (2004) 179 (https://doi.org/10.1016/j.lfs.2003.11.026)
27. M. F. Peintinger, D. V. Oliveira, T. Bredow, *J. Comput. Chem.* **34** (2013) 451 (https://doi.org/10.1002/jcc.23153).

Journal of the Serbian Chemical Society
JSCS@tmf.bg.ac.rs • www.shd.org.rs/JSCS
J. Serb. Chem. Soc. *87* (5) 561–573 (2022)
JSCS–5541
Original scientific paper
Published 18 February 2022

New rhodium(III)–ED3AP complex: Crystal structure, characterization and computational chemistry

MARKO D. RADOVANOVIĆ[1#], MARIJA S. RISTIĆ[1#], MATIJA ZLATAR[2#], FRANK W. HEINEMANN[3] and ZORAN D. MATOVIĆ[1]*

[1]*University of Kragujevac, Faculty of Science, Department of Chemistry, Radoja Domanovića 12, 34000 Kragujevac, Serbia,* [2]*University of Belgrade – Institute of Chemistry, Technology and Metallurgy, Njegoševa 12, 11000 Belgrade, Serbia and* [3]*University Erlangen-Nürnberg (FAU), Department of Chemistry and Pharmacy, Inorganic Chemistry, Friedrich-Alexander, Egerlandstraße 1, 91058 Erlangen, Germany*

(Received 30 December 2021, revised 14 January, accepted 15 January 2022)

Abstract: Only one (*trans*(O_5)-Na[Rh(ED3AP)]·3H_2O) of possible two isomers was synthesized and characterized by single crystal X-ray analysis, IR and UV–Vis spectroscopy. Computational analysis of both isomers was performed with three levels of theory (B3LYP/TZV, BP86/TZV, OPBE/TZV), which gave consistent results. The more stable isomer by total energy and ligand field stabilization energy (LFSE) was *trans*(O_5) which appeared in synthesis. The calculation of excited state energies complied with UV–Vis spectra, especially with OPBE functional. The results of excited state energy pointed out the differences among isomers in means of a splitting pattern of $^1T_{2g}$ excited state term. Both isomers have a strongly delocalized structure, according to the natural bonding orbital (NBO) analysis. NBO analysis shows that the *trans*(O_5) isomer is more stable than *trans*(O_5O_6) for approx. 87 kJ/mol. Therefore, only the *trans*(O_5) isomer is present in the reaction mixture.

Keywords: rhodium; EDTA; crystal structure; NBO; LFDFT.

INTRODUCTION

Metal complexes with EDTA-type of ligands (EDTA = ethylenediamine--*N*,*N*,*N'N'*-tetraacetate) are used in laboratory settings,[1] industrial processes,[2] in medicine,[3–5] environmental field[6,7] and biological systems.[8,9] The rhodium(III) and its complexes with EDTA-type ligands have been extensively investigated for many decades.[10–14] When it comes to the ED3AP ligand (ethylenediamine--*N*,*N*,*N'*-triacetato-*N'*-3-propionato anion), one cannot say that it is thoroughly investigated. The unsymmetrical hexadentate ED3AP ligand can form two geo-

* Corresponding author. E-mail: zmatovic@kg.ac.rs
# Serbian Chemical Society member.
https://doi.org/10.2298/JSC211230003R

metrical isomers depending on the position of the six-membered chelate rings: *trans*(O_5) and *trans*(O_5O_6) (Fig. 1). The literature data show that *trans*(O_5) ED3AP isomer is more stable of the two in the case of Co(III),[15] Cr(III),[16] Cu(II)[17] and Ni(II)[18] complexes. This outcome is explained by the low strain in the equatorial plane at the *trans*(O_5) isomer because the in-plane 5-5-6 the arrangement of the chelate rings makes the propionate ring less strained than the acetate ones. The six-membered propionate ring serves better for the formation of the less-strained ring in equatorial plane favouring the *trans*(O_5) isomer of $[Rh(ED3AP)]^-$ complexes, with 5-5-6 in-plane arrangement of rings.

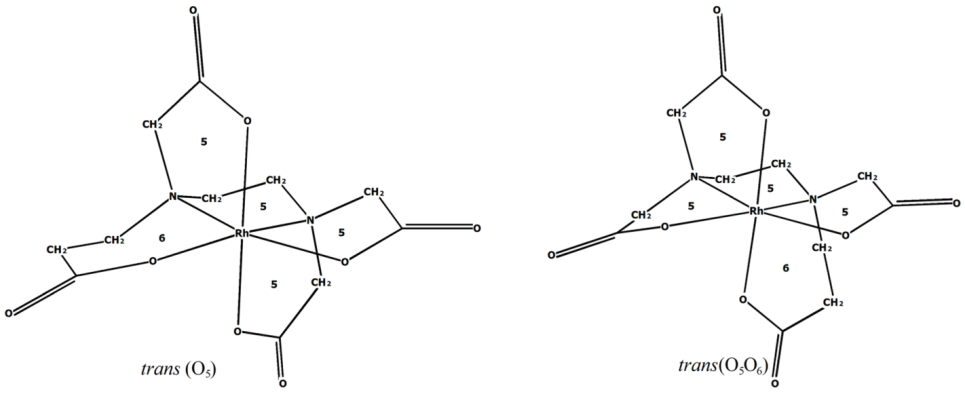

Fig. 1. Two possible geometrical isomers of the $[Rh(ED3AP)]^-$ complex. The size of chelate rings (five- or six- membered) is indicated.

Rhodium complexes are an important alternative to platinum-based complexes in cancer therapy. Many half-sandwich complexes of Rh have been reported with promising results,[19–21] as well as the octahedral rhodium complexes.[22,23] Also, rhodium complexes are known as antimicrobial agents.[24–27] However, there is insufficient data on the antitumor and the antimicrobial activity of rhodium complexes containing EDTA type of ligand.[11] Bearing this in mind, we have continued our research on complexes of Rh-EDTA type. Thus, in this paper, two isomers (*trans*(O_5) and *trans*(O_5O_6)) of $[Rh(ED3AP)]^-$ complex are investigated. In this paper a new rhodium (III) complex has been reported: $Na[Rh(ED3AP)]\cdot 3H_2O$. The IR, and UV–Vis spectra were discussed in relation to the geometry of the complex. Molecular mechanics and density functional theory (DFT) methods have been used to model the most stable geometric isomer and significant structural and energetic data were obtained. natural bonding orbital (NBO)[28] analysis is used to get insight into the energetics of these Werner-type of complexes. Ligand field density functional theory (LFDFT)[29] has been used to calculate the ligand field (LF) parameters and the excited state energies and rationalize the differences between two isomers.

EXPERIMENTAL

Reagents and physical measurements

All chemicals were purchased from Sigma–Aldrich and were used without any further purification. H_4ED3AP was prepared using a previously described procedure.[18] Elemental (C, H, N) analysis of the sample was carried out in the Center for Instrumental Analysis, Faculty of Chemistry, Belgrade. IR spectra (in KBr pellets) were recorded on a Perkin Elmer FT-IR spectrophotometer Spectrum One. Electronic absorption spectra were obtained using a double beam UV–Vis spectrophotometer model Cary 300 (Agilent Technologies, Santa Clara, CA, USA) with 1.0 cm quartz cells. The melting point was measured by the Stuart melting device with accuracy ±1 °C.

Preparation of the complex

The complex has been prepared by the previously reported procedure.[11] After elution with 0.1 mol dm^{-3} NaCl, a main yellow band was detected on the chromatographic column. The yellow band eluate was separated, evaporated, desalted using Sephadex G-10 resin and evaporated to 5 cm^3. After adding of 3 to 4 cm^3 of ethanol, the solution was left in a refrigerator for several days. After several days, the yellow crystals of the band were collected and air-dried. Yield: 0.15 g (6.22 %). Melting point: > 305 °C. Anal. Calc. for $C_{11}H_{20}N_2NaO_{11}Rh$ (482.19 g mol^{-1}): C, 27.40; H, 4.18; N, 5.81 %. Found: C, 27.50; H, 4.10; N, 5.76 %. IR (KBr, ν_{max} / cm^{-1}): 1664 ν(COO^-), 1623 ν(COO^-), 1567 ν(COO^-), 3475 ν(N–H). UV–Vis (H_2O, c = = 10^{-3} mol dm^{-3}): λ_{max} / nm (ε / dm^3 mol^{-1} cm^{-1}): 295(*sh*) (432), 343 (693).

X-ray crystallographic analysis

Details of crystal data, data collection, and refinement for *trans*(O_5)-Na[Rh(ED3AP)]·$3H_2O$ complex are given in Table S-I of the Supplementary material to this paper. The intensity data were collected using MoKα radiation (λ = 0.71073 Å) on a Bruker–Nonius Kappa CCD diffractometer, graphite monochromator. The data were corrected for Lorentz and polarization effects and the semiempirical absorption corrections were performed based on multiple scans using SADABS V2.06.[30] The structure was solved by direct methods (SHELXTL NT 6.12)[31] and refined by full-matrix least-squares procedures on F2 using SHELXL2016/6.[32] All non-hydrogen atoms were refined anisotropically. The positions of all hydrogen atoms were derived from a difference Fourier map, and their positional parameters were refined. The isotropic displacement parameters of all H atoms were tied to those of their corresponding carrier atoms by a factor of 1.2 or 1.5. Olex2 was used to prepare material for publication.[33]

Computational details

Geometries for Rh (III) complexes were optimized using Gaussian 16 C01 program (G16).[34] The Becke three-parameter exchange functional was employed in this study in conjunction with the Lee–Yang–Parr correlation hybrid functional (B3LYP)[35] and the TZVP basis set.[36] The systems were treated in restricted formalism. The calculations were done with polarizable continuum model (PCM), with water as a solvent, as implemented in the G16. The calculated structures were verified as local minima (all positive eigenvalues by frequency analysis). Starting geometries were taken either from the experimental X-ray structures or were pre-optimized using molecular mechanics. NBO employed in the Gaussian 16 C01 program was used with the same method/basis set, and for natural molecular orbital analysis, we used NBO 7.0.[28] We used the LFDFT to calculate excited state energies on either optimized or X-ray geometries. The LFDFT consists of four steps. Firstly, we performed an average of configuration (AOC) calculation, a spin-restricted calculation with 6 electrons distributed evenly

over 5 Kohn–Sham (KS) orbitals with dominantly Rh(III) 4d character. Using those AOC KS orbitals, in the second step, we calculated energies of all 210 Slater determinants (SD) originated from the d^6 configuration in a spin-unrestricted way. These SD energies were then used to determine the parameters of inter-electron repulsion (Racah's parameters) and eigenvalues, of the one-electron effective ligand-field (LF) Hamiltonian. These parameters were in the final step used to determine the excited state energies by diagonalizing the total LF Hamiltonian in the basis of SDs. LFDFT procedure was obtained using Amsterdam density functional (ADF)[37] program with three different functionals (B3LYP[35], BP86[38] and OPBE[39]) and Slater type TZP basis set. AOC calculations were performed with water included as a solvent through the conductor-like screening model (COSMO).

RESULTS AND DISCUSSION

Synthesis and spectral analysis of complexes

The hexadentate ED3AP ligand was used for the synthesis of the new *trans*(O_5)-[Rh(ED3AP)]$^-$ complex. The preparation of the ligand was reported previously.[18] The reaction between the equimolar amounts of $RhCl_3 \cdot 3H_2O$ and ED3AP in the water at 145 °C, was carried out, and column chromatography was used to separate the complex as described above. The corresponding rhodium (III) complex was obtained, as yellow crystals of *trans*(O_5)-Na[Rh(ED3AP)]·$3H_2O$ suitable for X-ray analysis. The complex was also characterized by elemental analysis, IR, UV–Vis, spectroscopy and single-crystal X-ray diffraction studies.

The carboxylate asymmetric stretching frequencies have been used as a criterion for distinguishing protonated (1700–1750 cm^{-1}) and coordinated carboxylate (1560–1680 cm^{-1}). The carboxylate asymmetric stretching of five-membered chelate rings are at higher energy (1600–1680 cm^{-1}) than the corresponding ones of six-membered chelate rings (1560–1600 cm^{-1}). The complex shows two high intensity band at 1664 and 1623 cm^{-1}, and these are assigned to asymmetric vibrations of the five-membered acetate rings in-plane and out-of-plane respectively (Fig. S-1, Supplementary material). The same complex shows one high intensity band at 1567 cm^{-1}, assigned to the carboxylate group of the six-membered in-plane 3-propionate ring. The absence of other vibrations in the 1700–1750 cm^{-1} area suggests that all carboxylate groups are coordinated.

Data of the UV–Vis spectra of the complex are presented in Fig. 2.

We also gave spectra of the *trans*(O_5)-[Rh(eddadp)]$^-$ complex[14] for comparison. The shapes of both spectra show two bands arising from the spin-allowed transitions ($^1A_{1g} \rightarrow {}^1T_{1g}$ and $^1A_{1g} \rightarrow {}^1T_{2g}$ in O_h assignment), but there are minor differences among them. *trans*(O_5)-[Rh(eddadp)]$^-$ has higher in energy transitions (lower wavelength) due to the stronger ligand field surrounding of the equatorial plane of the 656 chelate ring system, contrary to the 556 chelate ring system of our complex.

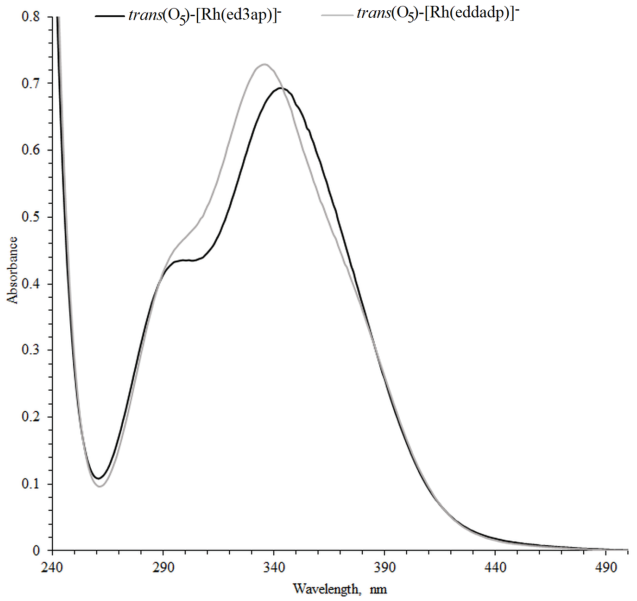

Fig. 2. Electronic absorption spectra of Rh(III) complexes in aqueous solution (c = 10^{-3} mol dm^{-3}): ━, *trans*(O_5)-[Rh(ED3AP)]$^-$ and ═, *trans*(O_5)-[Rh(eddadp)]$^-$.[14]

Description of the crystal structures

The structural diagram of the *trans*(O_5)-Na[Rh(ED3AP)]·3H_2O along with the packing in the crystals is illustrated in Fig. 3. Selected bond distances are listed in Table S-II, Supplementary material. The asymmetric unit contains one formula unit, comprising two moieties: the negatively charged rhodium complex [Rh(ED3AP)]$^-$ and Na^+ coordinated to three water molecules. Therefore, the orthorhombic unit cell contains eight units: four cations and four anions. The four cationic species (Na^+) are partially (triply) hydrated. The

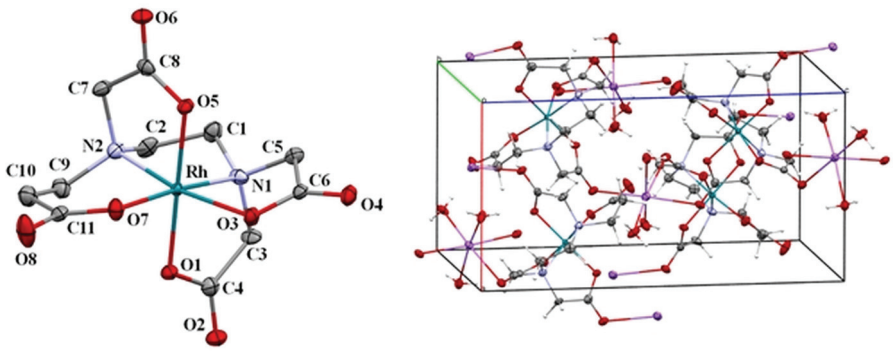

Fig. 3. Ortep diagram of the *trans*(O_5)-[Rh(ED3AP)]$^-$ complex anion and crystal packing view along *b* axis (50% probability ellipsoids).

trans(O_5) geometry of [Rh(ED3AP)]$^-$ entity contains Rh(III) center in a well approximated octahedral geometry. The rhodium(III) ion coordinates six donor atoms from the ligand: four deprotonated carboxylic oxygens and two amine nitrogen atoms.

The equatorial positions of the coordination octahedron are occupied by two deprotonated carboxylic oxygens (Rh-O3 2.053(2) Å, Rh-O7 2.043(2) Å) and the two nitrogen atoms of the ligand (Rh-N1 2.011(2) Å, Rh-N2 2.023(2) Å). The axial positions are occupied by two oxygen donor atoms of the third and fourth carboxyl (Rh-O5 2.006(2) Å, Rh-O1 1.999(2) Å). The second oxygen atom of the acetic in-plane carboxylic group interacts with the sodium ion (O4-Na1 2.516(2) Å). The Rh-ligand bond distances and angles (Table S-II) are comparable with the corresponding ones of analogous complexes.[10–13] The ethylenediamine E ring is in a twisted conformation. The puckering parameters are $q2$ = 0.452(2) Å and $\varphi 2$ = 266.6(2)°. The ideal values for a twisted conformation are $q2$ > 0 Å, $\varphi 2$ = 90°.[40] One of the five-membered rings adopted an envelope conformation, while the other two five-membered acetate rings are in a twisted conformation. Their puckering parameters are $q2$ = 0.122(2) Å, $\varphi 2$ = 183.1(1)° (RhO1C4C3N1), $q2$ = 0.474(2) Å, $\varphi 2$ = 157.4(3)° (RhO3C6C5N1) and $q2$ = 0.151(2) Å, $\varphi 2$ = = 162.1(9)° (RhO5C8C7N2). The equatorial six-membered propionate ring is in a half-chair conformation (RhN2C9C10C11O7) with puckering parameters: $q2$ = 0.362(2) Å, $q3$ = –0.382(2) Å, $\varphi 2$ = 110.1(3)°, θ = 136.5(2)°.

Computational chemistry

LFDFT. We used three different exchange-correlation functionals (BP86, OPBE, B3LYP) for AOC and SD calculations to determine the excited state energies through the LFDFT procedure on X-ray and B3LYP/TZVP optimized geometries. According to the Tanabe-Sugano diagram, the octahedral (O_h) low-spin d^6 complexes, such as Rh(III)-EDTA type complexes, give rise to two low spin excited states: $^1T_{1g}$ lower and $^1T_{2g}$ higher in energy. Both isomers (*trans*(O_5) and *trans*(O_5O_6)) of [Rh(ED3AP)]$^-$ complex are in octahedral coordination but with lower true symmetry (C_1 point group). Complexes have two N and two O donor atoms in the equatorial position, higher in the spectrochemical series than two axial O donor atoms. Because of that, Rh(III)-EDTA type complexes have a splitting pattern corresponding to D_{4h} symmetry (*i.e.*, holohedrized D_{4h} symmetry). Due to the unequal ligand surrounding in equatorial and axial positions, the lower energy $^1T_{1g}$ term is split to double degenerated ^1E_g and non-degenerated $^1A_{2g}$. The higher energy $^1T_{2g}$ term splits to double degenerate ^1E_g and non-degenerated $^1B_{2g}$ (Scheme S-1, Supplementary material).

In the case of ideal D_{4h} symmetry, a splitting pattern of four terms as described above is expected. In actual symmetry (C_1), which is contained in the non-empirical LF Hamiltonian, complete degeneracy removal is expected. This is

what is observed in LFDFT calculations (Table I). Still nearby in energy excitations may be considered as belonging to the degenerate ^1E_g term. The results of LFDFT calculation and their comparison with the experimental values of excited state energies for *trans*(O_5) isomer, which are also reported in this work, are given in Table I. As a consequence of the proximity of split transitions, only two are experimentally observed of the expected four. The average of three calculated values of the particular transition ($^1A_{1g}\rightarrow{}^1T_{1g}$ or $^1A_{1g}\rightarrow{}^1T_{2g}$) is compared with the experimental one, and the comparison is given as absolute error (AE, Table I). Considering the mean absolute error (MAE), we concluded that the results of OPBE functional are excellent on the X-ray geometry. The results are less accurate on B3LYP optimized structure no matter which functional is used. The geometry optimization by B3LYP overestimates metal-ligand bond distances (Table S-III, Supplementary material) and therefore LFDFT gives slightly lower energies of the excited states. These results indicate the importance of geometry used for excited state calculations. It is noteworthy that LFDFT calculations on B3LYP geometries are still accurate within 2000 cm^{-1}.

TABLE I. Energies (10^3 cm^{-1}) of the singlet electronic states from LFDFT and comparison with available experimental data

[Rh(ED3AP)]$^-$	Electronic state									
	trans(O_5)[a]				*trans*(O_5)[b]			*trans*(O_5O_6)[b]		
	B3LYP	BP86	OPBE	Exp.	B3LYP	BP86	OPBE	B3LYP	BP86	OPBE
$^1A_{1g}\rightarrow{}^1T_{1g}$	28.18	27.77	27.60	29.15	26.01	25.69	25.48	25.55	25.29	25.10
	28.63	28.27	28.15		26.42	26.13	25.97	25.82	25.54	25.36
	30.89	30.18	29.87		28.52	27.79	27.47	27.58	27.10	26.72
$^1A_{1g}\rightarrow{}^1T_{2g}$	35.54	34.19	33.59	33.90	33.35	32.22	31.61	31.85	31.57	30.94
	36.41	34.94	34.33		34.27	33.01	32.39	33.56	33.36	32.58
	37.84	36.60	35.98		35.37	34.33	33.73	34.47	34.56	33.82
AE ($^1A_{1g}\rightarrow{}^1T_{1g}$)	0.08	0.42	0.62		2.17	2.62	2.85			
AE ($^1A_{1g}\rightarrow{}^1T_{2g}$)	2.69	1.34	0.73		0.43	0.71	1.33			
MAE	1.39	0.88	0.67		1.30	1.67	2.09			

[a]X-ray structure; [b]B3LYP/TZVP optimized structure

We presented results from Table I in the form of a chart (Fig. 4) only for the optimized structures to discuss the relationship between the geometric isomers and the energies of their excited states and their splitting pattern.

There is no significant difference in the splitting of the excited states originating from $^1T_{1g}$ (lower in energy) in the case of both isomers. But the splitting of the $^1T_{2g}$ (higher in energy) term seems to be more related to the type of isomer. The ^1E_g ($^1T_{2g}$) is lower in energy than $^1B_{2g}$ in the case of the *trans*(O_5) isomer. In the case of the *trans*(O_5O_6), the opposite is observed. Furthermore, in *trans*(O_5O_6), the ^1E_g ($^1T_{2g}$) state is split more.

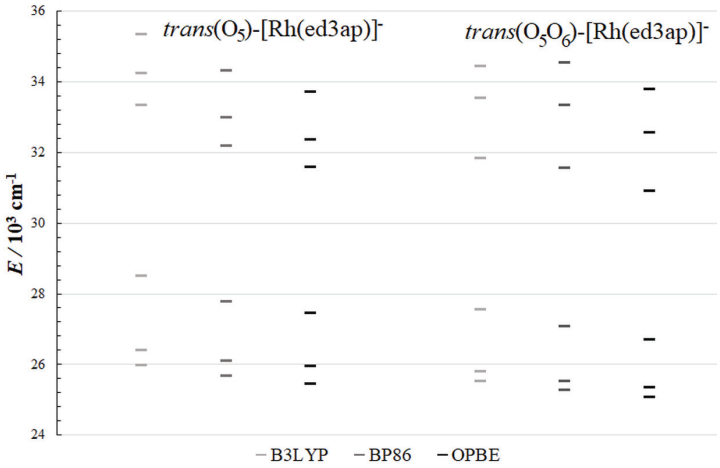

Fig. 4. Excited state energies of B3LYP/TZVP optimized structures for *trans*(O_5) and *trans*(O_5O_6) isomers of [Rh(ED3AP)]$^-$ complex obtained by LFDFT.

The calculation of the single-point (SP) energies by different exchange-correlation functionals (B3LYP, BP86, OPBE) were performed in order to interpret the stability of discussed isomers. SP energies were obtained on B3LYP optimized structures as well as $\Sigma\Delta(O_h)$ value. This parameter represents geometry distortion of the complex from the ideal octahedron. We also calculated the ligand field stabilization energy (LFSE) and collected all results in Table II. *trans*(O_5) isomer, with a 556-55 system of chelate rings, which is more adjustable to octahedral geometry and has lower value of $\Sigma\Delta(O_h)$ than *trans*(O_5O_6) isomer with his 555-56 system of chelate rings. The *trans*(O_5O_6) isomer has a higher value of LFSE (less stabilization) than the *trans*(O_5) isomer because of the more significant angle distortion. Consequently, the t_{2g} set (d_{xy}, d_{xz}, d_{yz}) is higher in energy. The more stable isomer is *trans*(O_5) because of LFSE's contribution to the total energy. The less stable *trans*(O_5O_6) isomer has not been isolated in the synthesis. All the results presented in Table II, are independent of the choice of exchange-correlation functional.

TABLE II. Relative and ligand field stabilization energies (E / kJ mol^{-1}) of optimized [Rh(ED3AP)]$^-$ isomers

Isomer	Ring system	$\Sigma\Delta(O_h)$[a]	State					
			B3YLP		BP86		OPBE	
			ΔE[b]	LFSE[c]	ΔE[b]	LFSE[c]	ΔE[b]	LFSE[c]
trans(O5)-[Rh(ED3AP)]$^-$	556–55	44	0.00	–406.26	0.00	–400.07	0.00	–398.55
trans(O5O6)-[Rh(ED3AP)]$^-$	555–56	66	24.49	–398.55	20.79	–392.52	24.70	–391.11

[a]The sum of the absolute values of the deviations from 90° of the twelve L–M–L' angles; [b]the isomer with the lowest energy minimum has been indicated with 0 kJ mol^{-1}; [c]ligand field stabilization energy in kJ mol^{-1}

NBO. NBO outputs from the Gaussian calculations were analyzed using the NBO 7.4 package. The empirical regularities in ML_n stoichiometry for d-block elements suggest a Rule of 12 ("duodectet rule"), governed by six d-block valence orbitals (one s plus five d), analogous to the four p-block counterparts (one s plus three p). Therefore, the idealized sd^{μ} hybrids for transition metal bonding (equivalent to sp^{λ} hybrids for main-group bonding) is proposed. NBO analysis exhibits duodectet-conforming Lewis-like bonding patterns for transition metal species throughout the d-block. According to the NBO procedure, the formation of a diatomic molecule leads to the key orbital transformation: NAO (natural atomic orbital) → NHO (natural hybrid orbital) → NBO. These NHOs present the key point in building NBOs and NLMOs (natural localized molecular orbitals) and will be evaluated in this paper. Within both molecules, there are three σRh-L 2c NBO pairs. These pairs enable bonding of Rh(III) with two nitrogens and one carboxylate oxygen. The rhodium bonds are highly polarized and according to the hybrid coefficients (*h*) of the Rh(III) ion, sd^2 hybridization may be deduced. This hybridization requires an M–L angle of 90°, which is satisfied in our case. It may be seen that BD Rh1-O5 orbital is stabilized by more than 80 kJ/mol, with respect to the other two BD Rh-N orbitals. These Rh(III)–L bonds are highly polarized with limited total orbital participation of Rh(III) (around 20 %). The polarity of the BD NBOs is best described by the "natural ionicity para-

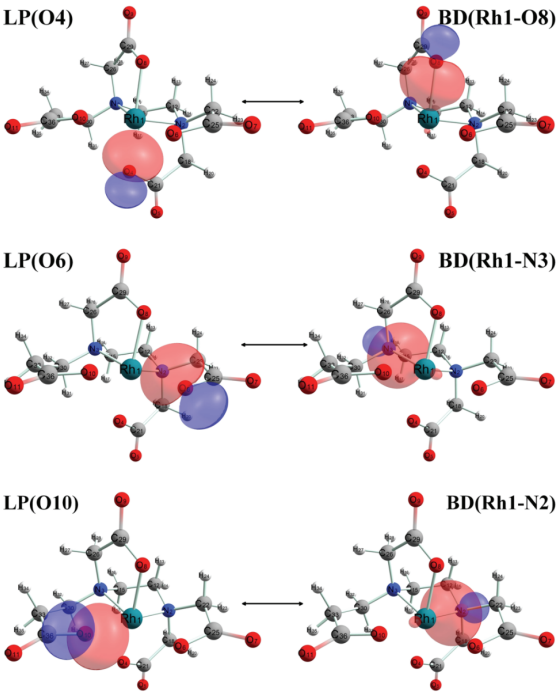

Fig. 5. 3-Center, 4-4lectron L:–Rh–:L' hyperbond orbitals.

meter, i_{AB}. One may ask about the other ligating atoms from ED3AP chelate. The answer that NBO offers might be dual. First, the NBO analysis does find three strong 3-center 4-electrons rhodium-ligand hypervalent bonds ("ω-bonding", Fig. 5 and Table III). As shown in Table III, each such 3c/4e L:–Rh–:L' ω-bond can be formulated in terms of distinct L + RhL' and LRh + L' resonance structures, each conforming to the 12e duodectet rule, but appearing in composite resonance-hybrid form as a 14e "hypervalent" species. However, the complex unit in whole corresponds to the 18e hypervalent center involving three 3c/4e ω bonds.

TABLE III. 3-Center, 4-Electron L:–Rh–:L' hyperbonds (L–Rh:L' <=> L:Rh–L')[a] of $[Rh(ED3AP)]^-$ isomers; threshold for detection: 33.3 %

Orb.	Hyperbond L : –Rh– : L'	L–Rh+:L', % / :L+Rh–L', %	OCC, electrons
		trans(O_5)	
1.	N 2 :–Rh 1– : O 10	56.1 / 43.9	3.9328
2.	N 3 : –Rh 1– : O 6	56.6 / 43.4	3.9390
3.	O 8 : –Rh 1– : O 4	50.3 / 49.7	3.9386
		trans(O_5O_6)	
1.	N 2 : –Rh 1– : O 10	58.4 / 41.6	3.9297
2.	N 3 : –Rh 1– : O 6	56.6 / 43.4	3.9258
3.	O 8 : –Rh 1– : O 4	52.6 / 47.4	3.9315

The donor–acceptor diagram depicts a universal quantum mechanical paradigm for energetically stabilizing the superposition of occupied and unoccupied localized orbitals in chemical interactions. As might be expected, the interaction of unperturbed donor $\varphi_i^{(0)}$ (valence LP) with acceptor $\varphi_{j*}^{(0)}$ (valence BD*) leads to the corresponding second-order i→j∗ of stabilization:

$$\Delta E^{(2)}_{i\rightarrow j*} = -2\langle\varphi_i^{(0)}|F|\varphi_{j*}^{(0)}\rangle^2/(\varepsilon_{j*}^{(0)} - \varepsilon_i^{(0)}) \quad (1)$$

For the *trans*(O_5O_6) isomer, this stabilization estimate, $\Delta E^{(2)}_{i\rightarrow i*}$, is 87 kJ/mol lower than for the *trans*(O_5) isomer. This result is in accordance with the calculated SP energies and is one of the reasons for the absence of the *trans*(O_5O_6) isomer in the reaction mixture.

CONCLUSION

We reported the investigation of two isomers (*trans*(O_5) and *trans*(O_5O_6)) of $[Rh(ED3AP)]^-$ complex. Only one of the possible two was synthesized and characterized. We determined the *trans*(O_5)-Na[Rh(ED3AP)]·3H_2O X-ray structure and characterized it by IR, and UV–Vis spectroscopy data of complex as well. We investigated the stability of two isomers by total energy and LFSE using different DFT levels of theory (B3LYP/TZV, BP86/TZV, OPBE/TZV). All DFT calculations are in agreement with each other. The total energy difference between *trans*(O_5) and *trans*(O_5O_6) isomer is beyond boundary energy we rep-

orted in our previous work[10]; therefore, the absence of *trans*(O_5O_6) isomer in the synthesis was expected. We used the same levels of theories for the LFDFT calculation of excited states. All three (B3LYP/TZV, BP86/TZV, OPBE/TZV) gave results in good agreement with the experimental ones (UV–Vis spectra). The best result was obtained with OPBE functional on the X-ray geometry (mean absolute error of only 670 cm^{-1}). By examining the splitting pattern of excited state energies, we determined an obvious difference in splitting the $^1T_{2g}$ term among isomers. In the case of the *trans*(O_5) isomer, the $^1E_g(^1T_{2g})$ term is lower in energy than the $^1B_{2g}$ term. For the *trans*(O_5O_6) isomer opposite is found. The NBO analysis suggests a strongly delocalized structure for both isomers. According to the NBO analysis, the *trans*(O_5) isomer is a more stable one for approx. 87 kJ/mol and the only present in the reaction mixture.

SUPPLEMENTARY MATERIAL

Additional data and information are available electronically at the pages of journal website: https://www.shd-pub.org.rs/index.php/JSCS/article/view/11533, or from the corresponding author on request.

Acknowledgement. This work is supported by the Ministry of Education, Science and Technological Development of Republic of Serbia (Agreement No. 451-03-9/2021-14/200122 and 451-03-9/2021-14/200026).

ИЗВОД

НОВИ РОДИЈУМ(III)–ED3AP КОМПЛЕКС: КРИСТАЛНА СТРУКТУРА, КАРАКТЕРИЗАЦИЈА И КОМПЈУТАЦИОНА ХЕМИЈА

МАРКО Д. РАДОВАНОВИЋ[1], МАРИЈА С. РИСТИЋ[1], МАТИЈА ЗЛАТАР[2], FRANK W. HEINEMANN[3] и ЗОРАН МАТОВИЋ[1]

[1]Универзитет у Крагујевцу, Природно–математички факултет, Институт за хемију, 34000 Крагујевац, [2]Универзитет у Београду, Институт за хемију, технологију и металургију, Његошева 12, 11000 Београд и [2]University Erlangen-Nürnberg (FAU), Department of Chemistry and Pharmacy, Inorganic Chemistry, Friedrich-Alexander, Egerlandstraße 1, 91058 Erlangen, Germany

Један (*trans*(O_5)-Na[Rh(ED3AP)]·3H_2O) од могућа два изомера синтетисан је и окарактерисан применом дифракције X-зрака на монокристалу, IR и UV–Vis спектроскопијом. Компјутерска анализа оба изомера обављена је помоћу три теоријска модела која су дала конзистентне резултате. Стабилнији изомер по укупној енергији и енергији стабилизације лигандног поља (LFSE) је *trans*(O_5) који је и изолован у синтези. Прорачун енергија ексцитованих стања дао је добру усаглашеност са UV–Vis спектром, посебно у случају прорачуна са OPBE функционалом. На основу резултата енергија ексцитованих стања уочене су разлике између изомера у начину цепања $^1T_{2g}$ терма. Оба изомера дају снажно делокализовану структуру судећи по NBO анализи. На основу NBO анализе, *trans*(O_5) изомер је стабилнији за 87 kJ/mol и једини је присутан у реакционој смеши.

(Примљено 30. децембра 2021, ревидирано 14. јануара, прихваћено 15. јануара 2022)

REFERENCES

1. C. Drouza, M. Vlasiou, A. D. Keramidas, *Dalt. Trans.* **42** (2013) 11831 (https://doi.org/10.1039/C3DT50619C)
2. E. Repo, J. K. Warchoł, A. Bhatnagar, M. Sillanpää, *J. Colloid Interface Sci.* **358** (2011) 261 (https://doi.org/10.1016/j.jcis.2011.02.059)
3. M. E. Markowitz, J. F. Rosen, *J. Pediatr.* **119** (1991) 305 (https://doi.org/10.1289/ehp.99107437)
4. K. Sakthithasan, P. Lévy, J. Poupon, R. Garnier, *Clin. Toxicol.* **56** (2018) 1143 (https://doi.org/10.1080/15563650.2018.1478424)
5. G. A. Lamas, O. M. Issa, *Curr. Cardiol. Rep.* **18** (2016) 20 (https://doi.org/10.1007/s11886-015-0690-9)
6. F. G. Kari, W. Giger, *Environ. Sci. Technol.* **29** (1995) 2814 (https://doi.org/10.1021/es00011a018)
7. H. Xue, L. Sigg, F. Günter Kari, *Environ. Sci. Technol.* **29** (1995) 59 (https://doi.org/10.1021/es00001a007)
8. J. Porath, J. Carlsson, I. Olsson, G. Belfrage, *Nature* **258** (1975) 598 (https://doi.org/10.1038/258598a0)
9. J. Carrasco-Castilla, A. J. Hernández-Álvarez, C. Jiménez-Martínez, C. Jacinto-Hernández, M. Alaiz, J. Girón-Calle, J. Vioque, G. Dávila-Ortiz, *Food Chem.* **135** (2012) 1789 (https://doi.org/10.1016/j.foodchem.2012.06.016)
10. M. S. Jeremić, M. D. Radovanović, F. W. Heinemann, M. M. Vasojević, Z. D. Matović, *Polyhedron* **169** (2019) 89 (https://doi.org/10.1016/j.poly.2019.04.053)
11. M. S. Jeremić, H. Wadepohl, V. V. Kojić, D. S. Jakimov, R. Jelić, S. Popović, Z. D. Matović, P. Comba, *RSC Adv.* **7** (2017) 5282 (https://doi.org/10.1039/C6RA26199J)
12. M. S. Jeremić, M. D. Radovanović, F. Bisceglie, V. V. Kojić, R. Jelić, Z. D. Matović, *Polyhedron* **156** (2018) 19 (https://doi.org/10.1016/j.poly.2018.08.075)
13. K. D. Gailey, D. J. Radanović, M. Djuran, B. E. Douglas, *J. Coord. Chem.* **8** (1978) 161 (https://doi.org/10.1080/00958977808073090)
14. D. J. Radanovic, K. D. Gailey, M. I. Djuran, B. E. Douglas, *J. Coord. Chem.* **10** (1980) 115 (https://doi.org/10.1080/00958978008079858)
15. D. J. Radanovic, V. D. Miletic, T. Ama, H. Kawaguchi, *Bull. Chem. Soc. Jpn.* **71** (1998) 1605 (https://doi.org/10.1246/bcsj.71.1605)
16. D. J. Radanović, N. Sakagami, V. M. Ristanović, S. Kaizaki, *Inorganica Chim. Acta* **292** (1999) 16 (https://doi.org/10.1016/S0020-1693(99)00164-4)
17. D. J. Radanovic, T. Ama, D. M. Gurešic, D. M. Ristanovic, D. D. Radanovic, H. Kawaguchi, *Bull. Chem. Soc. Jpn.* **73** (2000) 2283 (https://doi.org/10.1246/bcsj.73.2283)
18. V. D. Miletić, A. Meetsma, P. J. van Koningsbruggen, Z. D. Matović, *Inorg. Chem. Commun.* **12** (2009) 720 (https://doi.org/10.1016/j.inoche.2009.05.029)
19. R. Pettinari, F. Marchetti, C. Pettinari, F. Condello, A. Petrini, R. Scopelliti, T. Riedel, P. J. Dyson, *Dalt. Trans.* **44** (2015) 20523 (https://doi.org/10.1039/C5DT03037D)
20. F. Hackenberg, L. Oehninger, H. Alborzinia, S. Can, I. Kitanovic, Y. Geldmacher, M. Kokoschka, S. Wölfl, I. Ott, W. S. Sheldrick, *J. Inorg. Biochem.* **105** (2011) 991 (https://doi.org/10.1016/j.jinorgbio.2011.04.006)
21. S. Mukhopadhyay, R. K. Gupta, R. P. Paitandi, N. K. Rana, G. Sharma, B. Koch, L. K. Rana, M. S. Hundal, D. S. Pandey, *Organometallics* **34** (2015) 4491 (https://doi.org/10.1021/acs.organomet.5b00475)
22. S. Mollin, R. Riedel, K. Harms, E. Meggers, *J. Inorg. Biochem.* **148** (2015) 11 (https://doi.org/10.1016/j.jinorgbio.2015.01.005)

23. T.-S. Kang, W. Wang, H.-J. Zhong, J.-X. Liang, C.-N. Ko, J.-J. Lu, X.-P. Chen, D.-L. Ma, C.-H. Leung, *Biochim. Biophys. Acta - Gen. Subj.* **1861** (2017) 256 (https://doi.org/10.1016/j.bbagen.2016.11.032)
24. A. Lapasam, V. Banothu, U. Addepally, M. R. Kollipara, *J. Mol. Struct.* **1191** (2019) 314 (https://doi.org/10.1016/j.molstruc.2019.04.116)
25. A. Lapasam, L. Dkhar, N. Joshi, K. M. Poluri, M. R. Kollipara, *Inorg. Chim. Acta* **484** (2019) 255 (https://doi.org/10.1016/j.ica.2018.09.067)
26. L. Shadap, S. Diamai, V. Banothu, D. P. S. Negi, U. Adepally, W. Kaminsky, M. R. Kollipara, *J. Organomet. Chem.* **884** (2019) 44 (https://doi.org/10.1016/j.jorganchem.2019.01.019)
27. S. S. Hassan, *Appl. Organomet. Chem.* **32** (2018) e4170 (https://doi.org/10.1002/aoc.4170)
28. E. D. Glendening, C. R. Landis, F. Weinhold, *J. Comput. Chem.* **34** (2013) 2134 (https://doi.org/10.1002/jcc.23366)
29. M. Atanasov, C. A. Daul, C. Rauzy, *Chem. Phys. Lett.* **367** (2003) 737 (https://doi.org/10.1016/S0009-2614(02)01762-1)
30. *SADABS* v. 2.06, Bruker AXS, Inc., Madison, WI, 2002
31. G. M. Sheldrick, *Acta Cryst. A* **64** (2008) 112 (https://doi.org/10.1107/S0108767307043930)
32. G.M. Sheldrick, *Acta Cryst. C* **71** (2015) 3 (https://doi.org/10.1107/S2053229614024218)
33. O. V. Dolomanov, L. J. Bourhis, R. J. Gildea, J. A. K. Howard, H. Puschmann, *J. Appl. Crystallogr.* **42** (2009) 339 (https://doi.org/10.1107/S0021889808042726)
34. *Gaussian 16, Revision C.01*, Gaussian, Inc., Wallingford CT, 2016 (https://gaussian.com/relnotes)
35. P. J. Stephens, F. J. Devlin, C. F. Chabalowski, M. J. Frisch, *J. Phys. Chem.* **98** (1994) 11623 (https://doi.org/10.1021/j100096a001)
36. M. F. Peintinger, D. V. Oliveira, T. Bredow, *J. Comput. Chem.* **34** (2013) 451 (https://doi.org/10.1002/jcc.23153)
37. G. te Velde, F. M. Bickelhaupt, E. J. Baerends, C. Fonseca Guerra, S. J. A. van Gisbergen, J. G. Snijders, T. Ziegler, *J. Comput. Chem.* **22** (2001) 931 (https://doi.org/10.1002/jcc.1056)
38. J. P. Perdew, *Phys. Rev. B* **34** (1986) 7406 (https://doi.org/10.1103/PhysRevB.34.7406)
39. J. P. Perdew, K. Burke, M. Ernzerhof, *Phys. Rev. Lett.* **77** (1996) 3865 (https://doi.org/10.1103/PhysRevLett.77.3865)
40. D. Cremer, J. A. Pople, *J. Am. Chem. Soc.* **97** (1975) 1354 (https://doi.org/10.1021/ja00839a011).

Journal of the Serbian Chemical Society
JSCS@tmf.bg.ac.rs • www.shd.org.rs/JSCS
J. Serb. Chem. Soc. *87* (5) S117–S119 (2022) *Supplementary material*

SUPPLEMENTARY MATERIAL TO

New rhodium(III)–ED3AP complex: Crystal structure, characterization and computational chemistry

MARKO D. RADOVANOVIĆ[1], MARIJA S. RISTIĆ[1], MATIJA ZLATAR[2], FRANK W. HEINEMANN[3] and ZORAN D. MATOVIĆ[1]*

[1]*University of Kragujevac, Faculty of Science, Department of Chemistry, Radoja Domanovića 12, 34000 Kragujevac, Serbia,* [2]*University of Belgrade – Institute of Chemistry, Technology and Metallurgy, Njegoševa 12, 11000 Belgrade, Serbia and* [3]*University Erlangen-Nürnberg (FAU), Department of Chemistry and Pharmacy, Inorganic Chemistry, Friedrich-Alexander, Egerlandstraße 1, 91058 Erlangen, Germany*

J. Serb. Chem. Soc. *87* (5) (2022) 561–573

TABLE S-I. Crystal data and structure refinement for complex *trans*(O_5)-Na[Rh(ED3AP)]·3H_2O

Empirical formula	$C_{11}H_{20}N_2NaO_{11}Rh$
Formula weight	482.19
T / K	100(2)
Radiation	Mo-Kα (λ = 0.71073 Å)
Crystal system, space group	orthorhombic, $P2_12_12_1$
a, b, c / Å	8.7006(3), 11.2207(6), 16.8707(9)
α, β, γ / °	90, 90, 90
V / Å^3	1647.03(14)
Z	4
F(000)	976
$D_{calc.}$ / Mg m^{-3}	1.945
θ / °	6-20
μ / mm^{-1}	1.13
Crystal size, mm; color; shape	0.32×0.27×0.08; yellow; prism
Index ranges	h = −11→12, k = −15→14, l = −23→22
T_{min}, T_{max}	0.738, 0.910
No. of collected, independent and observed [$I > 2\sigma(I)$] reflections	26443, 4556, 4326
R_{int}	0.029
θ_{min}; θ_{max} / °	3.4; 29.6
Refinement method on F^2	Full-matrix least-squares on F^2
Reflections/restraints/parameters	4556/9/295
$R[F^2 > 2\sigma(F^2)]$, $wR(F^2)$, S	0.017, wR2 = 0.0363

* Corresponding author. E-mail: zmatovic@kg.ac.rs

TABLE S-I. Continued

Hydrogen site location	Difference Fourrier map. Only H-atom coordinates refined
Weighting scheme	$w = 1/[\sigma^2(F_o^2) + (0.0148P)^2 + 0.5898P]$, where $P = (F_o^2 + 2F_c^2)/3$
$\Delta\rho_{max}$; $\Delta\rho_{min}$ / e Å^{-3}	0.46; -0.49

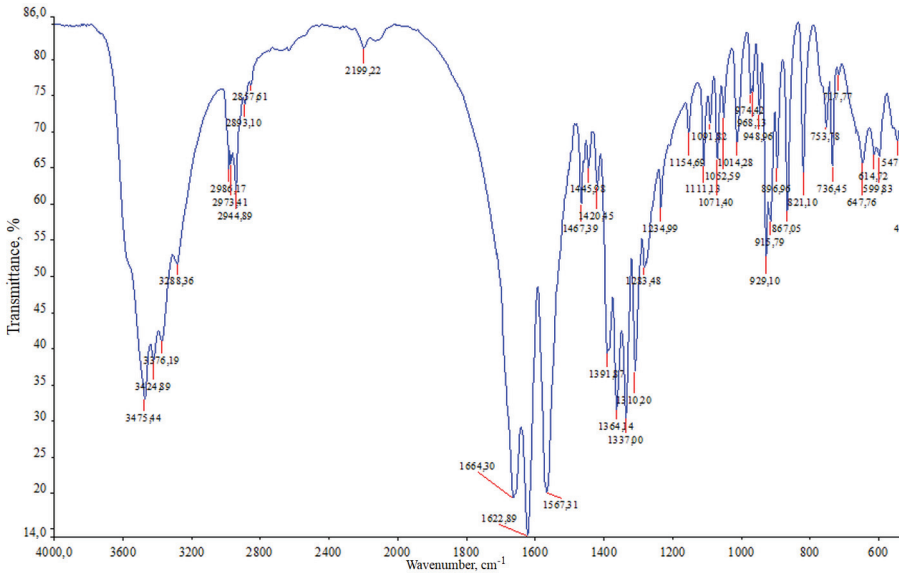

Fig. S-1. IR spectrum of *trans*(O_5)-Na[Rh(ED3AP)]·3H_2O complex

TABLE S-II. Selected bond distances and angles for *trans*(O_5)-Na[Rh(ED3AP)]·3H_2O

M-L bond lengths, Å			
Rh(1)-N(1)	2.011(2)	Rh(1)-O(3)	2.053(2)
Rh(1)-N(2)	2.023(2)	Rh(1)-O(5)	2.006(2)
Rh(1)-O(1)	1.999(2)	Rh(1)-O(7)	2.043(2)
Valence angles, °			
N(1)-Rh(1)-O(7)	175.12(7)	O(5)-Rh(1)-O(3)	90.21(7)
N(2)-Rh(1)-O(3)	167.88(7)	O(5)-Rh(1)-O(7)	89.53(7)
N(2)-Rh(1)-O(7)	93.83(7)	O(7)-Rh(1)-O(3)	97.03(7)
O(1)-Rh(1)-N(1)	85.59(7)	N(1)-Rh(1)-O(7)	175.12(7)
O(1)-Rh(1)-N(2)	96.43(7)	N(2)-Rh(1)-O(3)	167.88(7)
O(1)-Rh(1)-O(3)	88.97(7)	N(2)-Rh(1)-O(7)	93.83(7)
O(1)-Rh(1)-O(5)	178.99(7)	O(1)-Rh(1)-N(1)	85.59(7)
O(1)-Rh(1)-O(7)	89.99(7)	O(5)-Rh(1)-N(2)	84.49(7)
O(5)-Rh(1)-N(1)	94.86(7)	O(5)-Rh(1)-O(3)	90.21(7)
O(5)-Rh(1)-N(2)	84.49(7)		

TABLE S-III. Average bond distances of $[Rh(ED3AP)]^-$ isomers

$[Rh(ED3AP)]^-$	X-ray *trans*(O_5)	B3LYP optimized *trans*(O_5)	B3LYP optimized *trans*(O_5O_6)
average (Rh-N)	2.017	2.055	2.049
average (Rh-O)[a]	2.002	2.036	2.043
average (Rh-O)[b]	2.048	2.062	2.081

[a]average length of Rh-O axial oxygen
[b]average length of Rh-O equatorial oxygen

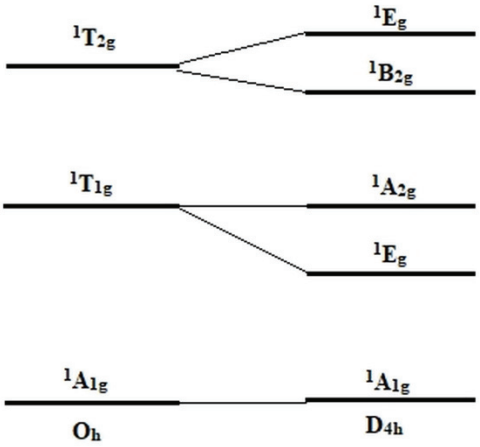

Scheme S-1. Therm splitting of d^6 complexes in Oh and D_{4h} symmetry.

Journal of the Serbian Chemical Society
JSCS@tmf.bg.ac.rs • www.shd.org.rs/JSCS

J. Serb. Chem. Soc. *87* (5) 575–587 (2022)
JSCS–5542

Original scientific paper
Published 23 March 2022

Theoretical calculation of newly synthesized tetrazolopyrimidine derivatives as a potential corrosion inhibitor

ERDEM ERGAN[1]*, NURULLAH SEKER[2], BEGUM CAGLA AKBAS[3] and ESVET AKBAS[2]

[1]*Department of Property Protection and Security, Van Security Vocational School, Van Yuzuncu Yil University, 65080, Van- Turkey,* [2]*Department of Chemistry, Faculty of Science, Van Yuzuncu Yil University, 65080 Van-Turkey and* [3]*Faculty of Pharmacy, University of Inonu, Malatya, Turkey*

(Received 19 April, revised 14 July, accepted 4 August 2021)

Abstract: In this work, we wanted to define a general and comprehensive strategy for the synthesis of tetrazolo[1,5-*a*]pyrimidine derivatives. For this purpose, we obtained new tetrazolo[1,5-*a*]pyrimidine molecules *via* the mercury-promoted desulfurization reaction, including hydrolysis, cyclizations, and eliminations. All of the molecules were characterized by FT-IR, ^{1}H-NMR, ^{13}C--NMR, and elemental analysis. On the other hand, the potentials of compounds as corrosion inhibitors were calculated at B3LYP/6-31G (d, p) level *via* density functional theory (DFT).

Keywords: desulfurization; DFT; characterization; quantum chemical studies; sodium azide.

INTRODUCTION

Corrosion is the deterioration of metal by reacting with chemicals or the environment. Corrosive solutions are used in many industrial applications. Acid solutions widely used in industry, especially in the cleaning process cause a significant mass loss on the surface.[1–3] Many methods are used to prevent corrosion. One of the methods of preventing corrosion is to use protective materials. Organic compounds are also one of the important materials used as protective materials.

The organic compounds containing π-bonds, phosphorus, sulfur, oxygen, and nitrogen as well as aromatic rings in their structure interacts with the metal surface and show high inhibition property.[4] The compounds containing both nitrogen and sulfur can provide excellent inhibition, compared with compounds containing only nitrogen or sulfur.[5] Generally, a strong interaction causes higher

* Corresponding author. E-mail: erdem_ergan@hotmail.com
https://doi.org/10.2298/JSC210419067G

inhibition efficiency, the inhibition increases in the sequence O < N < S.[6] It has been reported to increase the inhibition efficiency in general that compounds containing heteroatoms (S, N and O) with free electron pairs, delocalized π-electron aromatic rings, molecular weight, alkyl chains, and generally as a result of the existence of substituted groups. Compounds with π-bonds also generally exhibit good inhibitive properties due to the interaction of π-orbital with the metal surface.[7]

It is preferred that the compounds used for corrosion inhibiting purposes are not harmful to nature. For this reason, pyrimidine derivatives have attracted great attention due to their less environmentally damaging properties.[8] However; studies on pyrimidine are limited despite their ease of availability and corrosion inhibition properties.

Pyrimidine derivatives are among the important class of organic compounds. They exhibit broad biochemical effects due to the activity of nitrogen atoms in the ring and carbon atoms in the C2/C4/C6 position.[9] Due to these properties, pyrimidine derivative compounds are used as active ingredients in drugs such as uramustine, piritrexim, isethionate, tegafur, floxuridine, fluorouracil, cytarabine and methotrexate.[10] Pyrimidine derivatives are promising concerning corrosion inhibition.[11]

Experimental techniques like the weight-loss method, electrochemical impedance spectroscopy (*EIS*), potentiodynamic polarization, *etc.*, have been used to understand the corrosion process and its inhibition.[12,13] Although experiments mostly are time-consuming, costly, and lacking in explaining the mechanism of inhibition of the corrosion.[14,15] Thus, the quantum chemical calculation method was endorsed as a potent and easy tool to reduce the cost and time and can help in the interpretation of the experimental findings.[16,17]

Heakal *et al.*[18] used quantum chemical calculations to determine the structural and electronic properties of imidazole-pyrimidine-based new ionic compounds. They compared the theoretical inhibition yields of the compounds prepared in this way. Molecules chosen as inhibitors must be capable of donating electrons to the empty *d*-orbital of the metal and also be suitable for forming anti-feedback bonds. Pyrimidine compounds have these properties. Therefore, pyrimidine derivatives are expected to be excellent corrosion inhibitors at the industrial level.[19]

Quantum chemical calculations (QCCs) are widely used to find the corrosion inhibition reactivity of organic molecules. The effectiveness of an inhibitor can be related not only to its spatial molecular structure but also its molecular electronic structure. According to frontier orbital theory, the reaction of reactants mainly occurred on highest occupied molecular orbital (HOMO) and lowest unoccupied molecular orbital (LUMO), and the formation of a transition state is due to an interaction between the frontier orbitals of the reactants. So, it was imp-

ortant to investigate the distribution of HOMO and LUMO for the exploration of the inhibition mechanism.

The difference between E_{LUMO} and E_{HOMO} energies is called the energy gap (ΔE). It was generally acknowledged that low values of ΔE will provide good inhibition efficiency because the energy for removing an electron from the last occupied orbital will be low. For the theoretical calculation of the inhibitory effect of a molecule, it is necessary to know the ionization potential (I), the electron affinity (A), the chemical hardness-softness (S), the global electrophilicity index (ω), the interaction between the transmitted electron fraction index (ΔN), the interaction between back donations and non-linear optical (NLO) properties. All these values were calculated according to Shojaie *et al.* [20] using DFT-based QCCs in the Gaussian 09 software.[21]

EXPERIMENTAL

Chemicals and instruments

All chemicals and solvents used in the experiments were assured from Turkey representative of Sigma Aldrich and Fluka (Buchs, Switzerland). All reactions were monitored by thin-layer chromatography (TLC). TLC plates were based on silica gel 60 F254 aluminum plates with a 0.2 mm layer thickness (Merck Co., Darmstadt, Germany). The spots in TLC were determined by the UV lamp. Stuart (UK) SMP30 melting point apparatus was used to measure the melting points of the synthesized compounds. FT-IR spectra of compounds were measured in the range of 4000–400 cm^{-1} by using a Perkin Elmer Spectrum 100 FT-IR spectrometer (universal ATR sampling accessory). ^{1}H- and ^{13}C-nuclear magnetic resonance (NMR) spectra of compounds were measured in DMSO-d_6 by using a Bruker (Billerica, MA) AVANCDPX-400 MHz spectrometer at 400 and 100 MHz, respectively. Tetramethylsilane (TMS) was used as the internal reference. Elemental analyses were determined by using a Thermo Scientific (Pittsburgh, PA) Flash 2000 elemental analyzer. Full geometry optimizations of all molecules were performed using Gaussian09. The physical, analytical and spectral data for the compounds are given in the Supplementary material to this paper.

Synthesis

*(7-(4-(Methylthio)phenyl)-5-phenyl-4,7-dihydrotetrazolo[1,5-α]pyrimidin-6-yl)(phenyl) methanone (**6**)*. The mixture of (4-(4-(methylthio)phenyl)-6-phenyl-2-thioxo-1,2,3,4-tetrahydropyrimidin-5-yl)(phenyl)methanone (1 mmol),[22] sodium azide (2 mmol) and mercuric acetate (1 mmol) in acetic acid (5 mL) was stirred at 100 °C for 6 h. After completion of the reaction (monitored by thin-layer chromatography), the black sediment (HgS) was filtrated. Then water was added to the filtrate to give the crude product. It was recrystallized from ethyl alcohol.

*(7-(4-Hydroxyphenyl)-5-phenyl-4,7-dihydrotetrazolo[1,5-α]pyrimidin-6-yl)(phenyl) methanone (**7**)*. 0.386 g (4-(4-hydroxyphenyl)-6-phenyl-2-thioxo-1,2,3,4-tetrahydropyrimidin-5-yl)(phenyl) methanone (1 mmol),[23] sodium azide (2 mmol) and mercuric acetate (1 mmol) in acetic acid (5 mL) was stirred at 100 °C for 6 h. After completion of the reaction (monitored by thin-layer chromatography), the black sediment (HgS) was filtrated. Then water was added to the filtrate to give the crude product. It was recrystallized from methyl alcohol.

*(7-(4-Methoxyphenyl)-5-phenyl-4,7-dihydrotetrazolo[1,5-α]pyrimidin-6-yl)(phenyl) methanone (**8**)*.[24] 1 mmol (4-(4-methoxyphenyl)-6-phenyl-2-thioxo-1,2,3,4-tetrahydropyrimidin-5-

-yl)(phenyl)methanone,[25] sodium azide (2 mmol) and mercuric acetate (1 mmol) in acetic acid (5 mL) was stirred at 100 °C for 6 h. After completion of the reaction (monitored by thin-layer chromatography), the black sediment (HgS) was filtrated. Then water was added to the filtrate to give the crude product. It was recrystallized from isopropyl alcohol.

*(5,7-Diphenyl-4,7-dihydrotetrazolo[1,5-α]pyrimidin-6-yl)(phenyl)methanone (**9**)*.[24] 1 mmol (4,6-diphenyl-2-thioxo-1,2,3,4-tetrahydropyrimidin-5-yl)(phenyl)methanone,[26] sodium azide (2 mmol) and mercuric acetate (1 mmol) in acetic acid (5 mL) was stirred at 100 °C for 6 h. After completion of the reaction (monitored by thin-layer chromatography), the black sediment (HgS) was filtrated. Then water was added to the filtrate to give the crude product. It was recrystallization from butyl alcohol.

RESULTS AND DISCUSSION

Synthesis

Recently, structures change associated with mercury-promoted desulfurization reactions, including hydrolysis, cyclizations, and eliminations, have been reported.[27,28] Because of the strong thiophilic affinity of Hg^{2+}, mercuric acetate was used in the design of formation for HgS. We devised a strategy in which the azido group would be formed by desulfurization of 3,4-dihydropyrimidine-2-thiones using Hg^{2+}. The addition of the Hg^{2+} ion-induced the N_3^- to attack the 2-C atom of pyrimidine, followed by the removal of HgS and the formation of intramolecular guanylation. Finally, a stable cyclic product tetrazolo[1,5-α]pyrimidines were formed through an irreversible desulfurization reaction, as depicted in Scheme 1.

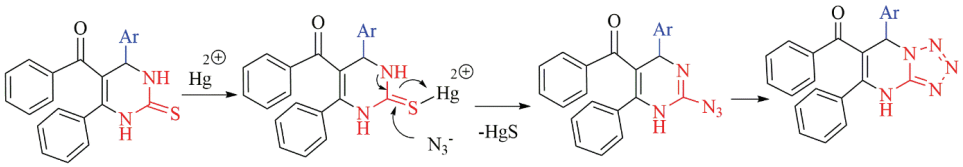

Scheme 1. Formation of tetrazolo[1,5-α]pyrimidines through an irreversible desulfurization reaction.

In this paper, we aimed to define a general and comprehensive strategy for the synthesis of tetrazolo[1,5-*a*]pyrimidine derivatives (Scheme 2).

We chose the reaction of compound **1** and sodium azide as a model reaction to optimize the reaction conditions. A series of experiments were performed to evaluate the feasibility of the formation of tetrazolo[1,5-α]pyrimidines. The results are shown in Table I. It can be said that compound **1**/NaN_3/mercuric(II) acetate (1:2:1) at 100 °C in acetic acid is the best result.

Analysis results of all synthesized compounds support the expected structure. Details of the analysis results are given in the Supplementary material. In addition to the structural analysis of the obtained compounds, the electronic properties were also calculated using computer calculation methods.

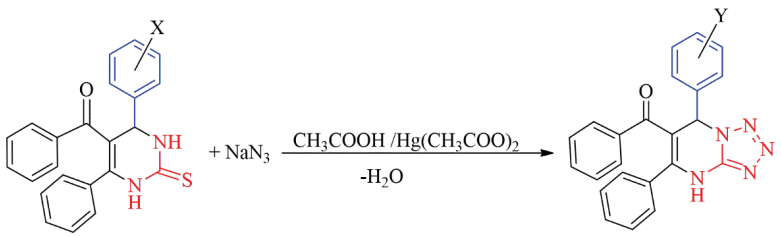

	X
1	4-SCH_3
2	4-OH
3	4-OCH_3
4	4-H

	Y
6	4-SCH_3
7	4-OH
8	4-OCH_3
9	4-H

Scheme 2. Desulfurization reaction for pyrimidine compounds.

TABLE I. Optimization of reaction conditions for compound **6**

Compound **1**:NaN_3:desulfurization reagent mole ratio	Solvent	Desulfurization reagent	T / °C	t / h	Yield, %
1:2:1	Acetic acid	Mercuric(II) acetate	25	10	–
1:2:1	Acetic acid	Mercuric(II) acetate	75	7	65
1:2:1	Acetic acid	Mercuric(II) acetate	100	6	85
1:2:1	Acetic acid	Mercuric(II) acetate	110	6	85
1:2:1	Methanol	Mercuric(II) acetate	65	6	60
2:4:1	Acetic acid	Mercuric(II) acetate	100	6	85
1:2:1	Acetic acid	Mercury(II) chloride	100	6	75
1:2:1	Acetic acid	Mercury(II) chloride	25	12	–

Computational analysis

Geometry optimizations of molecules were studied using Gaussian09. Calculations made DFT based on B3LYP and the 6-31G (d, p) orbital basis sets (Fig. 2).[21,29–31]

Quantum chemical parameters of synthesized compounds such as μ, I, A, χ, η, w, S, ΔN and $\Delta E_{\text{back donation}}$ were calculated according to Karzazi *et al.*[32] (Table II) using the Gaussian09 program. With this method, it is possible to predict the corrosion preventive effects of organic molecules.

The adsorption of the molecule to the metal surface causes the inhibitory effect. When the attachment occurs chemically, the ligand acts as an electron donor, and the metal acts as an electron acceptor (Fig. 3).

The inhibition effect of the molecule is related to the ground state geometry of the HOMO and LUMO structures (Fig. 4). The high HOMO region in the molecule acts as the favorite adsorption area due to its electron density.

Excellent corrosion inhibitors represented by organic compounds behaving, at the same time, on the one hand as electron donors to unoccupied d orbital of the metal surface to form coordinate covalent bonds, and on the other hand as the

acceptor of free electrons from the metal surface by using their antibonding orbitals to form feedback bonds. The LUMO energy level of molecules is the molecule's ability to accept electrons. When the LUMO energy level of the inhibitor molecule is lower, it is capable of accepting more electrons. The skill of the inhibitor to bind to the metal surface increases with increasing HOMO energy value and decreases LUMO energy value. Therefore, inhibitors with a lower E_{LUMO} value are more likely to be accepted onto the metal surface.

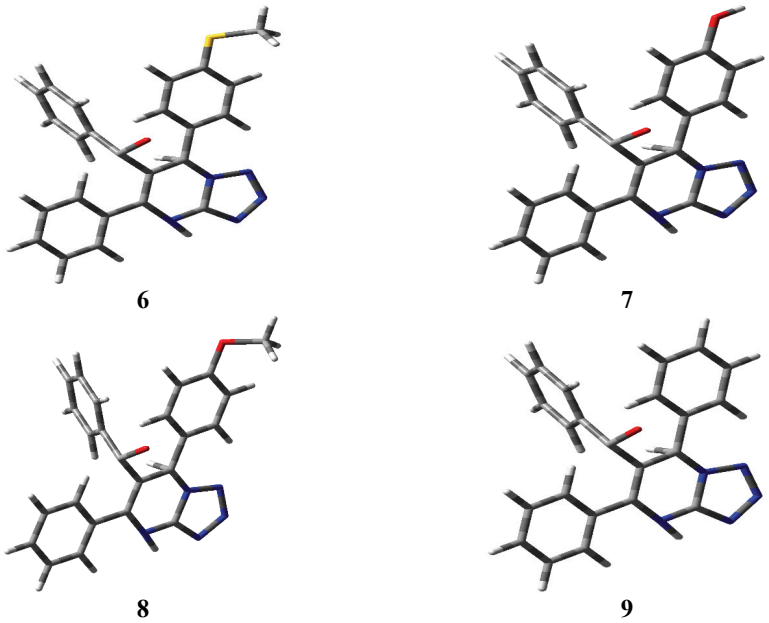

Fig. 2. Optimizations of all compounds.

TABLE II. The quantum chemical parameters for all compounds

Parameter	**6**	**7**	**8**	**9**
E_{HOMO} / eV	–4.9564	–5.5164	–5.5183	–6.1793
E_{LUMO} / eV	–3.4349	–3.4445	–3.4450	–1.9146
ΔE / eV	1.5214	2.0719	2.0733	4.2646
Ionization potential, eV	4.9564	5.5164	5.5183	6.1793
Electron affinity, eV	3.4349	3.4445	3.4450	1.9146
Chemical hardness, eV	0.7607	1.0359	1.0366	4.2647
Chemical softness, eV^{-1}	1.3146	0.9653	0.9646	0.2345
Electronegativity, eV	4.1956	4.4805	4.4815	4.0469
Transferred electrons fraction	1.8433	1.2161	1.2148	0.3463
Electrophilicity index	16.6809	12.9347	12.7732	52.437
Dipole moment, D[a]	5.0377	5.1767	5.1460	5.2688
$\Delta E_{back\ donation}$ / eV^{-1}	–0.1902	–0.2589	–0.2591	–1.0662

[a]1 D = 3.335×10^{30} C m

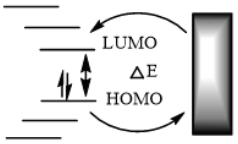

Fig. 3. Interaction of organic molecules with the metal surface.

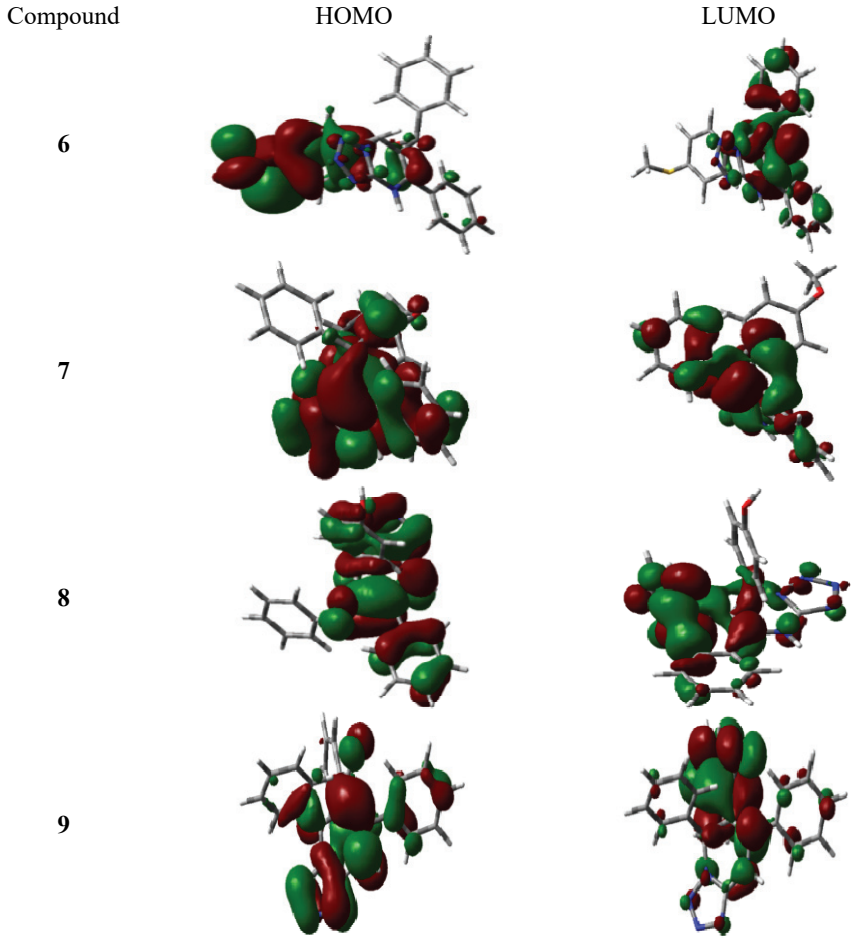

Fig. 4. HOMO and LUMO molecular orbitals.

The energy gap (ΔE) value indicates the difference between HOMO and LUMO energy levels. This value is an important parameter that shows the reactivity of the inhibitor molecule against adsorption on the metal surface. Low values of ΔE have been shown in previous studies to provide good inhibition.[33] A molecule with a low ΔE becomes more polarized and is generally associated with high chemical activity and low kinetic stability. These structures are called soft molecules.[34] In this study, ΔE values are listed as 9 > 8 > 7 > 6. As a result,

it can be said that molecule 6 can show good corrosion inhibitor performance (Table II).

The dipole moment (μ) of the molecule is an important parameter in determining the inhibition property. The increase in the dipole moment value increases the adsorption resolution.[35]

Chemical hardness (η) and softness (S) are other important properties used to measure the stability and reactivity of a molecule.[36,37] Molecule **6** with values of η = 0.7607 eV and softness S = 1.3146 eV will show the highest inhibition effect.

The fraction of electrons transferred (ΔN) values were also calculated (Table II). If $\Delta N < 3.6$, inhibition efficiency increases.[38–40] The global electrophilicity index (ω) and the $\Delta E_{\text{back donation}}$ values for the compounds demonstrate that compound **6** exhibit a good inhibitory effect (Table II).

Molecular electrostatic potentials (MEPs)

MEP provides information on reactive sites for electrophilic and nucleophilic attack and hydrogen bond interactions for compounds. MEPs were obtained at B3LYP/6-31+G (d,p) level for all compounds and are given in Fig. 5. The negative (red) regions of the MEP indicate electrophilic reactivity and the positive (blue) regions show nucleophilic reactivity.

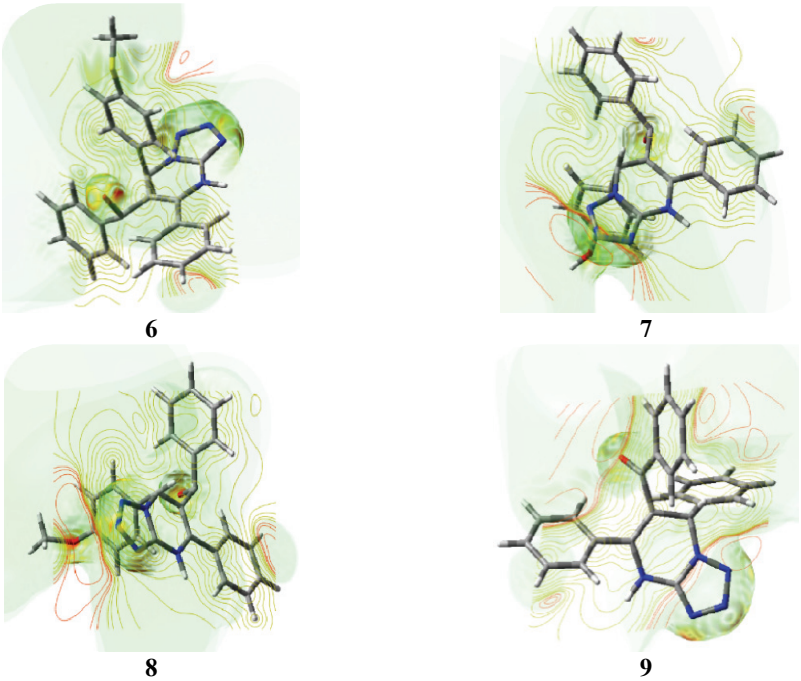

Fig. 5. MEPs of all molecules.

Non-linear optical (NLO) properties

NLO properties of compounds **6**–**9** were computed *via* the B3LYP/6-31+G (d,p) in the gas phase. Using the equations given below, the total dipole moment (μ_{tot}) by Eq. (1), mean polarizability (α_{tot}) by Eq. (2), and the average value of the first hyperpolarizability (β_{tot}) by Eq. (3) can be computed:

$$\mu_{tot} = \mu_x^2 + \mu_y^2 + \mu_z^2 \quad (1)$$

$$\alpha_{tot} = (\alpha_{xx} + \alpha_{yy} + \alpha_{zz})/3 \quad (2)$$

$$\beta_{tot} = [(\beta_{xxx} + \beta_{xyy} + \beta_{xzz})^2 + (\beta_{yyy} + \beta_{yxx} + \beta_{yzz})^2 + (\beta_{zzz} + \beta_{zxx} + \beta_{zyy})^2]^{0.5} \quad (3)$$

Calculated data and other components for the NLO are given in Table III.

TABLE III. Electric dipole moment μ, polarizability α_{tot} (10^{-33} esu*), and first hyperpolarizability β_{tot} (10^{-33} esu) for molecules **6**–**9** obtained by B3LYP level with the 6-31+g (d,p) basis set

Parameter	6	7	8	9
μ_x / D	1.7712	1.3178	1.8906	–0.4527
μ_y / D	0.1009	1.5123	0.3440	–1.3742
μ_z / D	–0.8864	–0.2771	–0.6759	–0.1959
μ_{tot}	17.1262	17.4944	17.5985	12.6132
α_{xx}	–64.7042	–57.1117	–63.0773	10.0268
α_{yy}	–61.7315	–60.0122	–59.3779	–12.1679
α_{zz}	–85.6467	–76.2526	–81.4938	2.1409
α_{tot}	–610.748	–556.879	–587.326	–0.0017
β_{xxx}	–24.2020	15.3040	–19.8924	–8.1824
β_{xyy}	21.5054	–9.2419	15.2620	–18.8274
β_{xzz}	28.5848	9.5182	28.2566	12.3043
β_{yyy}	8.9387	16.3674	12.4547	–55.1931
β_{yxx}	–2.7867	–4.2552	–8.6951	–6.3579
β_{yzz}	1.9177	22.7144	8.5003	–4.4225
β_{zzz}	–41.4856	–11.0272	–31.7697	1.0436
β_{zxx}	–7.3189	–28.6762	–29.1246	7.3687
β_{zyy}	–1.2435	–13.0927	0.2463	4.2575
β_{tot}	491.7667	562.7537	572.1984	594.120

Based on these data, it can be said that compounds with high dipole moment, high molecular polarizability, and high hyperpolarizability values will be more active. Based on the calculation results, it is seen that compounds **8** and **9**, which have the highest hyperpolarizability, will show more active NLO properties compared to other compounds.

In addition to these calculations, the intermolecular bond lengths, bond angles, and dihedrals of compound **6** were also calculated to serve as an example (Fig. 6 and Table IV).

* 1 esu = 3.336×10^{-10} C

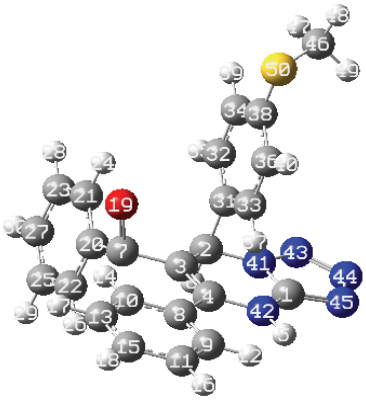

Fig. 6. The atom numbering for molecule **6**.

TABLE IV. Computed data are of selected bond lengths, angles, and dihedral angles for compound **6**

Bond	Bond length, Å	Bond angle, º	Dihedral angle, °
C(4)(3,2,1)	1.3899631	121.1386464	0.0026262
C(7)(3,2,1)	1.5400001	119.1112575	–179.998045
O(19)(7,3,2)	1.4300001	109.4712206	–90.0048931
H(5)(1,4,3)	2.1650737	56.7832079	179.994403
N(41)(2,1,4)	1.3803306	30.5550539	179.9931916
N(42)(1,41,2)	1.3802752	120.4036192	–0.0121285
N(43)(41,2,1)	1.4575035	132.5559472	179.9923687
N(44)(43,41,2)	1.4076826	108.1755697	–179.9890161
N(45)(44,43,41)	1.4071737	109.5727945	–0.0030415
C(46) (38,36,33)	2.3355950	131.6261913	–138.3953821
S(50)(46,38,36)	1.4300001	35.2500004	–84.4007167

CONCLUSION

The new tetrazolo[1,5-*α*]pyrimidine compounds were obtained by reaction of pyrimidine compounds with sodium azide. The structures of all molecules were determined by spectroscopic methods such as FT-IR, ^{1}H/^{13}C-NMR, and elemental analysis. The theoretical corrosion inhibition potentials of the compounds were investigated at the B3LYP/6-31G (d,p) level using density functional theory (DFT). In addition, molecular electrostatic potential maps and nonlinear optical (NLO) properties of the compounds were calculated theoretically. According to calculations, compound **6** is considered to be used as a good potential inhibitor for corrosion.

SUPPLEMENTARY MATERIAL

Additional data and information are available electronically at the pages of journal website: https://www.shd-pub.org.rs/index.php/JSCS/article/view/10683, or from the corresponding author on request.

Acknowledgement. This work was supported by the VanYYU, Project No: FYL-2018--7181.

ИЗВОД

ТЕОРИЈСКА ИЗРАЧУНАВАЊА НОВОСИНТЕТИСАНИХ ДЕРИВАТА ТЕТРАЗОЛОПИРИМИДИНА КАО ПОТЕНЦИЈАЛНИХ ИНХИБИТОРА КОРОЗИЈЕ

ERDEM ERGAN[1], NURULLAH SEKER[2], BEGUM CAGLA AKBAS[3] и ESVET AKBAS[2]

[1]*Department of Property Protection and Security, Van Security Vocational School, Van Yuzuncu Yil University, 65080, Van- Turkey,* [2]*Department of Chemistry, Faculty of Science, Van Yuzuncu Yil University, 65080 Van-Turkey и* [3]*Faculty of Pharmacy, University of Inonu, Malatya, Turkey*

У овом раду дефинисана је општа и свеобухватна стратегија за синтезу тетразоло[1,5-α]пиримидинских деривата. Добијени су нови тетразоло[1,5-α]пиримидински молекули у реакцији десулфуризације потпомогнуте живом, укључујући хидролизу, циклизацију и елиминацију. Сви молекули су окарактерисани са FT-IR, ^{1}H-NMR, ^{13}C--NMR и елементалном анализом. Са друге стране, потенцијали једињења као инхибитора корозије су израчунати на B3LYP/6-31G (d,p) нивоу теоријом функционала густине (DFT).

(Примљено 19. априла, ревидирано 14. јула, прихваћено 4. августа 2021)

REFERENCES

1. M. Lagrene, B. Mernari, M. Bouanis, M. Traisnel, F. Bentiss, *Corrosion Sci.* **44** (2002) 573 (https://doi.org/10.1016/S0010-938X(01)00075-0)
2. A. Yurt, S. Ulutas, H. Dal, *Appl. Surf. Sci.* **253** (2006) 919 (https://doi.org/10.1016/j.apsusc.2006.01.026)
3. S. Şafak, B. Duran, A. Yurt, G. Türkoğlu, *Corros. Sci.* **54** (2012) 25 (https://doi.org/10.1016/j.corsci.2011.09.026)
4. S. Shahabi, P. Norouzi, M. R. Ganjali, *Int. J. Electrochem Sci.* **10** (2015) 2646 (https://citeseerx.ist.psu.edu/viewdoc/download?doi=10.1.1.668.6592&rep=rep1&type=pdf)
5. J. Aljourani, M. A. Golozar, K. Raeissi, *Mater. Chem. Phys.* **121** (2010) 320 (https://doi.org/10.1016/j.matchemphys.2010.01.040)
6. A. Chetouani, A. Aouniti, B. Hammouti, N. Benchat, T. Benhadda, S. Kertit, *Corros. Sci.* **45** (2003) 1675 (https://doi.org/10.1016/S0010-938X(03)00018-0)
7. R. T. Loto, C. A. Loto, A P. I. Popoola, M. Ranyaoa, *Int. J. Phys. Sci.* **7** (2012) 2697 (https://www.researchgate.net/publication/313580988_Pyrimidine_derivatives_as_environmentally-friendly_corrosion_inhibitors_A_review)
8. K. Rasheeda, V. D. P. Alva, P. A. Krishnaprasad, S. Samshuddin, *Int. J. Corros. Scale Inhib*. **7** (2018) 48 (http://ijcsi.pro/papers/pyrimidine-derivatives-as-potential-corrosion-inhibitors-for-steel-in-acid-medium-an-overview/)
9. H. Dansena, H. J. Dhongade, K. Chandrakar, *Asian J. Pharm. Clin. Res*. **8** (2015) 171 (https://webcache.googleusercontent.com/search?q=cache:luNzlxY0zn8J:https://innovareacademics.in/journals/index.php/ajpcr/article/download/6283/2710+&cd=2&hl=tr&ct=clnk&gl=tr)
10. T. P. Selvam, C. R. James, P. V. Dniandev, S. K. Valzita, *Research in Pharm*. **2** (2012) 01 (https://updatepublishing.com/journal/index.php/rip/article/view/271)
11. M. Abdallah, E. A. Helal, A. S. Fouda, *Corros. Sci.* **48** (2006) 1639 (https://doi.org/10.1016/j.corsci.2005.06.020)

12. D-Q. Zhang, Q-R. Cai, X-M. He, L-X. Gao, G-D. Zhou, *Mater. Chem. Phys.* **112** (2008) 353 (https://doi.org/10.1016/j.matchemphys.2008.05.060)
13. M. A. Amin, M. M. Ibrahim, *Corros. Sci.* **53** (2011) 873 (https://doi.org/10.1016/j.corsci.2010.10.022)
14. N. A. Wazzan, I. Obot, S. Kaya, *J. Mol. Liq.* **221** (2016) 579 (https://doi.org/10.1016/j.molliq.2016.06.011)
15. B. Usman, I. Jimoh, B. A. Umar, *Appl. J. Environ. Eng. Sci.* **5** (2019) 66 (https://www.researchgate.net/publication/332195552_Theoretical_study_of_2_-3_4-dihydroxyphenyl_chroman-3_5_7-triol_on_corrosion_inhibition_of_mild_steel_in_acidic_medium)
16. Y. Atalay, F. Yakuphanoglu, M. Sekerci, D. Avcı, A. Başoğlu, *Spectrochim. Acta, A* **64** (2006) 68 (https://doi.org/10.1016/j.saa.2005.06.038)
17. E. E. Ebenso, T. Arslan, F. Kandemirli, N. Caner, I. Love, *Int. J. Quantum Chem*. **110** (2010) 1003 (https://doi.org/10.1002/qua.22249)
18. F. E. T. Heakal, S. A. Rizk, A. E. Elkholy, *J. Mol. Struct.* **1152** (2018) 328 (https://doi.org/10.1016/j.molstruc.2017.09.079)
19. E. Akbas, E. Yildiz, A. Erdogan, *J. Serbian Chem. Soc.* **85** (2020) 481 (https://doi.org/10.2298/JSC190326081A)
20. F. Shojaie, N. M. Baghini, *Int. J. Ind. Chem.* **6** (2015) 297 (https://doi.org/10.1007/s40090-015-0052-x)
21. *Gaussian 09, Revision E.01,* Gaussian, Inc., Wallingford, CT, 2009 (http://gaussian.com/g09citation/)
22. E. Akbas, E. Ergan, E. Sahin, S. Ekin, M. Cakir, Y. Karakus, *Phosphorus Sulfur Silicon Relat. Elem.* **194** (2019) 796 (https://doi.org/10.1080/10426507.2018.1550489)
23. E. Akbas, A. Levent, S. Gumus, M. R. Sumer, I. Akyazi, *Bull. Korean Chem. Soc.* **31** (2010) 3632 (https://doi.org/10.5012/bkcs.2010.31.12.3632)
24. E. Akbas, S. Celik, E. Ergan, A. Levent, *J. Chem. Sci.* **131** (2019) 30 (https://doi.org/10.1007/s12039-019-1602-0)
25. E. Ergan, E. Akbas, A. Levent, E. Sahin, M. Konus, N. Seferoglu, *J. Mol. Struct.* **1136** (2017) 231 (https://doi.org/10.1016/j.molstruc.2017.02.001)
26. F. Aslanoglu, E. Akbas, M. Sonmez, B. Anil, *Phosphorus Sulfur Silicon Relat. Elem.* **182** (2007) 1589 (https://doi.org/10.1080/10426500701263554)
27. Y. K. Yang, K. J. Yook, J. Tae, *J. Am. Chem. Soc.* **127** (2005) 16760 (https://doi.org/10.1021/ja054855t)
28. K. C. Song, J. S. Kim, S. M. Park, K. C. Chung, S. Ahn, S. K. Chang, *Org. Lett.* **8** (2006) 3413 (https://doi.org/10.1021/ol060788b)
29. A. D. Becke, *J. Chem. Phys.* **96** (1992) 2155 (https://doi.org/10.1063/1.462066)
30. A. D. Becke, *J. Chem. Phys.* **98** (1993) 1372 (https://doi.org/10.1063/1.464913)
31. C. Lee, W. Yang, R. G. Parr, *Phys. Rev., B* **37** (1988) 785 (https://doi.org/10.1103/PhysRevB.37.785)
32. Y. Karzazi, M. E. A. Belghiti, A. Dafali, B. Hammouti, *J. Chem. and Pharm. Res*. **6** (2014) 689 (https://www.jocpr.com/abstract/a-theoretical-investigation-on-the-corrosion-inhibition-of-mild-steel-by-piperidine-derivatives-in-hydrochloric-acid-sol-2763.html)
33. H. Zarrok, A. Zarrouk, R. Salghi, H. Oudda, B. Hammouti, M. Assouag, M. Taleb, M. Ebn Touhami, M. Bouachrine, S. Boukhris, *J. Chem. Pharm. Res.* **4** (2012) 5056 (https://www.jocpr.com/articles/gravimetric-and-quantum-chemical-studies-of-14acetyl24chlorophenylquinoxalin14hylacetone-as-corrosion-inhibitor-for-carb.pdf)

34. T. T. Adejumo, N. V. Tzouras, L. P. Zorba, D. Radanovic, A. Pevec, S. Grubišic, D. Mitic, K. K. Andelkovic, G. C. Vougiokalakis, B. Cobeljic, I. Turel, *Molecules* **25** (2020) 4043 (https://doi.org/10.3390/molecules25184043)
35. X. Li, S. Deng, H. Fu, T. Li, *Electrochim. Acta* 54 (2009) 4089 (https://doi.org/10.1016/j.electacta.2009.02.084)
36. N. Caliskan, E. Akbas, *Mater. Corros.* **63** (2012) 231 (https://doi.org/10.1002/maco.201005788)
37. N. Caliskan, E. Akbas, *Mater. Chem. Phys.* **126** (2011) 983 (https://doi.org/10.1016/j.matchemphys.2010.11.051)
38. R. Hasanov, M. Sadikoglu, S. Bilgic, *Appl. Surf. Sci.* **253** (2007) 3913 (https://doi.org/10.1016/j.apsusc.2006.08.025)
39. F. Bentiss, M. Lagrenée, *J. Mater. Environ. Sci.* **2** (2011) 13 (https://www.jmaterenvironsci.com/Document/vol2/3-JMES-62-2011-Bentiss2.pdf)
40. P. Udhayakala, T. V. Rajendiran, S. Gunasekaran, *J. Advanced Sci. Res.* **3** (2012) 71 (http://eds.b.ebscohost.com/eds/pdfviewer/pdfviewer?vid=1&sid=85d1e953-13bc-4e39-94f0-6c41acdeacb8%40sessionmgr102).

Journal of the Serbian Chemical Society
JSCS@tmf.bg.ac.rs • www.shd.org.rs/JSCS
J. Serb. Chem. Soc. 87 (5) S120–S126 (2022) *Supplementary material*

SUPPLEMENTARY MATERIAL TO

Theoretical calculation of newly synthesized tetrazolopyrimidine derivatives as a potential corrosion inhibitor

ERDEM ERGAN[1]*, NURULLAH SEKER[2], BEGUM CAGLA AKBAS[3] and ESVET AKBAS[2]

[1]*Department of Property Protection and Security, Van Security Vocational School, Van Yuzuncu Yil University, 65080, Van- Turkey,* [2]*Department of Chemistry, Faculty of Science, Van Yuzuncu Yil University, 65080 Van-Turkey and* [3]*Faculty of Pharmacy, University of Inonu, Malatya, Turkey*

J. Serb. Chem. Soc. 87 (5) (2022) 575–587

*The spectral data of (7-(4-(methylthio)phenyl)-5-phenyl-4,7-dihydrotetrazolo-[1,5-α]pyrimidin-6-yl)(phenyl) methanone (**6**)*

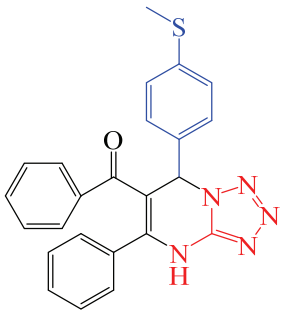

M.p.: 260-262ºC; IR (KBr, υ, cm^{-1}) 3218, 3084, 2960, 1692, 1623, 1582, 1549; ^{1}H NMR (300 MHz, DMSO-*d*6): δ (ppm) 11.32 (s, 1H, NH), 7.41-6.99 (m, 14H, $H_{arom.}$), 6.88 (s, 1H, CH), 2.40 (s, 3H, SCH_3). ^{13}C-NMR (DMSO-d_6): 194.73 (benzoyl), 149.66, 139.32, 139.27, 136.86, 133.85, 131.69, 130.46, 130.18, 129.06, 128.64, 128.42, 127.95, 126.20, 107.69, 60.54, 14.73.

* Corresponding author. E-mail: erdem_ergan@hotmail.com

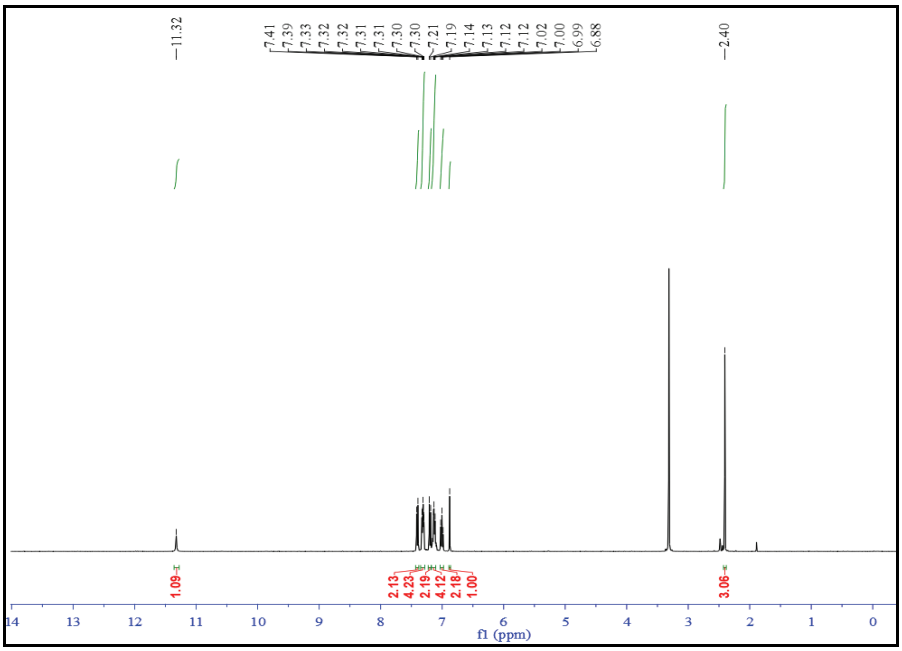

Fig. S-1. ^{1}H-NMR spectra of the compound **6**.

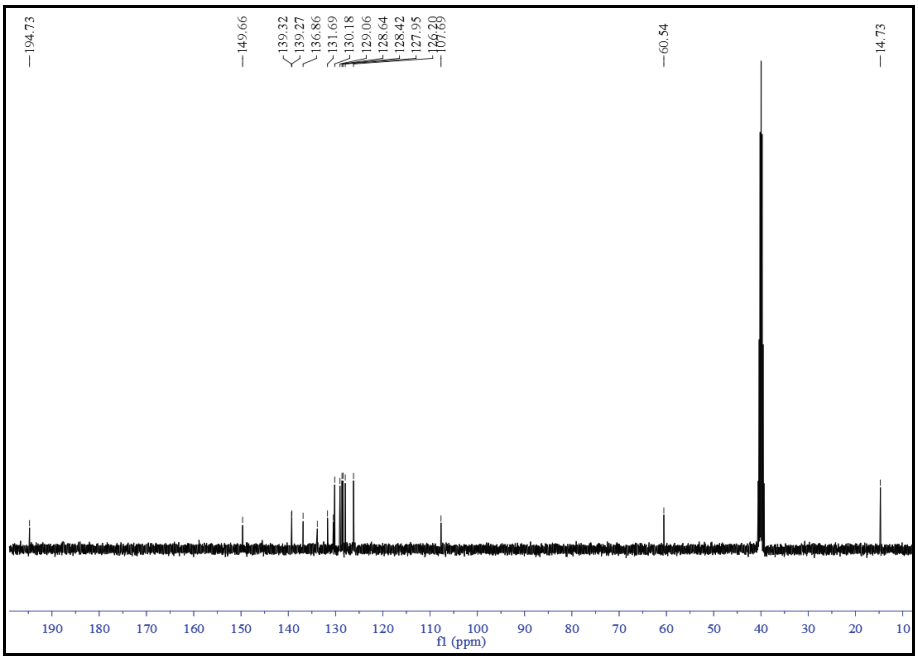

Fig. S-2. ^{13}C-NMR spectra of the compound **6**.

*The spectral data of (7-(4-hydroxyphenyl)-5-phenyl-4,7-dihydrotetrazolo[1,5-α]-pyrimidin-6-yl)(phenyl) methanone (**7**)*

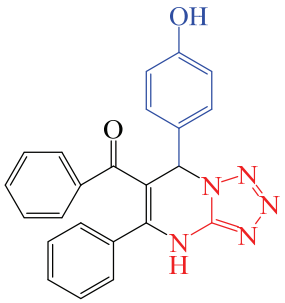

M.p.: 252-253ºC; IR (KBr, υ, cm^{-1}) 3082, 2963, 1690, 1622, 1584, 1541; ^{1}H NMR (300 MHz, DMSO-*d*6): δ (ppm) 11.23 (s, 1H, OH), 9.55 (s, 1H, NH), 7.33-6.99 (m, 12H, $H_{arom.}$) 6.80 (s, 1H, CH), 6.69-6.66 (m, 2H, $H_{arom.}$). ^{13}C-NMR (DMSO-d_6): 194.90 (benzoyl), 157.98, 149.62, 144.47, 139.16, 133.86, 131.75, 130.84, 130.07, 129.34, 129.05, 128.42, 127.96, 123.72, 115.79, 108.29, 60.58.

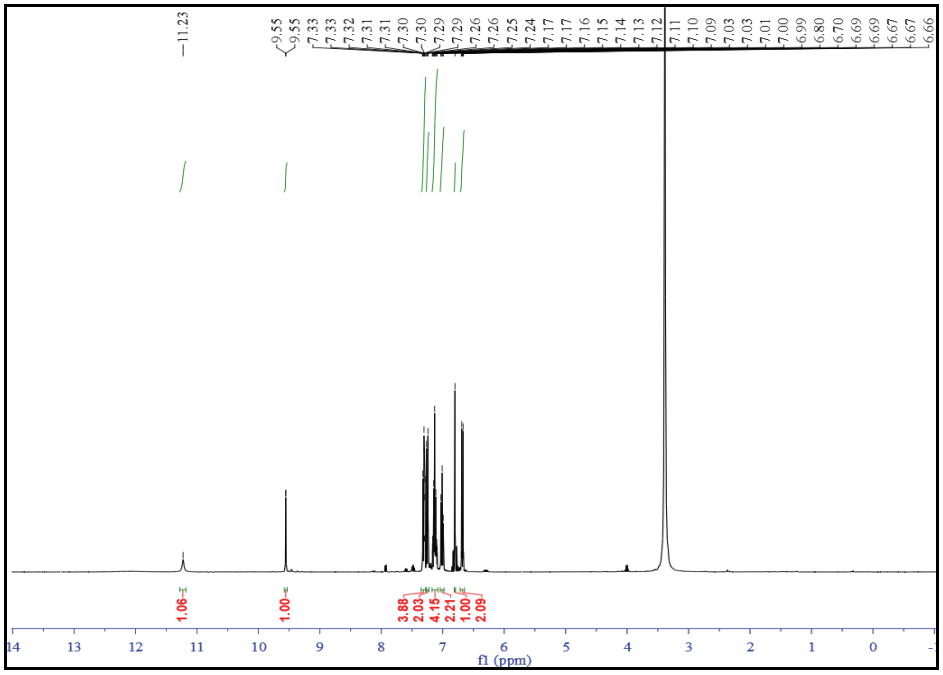

Fig. S-3. ^{1}H-NMR spectra of the compound **7**.

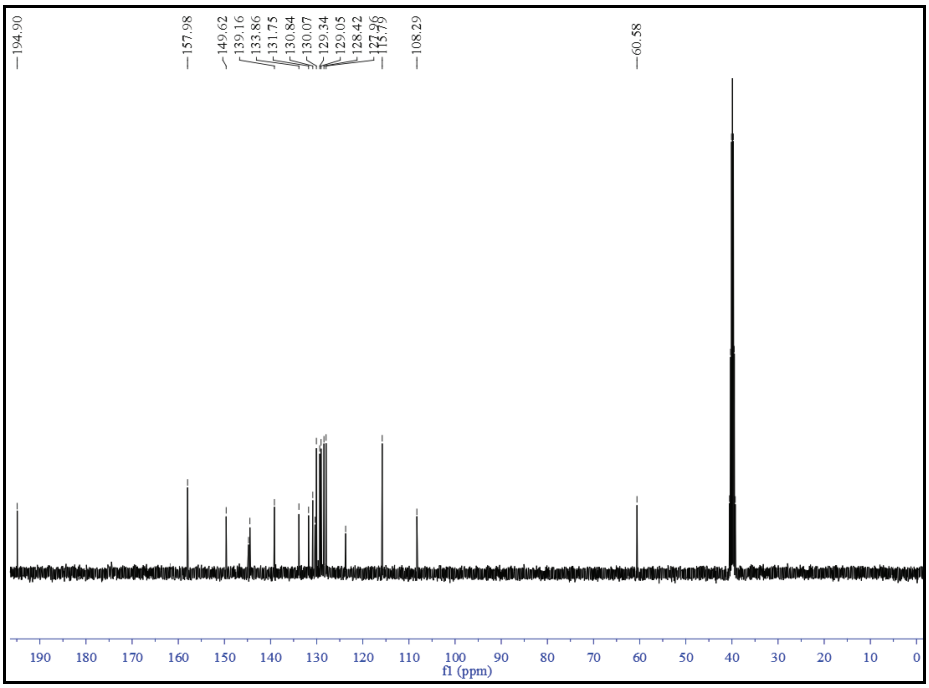

Fig. S-4. ^{13}C-NMR spectra of the compound **7**.

*The spectral data of (7-(4-methoxyphenyl)-5-phenyl-4,7-dihydrotetrazolo[1,5-α]-pyrimidin-6-yl)(phenyl) methanone (**8**)*

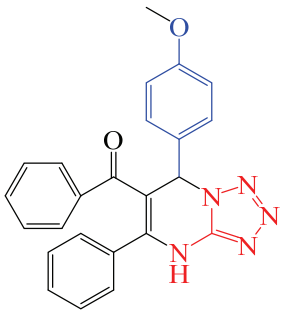

M.p.: 267-268ºC; IR (KBr, υ, cm^{-1}) 3216, 2966, 1696, 1628, 1588, 1545; ^{1}H NMR (300 MHz, DMSO-*d*6): δ (ppm) 11.29 (s, 1H, NH), 7.39-6.86 (m, 15H, $H_{arom.}$ and CH), 3.68(s, 3H, O-CH_3). ^{13}C-NMR (DMSO-d_6): 196.27 (benzoyl), 159.22, 145.17, 139.36, 135.39, 132.91, 131.47, 130.38, 130.32, 128.95, 128.26, 128.17, 128.00, 114.40, 110.71, 55.57, 55.31.

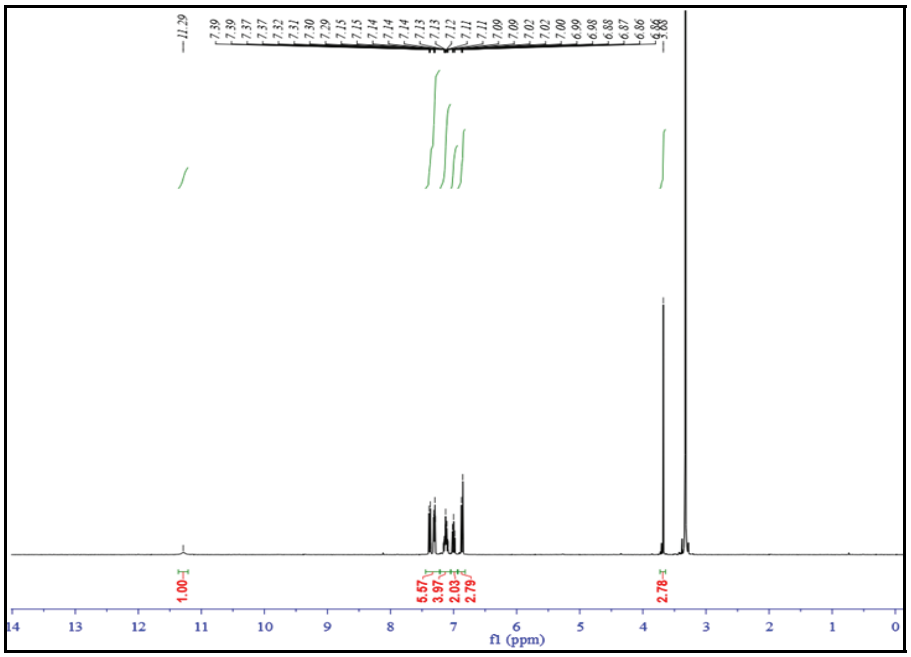

Fig. S-5. ^{1}H-NMR spectra of the compound **8**.

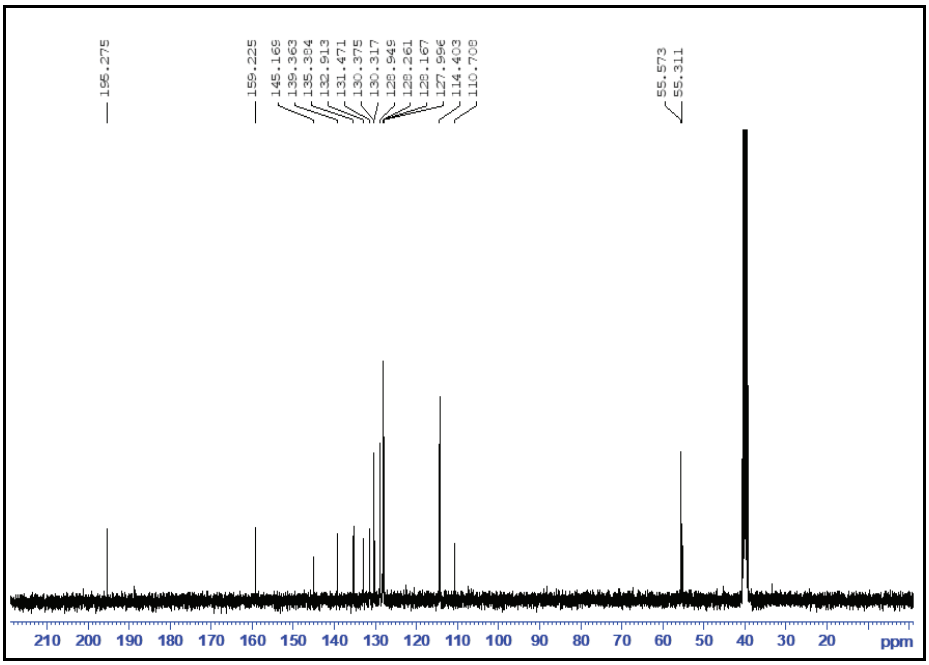

Fig. S-6. ^{13}C-NMR spectra of the compound **8**.

*The spectral data of (5,7-diphenyl-4,7-dihydrotetrazolo[1,5-α]pyrimidin-6-yl)-(phenyl)methanone (**9**)*

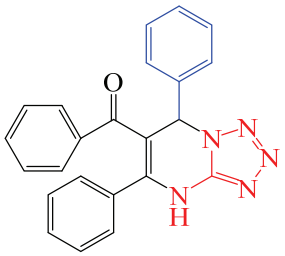

M.p.: 260-262ºC; IR (KBr, υ, cm^{-1}) 3218, 2973, 1694, 1628, 1588, 1547; ^{1}H NMR (300 MHz, DMSO-*d*6): δ (ppm) 11.33 (s, 1H, NH), 7.47-6.98 (m, 15H, $H_{arom.}$), 6.91 (s, 1H, CH). ^{13}C-NMR (DMSO-d_6): 194.77 (benzoyl), 149.77, 145.24, 140.37, 139.25, 133.83, 131.68, 130.46, 130.16, 129.19, 129.03, 128.42, 128.03, 127.92, 107.83, 60.96.

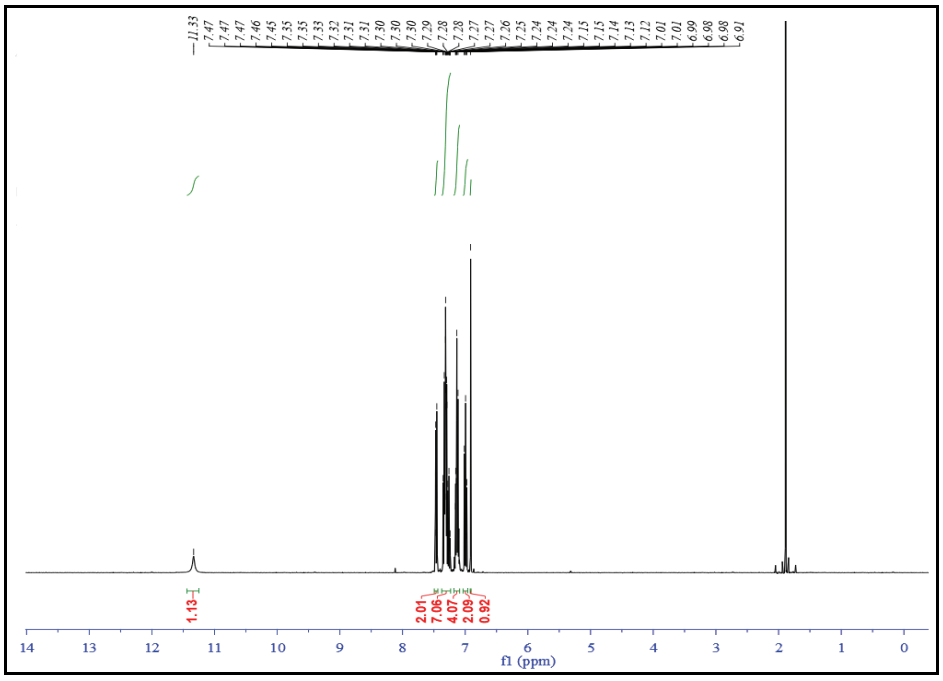

Fig. S-7. ^{1}H-NMR spectra of the compound **9**.

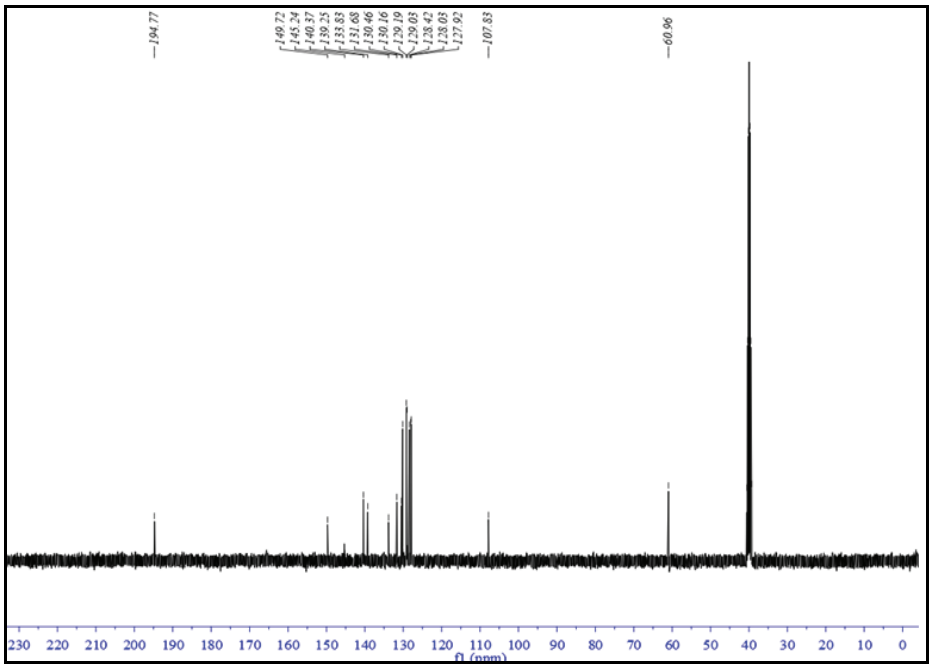

Fig. S-8. ^{13}C-NMR spectra of the compound **9**.

Journal of the Serbian Chemical Society
JSCS-info@shd.org.rs • www.shd.org.rs/JSCS
J. Serb. Chem. Soc. *87* (5) 589–601 (2022)
JSCS–5543
Original scientific paper
Published 28 April 2022

Use of experimental design to evaluate the adsorption of chromium (VI) by alginate/polyaniline beads

BELKHODJA ABDELMAJID[1,2]*, AMAL BENKHALED[1], TARIK ATTAR[1,3], SMAIN BOUSALEM[2] and ESMA CHOUKCHOU BRAHAM[1]**

[1]*Laboratory of Toxicomed, University Abou Beker Belkaid Tlemcen, BP119, 13000 Tlemcen, Algeria,* [2]*Laboratory of Applied Chemistry, University Belhadj Bouchaib, Ain Témouchent, Algeria and* [3]*Higher School of Applied Sciences of Tlemcen, BP 165, Bel Horizon, 13000 Tlemcen, Algeria*

(Received 24 July, revised 25 October, accepted 1 December 2021)

Abstract: Low-cost decorated sodium alginate beads with polyaniline (Alg@PANI beads) were easily prepared using a cross-linking method, and employed for the adsorption of Cr(VI) from aqueous solutions. The effect of several influencing parameters, including temperature, contact time, Cr(VI) concentration, and adsorbent dosage, was investigated and optimized using central composite design (CCD) under response surface methodology (RSM). The analysis of variance (ANOVA) of the quadratic model and the analyzed model revealed that the models were statistically significant, with a low *P*-value (<0.0001) and a high correlation coefficient value (R^2 = 0.93). The optimum parameters for total adsorption were as follows: adsorbent dose 0.027 g, pH 2, contact time 45 min, temperature 38 °C, and Cr(VI) concentration 29.24 ppm. The findings of this study indicate that the prepared Alg@PANI beads could be effectively used to remove Cr(VI) ions from aqueous solutions.

Keywords: bioadsorbent; central composite design; response surface; ANOVA.

INTRODUCTION

The discharge of different hazardous materials into the environment, such as heavy metals, causes a large pollution issue that can affect the quality of air, water and soil. Chromium is one of the most common heavy metal contaminants. Generally, chromium exists in several stable oxidation states, *i.e.*, Cr(0), trivalent Cr(III) and hexavalent Cr(VI) species. The hexavalent form Cr(VI) causes serious health effects, such as liver damage, pulmonary congestion, shortness of breath, coughing, and wheezing.[1] Traditional sewage methods for the removal of Cr(VI) from aqueous solutions, such as chemical precipitation,[2] membrane separ-

*,** Corresponding authors. E-mail: (*)majid92t@gmail.com; (**)esma_sid@yahoo.fr
https://doi.org/10.2298/JSC210724104A

ation,[3] adsorption,[4,5] ion exchange,[6] electrolysis[7] and coagulation[8] have been shown to be efficient. However, due to its high performance, low cost, ease of use, and lack of polluting by-products, the adsorption process has been extensively studied and widely applied on a large scale.[9–11]

Many adsorbents have been studied for the removal of Cr(VI) from aqueous solutions, including activated carbon, graphene and magnetic nanoparticles.[12,13] In recent years, low-cost adsorbents, such as biopolymers, have received much interest due to their ability to adsorb harmful heavy metal ions while still being environmentally friendly. The current example is alginate (Alg), a salt of alginic acid, which is a natural polysaccharide extracted from brown macroalgae, which consists of the anionic bloc of (1→4) linked α-L-gluronic acid (G) and β-D-mannuroric acid.[14] Thus, numerous physiochemical modifications of alginate, such as grafting and composite formation, have been developed to improve its weak mechanical stability, rigidity and adsorption properties.[15,16]

Furthermore, polyaniline, a common conductive polymer, has attracted the attention of researchers in recent years due to its low cost, ease of synthesis and environmental stability.[17,18] Then, most studies about adsorption focused on the use of polyaniline and its composites because they contain large amounts of aniline and imine nitrogen.[19]

A traditional study can be conducted to determine the best conditions of the effect treatment, but it requires more time and reactive products, which raises the cost invested in the study and the design of the treatment. Hence, predictive analytics studies were used by scientists for resolving environmental problems.[18,20,21] Thus, response surface methodology (RSM) can be used to study the effect of different variables influencing the removal of Cr(VI) from water in order to determine the best possible operating conditions.

Hence, in this study, alginate beads were decorated with polyaniline to prepare non-toxic Alg@PANI beads, and their activity and properties for adsorbing Cr(VI) in an aqueous solution were studied. The influence of different variables, namely temperature, contact time, Cr(VI) concentration, and adsorbent dosage, were investigated and optimized by central composite design combined with response surface methodology. Furthermore, the optimum parameters of the adsorption of chromium *via* Alg@PANI beads were optimized.

EXPERIMENTAL

Materials and methods

Aniline was purchased from Sigma–Aldrich and was distilled before use. All other chemicals, including sodium alginate, were purchased from Sigma–Aldrich and BIOCHEM, and used without further purification. Double distilled water was used in all experiments.

The method of preparation of 1000 ppm stock solution of Cr(VI) consisted of the dissolution of 2.829 g of $K_2Cr_2O_7$ in 1 L of double-distilled water, and standard solutions were

prepared by successive dilution. The pH of the standard solution was 6.5, which corresponds to the predominant species of CrO_4^{2-}.[22]

Preparation of Alg@PANI beads

A low-cost adsorbent was prepared by the polymerization of aniline on the surface of Alg beads. A solution of 2 % of sodium alginate was prepared by mixing the fine sodium alginate powder with double distilled water and stirring for 3 h. Separately, 0.05 M $CaCl_2$ was prepared, and both of the solutions were left standing overnight in a refrigerators. The alginate solution was then added dropwise into 500 mL of $CaCl_2$ solution under gentle stirring at room temperature. Upon contact with the cross-linker solution, calcium-alginate beads, denoted Alg beads, were formed and left to stabilize overnight. The excess of the cross-linker solution was removed by filtration.[15]

In order to activate the surface of the Alg beads, they were soaked by gentle stirring in a solution of HCl (1 M) for 1 h at room temperature. Then, a known amount of aniline was added and after 2 h, ammonium persulfate solution was added dropwise, and the reaction was allowed to proceed for 6 h at room temperature. The final synthesized product was filtered and washed several times with double distilled water and then left to air dry for 48 h.

Batch adsorption experiments

The adsorption studies of Cr(VI) on Alg@PANI beads were performed on the batch scale in the laboratory. Adsorbate solution (25 mL) was treated with a known amount of adsorbent at 150 rpm for a defined contact time under determined concentration and temperature conditions. The pH of the adsorption medium was adjusted with 0.1 M NaOH and HCl solutions in the range from 1 to 8. After the desired contact time, the adsorbate and adsorbent were separated by filtration and the residual adsorbate concentration was determined using a UV-spectrophotometer (Optizen 1412V model) at 540 nm by measuring the optical density of the resultant purple complex of Cr(VI) with 1,5-diphenylcarbazide.[23] The removal percentage (R) of the adsorbate was computed using Eq. (1):

$$R = 100\frac{C_0 - C_t}{C_0} \tag{1}$$

where C_t and C_0 are the final and initial concentrations of the adsorbate in ppm.

Experimental design

In this study, a central composite design (CCD) was chosen to assess the relationship between the variables and to evaluate the optimal conditions for the experiments.[24] Design Expert 8.0.7.1 Trial software was used for generating the statistical experimental design and analyzing the observed data. The factor levels were coded as −1 (low), 0 (central point) and 1 (high), and star points +2 (+α) and −2 (−α). According to some preliminary experiments, Table I shows the studied parameters consisting of temperature (X_1), contact time (X_2), Cr(VI) concentration (X_3) and adsorbent dosage (X_4). A quadratic equation was developed by using the second-degree polynomial equation to express the correlation between response and the selected variables, which was defined as:

$$Y = \beta_0 + \sum_{i=1}^{4}\beta_i X_i + \sum_{i=1}^{4}\sum_{j=1}^{4}\beta_{ij} X_i X_j + \sum_{i=1}^{4}\beta_{ii} X_i^2 \tag{2}$$

where Y is the predicted response; β_0, β_i, β_{ii} and β_{ij} are the unknown regression coefficients; and X_i, X_j, X_i^2 are the coded values and interaction terms of the variables.

TABLE I. Central composite design experimental factors and levels

Factor		Level			Star points, $\alpha = 2$	
		Low (−1)	Middle (0)	High (+1)	$-\alpha$	$+\alpha$
X_1	Temperature, °C	25	35	45	15	55
X_2	Contact time, min	30	45	60	15	75
X_3	Cr (VI) concentration, ppm	25	45	65	5	85
X_4	Adsorbent dose, g	0.015	0.025	0.035	0.005	0.045

RESULTS AND DISCUSSION

Characterization of adsorbent

Point of zero charges (pH$_{PZC}$). pH$_{PZC}$ is the pH value at which the total surface charge of an adsorbent is zero.[25] A pH-drift approach was used to determine the pH$_{PZC}$ of the Alg@PANI beads.[26] The sample was measured in NaCl electrolyte solutions of varying ionic strength (0.1, 0.01 and 0.001 mol/L). As can be seen in Fig. 1, the pH$_{PZC}$ value of Alg@PANI was found at 6.5±0.2. The composite reacts as a negative surface when the pH of the solution is >pH$_{PZC}$ and as a positive surface when the pH of the solution <pH$_{PZC}$.

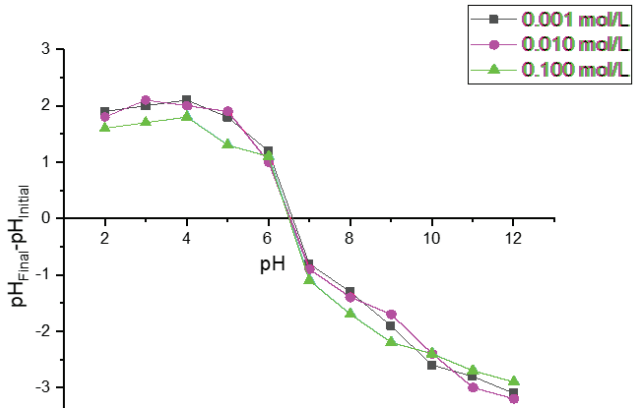

Fig. 1. Point of zero charge of Alg@PANI beads.

FTIR analysis. the functional groups of the formed beads were analyzed by Fourier transform infrared spectroscopy (FTIR, Agilent Technologies Cary 600 Series) in the 500-4000 cm^{-1} region (Fig. 2). With such a minor change, the spectrum of Alg@PANI is very similar to the Alg spectrum. The peaks at about 3241, 1592, 1419 and 1024 cm^{-1} in the alginate spectrum (Fig. 2, a) are assigned to the –OH, –COO– (asymmetric), –COO– (symmetric) groups, and oxygen stretching in cyclic ether bridge, respectively.[27] The spectrum of Alg@PANI beads (Fig. 2, b) shows an absorption peak at 3286 and 1731 cm^{-1}, which are related, respectively, to OH and the carboxyl groups in the alginate blocks after combination with the imine groups of PANI.[28] In addition, other PANI specific

peaks appeared in the spectrum of the Alg@PANI beads, *i.e.*, C=C stretching vibration of quinoid and benzenoid rings at 1577 and 1309 cm^{-1}, C–N stretching vibrations of secondary amine at 1230 cm^{-1} and C–H stretching of aromatic rings. These peaks are indicate the presence of PANI and are according with literature data.[29,30]

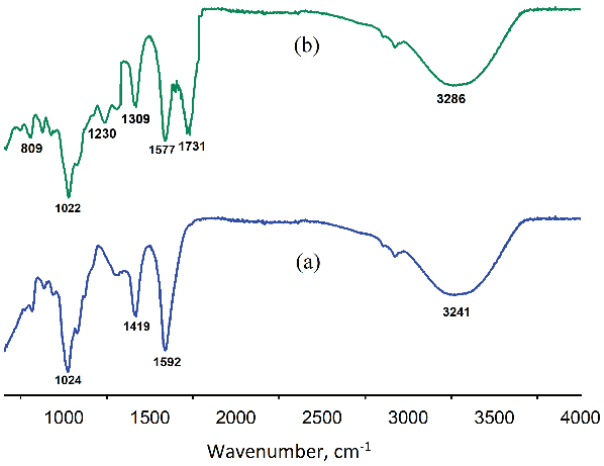

Fig. 2. FTIR spectra of Alg (a) and Alg@PANI (b).

Effect of pH

It is well known that chromium species can exist in different forms,[3] *i.e.*, H_2CrO_4, $HCrO_4^-$, $HCr_2O_7^-$, $Cr_2O_7^{2-}$ and CrO_4^{2-}. Whereby, H_2CrO_4 is the main form at pH < 2, while in the pH range 2 to 6, the predominant species are $HCrO_4^-$ and $Cr_2O_7^{2-}$ and CrO_4^{2-} is the main precipitated form of Cr(VI) at pH > 6.

The effect of solution pH for removal of Cr(VI) on Alg@PANI beads was separately investigated in the pH ranges between 1 and 8 (Fig. 3), and results revealed that the adsorption capacity reached the maximum value at pH 2.

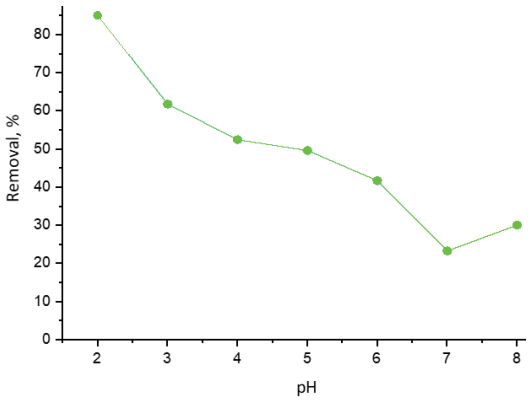

Fig. 3. Effect of the pH on Cr(VI) adsorption onto Alg@PANI beads.

This behavior could be attributed to the attraction between these anionic species of chromium and the positively charged surface of Alg@PANI beads (carboxylate, hydroxyl, and amine groups) at lower solution pH values, *i.e.* at pH values lower than pH_{PZC}.

Central composite design

Relationship between temperature, contact time, initial concentration of Cr(VI) in the solution and adsorbent dosage is indicated in Table II and shows the results of the removal of chromium from the aqueous solution by Alg@PANI beads.

TABLE II. Experimental design factors coded, real values, and predicted removal values by RSM-CCD

Run	Coded value				Real value				Removal, %		
	X_1	X_2	X_3	X_4	T / °C	t / min	C / ppm	Dose, g	Experimental	Predicted by RSM-CCD	Difference
1	–1	–1	–1	–1	25	30	25	0.015	76.2	74.1	2.1
2	+1	–1	–1	–1	45	30	25	0.015	80.3	82.8	–2.5
3	–1	+1	–1	–1	25	60	25	0.015	81.6	82.6	–1.0
4	+1	+1	–1	–1	45	60	25	0.015	85.3	84.1	1.2
5	–1	–1	+1	–1	25	30	65	0.015	71.9	71.5	0.4
6	+1	–1	+1	–1	45	30	65	0.015	75.5	75.4	0.1
7	–1	+1	+1	–1	25	60	65	0.015	81.7	80.1	1.6
8	+1	+1	+1	–1	45	60	65	0.015	74.8	76.9	–2.1
9	–1	–1	–1	+1	25	30	25	0.035	85.3	85.3	0.0
10	+1	–1	–1	+1	45	30	25	0.035	94.4	95.8	–1.4
11	–1	+1	–1	+1	25	60	25	0.035	94.7	94.5	0.2
12	+1	+1	–1	+1	45	60	25	0.035	95.4	97.8	–2.4
13	–1	–1	+1	+1	25	30	65	0.035	76.0	76.9	–0.9
14	+1	–1	+1	+1	45	30	65	0.035	81.6	82.6	–1.0
15	–1	+1	+1	+1	25	60	65	0.035	86.7	86.3	0.3
16	+1	+1	+1	+1	45	60	65	0.035	83.1	84.9	–1.8
17	–2	0	0	0	15	45	45	0.025	68.2	70.4	–2.2
18	+2	0	0	0	55	45	45	0.025	77.8	77.7	0.1
19	0	–2	0	0	35	15	45	0.025	80.2	79.4	0.8
20	0	+2	0	0	35	75	45	0.025	99.1	90.0	9.1
21	0	0	–2	0	35	45	5	0.025	98.6	97.6	1.0
22	0	0	+2	0	35	45	85	0.025	82.8	82.0	0.8
23	0	0	0	–2	35	45	45	0.005	74.1	74.8	–0.7
24	0	0	0	+2	35	45	45	0.045	96.6	94.0	2.6
25	0	0	0	0	35	45	45	0.025	98.9	98.6	0.3
26	0	0	0	0	35	45	45	0.025	98.4	98.6	–0.2
27	0	0	0	0	35	45	45	0.025	98.5	98.6	–0.1

The ANOVA analysis for response surface reduced quadratic model, using *P*-value and *F*-value to evaluate the regression coefficients of the model equation is reported in Table III. The model *F*-value of 25.80 indicates the model is sig-

nificant. Furthermore, the value of 111.50 implies the lack of fit of the *F*-value is significant. It has been reported that values of *P* less than 0.05 indicate the model terms are significant. On the other hand, values greater than 0.1 indicate the model terms are not significant.[31] In the present case, the linear coefficients X_1, X_2, X_3 and X_4, their interactions X_1X_2 and X_3X_4 and the quadratic effects X_1^2, X_2^2, X_3^2 and X_4^2 are significant model terms. shown The quadratic model equation for Cr(VI) removal and their corresponding coded values are shown in Eq. (3):

$$\begin{aligned}\text{Removal} = 98.60 + 1.48X_1 + 3.33X_2 - 3.90X_3 + 4.79X_4 - 1.78X_1X_2 - \\ - 1.18X_1X_3 + 0.46X_1X_4 + 0.031X_2X_3 + 0.19X_2X_4 - 1.43X_3X_4 - \\ - 6.72X_1^2 - 2.55X_2^2 - 2.69X_3^2 - 3.63X_4^2\end{aligned} \quad (3)$$

TABLE III. Analysis of variance (ANOVA) for the CCD model

Source	Sum of squares	Degree of freedom	Mean square	*F*-value	*P*-value Prob > *F*	Significance
Model	2353.39	14	168.10	25.80	< 0.0001	Significant
X_1	52.51	1	52.51	8.06	0.0149	
X_2	266.00	1	266.00	40.82	< 0.0001	
X_3	364.26	1	364.26	55.90	< 0.0001	
X_4	550.08	1	550.08	84.42	< 0.0001	
X_1X_2	50.77	1	50.77	7.79	0.0163	
X_1X_3	20.33	1	20.33	3.43	0.0889	
X_1X_4	3.33	1	3.33	0.51	0.4883	
X_2X_3	0.016	1	0.016	0.002398	0.9617	
X_2X_4	0.60	1	0.60	0.092	0.7666	
X_3X_4	32.78	1	32.78	5.03	0.0446	
X_1^2	962.13	1	802.24	147.65	< 0.0001	
X_2^2	139.06	1	256.84	21.34	0.0006	
X_3^2	111.94	1	103.94	17.18	0.0014	
X_4^2	280.82	1	268.07	43.10	< 0.0001	
Residual	78.19	12	6.52	–	–	–
Lack of fit	78.05	10	7.81	111.50	0.0089	Significant
Pure error	0.14	2	0.070	–	–	–
Total SS	2431.58	26	–	–	–	–

The thorough awareness of the effect of each factor on the response, as well as their interactions, can be seen in Eq. (3). In the equation, a positive sign denotes a synergistic effect, while a negative sign denotes an antagonistic effect. The comparison of observed and predicted Cr(VI) removal values (Table II) yielded a high correlation coefficient R^2 of 0.8150, which is in good agreement with the adjusted R^2_{adj} value of 0.9303. This is illustrated in Fig. 4, while the plot of the predicted values *vs*. experimental values for the removal percentage of Cr(VI) revealed a good fit, indicating the validity of the regression model.

The relationship between relevant model terms and the three dimensional contours of the optimal response is graphically depicted in Fig. 5. These plots were constructed using fixed and optimum values of other variables for a specific combination of factors.

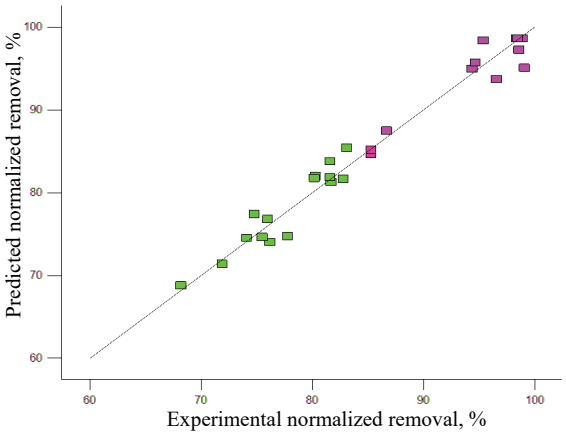

Fig. 4. The experimental data *vs.* the predicted data of normalized removal of Cr(VI).

The interaction of the adsorbent dosage with contact time, temperature and Cr(VI) concentration are presented in Fig. 5a–c, respectively. An increased removal percentage of chromium was observed with increasing adsorbent dosage. This is due to the presence of additional vacant adsorption sites with increasing adsorbent dose, which led to an enhanced caption of metals. At lower amounts of Alg@PANI beads, the removal percentage decreased because of the smaller numbers of active sites.

The 3D curvature of the response surfaces shown in Fig. 5c–e for the Cr(VI) concentration showed changes in the percentage removal as a function of adsorbent dosage and other factors with interaction between them. As can be seen, the removal percentage decreases upon increasing the initial concentration of the Cr(VI) solution. At lower concentrations, the amount of adsorbent used was greater than the amount of metal ions used, and the adsorption sites could easily catch the Cr(VI) ions. On the contrary, at higher concentrations, the decrease in removal percentage was due to a decrease in available adsorption sites, indicating that the entire surface sites on Alg@PANI beads was saturated using a certain Cr(VI) concentration. Furthermore, higher Cr(VI) concentrations may cause more offensive forces within the solid particles and solute molecules, causing a reduction in the removal of metal ions.

The effect of contact time on the removal percentage and the interaction of diffrent factors with it are illustrated in Figs. 5a, d and f. The results showed that the maximum rate of removal percentage was achieved after 30 min. However,

extending the contact time had no affect on the rate of Cr(VI) adsorption because all the active adsorption sites had been saturated after 30 min of contact.

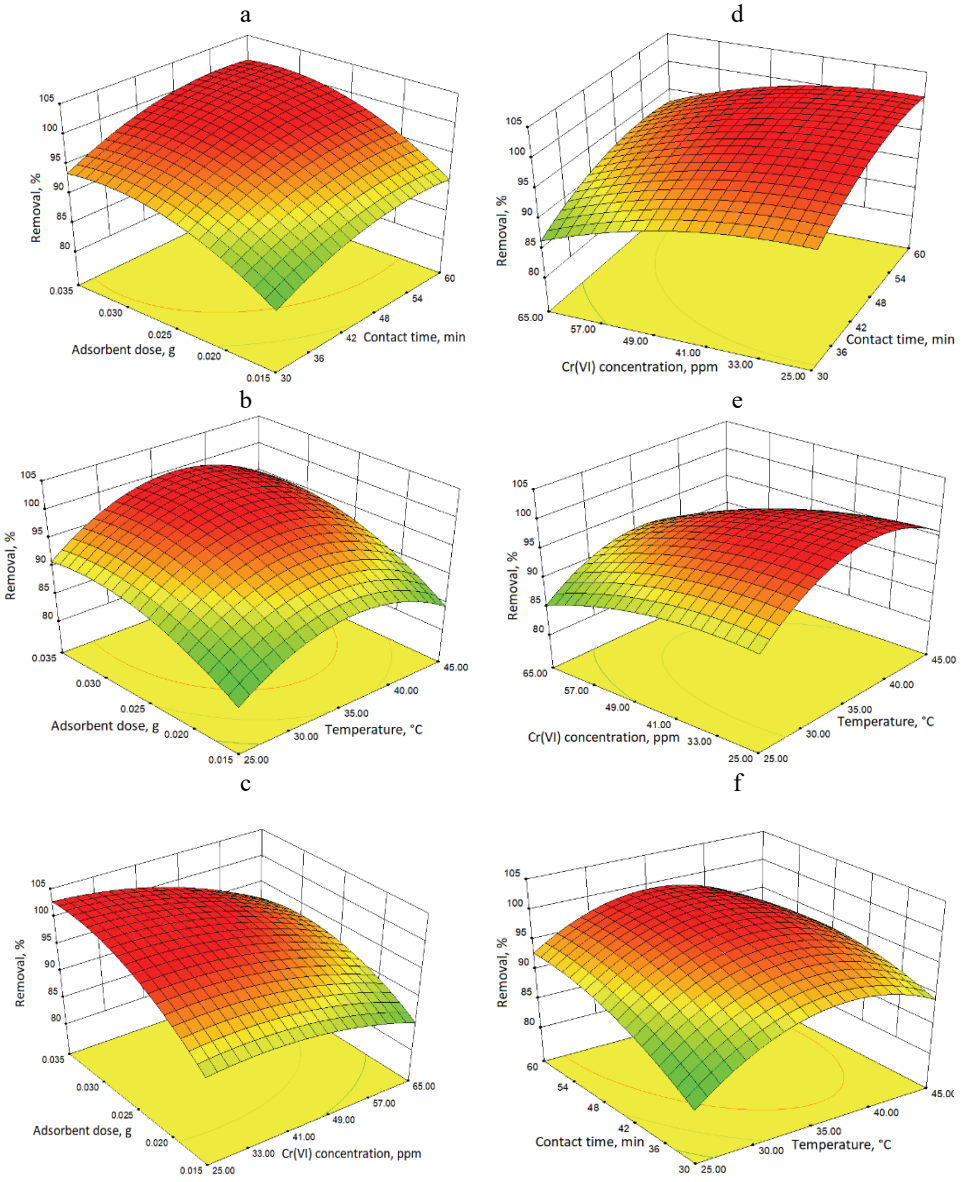

Fig. 5. Response surfaces for the CCD: a) adsorbent dosage–contact time; b) adsorbent dosage–temperature; c) adsorbent dosage–Cr(VI) concentration; d) Cr(VI) concentration–contact time; e) Cr(VI) concentration–temperature; f) contact time–temperature.

The response surfaces plots for the effect of temperature and its interaction with adsorbent dosage, Cr(VI) concentration and contact time are shown in Fig. 5b, e and f, respectively. With rising temperature, the percentage removal of Cr(VI) increased which indicates the endothermic nature of the adsorption process.

In this study, design expert software was used to determine the optimal parameter values for the adsorption of Cr(VI) by Alg@PANI beads. In addition, the optimal conditions for total adsorption (Fig. 6) were obtained at optimum conditions set as: adsorbent dose = 0.027 g, pH 2, time = 45 min, temperature = = 38 °C and Cr(VI) concentration = 29.24 ppm. The optimal operating conditions were determined in order to lead to higher yields, with the minimum adsorption mass and maximum concentration.[24] Then, the optimum removal of 88.62 % was achieved with a minimum dose = 0.018 g, contact time = 47 min, temperature = = 31.4 °C and Cr(VI) concentration = 65 ppm.

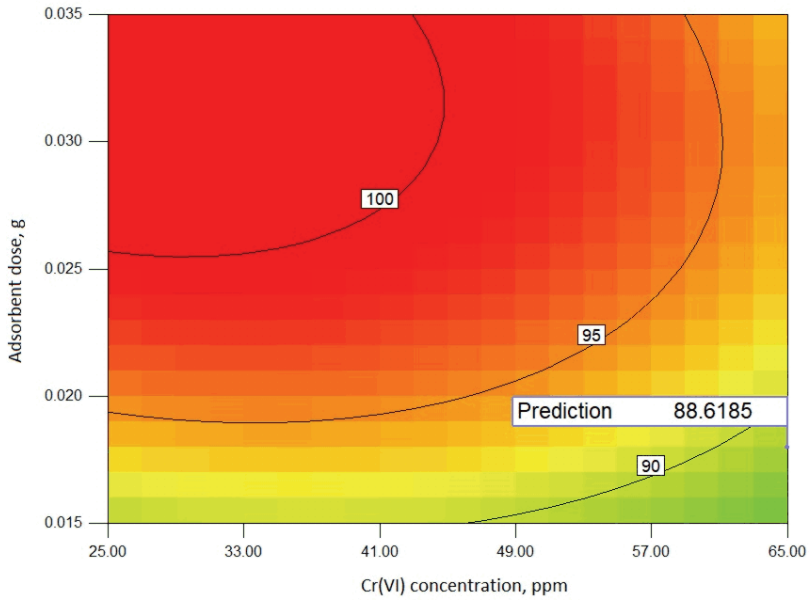

Fig. 6. Optimum removal efficiency (contour plot obtained from RSM optimization).

CONCLUSIONS

The experimental design methodology was used in this study to optimize Cr(VI) removal by Alg@PANI beads. Temperature, contact time, Cr(VI) concentrations, and adsorbent dose were evaluated as operational variables for the optimization of the treatment process and statistical analysis of model response interaction were studied. As a result, the majority of the impacts are substantial, and the *P*-value of the model was less than 0.05 (*P*-value = 0.0089), indicating that composite central design of the model is appropriate for the explored systems.

The total efficiency of Cr(VI) removal was reached under the optimum conditions, *i.e*., adsorbent dose of 0.027 g, pH 2, time 45 min, temperature 38 °C and Cr(VI) initial concentration of 29.24 ppm. Moreover, using the minimum amount of adsorbent (0.018 g) and a high concentration of Cr(VI) (65 ppm), the adsorption rate was 88.62 %. Finally, this strategy of modelization offers a cost-effective way to obtain specific information in a short period with a small number of experiments.

Acknowledgements. The authors thank the Laboratory of Catalysis and Synthesis in Organic Chemistry (LCSCO) for the analysis. The authors wish to thank the Directorate General for Scientific Research and Technological Development (DGRSDT), the University of Tlemcen and University of Ain Temouchent for the financial support.

ИЗВОД

ЕКСПЕРИМЕНТАЛНИ ДИЗАЈН ЗА ИСИТИВАЊЕ АДСОРПЦИЈЕ ХРОМА(VI) НА АЛГИНАТ/ПОЛИАНИЛИН ПЕРЛАМА

BELKHODJA ABDELMAJID[1,2], AMAL BENKHALED[1], TARIK ATTAR[1,3], SMAIN BOUSALEM[2] и ESMA CHOUKCHOU BRAHAM[1]

[1]*Laboratory of Toxicomed, University Abou Beker Belkaid Tlemcen, BP119, 13000 Tlemcen, Algeria,* [2]*Laboratory of Applied Chemistry, University Belhadj Bouchaib, Ain Témouchent, Algeria и* [3]*Higher School of Applied Sciences of Tlemcen, BP 165, Bel Horizon, 13000 Tlemcen, Algeria*

У овом раду су јефтине, натријумом-алгинатне перле са превлаком од полинаилина (Alg@PANI перле) добијене једноставном методом унакрсног повезивања и примењене за адсорпцију Cr(VI) из водених раствора. Испитиван је утицај неколико параметара, укључујући температуру, време контакта, концентрацију Cr(VI) и дозу адсорбента, и оптимизован користећи дизајн централног композита (CCD) применом методологије површине одговора (RSM). Анализа варијансе (ANOVA) квадратног модела и анализираног модела показала је да су модели статистички значајни, са малом *P*-вредношћу (< 0,0001) и већом вредношћу корелационог коефицијента (R^2 = 0,93). Оптимални параметри за тоталну адсорпцију су били: доза адсорбента = 0,027 g, pH 2, време контакта = 45 min, температура = 38 °C, и концентрација Cr(VI) = 29,24 ppm. Резултати овог истраживања указују да припремљене Alg@PANI перле могу бити коришћене за успешно уклањање Cr(VI) јона из водених раствора.

(Примљено 24. јула, ревидирано 25. октобра, прихваћено 1. децембра 2021)

REFERENCES

1. R. Kumar, S. Kim, K. Kim, S. Lee, H. Park, *Appl. Geochem.* **88** (2017) 113 (https://doi.org/10.1016/j.apgeochem.2017.04.002)
2. C. R. Ramakrishnaiah, B. Prathima, *Int. J. Eng. Res. Appl.* **2** (2012) 599 (https://www.academia.edu/download/28318905/CT22599603.pdf)
3. P. Y. He, Y. J. Zhang, H. Chen, Z. C. Han, L. C. Liu, *J. Hazard. Mater.* **392** (2020) 122359 (https://doi.org/10.1016/j.jhazmat.2020.122359)
4. M. Bilal, J. Ali, N. Hussain, M. Umar, S. Shujah, D. Ahmad, *J. Serb. Chem. Soc.* **85** (2020) 265–277 (https://doi.org/10.2298/JSC181108001B)

5. J. S. Marciano, R. R. Ferreira, A. G. de Souza, R. F. S. Barbosa, A. J. de Moura Junior, D. S. Rosa, *Int. J. Biol. Macromol.* **181** (2021) 112 https://doi.org/10.1016/j.ijbiomac.2021.03.117)
6. H. Wang, X. Song, H. Zhang, P. Tan, F. Kong, *J. Hazard. Mater.* **384** (2020) 121459 (https://doi.org/10.1016/j.jhazmat.2019.121459)
7. F. A. Soriano Moranchell, J. M. Sandoval Pineda, J. N. Hernández Pérez, U. S. Silva--Rivera, C. A. Cortes Escobedo, R. de Guadalupe González Huerta, *Int. J. Hydrog. Energy* **45** (2020) 13683 (https://doi.org/10.1016/j.ijhydene.2020.01.050)
8. I. A. Katsoyiannis, M. Xanthopoulou, A. I. Zouboulis, *Appl. Sci.* **10** (2020) 802 (https://doi.org/10.3390/app10030802)
9. C. B. Esma, B. K. Ismet, B. Amel, S. A. Rim, H. Djawhar, D. Zoulikha, *J. Macromol. Sci. A* **52** (2015) 273 (https://doi.org/10.1080/10601325.2015.1007272)
10. A. Gadiri, A. Benkhaled, E. Choukchou-Braham, J. Macromol. Sci. **55** (2018) 393 (https://doi.org/10.1080/10601325.2018.1453258)
11. D. Heddi, A. Benkhaled, A. Boussaid, E. Choukchou-Braham, *Phys. Chem. Res.* **7** (2019) 731 (https://dx.doi.org/10.22036/pcr.2019.179510.1625)
12. U. O. Aigbe, O. A. Osibote, *J. Environ. Chem. Eng.* **8** (2020) 104503 (https://doi.org/10.1016/j.jece.2020.104503)
13. Z. Djemaa, K. I. Benabadji, E. Choukchou-braham, A. Mansri *J. Macromol. Sci.* 50 (2013) 679 (https://doi.org/10.1080/10601325.2013.792194)
14. K. Varaprasad, T. Jayaramudu, V. Kanikireddy, C. Toro, E. R. Sadiku, *Carbohydr. Polym.* **236** (2020) 116025 (https://doi.org/10.1016/j.carbpol.2020.116025)
15. A. M. Omer, R. E. Khalifa, Z. Hu, H. Zhang, C. Liu, X. Ouyang, *Int. J. Biol. Macromol.* **125** (2018) 1221 (https://doi.org/10.1016/j.ijbiomac.2018.09.097)
16. G. Cattelan, A. Guerrero Gerbolés, R. Foresti, P. P. Pramstaller, A. Rossini, M. Miragoli, C. Caffarra Malvezzi, *Front. Bioeng. Biotechnol.* **8** (2020) (https://doi.org/10.3389/fbioe.2020.00414)
17. W. A. Amer, M. M. Omran, M. M. Ayad, *Colloids Surf.* **562** (2018) 203 (https://doi.org/10.1016/j.colsurfa.2018.10.081)
18. E. Sharifpour, M. Ghaedi, A. Asfaram, M. Farsadrooh, E. A. Dil, H. Javadian, *Int. J. Biol. Macromol.* **152** (2020) 913 (https://doi.org/10.1016/j.ijbiomac.2020.02.236)
19. Y. Jiang, Z. Liu, G. Zeng, Y. Liu, B. Shao, Z. Li, Y. Liu, *Int. J. Biol. Macromol*. **25** (2018) 6158 (https://doi.org/10.1007/s11356-017-1188-3)
20. L. K. F. Araújo, A. A. Albuquerque, W. C. O. Ramos, A. T. Santos, S. H. V Carvalho, J. I. Soletti, M. D. Bispo, *Environ. Dev. Sustain.* **23** (2021) 11732 (https://doi.org/10.1007/s10668-020-01137-7)
21. E. Cheraghipour, M. Pakshir, *J. Environ. Chem. Eng.* **9** (2021) 104883 (https://doi.org/10.1016/j.jece.2020.104883)
22. M. Chabane, C. Melkaoui, B. Dahmani, S. Zahia Belalia, *Ann. Chim. Sci. Des Mater.* **44** (2020) 311 (https://doi.org/10.18280/acsm.440502)
23. A. Lace, D. Ryan, M. Bowkett, J. Cleary, *Int. J. Environ. Res. Public Health* **16** (2019) 1803 (https://doi.org/10.3390/ijerph16101803)
24. K. Azoulay, I. Bencheikh, A. Moufti, A. Dahchour, J. Mabrouki, S. El Hajjaji, *Chem. Data Collect.* **27** (2020) 100385 (https://doi.org/10.1016/j.cdc.2020.100385)
25. T. E. Abilio, B. C. Soares, J. C. José, P. A. Milani, G. Labuto, E. N. V. M. Carrilho, *Environ. Sci. Pollut. Res.* 28 (2021) 24816 (https://doi.org/10.1007/s11356-020-11726-8)

26. M. Pashai Gatabi, H. Milani Moghaddam, M. Ghorbani, *J. Mol. Liq.* **216** (2016) 117 (https://doi.org/10.1016/j.molliq.2015.12.087)
27. W. Zhao, P. Yuan, X. She, Y. Xia, S. Komarneni, K. Xi, Y. Che, X. Yao, D. Yang, *J. Mater. Chem. A* **3** (2015) 14188 (https://doi.org/10.1039/C5TA03199K)
28. N. Jiang, Y. Xu, Y. Dai, W. Luo, L. Dai, *J. Hazard. Mater.* **215**–**216** (2012) 17 (https://doi.org/10.1016/j.jhazmat.2012.02.026)
29. G. A. O. Fang, C. Yang, A. N. Liang, T. A. N. Ruiqin, L. I. Xiaomin, W. Guanghui, *J. Wuhan Univ. Technol. Mater. Sci.* **30** (2015) 1147 (https://doi.org/10.1007/s11595-015-1286-3)
30. R. Karthik, S. Meenakshi, *Int. J. Biol. Macromol.* **72** (2015) 711 (https://doi.org/10.1016/j.ijbiomac.2014.09.023)
31. R. A. Abbas, A. A. R. Farhan, H. N. Abdalraheem Al Ani, A. C. Nechifor, *Rev. Chim.* **70** (2019) 1108 (https://doi.org/10.37358/rc.19.4.7074).

Journal of the Serbian Chemical Society
JSCS-info@shd.org.rs • www.shd.org.rs/JSCS
J. Serb. Chem. Soc. *87* (5) 603–614 (2022)
JSCS–5544
Original scientific paper
Published 25 March 2022

Design and implementation of low-cost portable potentiostat based on WeChat

XIAOYAN SHEN[1,2], ZIQIANG LI[1], LEI MA[1]*, XIONGHENG BIAN[1], XINGSI CHENG[1] and XIONGJIE LOU[1]

[1]*School of Information Science and Technology, Nantong University, Nantong, 226019, China and* [2]*Nantong Research Institute for Advanced Communication Technologies, Nantong, 226019, China*

(Received 10 October, revised 28 December 2021, accepted 28 February 2022)

Abstract: The potentiostat is critical in the development of electrochemical systems; however, its cumbersome detection and high cost considerably limit its large-scale application. To provide an affordable alternative to developing countries and resource-constrained areas, this study designs an electrochemical detection system based on smartphones, which uses Bluetooth Low Energy to convert open-source potentiostat data based on PSoC-5LP. The WeChat application on the smartphone provides an interface for entering experimental parameters and visualizing the results in real time. The smartphone-based electrochemical detection system has a simple design and reduces the size (10×3×0.3 cm^3) and the cost of the hardware ($ 18). The system performs the most commonly used cyclic voltammetry for electrochemical detection, with results that are comparable to those obtained using a commercial potentiostat and an error rate of 1.3 %. In the classical teaching experiment of electrochemical determination of ascorbic acid in orange juice samples, the measured value of the system is 0.367±0.012 mg/mL, compared with the standard reference value of 0.37 mg/mL, which is obviously a convincing value. Therefore, this system is a low-cost, reliable alternative to a potentiostat for research, education or product integration development.

Keywords: cyclic voltammetry; point-of-care testing; smartphone; Bluetooth.

INTRODUCTION

Electrochemistry studies chemical reactions at the interfaces of electronic and ion conductors and charge transfer between molecules and electrodes.[1] It may be used in wearable devices and for analysis in applications such as clinical diagnosis, environmental, industrial, and food monitoring, and quality control.[2–6] Data are obtained by monitoring electron transfer at the conductor interface and

* Corresponding author. E-mail: malei@ntu.edu.cn
https://doi.org/10.2298/JSC211030018S

the redox peak intensities of substances involved in the reaction. A critical monitoring device in bioelectrochemical research is the potentiostat, which measures the current passing between the two electrodes by controlling the voltage between the working and counter electrodes (WE and CE, respectively).[7] Although progress in electronic technology reduced the volume of the traditional commercial potentiostat,[8,9] the use of commercial potentiostats remains cumbersome and costly, resulting in clear limitations in cost, portability, and analysis time. Furthermore, their components and circuits are confidential. Hence, for researchers who conduct rapid electrochemical analysis in the field and require the use of a potentiostat for research, education, or product integration development, there are clear, considerable challenges in using a commercial potentiostat.

Point of care testing (POCT) technology is critical in promoting electrochemical detection. This is a rapid detection technology that is used in the field, instead of being limited to the laboratory setting.[10] Compared with the traditional central laboratory,[11] POCT exhibits the advantages of small equipment, simple operation, lower sample consumption, lack of required pre-processing, and instant reporting of results, particularly with the short duration of sample analysis.[12]

Currently, >67 % of the global population own mobile phones, and >50 % of the population own smartphones with advanced computing and connectivity capabilities.[13,14] The rapid development of smartphones resulted in them becoming the most widely used mobile devices. Smartphones exhibit the advantages of programmable systems, high-speed computing, and sizable data storage, and may be used as integrated platforms to receive, analyze and display data. They are critical portable devices and the most sought-after analytical equipment in the field of biosensing.[15,16] Currently, smartphones are mainly involved in the design of optical biosensor systems.[17,18] In recent years, with the progression of electrochemical research, the wireless combination of smartphones and portable potentiostats *via* Bluetooth favors on-site electrochemical analysis in areas with limited resources,[19] which effectively achieves POCT. Additionally, this may overcome the limitations of commercial electrochemical workstations to a considerable extent. The emergence of this design promotes the application of smartphones in the field of bioelectrochemical sensing.[20–23]

WeChat Mini Program is an application service that may be run in WeChat. It was developed by Tencent and launched on January 9, 2017. Its emergence overcomes the multi-platform and compatibility issues that exist in the development of native applications for smart mobile terminals. Native application development tools (such as Android studio) employ Java language as the basic development language, with the concomitant disadvantages of Java language development, such as high memory usage and running on virtual machines.[24] Conversely, WeChat applet development employs JavaScript language as the basic development language, which relies on browser engines for compilation, ana-

lysis, and rendering, and enables the creation of better interactive pages, which users appreciate.

This study involves the design of a portable, low-cost, smartphone-based electrochemical cyclic voltammetry (CV) system. This system consists of the following main components: smartphone, handheld detector and three-electrode system. The smartphone is used to receive and process data *via* the WeChat applet and display the results. The handheld detector is based on an embedded development board; it is used to perform CV based on the applied excitation voltage, detect feedback within the three-electrode system, and transmit the obtained data to the smartphone. The three-electrode system participates in the chemical redox reaction in the electrolyte solution and measures electron transfer during the reaction. The performance of this system is verified by comparing the results with those of commercial electrochemical systems. Moreover, the practicability of the system in educational application is verified.

EXPERIMENTAL

Design of smartphone-based electrochemical detection system

The overall system operation is shown in Fig. 1. The chemical reaction in the electrochemical cell generates an analog electrical signal, which is recorded using the handheld detector and converted into digital signals. These signals are transmitted to the smartphone *via* Bluetooth. The WeChat applet then visualizes the data on the screen of the smartphone.

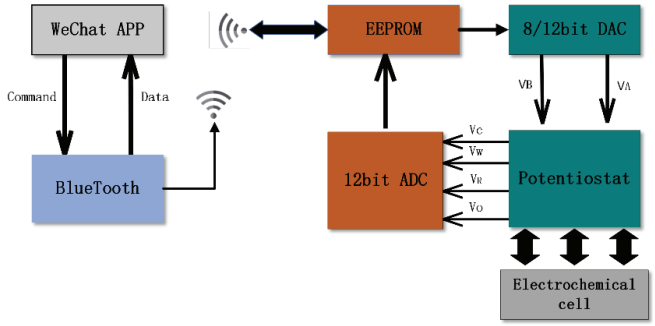

Fig. 1. Electrochemical detection system based on a smartphone.

Design of the hand-held cv detector

The design of the detection module is the key to the portability of the entire system. Therefore, the design employed a small PSoC-5LP development board (part number CY8CKIT-059, purchased from Future Electronics, Shanghai, China), and the microcontroller unit CY8C5888LTI-LP097. The low-cost chip exhibited satisfactory experimental accuracy. Additionally, the programmable system on a chip (PSoC) Creator programmable environment (Cypress Semiconductor, San Jose, California) configured by PSoC 5LP integrated various functional circuit modules, including operational, transimpedance, and programmable gain amplifiers, comparators, mixers, segment liquid crystal displays, CapSense touch sensors, dig-

ital-to-analog converters (DACs), and analog multiplexers (AMuxs),[25] which satisfied the requirements of detection module design.

To control the voltage between the electrodes, a voltage control circuit was designed, as shown in Fig. 2a. The circuit may employ 8-bit voltage DAC (VDAC) or 12-bit voltage DAC (DVDAC). DVDAC can control the voltage that may rapidly switch between two values. This renders the DVDAC output voltage a weighted average of the input values, that may be used for improving the accuracy of the DA conversion. However, this type of switching produces noise and causes interference to signal. Thus, a small capacitor C(100nF) should be placed at the output to improve the voltage resolution, and the circuit may also be used to select the DAC to employ an AMux sensing electrode. The operational amplifier may buffer the voltage and provide a feedback electrical signal from the reference electrode (RE).[26,27]

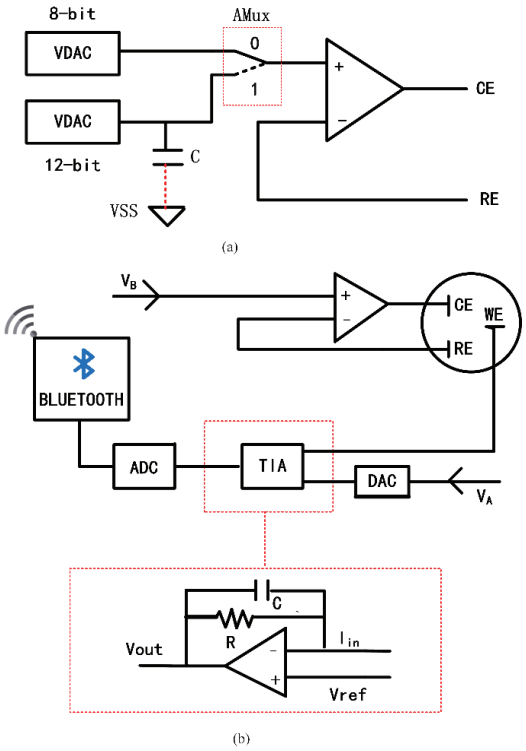

Fig. 2. a) Voltage control circuit. b) Potentiostat circuit diagram.

The core circuit design of the module is shown in Fig. 2b. The circuit mainly consists of a voltage control circuit, transimpedance amplifier (TIA), Digital to analog converter (DAC), and an analog-to-digital converter (ADC). When the module is used in CV detection, the output amplifier of the voltage control circuit adjusts the potential of the CE and feeds back the potential to the RE to ensure that the potential of the RE is consistent with the output of the reference potential of the DAC. The transimpedance amplifier (TIA) mainly measures the electrical signal feedback at the WE, converts the ADC signal to a digital electrical signal, and uploads it to the smartphone terminal *via* Bluetooth communication.

Bluetooth communication module and three-electrode system

The Bluetooth communication module transferred the data between the potentiostat and WeChat applet. This system employed the HC-08 module owing to the following: 1) the small, low-cost microprocessor exhibited low power consumption. 2) Compatibility with Apple and Android, which are two mainstream smartphone operating systems, yielding numerous possibilities in system software design. 3) It could provide a wide bandwidth for data transmission and transmit all original data to the smartphone within the working distance of the communication module.

The electrochemical cell module generally consists of two- or three-electrode systems. However, in a two-electrode system, the polarization current passing through the electrodes causes voltage changes, interfering with the constant voltage between the electrodes, which causes large experimental errors. Compared with the two-electrode system, the three-electrode system possesses an RE, which provides a stable reference potential during measurement, eliminates the large error of electrode potential caused by polarization current to stabilize the working electrode, and ensures the accuracy of the measurement.[28] The electrochemical cell module of this system was designed as a three-electrode system. The details of the electrode materials are as follows: the WE was a glassy carbon electrode (Shanghai Chuxi Industrial Co., Ltd; diameter: 10 mm; length: 80 mm), the CE was a platinum electrode (Shanghai Chuxi Industrial Co., Ltd; diameter: 1 mm; length: 60 mm), and the RE was a saturated calomel electrode (Shanghai Chuxi Industrial Co., Ltd; diameter: 9 mm; length: 120 mm).

Design of the WeChat applet

This study developed a WeChat applet (Fig. 3b–d) by using WeChat developer tools (Tencent, China, Version 1.03). It connects a smartphone to a handheld CV detector *via* Bluetooth to control CV, process real-time data, and plot cyclic voltammograms. The basic process of the software application (Fig. 3a) is as follows: first, open the application software, initiate Bluetooth, enter the detection interface and pair with the Bluetooth module of the lower computer. Second, log in using a WeChat account, and select CV detection mode. Enter the parameter-setting interface, and after accurately entering the specific initial parameters, click "OK" to enter the detection interface. Subsequently, the lower computer detects according to the set detection method and corresponding parameters, and the measured data is transferred via Bluetooth. Subsequently, the WeChat applet on the mobile phone plots and presents the voltage–current curve.

System performance evaluation

To evaluate the performance of the system, a commercial potentiostat and the system were used to perform CV studies on a 5 mM potassium ferricyanide solution and the results were compared to obtain the peak oxidation current error rate of the system. The experimental sweep voltage range was 800 to –400 mV, sweep rate was 50 mV/s. The error rate equation is:

$$\text{Distinction} = \frac{I_\text{d} - I_\text{c}}{I_\text{c}} \quad (1)$$

where I_d is the oxidation peak current measured using the system and I_c is the oxidation peak current measured using the commercial potentiostat.

The ferrocyanide cyclic voltammograms were recorded at 0.31, 0.62, 1.25, 2.5 and 5 mM (sweep rate of 50 mV/s, sweep voltage of –400–800 mV) and different scanning rates at 5 mM (sweep rate of 10–100 mV/s and sweep voltage of –1000–800 mV) using the system.

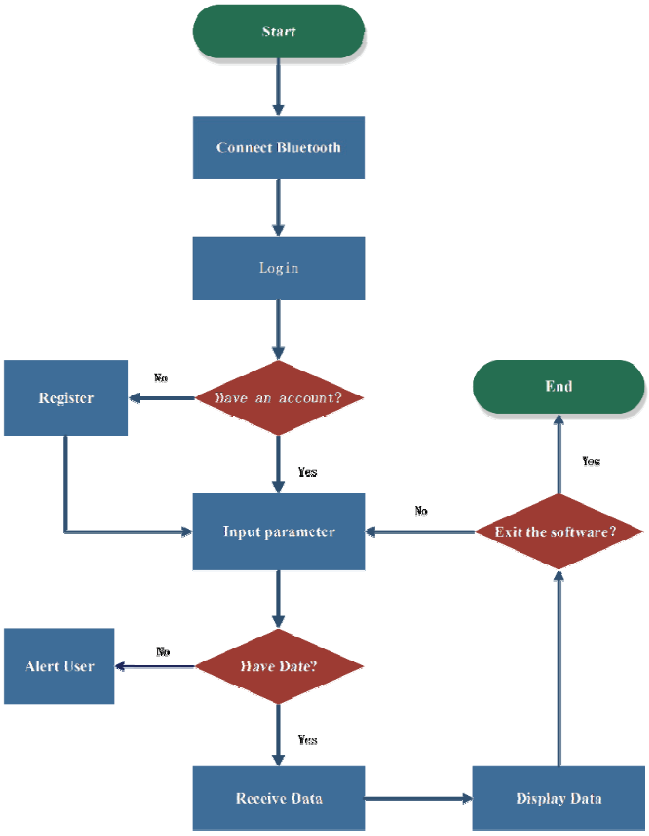

(a)

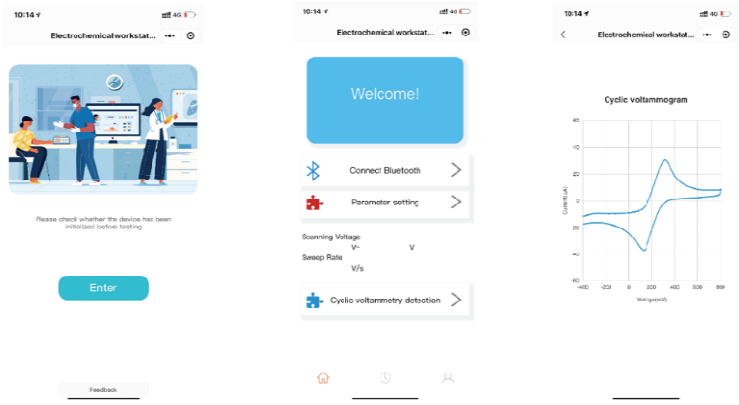

(b) (c) (d)

Fig. 3. a) WeChat applet operation. b–d) WeChat applet interface.

RESULTS AND DISCUSSION

In the ferricyanide/ferrocyanide redox pair, the half reaction (2):

$$[Fe(CN)_6]^{3-} + e^- \leftrightarrow [Fe(CN)_6]^{4-} \quad (2)$$

rapidly exchanges electrons with the WE.[29] The CV response of the redox pair shows the oxidation $Fe^{2+} \rightarrow Fe^{3+}$ and reduction $Fe^{3+} \rightarrow Fe^{2+}$ peaks of the electroactive substances, resulting in the characteristic current-potential curve of the reaction.[29] Fig. 4a shows that the detection results of the smartphone-based electrochemical CV detection system and those of the commercial potentiostat exhibit similar characteristic reversible redox peaks, but there are some differences in the traces. These differences, several of which may be owing to electrochemical changes over time within the electrodes,[30] may also be caused by a slight voltage offset of the on-board amplifier of the embedded development board. Fig. 4b shows the measured oxidation peak currents – the difference is 0.47 μA with an error rate of 1.3 %.

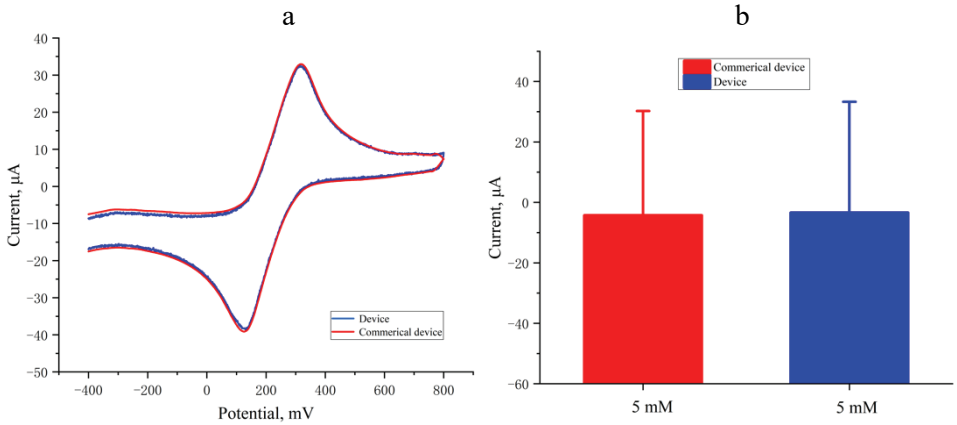

Fig. 4. a) Cyclic voltammograms obtained using the Proposed system and commercial potentiostat. b) Oxidation peak currents measured using the Proposed system and commercial potentiostat.

Table I summarizes the parameters of the proposed system and commercial potentiostat. The proposed system has lower cost, weight, and dimensions than the commercial potentiostat. However, its voltage range is narrower than that of the commercial device.

TABLE I. Comparison of parameters between self-made system and commercial Potentiostat

Potentiostat	Voltage range	ADC resolution	Cost, $	Weight, g	Dimensions, cm^3
PSoC-device	±2 V	12-bits[c]	18.03	65	10×3×0.3
Commerical-device	±10 V	24-bits	80–120	2000	37×23×12

As shown in Fig. 5a, the redox peak current increases with increasing sweep rate. A good relationship between the redox peak current and the square root of the sweep rate is observed (Fig. 5b). The correlation coefficients of the oxidation and reduction currents and the square root of the sweep rate are 0.9987 and 0.9966, respectively. According to the relationship between the peak current and square root of the scan rate based on the Randles-Sevcik equation,[31] the electron transfer reaction at the electrode surface is governed by diffusion.

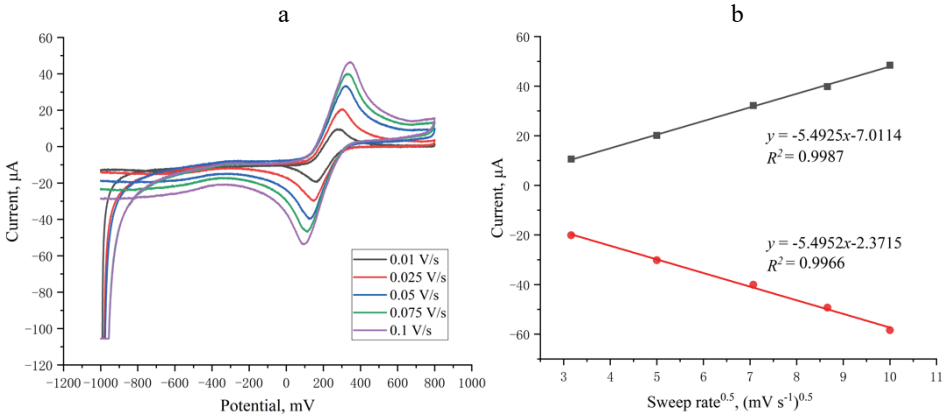

Fig. 5. a) Cyclic voltammograms of potassium ferricyanide solution at sweep rates of 10–100 mV/s. b) Linear relationships between the square root of the sweep speed and the peak redox currents. Black line, oxidation current; red line, reduction current.

Fig. 6a shows the peak currents of the system using 0.31–5 mM potassium ferricyanide solution. The data follow Fick's first law, as the electron diffusion rate is proportional to the reactant concentration, the current increases with the reactant concentration, and the oxidation and reduction peak currents exhibit linear relationships with the reactant concentration. The correlation coefficients are 0.99056 and 0.99502 (Fig. 6b), respectively. The system exhibits good stability.

To verify the applicability of the proposed system, in school general chemistry lab course, we used it to determine the concentration of ascorbic acid in orange juice. In the experiment, four 20 ml orange juice samples ((Nongfu Spring, China) were prepared. One sample was unmodified, whereas in the other three, 10 ml of ascorbic acid standard solutions with different concentrations (0.1, 0.2 and 0.3 mg/mL) were added. In order to increase the conductivity of the solution, an appropriate amount of KCl was added to the orange juice to make up the concentration to 1 M. Then, the system was used to detect the cyclic voltammograms of the four samples (Fig. 7 a) over the sweep voltage range of 200–900 mV and at the sweep rate of 100 mV/s. In order to quantify ascorbic acid in

orange juice, the current corresponding to 550 mV was selected as the standard, because the samples contain ascorbic acid, a redox active substance in orange juice, and the oxidation of other substances in orange juice occurs, causing the current rise to >550 mV.[32]

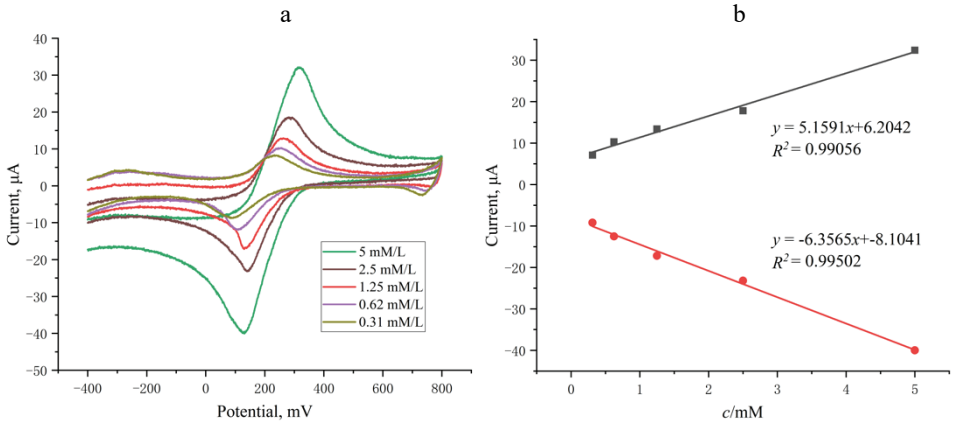

Fig. 6. a) Cyclic voltammograms of potassium ferricyanide solution at concentrations of 0.31–5 mM. b) Linear relationships between the potassium ferricyanide concentration and the redox peak currents. Black line, oxidation current; red line, reduction current.

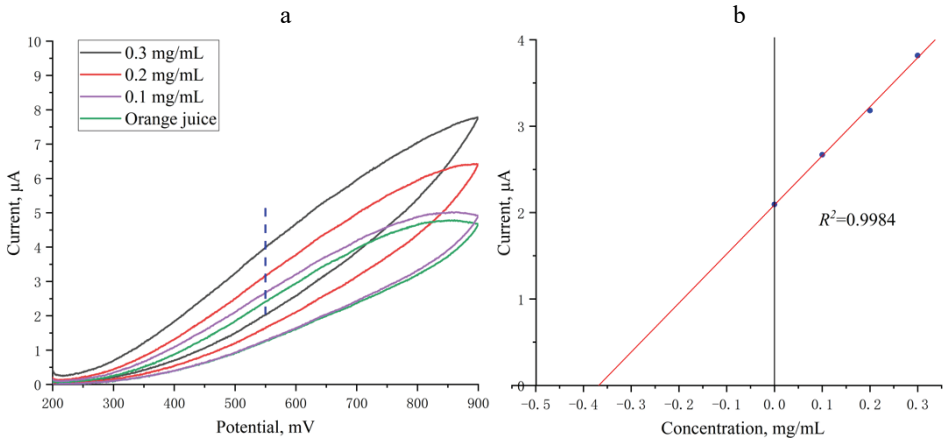

Fig 7. a) The original current traces of cyclic voltammetry experiments in four kinds of orange juice. b) The linearity of the oxidation current observed at 550 mV was compared with the linearity of the ascorbic acid standard solution.

The linear diagram of the current corresponding to 550 mV and that of the added ascorbic acid standard solution (Fig. 7b) is extrapolated to the zero current on the *x*-axis. The ascorbic acid concentration in the non-modified orange juice

sample is measured to be 0.367±0.012 mg/mL. The result obtained through the proposed system is comparable to the ascorbic acid value of 0.37 mg/mL prescribed by the orange juice nutrition panel.

CONCLUSIONS

This study designed a chemical CV detection system based on a smartphone, which combines a handheld CV detection module with wireless Bluetooth Low Energy and a smartphone. To compare the performances of the system and that of the traditional commercial constant potential studies were conducted, using potassium ferricyanide electrolyte solution, with satisfactory results. Additionally, compared with the traditional commercial potentiostat, this system exhibited the following advantages: 1) the system hardware test equipment has small volume and low cost (US $18.03), and it can be used as an educational tool with special value. In the experiment of determining the content of ascorbic acid in orange juice, the value obtained by using this system is almost consistent with the standard value. From the perspective of education, the operation of the system is very simple, which is conducive to students' learning and use. 2) In addition to educational purposes, the system will provide a cheap POCT platform for electrochemical analysis in some developing countries. 3) The software design of the system was based on the WeChat interface, which enabled broad software compatibility with different systems. However, the system only realizes cyclic voltammetry detection, and other electrochemical detection methods, such as square wave voltammetry and differential pulse voltammetry, that need to be further developed. In addition, the system can develop in the direction of the Internet of Things in the future, thus it will be a good choice to use cloud services to process and store data.

Acknowledgments. This work was supported by the National Natural Science Foundation of China Under Grant (No. 81371663) and National Natural Science Foundation of China (No. 61534003) and the "Six talents peaks" Project (SWYY-116), the "226 Engineering" Research Project of Nantong Government and the Opening Project of State Key Laboratory of Bioelectronics, Southeast University. This work was also supported by Nantong science and technology program (JC2020009); Ministry of Education in China Liberal arts and Social Sciences Foundation (17YJC890022), Natural Science Foundation of Jiangsu Province (BK20170448), Jiang Su Liberal arts and Social Sciences Foundation (17TYC003).

ИЗВОД

ДИЗАЈН И ПРИМЕНА ЈЕФТИНОГ ПРЕНОСИВОГ ПОТЕНЦИОСТАТА ЗАСНОВАНОГ НА АПЛИКАЦИЈИ WeChat

XIAOYAN SHEN[1,2], ZIQIANG LI[1], LEI MA[1], XIONGHENG BIAN[1], XINGSI CHENG[1] и XIONGJIE LOU[1]

[1]*School of Information Science and Technology, Nantong University, Nantong, 226019, China* и [2]*Nantong Research Institute for Advanced Communication Technologies, Nantong, 226019, China*

Потенциостат је кључни инструмент у развоју неког електрохемијског система, међутим његове димензије и висока цена значајно ограничавају његову примену. Да би се обезбедила алтернатива која је ценовно прихватљива за земље у развоју и областима са ограниченим ресурсима, у овој студији је дизајниран систем за електрохемисјко мерење заснован на паметним телефонима који користе Bluetooth мале потрошње за конверзију података из потенциостата отвореног софтвера базираног на PSoC-5LP. Апликација WeChat за паметне телефоне обезбеђује интерфејс за унос експерименталних параметара и за визуелизацију резултата у реалном времену. Електрохемијски систем за мерење базиран на паметном телефону је једноставног дизајна, малих димензија (10×3×0,3 cm^3) и ниске цене хардвера (18 $). Систем омогућава извођење цикличне волтаметрије као најчешће коришћене методе за електрохемијску детекцију и даје резултате који су поредиви са комерцијалним потенциостатима са нивоом грешке од 1,3%. У класичном школском експерименту електрохемијске детекције аскорбинске киселине у соку од поморанце измерена је вредност 0.367±0.012 mg/mL која је веома блиска стандардној референтној вредности од 0.37 mg/mL. Из тога следи да је овај систем јефтина и поуздана алтернатива потенциостату за истраживачки рад, образовање и интегрисани развој производа.

(Примљено 10. октобра, ревидирано 28. децембра 2021, прихваћено 28. фебруара 2022)

REFERENCES

1. C. Lefrou, P. Fabry, J. C. Poignet, *Electrochemistry: the basics, with examples*, Springer, Berlin, 2012, pp. 1–353 (https://doi.org/10.1007/978-3-642-30250-3)
2. P. Redon, A. Shahzad, T. Iqbal, W. Wijns, *Bioengineering* **8** (2021) 1 (https://doi.org/10.3390/bioengineering8020028)
3. P. Mohankumar, J. Ajayan, T. Mohanraj, R. Yasodharan, *Measurement* **167** (2021) 108293 (https://doi.org/10.1016/j.measurement.2020.108293)
4. S. Kurbanoglu, C. Erkmen, B. Uslu, *TrAC Trends Anal. Chem*. **124** (2020) 115809 (https://doi.org/10.1016/j.trac.2020.115809)
5. S. Campuzano, P. Yáñez-Sedeño, J. M. Pingarrón, *Sensors (Switzerland)* **20** (2020) 1 (https://doi.org/10.3390/s20185125)
6. T. Dobbelaere, P. M. Vereecken, C. Detavernier, *HardwareX* **2** (2017) 34 (https://doi.org/10.1016/j.ohx.2017.08.001)
7. D. A. Skoog, F. J. Holler, S. R. Crouch, *Principles of Instrumental Analysis*, Cengage Learning, Boston, MA, 2017 (ISBN 10 1-305-57721-3)
8. *Portable potentiostats*, Metrohm, http://www.metrohm-autolab.com/Products/Echem/PortablePot/PortablePotentiostats.html (accessed on Jan 4, 2021)
9. *Portable potentiostat*, BioLogic Science Instruments, http://www.bio-logic.net/en/products/potentiostat-galvanostat-eis/pg581-portable-potentiostatgalvanostat/ (accessed on Jan 4, 2021)
10. J. Wiencek, J. Nichols, *Expert Rev. Mol. Diagn*. **16** (2016) 415 (https://doi.org/10.1586/14737159.2016.1141678)

11. A. Warsinke, *Anal. Bioanal. Chem.* **393** (2009) 1393 (https://doi.org/10.1007/s00216-008-2572-0)
12. J. H. Nichols, *Contemp. Pract. Clin. Chem.*19 (2020) 323 (https://doi.org/10.1016/B978-0-12-815499-1.00019-3)
13. *Smartphone Users Worldwide 2016–2021*, Available online: https://www.statista.com/statistics/330695/number-of-smartphone-users-worldwide/ (accessed on Jan 10, 2021)
14. *Number of smartphone users worldwide from 2014 to 2020*, Statista, https://www.statista.com/statistics/330695/number-of-smartphone-users-worldwide/ (accessed on Jan 10, 2021)
15. D. Quesada-González, A. Merkoçi, *Biosens. Bioelectron*. **92** (2017) 549 (https://doi.org/10.1016/j.bios.2016.10.062)
16. D. Zhang, Q. Liu, *Biosens. Bioelectron.* **75** (2016) 273 (https://doi.org/10.1016/j.bios.2015.08.037)
17. S. Dutta, *TrAC, Trends Anal. Chem.* **110** (2019) 393 (https://doi.org/10.1016/j.trac.2018.11.014)
18. N. Seddaoui, A. Amine, *Talanta* **30** (2021) 122346 (https://doi.org/10.1016/j.talanta.2021.122346)
19. A. Ainla, M. P. S. Mousavi, M.-N. Tsaloglou, J. Redston, J. G. Bell, M. T. Fernández--Abedul, G. M. Whitesides, *Anal. Chem.* **90(10** (2018) 6240 (https://doi.org/10.1021/acs.analchem.8b00850)
20. J. Li, P. B. Lillehoj, *ACS Sens.* **6** (2021) 1270 (https://pubs.acs.org/doi/10.1021/acssensors.0c02561)
21. V. Caratelli, A. Ciampaglia, J. Guiducci, G. Sancesario, D. Moscone, F. Arduini, *Biosens. Bioelectron.* **165** (2020) 112411 (https://doi.org/10.1016/j.bios.2020.112411)
22. D. Ji, L. Liu, S. Li, C. Chen, Y. Lu, J. Wu, Q. Liu, *Biosens. Bioelectron.* **98** (2017) 449 (https://doi.org/10.1016/j.bios.2017.07.027)
23. J. Monge, O. Postolache, A. Trandabat and S. Macovei, in *2020 International Conference and Exposition on Electrical And Power Engineering (EPE)*, 2020, pp. 695–698 (https://doi.org/10.1109/EPE50722.2020.9305567)
24. *Android vs iOS Development: Pros and Cons of Each Platform*, https://scand.com/company/blog/android-vs-ios-development (accessed on Jan 20, 2021)
25. *32-bit Arm Cortex-M3 PSoC 5LP*, https://www.cypress.com/products/32-bit-arm-cortex-m3-psoc-5lp (accessed on March 5, 2021)
26. *Operational Amplifier (Opamp)*, https://www.cypress.com/documentation/component-datasheets/operational-amplifier-opamp (accessed on March 5, 2021)
27. *Trans-Impedance Amplifier (TIA)*, https://www.cypress.com/documentation/component-datasheets/trans-impedance-amplifier-tia (accessed on March 5, 2021)
28. A. J. Bard, L. R. Faulkner, *Fundamentals and applications: Electrochemical methods*, John Wiley & Sons, Hoboken, NJ, 2001, pp. 580–632 (ISBN 978-0-471-04372-0)
29. M. D. M. Dryden, A. R. Wheeler, *PloS One* **10** (2015) e0140349 (https://doi.org/10.1371/journal.pone.0140349)
30. A. Fick, *Ann. Phys.* **170** (1855) 59 (https://doi.org/10.1002/andp.18551700105)
31. N. S. Neghmouche, T. Lanez, *Int. Lett. Chem. Phys. Astron.* (2013) 37 (https://doi.org/10.18052/www.scippress.com/ILCPA.9.37).
32. D. King, J. Friend, J. Kariuki, *J. Chem. Educ.* **87** (2010) 507 (http://pubs.acs.org/jchemeduc).

Journal of the Serbian Chemical Society
JSCS@tmf.bg.ac.rs • www.shd.org.rs/JSCS

J. Serb. Chem. Soc. *87* (5) 615–628 (2022)
JSCS–5545

Original scientific paper
Published 2 February 2022

Optimization of chromatographic separation of aripiprazole and impurities: Quantitative structure–retention relationship approach

BOJANA SVRKOTA, JOVANA KRMAR, ANA PROTIĆ, MIRA ZEČEVIĆ and BILJANA OTAŠEVIĆ*

Department of Drug Analysis, University of Belgrade - Faculty of Pharmacy, Vojvode Stepe 450, 11221 Belgrade, Serbia

(Received 9 July, revised 21 October, accepted 3 November 2021)

Abstract: A new optimization strategy based on the mixed quantitative structure–retention relationship (QSRR) model is proposed for improving the RP-HPLC separation of aripiprazole and its impurities (IMP A-E). Firstly, experimental parameters (EPs), namely mobile phase composition and flow rate, were varied according to Box–Behnken design and thereafter, an artificial neural network (ANN) as a QSRR model was built correlating EPs and selected molecular descriptors (ovality, torsion energy and non-1,4-van der Waals energy) with the log-transformed retention times of the analytes. Values of the root mean square error (*RMSE*) were used for an estimation of the quality of the ANNs (0.0227, 0.0191 and 0.0230 for the training, verification and test set, respectively). The separations of critical peak pairs on chromatogram (IMP A-B and IMP D-C) were optimized using ANNs for which the EPs served as inputs and the log-transformed separation criteria *s* as the outputs. They were validated by application of leave-one-out cross-validation (*RMSE* values 0.065 and 0.056, respectively). The obtained ANNs were used for plotting response surfaces upon which the analyses chromatographic conditions resulting in optimal analytes retention behaviour and the optimal values of the separation criteria *s* were defined. The optimal conditions were 54 % of methanol at the beginning and 79 % of methanol at the end of gradient elution programme with a mobile phase flow rate of 460 μL min^{-1}.

Keywords: gradient elution; high performance liquid chromatography; artificial neural networks.

INTRODUCTION

In various fields of pharmaceutical research, high performance liquid chromatography (HPLC) is an indispensable tool for analytical testing. Due to their

* Corresponding author. E-mail: biljana.otasevic@pharmacy.bg.ac.rs
https://doi.org/10.2298/JSC210709092S

widespread use, there is a pronounced need for efficient and improved method development. Whereby the numerous factors affecting HPLC separation, including a large amount of available equipment and the determination of the conditions which ensure optimal method performance, can be extremely challenging. For improving a systematic survey of experimental space for optimal conditions, software-dependent tools can accelerate the development of a given method.[1] The traditionally predominant approach was based on the "trial and error" concept, which was exceedingly time and resources consuming. Nowadays, this approach is considered outdated and is efficiently suppressed by the emergence of more sophisticated chemometric tools. Since chemometric tools are based on reliable mathematical-statistical principles, the experimental work is successfully planned in advance and the resource requirements for its execution are reduced.[2] Chemometric techniques mainly used in HPLC method optimization are design of experiments (DoE) and quantitative structure–retention relationships (QSRR) approach. Within the DoE framework, analyte retention behaviour is mathematically associated with the values of experimental parameters. However, with the help of established DoE models, it is possible to develop an optimal method only for substances for which retention data have been obtained through experiments. In order to achieve a superior predictive dimension of applied modelling technique, it is necessary to involve the chemical–physical properties that are known independently of experimental work. This can be provided with QSRR studies.[3] Explicitly, QSRR models have the possibility of relating chromatographic retention behaviour to numerically expressed chemical information embedded in the molecule structure in the form of molecular descriptors (MDs).[4] This implies that the most common QSRR models are limited to predicting the retention behaviour only at constant values of the experimental parameters (EP). Therefore, when QSRR studies are motivated by practical goals, such as method optimization, EPs have to be included in the model as relevant variables (predictors or inputs).[5]

Models referred to as mixed QSRR models are more complex than the aforementioned classical ones since they explain retention behaviour in context of both, EPs and MDs.[4,6] A significant part of QSRR model building is the technique used for determining the mathematical relationship between MDs and retention behaviour. The most widely applied model-building techniques are multiple linear regression (MLR) and artificial neural networks (ANN).[3] With regards to the introduction of additional inputs, it is reasonable to expect that more sophisticated analytical tools should be used. At the same time, when the specific chromatographic system of interest comprises analytes with different polarities and a gradient elution program is consequently applied, nonlinear behaviour of the system is expected.[7] In such cases, nonlinear tools such as ANN are preferable for QSRR model building. ANN is a biologically inspired machine learning algorithm that mimics the functioning of the human brain.[8] In comparison to

the classical statistical methods, ANN does not require previous knowledge about mathematical relationships between dependent and independent variables and has better predictive abilities.[4,5,8]

Difficulties in substantial method development for quality assessment purposes were present during the separation of aripiprazole (AR) and its impurities, the structures of which are presented in Fig. 1. Generally, impurities that can originate from raw materials, arise during drug product manufacturing (process-related), or appear as a result of drug degradation can impair the quality of an active substance or product.[9,10] Therefore, a reliable and optimized method for analysis of AR and its impurities had to be introduced. In the literature, IMP A, B, D and E are recognized as degradation products that can arise from various stress conditions,[11–13] while IMP A–D are also identified as process-related.[14] A literature survey revealed that HPLC methods were dominantly developed for the separation of AR and its known impurities.[13–20] It was noticed that octyl (C8) or octadecyl (C18) are the most commonly applied stationary phases. Unfortunately, in all these methods, the overall quality of the chromatographic separations was not quite adequate, because either the peaks of IMP E and AR were significantly close to each other or/and IMP E eluted after the peak of the active pharmaceutical ingredient (API).[13–16]

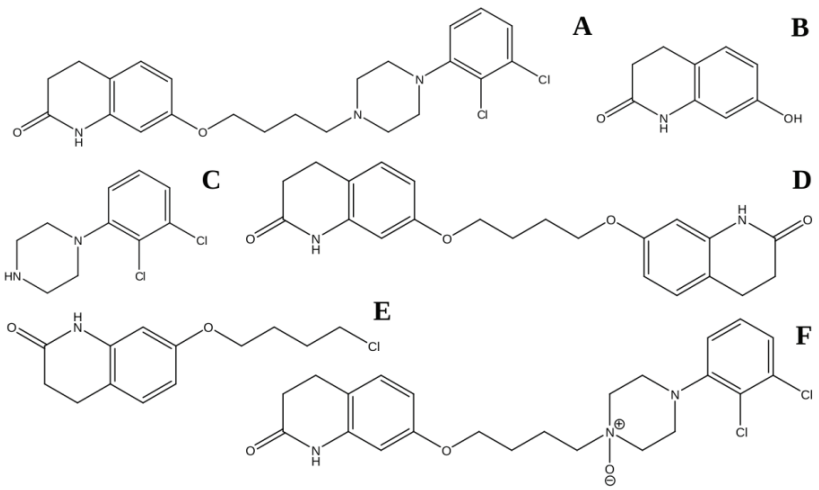

Fig. 1. Chemical structures of: A) aripiprazole, B) impurity A, C) impurity B, D) impurity C, E) impurity D and F) impurity E.

In practice, with such an elution, the tail of the API peak may overlap with a much smaller peak of the following impurity, which eventually occurs with long lifecycle methods and/or during problematic inter-laboratory analytical method transfer and consequently affects the identification and quantification impurity as

well as the estimation of the overall AR quality. Therefore, separation conditions with different selectivity could be beneficial. In order to meet these demands, an RP-HPLC method was developed for the separation of AR and its impurities using a nonconventional stationary phase, a phenyl-hexyl column, able to produce diverse selectivity. A gradient elution program was employed for overcoming the difficulties in separation of molecules with different log *D* and log *P* features (Table S-I of the Supplementary material to this paper). Such a situation was also recognized by other authors who attempted to address this issue by using different HPLC modes starting from gradient elution in RP-HPLC,[13,16,18–20] then with micellar[6] and ion-pair chromatography.[14,15] The retention mechanisms involved into later separation processes are more complex due to the application of additives to the mobile phase and the consequent presence of secondary equilibriums. In addition, from the practical point of view, these chromatographic systems are considered as less attractive due to prolonged system equilibration and significantly reduced column lifetime. On the contrary, the advantage of the RP mode is reflected in its simpler retention mechanism that enables easier interpretation, better understanding and faster method optimization.

The QSRR strategy was applied in two reported studies. Nikolić *et al.* built a classical QSRR model in order to predict the retention times of impurities while central composite design was used for defining the optimal chromatographic conditions.[21] In such a way, the overall optimization method concept did not rely on the QSRR model; rather its predicting ability was the focus. Snoj Ekmečić *et al*. applied a solvatic retention model.[18] Although this approach gives insight into the physical meaning of the separation process, it has a lower ability in defining the experimental space compared to QSRR with computed MDs. Bearing in mind the optimization of the chromatographic method was the principal goal, the use of QSRR with computed MDs is considered the tool of choice.[3,7] To the best of knowledge, this is the first research where a mixed QSRR-ANN model was used as an optimization tool for the development of a superior method for the separation of aripiprazole and its impurities.

EXPERIMENTAL

Chemicals and reagents

All chemicals used were of analytical grade. Reference standard substances of aripiprazole (7-[4-[4-(2,3-dichlorophenyl)piperazin-4-ium-1-yl]butoxy]-3,4-dihydro-1*H*-quinolin-2-one) and impurities IMP A (7-hydroxy-3,4-dihydro-1*H*-quinolin-2-one), IMP B (1-(2,3-dichlorophenyl)--piperazine), IMP C (1,4-bis[[3,4-dihydro-2(1*H*)-quinolinone]7-oxy]butane), IMP D (7-(4-chlorobutoxy)-3,4-dihydro-1*H*-quinolin-2-one) and IMP E (7-[4-[4-(2,3-dichlorophenyl)-1-oxidopiperazin-4-ium-1-yl]butoxy]-3,4-dihydro-1*H*-quinolin-2-one), purchased from Orchid Chemicals & Pharmaceuticals (Chennai, India), were utilized for the preparation of the working mixture solution for chromatographic analyses. The mobile phase was composed of LC–MS grade methanol (MeOH, Fluka, Switzerland), water HPLC grade purified with simplicity 185 water purification system (Millipore, USA) and acetic acid analytical grade (Sigma–Aldrich).

Preparation of standard and work solutions

The standard stock solution of Aripiprazole was prepared by dissolving the respective amount of the standard substance in MeOH to attain a concentration of 2 mg mL^{-1}. Dissolving was ultrasonically assisted for 5 min using an ultrasonic bath (Fungilab, Barcelona, Spain). For preparing the individual standard stock solutions of the impurities, the respective amounts were dissolved in MeOH assisted with ultrasonication for 5 min. The solutions of the impurities were attained in concentrations of 20 μg mL^{-1}. The working mixture solution was prepared by transferring 1 mL of each standard solution to a 10-mL volumetric flask and filling to volume with a mixture of aqueous part of the mobile phase and MeOH (50:50). The concentration of working solution was 200 μg mL^{-1} of aripiprazole and 2 μg mL^{-1} of each of impurities.

Chromatographic conditions and equipment

A Thermo Accela UHPLC system (Thermo Fisher Scientific Inc., USA) equipped with an autosampler, pump and PDA detector was used for the experimental runs. The chromatographic separations were performed with a Kinetex RP-phenyl-hexyl column (100 mm×4.6 mm, 2.6 μm, Phenomenex Inc., USA). The column temperature was set at 25 °C and the UV detection wavelength was 254 nm. The mobile phase consisting of a methanol/water mixture was composed according to the Box–Behnken design of experiments (Table I) created using Design-Expert 7.0.0 software (Stat-Ease Inc., USA). The pH of the aqueous phase was adjusted to 4.7 using the acetic acid and a pH-meter with a combined electrode, PHM 220 (Radiometer, Denmark). The mobile phase was freshly prepared and filtered before use through Whatman 47 mm Glass/mesh system with membrane carrier and a 0.22 μm pore size membrane filter (Kinesis Inc., USA). The elution program consisted of a 6 min isocratic elution with the initial MeOH (s_{MeOH}) and water mixture, followed by a 1 min gradient that reached final MeOH (e_{MeOH}) and water content that was maintained until the end of the analysis. The chromatograms were gathered using ChromQuest 5.0 software (Thermo Fisher Scientific Inc., USA).

QSRR model development

For QSRR model building, MDs and EPs were determined as independent variables while the dependent variable was the log-transformed retention time of the studied analytes (log t_r). The structures of the molecules were first generated with ChemDraw Ultra 7.0 software (Perkin Elmer, USA). Then, they were utilized for an estimation of the molecular p*K*a and ionization forms using MarvinView 6.1.6 (ChemAxon Ltd., Hungary). Structure energy minimization and computation of MDs were provided with Chem3D® Ultra 7.0 software (Cambridge Soft Corporation, USA). Computation of MDs was performed after minimizing the energy of solute structures *via* the semi-empirical MOPAC/PM3 method. The computations resulted in total of 37 MDs that included: dipole length – *DPLL*; electronic energy – *ElcE;* formal charge – *Charge;* HOMO energy – *HOMO;* LUMO energy – *LUMO;* repulsion energy – *NRE*; total energy –*TotE;* Balaban index – *BIndx*; cluster count – *ClsC*; Connolly accessible area – *SAS*; Connolly molecular area – *MS*; Conolly solvent–excluded volume – *SEV*; diameter – *Diam*; exact mass – *Mass*; molecular topological index – *TIndx*; molecular weight – *MW*; ovality – *O*; principle moment of inertia *X*, *Y* and *Z* – *PMIX*, *PMIY*, *PMIZ*; radius – *Rad*; shape attribute – *ShpA*; shape coefficient – *ShpC*; sum of degrees – *SDeg*; sum of valence degrees – *SVDe*; total connectivity – *TCon*; total valence connectivity – *TVCon*; Wiener index – *WIndx*; bend energy – *Eb*; molar refractivity – *MR*; non–1,4–VDW E – *Ev*; partition coefficient (octanol/water) – *C* log *P*; stretch–bend energy – *Esb*; stretch energy – *Es*;

torsion energy – *Et*; VDW 1,4 energy – *E14*; total energy – *E* (Table S-II of the Supplementary material). When calculating the values of MDs, the percentage of existing ionization forms present at the mobile phase pH was taken into account. Descriptors were selected taking into account correlation coefficient. That is, in order to avoid multicollinearity, one of two variables were discarded if the correlation between them was higher than 0.9 ($|r| > 0.9$). The MDs correlation was evaluated using Microsoft Office Excel 2010 (Microsoft, WA). Furthermore, MDs with the highest impact on the system behaviour were identified using MLR, with the stepwise inclusion of independent variables in the model. MLR was performed with SPSS software (SPSS, USA).

ANN was used as a tool for *QSRR* model building as well as for modelling of separation criteria (*s*). Multilayer perception (MLP) feed forward neural networks were used consisting of neurons (processing units) arranged in 3 layers: input, hidden and output and connected by bonds with assigned weights. The networks were trained with a backpropagation algorithm. Logistic transformation was applied in the second and third layer. The model validity was estimated with root mean square error (*RMSE*). An increase in the *RMSE* value indicated overfitting which was a signal to stop the network training. Regression statistics was used to evaluate model fitting to experimentally obtained data. Separate MLPs were trained to model separation criteria ($s_{B\text{-}A}$, $s_{C\text{-}D}$). MLPs were trained on a data set consisting of 13 cases obtained during BBD. Each MLP included 3 inputs (EPs), 2 hidden neurons, and 1 output (log $s_{B\text{-}A}$ or log $s_{C\text{-}D}$). In the MLP used for modelling log $s_{B\text{-}A}$, logistic transformation was applied in the hidden and output layer. For MLP used for log $s_{C\text{-}D}$ estimation, logistic transformation was used in the second and hyperbolic transformation in the third layer. Leave-one-out cross-validation (LOO-CV) was used for an estimation of the generalization ability of the algorithms, which was evaluated using LOO-CV *RMSE*. All ANN models were developed and validated with Statistica Neural Network software (StatSoft Inc., USA).

RESULTS AND DISCUSSION

During the development process of the HPLC method, the type of stationary phase and the composition of eluent were selected before optimization of the method. The domain of chromatographic parameters was selected with respect to the different physicochemical characteristics (values of log *P* and log *D* taking into account the respective pH) of the investigated analytes (Table S-I). Gradient elution was introduced to move strongly retained compounds, while having the least hydrophobic analytes well resolved. Additionally, an inspection of chemical structures of all compounds (Fig. 1) revealed that each of them contained at least one aromatic ring for which it was reasonable to expect that π-electrons could potentially be involved in the separation process. Therefore, a phenyl-hexyl column, the retention mechanism of which is based on π–π and hydrophobic interactions, was considered as the proper choice for the separation of this type of analyte.[22] Following the selection of column, a thorough review of the constituents of the mobile phase was performed. It has already been proven that acetonitrile can suppress π–π interactions.[23] Therefore, MeOH was considered as the organic solvent of choice. The additional benefit of using MeOH was also reflected in its toxicological profile since MeOH is a less environmentally hazardous organic solvent compared to acetonitrile.[24]

Given that the pH value of the aqueous phase also influences the separation process of ionisable compounds, the working pH value was set. The preliminary experiments revealed that a pH of the aqueous phase set at 4.7 contributed to better separation of the compounds compared to the usually applied pH 3.0, due to a shift in the ionization state of IMP E. Molecules ionization states under these conditions are presented in Table S-I. All these considerations pointed out that the following EPs are the most significant for the intended method development: MeOH content at the start of the gradient elution program (s_{MeOH}) within range 50–60 %; MeOH content at the end of gradient elution program (e_{MeOH}) within the 75–85 % and the mobile phase flow rate (F) varied within 400–500 μL min^{-1}.

In order to provide a proper description of experimental space, DoE methodology was applied. The response surface design by means of three level Box–Behnken design (BBD) was favoured as more economical and efficient due to smaller number of runs comparing to other optimization designs (such as central composite design).[25] BBD is rotatable design meaning that all the experimental points are equally distant from the central point and lie on a sphere when presented in 3D space.[8,26] The number of experiments to be performed according to BBD in the presented research resulted in a total of 13 runs (Table I). Although the value of DoE in method optimization is unquestionable, the obtained mathematical models are not completely in agreement with experimental outcomes, which is reflected in the coefficients of determination, R^2 (Table II). Therefore, the data gathered using DoE was further implemented into QSRR-ANN model.[8]

TABLE I. Experimental plan with EPs and experimentally obtained responses

Content, %		Flow rate, mL min^{-1}	Retention time, min						s / min	
s_{MeOH}	e_{MeOH}		IMP A	IMP B	IMP D	IMP C	IMP E	AR	B-A	C-D
50	75	450	2.50	3.63	11.93	13.19	15.08	18.58	0.977	0.860
60	75	450	2.37	2.96	10.77	12.23	14.20	17.25	0.161	1.019
50	85	450	2.50	4.00	11.00	11.54	12.60	15.94	1.156	0.096
60	85	450	2.37	2.96	9.99	10.54	11.38	13.84	0.152	0.273
50	80	400	2.82	4.46	12.34	13.36	15.09	19.47	1.128	0.507
60	80	400	2.79	3.45	11.40	12.53	14.22	18.22	0.397	0.669
50	80	500	2.26	3.49	11.01	11.81	13.13	16.52	1.010	0.389
60	80	500	2.23	2.79	10.27	11.19	12.51	15.56	0.141	0.481
55	75	400	2.48	3.76	13.36	15.49	18.57	23.32	0.846	1.932
55	85	400	2.77	3.65	10.91	11.45	12.44	15.56	0.654	0.197
55	75	500	2.19	3.09	11.74	13.42	15.78	19.50	0.367	1.238
55	85	500	2.19	3.09	10.24	10.76	11.66	14.50	0.329	0.121
55	80	450	2.44	3.37	11.21	11.71	13.63	17.30	0.463	0.460

The overall goal of this study was to develop an optimization strategy that would enable the appropriate chromatographic separation of all peaks in the shortest possible time. At the same time, it was necessary to avoid non-retention

behaviour of the first eluting peak corresponding to IMP A. Accordingly, the following responses were selected. The total analysis time was estimated according to the retention time of the last eluting peak (t_{rAR}). The retention time of IMP A (t_{rIMPA}) was monitored to establish separation from the peak of the mobile phase. The quality of the separation between neighbouring peaks of analytes was estimated using the separation criterion *s* that has lately been recognized as a superior descriptor of separation in gradient elution methods known for susceptibility to baseline variations and peak shape irregularities.[27] This criterion represents the difference between the time when the first peak ends (t_{r1e}) and the time when next peak begins (t_{r2b}). This can be defined with following equation: $s = = t_{r2b}–t_{r1e}$. In this respect, the baseline separations between IMP A-B and IMP D-C peak pairs were assessed according to the calculated values of $s_{B\text{-}A}$ and $s_{C\text{-}D}$, respectively (Table I) with an appropriate acceptance criterion $s > 0$. The retention times of interest were modelled using QSRR-ANN, and *s* criteria were modelled using ANNs specially developed for the purpose.

TABLE II. Statistically evaluated BBD mathematical models using coded factor values; Equations obtained using Design Expert 7.0.0 software

Mathematical model	R^2	Adj. R^2	Pred. R^2
$t_{rIMPA} = 2.45 – 0.25F$	0.8300	0.8179	0.7563
$\log s_{B\text{-}A} = -0.34 – 0.37s_{MeOH} – 0.14F$	0.9124	0.8989	0.8508
$\log s_{C\text{-}D} = -0.34 – 0.093s_{MeOH} – 0.44e_{MeOH} – 0.083F$	0.9294	0.9118	0.8604
$\log t_{rAR} = 1.23 – 0.058e_{MeOH} – 0.031F$	0.7428	0.7032	0.5800

In order to ensure a reliable building of a QSRR model, selection of MDs was carefully driven. The types of MDs were selected using general knowledge of the RP-HPLC separation mechanism. From initially calculated 37 MDs, 13 MDs (*DPLL*, *HOMO*, *LUMO*, *SAS*, *O*, *PMIX*, *ShpC*, *TVCon*, *Ev*, *C log P*, *Esb*, *Es* and *Et*) were retained based on the level of mutual correlation of the MDs ($|r| < 0.9$). This MDs selection procedure was applied in order to avoid multicollinearity and overfitting of the obtained model. From the pool of all independent variables (MDs and EPs), the statistically influential inputs were extracted using MLR. The set of the most significant independent variables indicated that the chromatographic system was dominantly influenced by 3 EPs (s_{MeOH}, e_{MeOH}, *F*) and 4 MDs (*O*, *Ev*, *ShpC*, *Et*). Further inspection of the MDs values indicated that *ShpC* had identical value for 3 of the 6 analytes, which would eventually negatively affect the training of the ANN. Since the quality and predicting ability of the model can be preserved in reduced QSRR when selection of attributes is good,[27] it was decided to remove *ShpC* from the data set.

The aforementioned independent variables (s_{MeOH}, e_{MeOH}, *F*, *O*, *Et*, *Ev*) were used as inputs for the MLP, while log-transformed retention times of the analytes ($\log t_r$) represent output variable. Thus, the QSRR-ANN architecture consisted of 6

neurons in the input, 4 neurons in the hidden and 1 neuron in the output layer. It was decided to use the multilayer perception ANN due to its proven simplicity and efficiency. MLP is a feed forward ANN trained with a backpropagation algorithm meaning that it computes the error and adjusts the weights backwards through layers, from output to inputs, until the error is minimized.[4] The output was transformed *via* log-function in order to provide normal distribution of the outcome variable. Even though normal distribution of the measured data is not necessary for an ANN to function, in some cases it can improve the performance of a network. Engagement of log-transformation, with the ability of narrowing the response value interval, resulted in significantly better learning ability of an ANN, lower errors and satisfying overall statistical performance.[6] The network was trained using 78 cases (13 cases of BBD for each of the 6 compounds), divided into training, verification, and test set. The training set contained 52 cases, and the verification and test sets contained 13 cases each. The training and verification sets were formed randomly, while the test set contained only cases related to IMP C. This was done intentionally, so that the real predictive ability of the developed model can be estimated for an analyte previously unseen by the network. The learning rate of the ANN was set to 0.3 and momentum to 0.1. The ANN weights are presented in Table S-III of the Supplementary material. The predictive power of the obtained network was validated using internal and external validation.[28] IMP C was used for the external validation and cross-verification with verification data set was applied as an internal type of validation. Low and balanced *RMSE* values indicated good predictive ability of the network. Furthermore, regression statistics and the correlation coefficient values of the model indicated good fitting of the predicted model to experimental data (Table III).[29]

TABLE III. Statistical performance of the QSRR-ANN developed model

Parameter	Training log (t_r / min)	Verification log (t_r / min)	Test log (t_r / min)
Data mean	0.8634	0.8902	1.0859
Data *S.D.*	0.3442	0.3759	0.0462
Error mean	–0.0005	0.0072	0.0154
Error *S.D.*	0.0229	0.0184	0.0178
Abs E. mean	0.0176	0.0144	0.0194
S.D. ratio	0.0665	0.0490	0.3858
Correlation	0.9978	0.9989	0.9253
RMSE	0.0227	0.0191	0.0230

Considering that $s_{B\text{-}A}$ and $s_{C\text{-}D}$ could not be estimated by the means of the QSRR-ANN model, they were evaluated using other ANNs. Although it is uncommon for ANNs to model small data sets, they still can be considered in circumstances where classical regression modelling tools are not applicable. Due to the questionable reliability of such ANN, the quality of the model needs

verification applying robustification methods. One of these methods refers to *V*-fold cross-validation, where *V* is the number of folds. Special case where number of cases is equal to number of folds refers to LOO-CV.[30] In this research, the LOO-CV *RMSE* values were 0.0648 and 0.0560 for log $s_{B\text{-}A}$ and log $s_{C\text{-}D}$, respectively (Table S-IV of the Supplementary material). These results indicate good reliability of the whole dataset of the obtained model. Since none of two peak pairs was favoured, the most similar *s* values, still reflecting baseline separation, were striven for. The established ANNs (Tables S-V and S-VI of the Supplementary material) were further used to obtain response surfaces that were then used for visual inspection of the influence of EPs on the responses (Fig. 2).

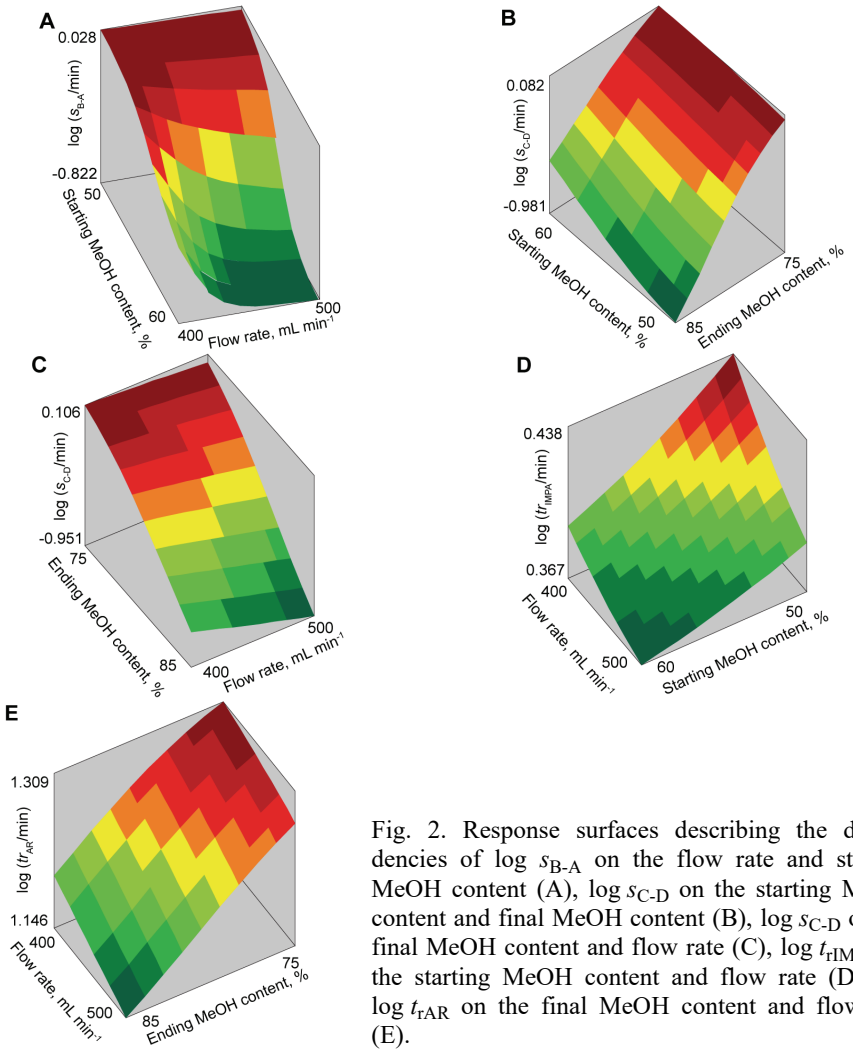

Fig. 2. Response surfaces describing the dependencies of log $s_{B\text{-}A}$ on the flow rate and starting MeOH content (A), log $s_{C\text{-}D}$ on the starting MeOH content and final MeOH content (B), log $s_{C\text{-}D}$ on the final MeOH content and flow rate (C), log t_{rIMPA} on the starting MeOH content and flow rate (D) and log t_{rAR} on the final MeOH content and flow rate (E).

Choosing the optimal EPs values was a challenging task due to the opposed influences they demonstrated towards all the observed responses. The lower values of all EPs enabled satisfactory baseline separations of neighbouring peaks to be achieved. On the contrary, higher EPs values reduced the analysis time. Among the EPs, the flow rate had a very low influence on both separation criteria (Fig. 2). In the region of the highest EPs values where good peak separation was preserved, the selection of optimal conditions was made mainly to suite the total analysis time. F values higher than 460 μL min^{-1} disrupt an adequate separation between critical peak pairs. Thus, even though this reduces the analysis runtime, a flow rate set to 460 μL min^{-1} was considered as optimal. The factor e_{MeOH} had a greater influence on $s_{C\text{-}D}$ and the maximal value that preserves a good $s_{C\text{-}D}$ was defined to be 79 %. Optimal s_{MeOH} was chosen bearing in mind that values greater than 54 % rapidly decreased $s_{B\text{-}A}$. Furthermore, the selected values of s_{MeOH} and flow rate resulted in satisfactory t_{rIMPA} values. Finally, the values of the EPs providing appropriate meeting of all method optimization goals were: s_{MeOH} = 54 %, e_{MeOH} = 79 % and F = 460 μL min^{-1}. The predicted t_r values were 2.46, 3.31, 12.60, 11.12, 13.89 and 17.83 min for IMP A-E and AR, respectively, while the predicted s values were $s_{B\text{-}A}$ = 0.630 min and $s_{C\text{-}D}$ = 0.591 min. The obtained results were in accordance with experimentally obtained values for t_r (2.49, 3.48, 12.34, 11.37, 13.85 and 17.47 min for IMP A-E and AR, respectively) and s ($s_{B\text{-}A}$ = 0.560 min, $s_{C\text{-}D}$ = = 0.580 min), as presented in Fig. 3.

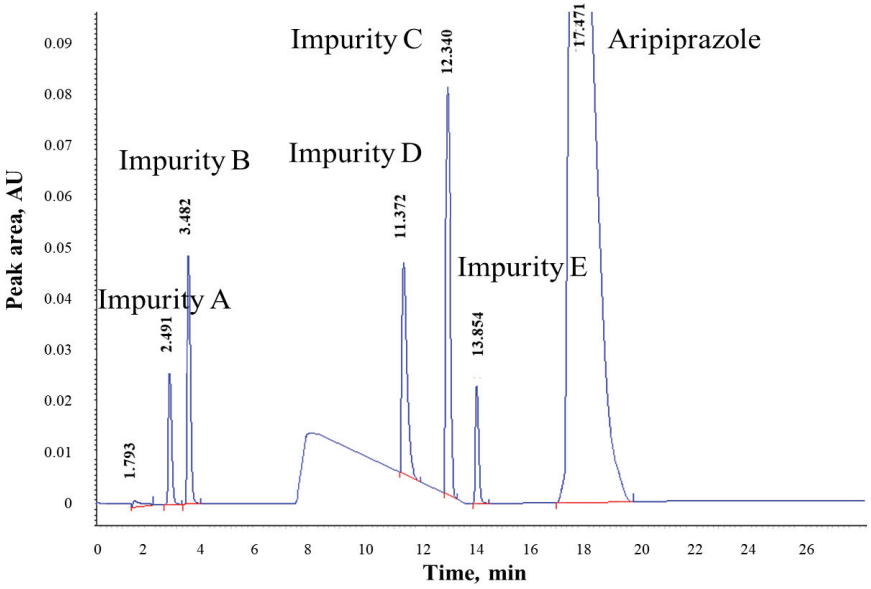

Fig. 3. Chromatogram recorded under optimal conditions.

CONCLUSIONS

An improved RP-HPLC method intended for the evaluation the purity of AR was developed using a mixed QSRR-ANN model as an optimization tool. The experimental conditions providing adequate separations in a reasonable analysis time were determined (s_{MeOH} = 54 %, e_{MeOH} = 79 % and F = 460 μL min^{-1}). Furthermore, the demonstrated good predictive power of the built models enable future spreading of the current research to other AR related topics, meaning that it is reasonable to suggest that the noted chromatographic behaviour predictions could serve as a starting point in development of analytical procedures aimed at AR stability studies as well as investigations of AR in different biological samples.

SUPPLEMENTARY MATERIAL

Additional data and information are available electronically at the pages of journal website: https://www.shd-pub.org.rs/index.php/JSCS/article/view/10939, or from the corresponding author on request.

Acknowledgment. This research was funded by the Ministry of Education, Science and Technological Development of the Republic of Serbia through a Grant Agreement with University of Belgrade – Faculty of Pharmacy No: 451-03-9/2021-14/200161.

ИЗВОД

ОПТИМИЗАЦИЈА ХРОМАТОГРАФСКОГ РАЗДВАЈАЊА АРИПИПРАЗОЛА И НЕЧИСТОЋА: ПРИСТУП КВАНТИФИКОВАЊА ОДНОСА СТРУКТУРЕ И РЕТЕНЦИОНОГ ПОНАШАЊА

БОЈАНА СВРКОТА, ЈОВАНА КРМАР, АНА ПРОТИЋ, МИРА ЗЕЧЕВИЋ и БИЉАНА ОТАШЕВИЋ

Катедра за аналитику лекова, Универзитет у Београду – Фармацеутски факултет, Војводе Степе 450, 11221 Београд

Нова оптимизациона стратегија заснована на грађењу мешовитих модела за квантификовање односа структуре и ретенционог понашања (QSRR) предложена је за унапређење RP-HPLC раздвајања арипипразола и његових нечистоћа (IMP A-E). Експериментални параметри (EP), састав мобилне фазе и брзина протока, варирани су најпре у складу са Box–Behnken дизајном, а затим је награђена вештачка неуронска мрежа као QSRR модел који повезује EP и одабране молекуларне дескрипторе (овалност, торзиона енергија и не-1,4-ван дер Валсова енергија) са логаритамски трансформисаним ретенционим временом аналита. Вредности средње квадратне грешке (*RMSE*) коришћене су за процену квалитета мреже (0,0227, 0,0191 и 0,0230 за тренинг, верификацију и тест сет, редом). Раздвајање критичних парова пикова на хроматограму (IMP A-B и IMP D-C) оптимизовано је коришћењем мрежа за које су EP послужили као улази, а логаритамски трансформисани критеријуми сепарације *s* као излази. Ове мреже су валидиране применом унакрсне валидације изостанка (*RMSE* вредности, редом, 0,065 и 0,056). На основу награђених мрежа, конструисани су дијаграми површина одговора чијом анализом су дефинисани услови при којима се постиже оптимална ретенција аналита, односно вредности критеријума сепарације *s*, а који су подразумевали 54 % метанола на почетку и 79 % на крају програма градијентног елуирања са брзином протока мобилне фазе од 460 mL min^{-1}.

(Примљено 9. јула, ревидирано 21. октобра, прихваћено 3. новембра 2021)

REFERENCES

1. F. T. Mattrey, A. A. Makarov, E. L. Regalado, F. Bernardoni, M. Figus, M. B. Hicks, J. Zheng, L. Wang, W. Schafer, V. Antonucci, S. E. Hamilton, K. Zawatzky, C. J. Welch, *Trends Anal. Chem.* **95** (2017) 36 (https://doi.org/10.1016/j.trac.2017.07.021)
2. P. K. Sahu, N. R. Ramisetti, T. Cecchi, S. Swain, C. S. Patro, J. Panda, *J. Pharm. Biomed. Anal.* **147** (2018) 590 (https://doi.org/10.1016/j.jpba.2017.05.006)
3. P. R. Haddad, M. Taraji, R. Szücs, *Anal Chem.* **93** (2020) 228 (https://doi.org/10.1021/acs.analchem.0c04190)
4. J. Golubović, A. Protić, B. Otašević, M. Zečević, *Talanta* **150** (2016) 190 (https://doi.org/10.1016/j.talanta.2015.12.035)
5. A. A. D'Archivio, M. A. Maggi, F. Ruggieri, *J. Sep. Sci.* **37** (2014) 1930 (https://doi.org/10.1002/jssc.201400346)
6. J. Krmar, M. Vukićević, A. Kovačević, A. Protić, M. Zečević, B. Otašević, *J. Chromatogr., A* **1623** (2020) 461146 (https://doi.org/10.1016/j.chroma.2020.461146)
7. A. A. D'Archivio, M. A. Maggi, F. Ruggieri, *Anal. Bioanal. Chem.* **407** (2015) 1181 (https://doi.org/10.1007/s00216-014-8317-3)
8. M. A. Bezerra, R. E. Santelli, E. P. Oliveira, L. S. Villar, L. A. Escaleira, *Talanta* **76** (2008) 965 (https://doi.org/10.1016/j.talanta.2008.05.019)
9. ICH Topic Q3A (R2), *Impurities in new drug substances*, 2006, https://www.ema.europa.eu/en/documents/scientific-guideline/ich-q-3-r2-impurities-new-drug-substances-step-5_en.pdf (accessed Feb 16, 2021)
10. ICH Topic Q3B (R2), *Impurities in new drug products*, 2006, https://www.ema.europa.eu/en/documents/scientific-guideline/ich-q-3-b-r2-impurities-new-drug-products-step-5_en.pdf (accessed Feb 16, 2021)
11. C. M. El-Maraghy, H. Salem, S. M. Amer, M. Nebsen, *Anal. Chem. Lett.* **9** (2019) 258 (https://doi.org/10.1080/22297928.2019.1585286)
12. K. S. V. Srinivas, R. Buchireddy, G. Madhusudhan, K. Mukkanti, P. Srinivasulu, *Chromatographia* **68** (2008) 635 (https://doi.org/10.1365/s10337-008-0739-7)
13. G. V. R. Reddy, A. P. Kumar, B. V. Reddy, P. Kumar, H. D. Gauttam, *Eur. J. Chem.* **1** (2010) 20 (https://doi.org/10.5155/eurjchem.1.1.20-27.11)
14. N. Djordjević Filijović, A. Pavlović, K. Nikolić, D. Agbaba, *Acta Chromatogr.* **26** (2014) 13 (https://doi.org/10.1556/achrom.26.2014.1.15)
15. M. Rmandić, A. Malenović, *J. Sep. Sci.* **43** (2020) 3242 (https://doi.org/10.1002/jssc.201900985)
16. M. V. V. N. Murali Krishna, S. V. Rao, N. V. S. Venugopal, *J. Liq. Chromatogr. Relat. Technol.* **40** (2017) 741 (https://doi.org/10.1080/10826076.2017.1357572)
17. F. Soponar, M. Sandru, V. David, *J. Liq. Chromatogr. Relat. Technol.* **39** (2016) 70 (https://doi.org/10.1080/10826076.2015.1126729)
18. T. Snoj Ekmečić, I. Kralj Cigic, *Acta Chim. Slov.* **66** (2019) 958 (http://dx.doi.org/10.17344/acsi.2019.5189)
19. *European Pharmacopoeia*, 9th ed., The Council of Europe, Strasburg, 2017
20. *The United States Pharmacopeia*, 42nd revision, United States Pharmacopeia Convention, Rockville, MD, 2019
21. K. Nikolić, N. Djordjević Filijović, B. Maričić, D. Agbaba, *J. Sep. Sci.* **36** (2013) 3165 (https://doi.org/10.1002/jssc.201300477)
22. K. Croes, A. Steffens, D. H. Marchand, L. R. Snyder, *J. Chromatogr., A* **1098** (2005) 123 (https://doi.org/10.1016/j.chroma.2005.08.090)

23. M. Yang, S. Fazio, D. Munch, P. Drumm, *J. Chromatogr., A* **1097** (2005) 124 (https://doi.org/10.1016/j.chroma.2005.08.028)
24. ICH Topic Q3C (R6), *Residual solvents*, 2006, https://www.ema.europa.eu/en/documents/regulatory-procedural-guideline/ich-guideline-q3c-r8-impurities-guideline-residual-solvents-step-5_en.pdf (accessed Feb 16, 2021)
25. E. Yabalak, O. Gomez, B. G. Sonmez, *J. Serb. Chem. Soc.* **83** (2018) 489 (https://doi.org/10.2298/JSC170909113Y)
26. S. L. Ferreira, R. E. Bruns, E. G. da Silva, W. N. Dos Santos, C. M. Quintella, J. M. David, J. B. de Andrade, M. C. Breitkreitz, I. C. Jardim, B. B. Neto, *J. Chromatogr., A* **1158** (2007) 2 (https://doi.org/10.1016/j.chroma.2007.03.051)
27. B. Otašević, J. Šljivić, A. Protić, N. Maljurić, A. Malenović, M. Zečević*, Microchem. J.* **145** (2019) 655 (https://doi.org/10.1016/j.microc.2018.11.033)
28. M. A. Fouad, E. H. Tolba, M. A. El-Shal, A. M. El Kerdawy, *J. Chromatogr., A* **1549** (2018) 51 (https://doi.org/10.1016/j.chroma.2018.03.042)
29. Y. Cao, S. Yao, X. Wang, T. Yao, H. Song, *J. Serb. Chem. Soc.* **82** (2017) 399 (https://doi.org/10.2298/JSC160725013D)
30. M. De Lozzo, P. Klotz, B. Laurent, *Eng. Appl. Artif. Intell.* **26** (2013) 2270 (https://doi.org/10.1016/j.engappai.2013.07.001).

Journal of the Serbian Chemical Society
JSCS@tmf.bg.ac.rs • www.shd.org.rs/JSCS
J. Serb. Chem. Soc. 87 (5) S127–S129 (2022) *Supplementary material*

SUPPLEMENTARY MATERIAL TO

Optimization of chromatographic separation of aripiprazole and impurities: Quantitative structure–retention relationship approach

BOJANA SVRKOTA, JOVANA KRMAR, ANA PROTIĆ, MIRA ZEČEVIĆ and BILJANA OTAŠEVIĆ*

Department of Drug Analysis, University of Belgrade - Faculty of Pharmacy, Vojvode Stepe 450, 11221 Belgrade, Serbia

J. Serb. Chem. Soc. 87 (5) (2022) 615–628

TABLE S-I. Values of log *P* and log *D* for the tested analytes*

Compound	pK_a	log *P*	log *D*		Amount of ionization form, %			
			pH 3.0	pH 4.7	at pH 3.0		at pH 4.7	
					Neutral	Cation	Neutral	Cation
IMP A	9.21	1.21	1.21	1.21	100	0	100	0
IMP B	8.82	2.75	-0.49	-0.43	0	100	0	100
IMP C	13.21; 13.81	3.12	3.12	3.12	100	0	100	0
IMP D	13.51	2.60	2.60	2.60	100	0	100	0
IMP E	3.73; 13.51	3.78	3.71	3.77	16	84	90	10
Aripiprazole	7.46; 13.51	4.90	1.45	2.21	0	100	0	100

* Values obtained with MarvinView 6.1.6 software

TABLE S-II. Values of the molecular descriptors for the tested analytes**

pH 4.7	Aripiprazole	ImpA	ImpB	ImpC	ImpD	ImpE	Average	SD	RSD
SAS, Å^2	634.862	273.278	341.850	5606.222	416.452	645.140	1319.634	1922.037	145.649
MS, Å^2	406.347	155.716	206.327	378.030	250.729	413.149	301.716	101.820	33.747
SEV, Å^3	360.380	120.307	178.063	310.906	201.820	366.442	256.320	94.454	36.850
Mass, g mol^{-1}	448.156	163.063	231.046	380.174	253.087	463.143	323.112	113.649	35.173
Charge	1.526 10^{-5}	0	1.526 10^{-5}	0	0	0	5.087 10^{-6}	7.194 10^{-6}	141.421
MW / AMU	449.402	163.177	232.133	380.446	253.730	464.394	323.880	113.918	35.173
O	1.659	1.321	1.348	1.703	1.507	1.668	1.535	0.154	10.060
PMIX / g mol^{-1} Å^2	2194.300	230.895	445.371	533.635	275.057	2047.790	954.508	832.063	87.172
PMIY / g mol^{-1} Å^2	12786.400	816.627	1585.570	17237.400	4849.740	17033.500	9051.540	6902.642	76.259
PMIZ /g mol^{-1} Å^2	14054.500	1031.900	1831	17709.300	5081.160	17982.500	9615.060	7188.624	74.764
MR	12.225	4.460	5.998	10.598	6.807	12.378	8.744	3.200	35.679
C log *P*	5.219	0.629	3.072	3.107	2.671	4.790	3.248	1.500	46.192
Eb / Kcal mol^{-1}	6.463	1.588	1.243	6.129	4.149	8.440	4.669	2.617	56.042
Ev / Kcal mol^{-1}	-0.028	-1.882	-4.103	-3.683	1.790	1.693	-1.036	2.366	228.459
Es / Kcal mol^{-1}	27.752	6.071	21.131	0.778	6.290	32.686	15.785	12.022	76.162
Esb / Kcal mol^{-1}	0.443	-0.053	0.093	0.228	-0.267	-0.008	0.073	0.223	308.010
Et / Kcal mol^{-1}	0.297	0.065	0.010	0.012	0.085	0.082	0.092	0.097	105.222

* Corresponding author. E-mail: biljana.otasevic@pharmacy.bg.ac.rs

pH 4.7	Aripiprazole	ImpA	ImpB	ImpC	ImpD	ImpE	Average	SD	RSD
E / Kcal mol^{-1}	55.387	7.436	28.203	11.329	20.545	65.551	31.408	21.782	69.352
E14 / Kcal mol^{-1}	20.460	1.647	9.828	7.866	8.499	22.659	11.826	7.374	62.350
DPLL, eV	5.369	3.771	3.449	0.184	2.576	2.206	2.926	1.587	54.255
ElcE, eV	-41611.200	-10471.300	-14473	-33306	-17685.500	-42828.200	-26729.200	13039.864	48.785
HOMO , eV	-1.729	-8.881	-1.319	-8.834	-8.873	-8.874	-6.418	3.463	53.955
LUMO, eV	-0.044	0.084	0.133	0.077	0.098	-0.405	-0.009	0.185	1988.073
NRE, eV	36274.100	8346.990	11854.900	28464.200	14578.400	37185.600	22784.032	11668.033	51.211
TotE, eV	-5337.090	-2124.320	-2618.11	-4841.810	-3107.070	-5642.670	-3945.178	1378.520	34.942
BIndx	1258736	19099	40414	914045	118842	1421449.000	628764.167	589415.962	93.742
ClsC	30	12	14	28	17	31	22	7.853	35.695
Diam	18	6	7	17	11	18	12.833	5.080	39.584
TIndx	22957	1387	2120	19444	4174	23847	12321.500	9888.517	80.254
Rad	9	3	4	9	6	9	6.667	2.494	37.417
ShpA	28.033	10.083	12.071	26.036	15.059	29.032	20.052	7.833	39.063
ShpC	1	1	0.75	0.889	0.833	1	0.912	0.097	10.611
SDeg	66	26	30	62	36	68	48	17.663	36.799
SVDe	92.556	44	38.5556	98	53.778	99.556	71.074	26.100	36.722
TCon	1.392 10^{-5}	0.014	0.007	2.411 10^{-5}	0.002	1.206 10^{-5}	0.004	0.005	131.245
TVCon	2.166 10^{-7}	0.001	0.002	6.279 10^{-8}	1.421 10^{-4}	7.910 10^{-8}	4.480 10^{-4}	0.001	160.538
WIndx	3204	185	291	2652	590	3400	1720.333	1388.551	80.714

**Values obtained using Chem3D Ultra 7.0 software

TABLE S-III. Weight values for QSRR-ANN

Neuron unit	*h1#01*	*h1#02*	*h1#03*	*h1#04*	log t_r
Threshold	-0.1495	-0.3591	2.18358	0.3097661	-0.1003
s_{MeOH}	-0.405927	-0.6614	-0.3095	0.3783298	
e_{MeOH}	0.5581015	-0.09984	-1.592106	-0.1448	
F	-0.2832	0.851204	-0.5773	0.3834429	
O	1.034471	-0.3111	1.131429	-7.023405	
Ev	0.6841513	0.0851934	0.09666	0.2688041	
Et	0.3471714	-0.2554	1.808066	1.602358	
h1#01					0.7634846
h1#02					-0.01301
h1#03					3.178396
h1#04					-6.083286

TABLE S-IV. Values of *RMSE* for ANNs trained during LOO-CV for log s_{B-A} and log s_{C-D}

Test case No.	log s_{B-A}			log s_{C-D}		
	Training *RMSE*	Verification *RMSE*	Test *RMSE*	Training *RMSE*	Verification *RMSE*	Test *RMSE*
1	0.0292	0.0357	0.0274	0.1232	0.0261	0.0024
2	0.0352	0.0630	0.0513	0.0944	0.0141	0.0528
3	0.0295	0.0525	0.0621	0.0939	0.0031	0.1638
4	0.0378	0.0611	0.0653	0.1613	0.0020	0.0038
5	0.0513	0.0740	0.0127	0.0878	0.0520	0.0223
6	0.0617	0.0193	0.2480	0.0763	0.0953	0.0171
7	0.0573	0.0686	0.0218	0.1243	0.0282	0.0393
8	0.0802	0.0811	0.0853	0.1153	0.0145	0.0274
9	0.0640	0.0892	0.0066	0.0581	0.0056	0.2760
10	0.0764	0.0207	0.0877	0.0763	0.0464	0.0279
11	0.0998	0.0703	0.0695	0.0693	0.0354	0.0594
12	0.0895	0.0603	0.0538	0.0765	0.0386	0.0315

TABLE S-IV. Continued

Test case No.	log s_{B-A}			log s_{C-D}		
	Training *RMSE*	Verification *RMSE*	Test *RMSE*	Training *RMSE*	Verification *RMSE*	Test *RMSE*
13	0.0908	0.0192	0.0510	0.0688	0.0351	0.0049
Average *RMSE*	0.0617	0.0550	0.0648	0.0943	0.0305	0.0560

TABLE S-V. Weight values for ANN to optimized log s_{B-A}

Neuron unit	*h1#01*	*h1#02*	log s_{B-A}
Threshold	-1.405131	-1.756968	3.721817
s_{MeOH}	-0.0548	-5.093693	
e_{MeOH}	0.1236208	-0.1554	
F	-4.129496	0.8476573	
h1#01			4.327358
h1#02			6.393134

Journal of the Serbian Chemical Society
JSCS@tmf.bg.ac.rs • www.shd.org.rs/JSCS
J. Serb. Chem. Soc. *87* (5) 629–640 (2022)
JSCS–5546
Original scientific paper
Published 16 May 2022

Antimicrobial and anticancer activities of copolymers of tri-*O*-acetyl-D-glucal and itaconic anhydride

CHETANA DEOGHARE[1], SHRUTI BALAJI[2], SAVITHA DHANDAPANI[3], HONEY SRIVASTAVA[4], ANASUYA GANGULY[5]* and RASHMI CHAUHAN[4]**

[1]Department of Chemistry, Institute of Sciences, Humanities and Liberal Studies, Indus University, Rancharda, via Silaj, Ahmedabad - 382115, Gujarat, India, [2]PlantaCorp GmbH, 20097 Hamburg, Germany, [3]Temasek Life Sciences Laboratory, National University of Singapore – 117604, Singapore, [4]Department of Chemistry, BITS-Pilani, K. K. Birla Goa Campus, Goa, India and [5]Department of Biological Sciences, BITS-Pilani, K. K. Birla Goa Campus, Goa, India

(Received 28 August, revised and accepted 10 December 2021)

Abstract: This paper reports the synthesis and characterization of monomers itaconic anhydride (IA) and tri-*O*-acetyl-D-glucal (TAG) as well as 4,6-di-*O*--acetyl-D-glucal (PSG). The homopolymers and copolymers of IA and TAG were synthesized *via* free radical copolymerization in bulk, using azobisisobutyronitrile as an initiator with different feed ratios of monomers. Their structural, molecular and thermal characterization was done using ^{1}H-NMR spectroscopy, gel permeation chromatography and differential scanning calorimetry, respectively. The glass transition temperature (T_g) of copolymers was found in the range of 139–145 °C. The highest T_g was found for IA–TAG2 copolymers, whereas IA–TAG4 copolymer showed lowest T_g. The molecular weight of the copolymers was in the range 5157–5499 g mol^{-1}. The monomer TAG undergoes Ferrier rearrangement in water to give PSG. The antimicrobial activity of IA, TAG, PSG and IA–TAG copolymers was studied using the minimum microbicidal concentration-broth dilution method. TAG, IA and PSG, as well as homopolymer and copolymers of IA and TAG are excellent antimicrobial agents.

Keywords: free radical polymerization; glass transition temperature; homopolymer; Ferrier rearrangement; cytotoxicity; antibacterial activity.

INTRODUCTION

The number of aggressive infections is on the rise, accompanied by an increase in the number of antibiotic resistant microorganisms. Therefore, the need to screen for novel anti-microbial compounds is imperative.[1,2] The identification of

*,** Corresponding authors. E-mail: (*)ganguly@goa.bits-pilani.ac.in; (**)rchauhan@goa.bits-pilani.ac.in
https://doi.org/10.2298/JSC210828108D

anti-cancer drugs is another thrust area of research. Environmental and economic concerns necessitate the use of polymer from renewable resources.[3,4] Polymers based on renewable resources such as plant and agro-industrial waste are of considerable interest as substitutes for petroleum-based materials.[5,6] Such materials are attractive from an environmental perspective, especially if they are biodegradable. In this regard, glucose or fructose can be a good source of monomers as they are available in abundance and at a low cost.[7] Tri-O-acetyl-D-glucal (TAG) and itaconic anhydride (IA) both can be obtained from renewable resources, *i.e.*, D-glucose and itaconic acid (ITA), respectively. IA is produced from the pyrolysis of citric acid or through the fermentation of carbohydrates forming ITA followed by its dehydration to form the anhydride.[8,9] IA can be polymerized or copolymerized with various other monomers by free radical reactions. IA is more reactive than maleic anhydride and is an alternative monomer for introducing polar functionality into polymers.[10–12] Polyacrylate derivatives containing IA moieties have been prepared using the microwave irradiation technique.[13] From the various heterocyclic derivatives prepared from IA precursor by Narayana *et al.*[14] good antibacterial activity was shown by 1-(4-iodophenyl)-3-methylidenepyrrolidine-2,5-dione, whereas the derivatives 1-(4-chlorophenyl)-3-methylidenepyrrolidine-2,5-dione and 3-methylidene-1-(1,3-thiazol-2-yl)pyrrolidine-2,5--dione showed promising antifungal properties. [^{18}F]2-fluoro-2-deoxy-β-D-allose ([^{18}F]2-FDβA) was synthesized from TAG in a two-step reaction and was shown to be a possible candidate as a radiotracer for breast tumour detection.[15] Han *et al*. reported the biological activity of TAG-maleic anhydride copolymer by MTT method and ID_{50}-values against tumour cells.[16] Recently antibacterial active films were prepared from poly(itaconic acid), which was functionalized with quaternized thiazole group and incorporated in gelatine and oxidized starch. These films also showed antioxidant capacity.[17]

In our study, TAG and IA were synthesized from D-glucose and ITA, respectively, and PSG was prepared from TAG. The copolymers of TAG and IA were prepared using bulk polymerization under free-radical conditions. The polymerization was carried out under nitrogen atmosphere using AIBN as an initiator at 60 °C. The copolymers were prepared using different compositions. The ratio of IA to TAG varied as follows: 9:1, 8:2, 7:3, 6:4 and 5:5. The structural characterization of the obtained copolymers was done by ^{1}H-NMR spectroscopy. Thermal and molecular characterizations were done using DSC, and GPC respectively. Here we propose the use of TAG, IA, PSG and homopolymer and copolymers of IA and TAG as potential antimicrobial as well as anticancer agents.

EXPERIMENTAL

Materials

Itaconic acid (99.0 %), phosphorus pentoxide (95.0 %), D-glucose (95.0 %), perchloric acid (98.0 %), red phosphorus (95.0 %), bromine (95.0 %), acetic acid (98.0 %), sodium

acetate (99.5 %), zinc dust (99.0 %), copper sulphate (95.5 %), azobisisobutyronitrile (AIBN) (95.0 %), silica gel (60-120 mesh) for column chromatography, were used as supplied. Chloroform (99.7 %) and acetic anhydride (98.0 %) were distilled before use. All the above chemicals were obtained from S. D. Fine Chem Limited, Mumbai, India.

Methods

FT-IR spectrum of the IA was recorded on a Shimadzu IR-Affinity-1, FT-IR spectrophotometer in the region from 4000 to 400 cm^{-1} using the KBr pellet method. The ^{1}H-NMR spectra were obtained by dissolving the samples in deuterated chloroform ($CDCl_3$) using a Brucker AV III 500 MHz FT-NMR or a Brucker DRX500 spectrometer. Chemical shifts (δ in ppm) are given relative to tetramethylsilane. Differential scanning calorimeter (DSC) was used for the melting point and to check the purity of the monomers and for determination of glass transition temperature (T_g) of polymers. DSC scans were recorded in nitrogen atmosphere at a heating rate of 10 °C /min by using 3±1 mg of powdered samples using Discovery SDT 650, TA Instruments, TGA-DSC. The molecular weight and polydispersity index of obtained copolymers were calculated using Perkin Elmer Series 200 system equipped with column: PL gel 5 microns Mixed D: 300 mm×7.5 mm using THF as mobile phase at a flow rate of 1.0 mL min^{-1} and refractive index detector.

Culture of bacterial and fungal cultures

1 % cultures of *Escherichia coli* (strain no. MTCC 2345) and *Staphylococcus aureus* (Strain no. MTCC 737) were cultured overnight at 37 °C with constant shaking in nutrient broth (HiMedia). They were sub-cultured the next morning at 1 % in nutrient broth and allowed to grow under the same culture conditions as described above for 6 h (end of log phase). *Streptococcus pyogenes* (strain no. MTCC 442) and *Pseudomonas aeruginosa* (strain no. MTCC 741) were cultured under similar conditions in Brain Heart Infusion (BHI) medium (HiMedia) while *Candida albicans* (strain no. MTCC 183) was cultured in MGYP medium (malt extract (3 mg mL^{-1}), glucose (10 mg mL^{-1}), yeast extract (3 mg mL^{-1}) and peptone (5 mg mL^{-1}), all obtained from HiMedia.

*Estimation of minimum microbicidal concentration (*MMC*)-broth dilution method*

At the end of the log phase of the cultures, the optical densities (*OD*) were estimated at a wavelength of 600 nm, and the cultures were diluted to an *OD* of 0.2. Since 1 *OD* was taken to correspond to 5×10^8 cells mL^{-1}, 20 μL of the diluted culture was added to 980 μL of twice the concentrations of the respective culture broths so that the final concentration of cells was 2×10^6 cells mL^{-1}. 100 μL of cell suspensions were then plated out in flat bottomed 96-well plates (Tarsons). 100 μL of the autoclaved test sample in different concentrations were added correspondingly. Cultures with only sterile distilled water were used as negative controls while cultures with 100 μL of commercially available antibacterial/antimycotic solution (HiMedia) containing penicillin (100 U), streptomycin (0.1 mg) and amphotericin B (0.25 μg) were used as positive controls. All cultures were performed in duplicates. The cultures were incubated for 24 h at 37 °C. The *MMC* was taken as the concentration at which no growth was observed (comparable to positive control).

Culture of A549 cell line

A549 human lung adenocarcinoma cell lines were cultured in Dulbecco's modified Eagle medium (DMEM containing Phenol red; HiMedia) with 10 % Foetal bovine serum (FBS; HiMedia) at 37 °C in a humidified incubator with 5 % CO_2.

Trypan blue viability assay

A549 cells of >95 % viability were plated out at a cell density of 1.5×10^5 cells mL^{-1} in a 24-well plate (Tarsons) and cultured overnight at 37 °C in a humidified incubator with 5 % CO_2. The next day, the spent medium was completely removed and equal volumes of fresh medium and autoclaved 2× concentration of polymers were added to different wells and incubated for a further 12 h and 24 h at 37 °C and 5 % CO_2. Cultures sans polymers were used as a negative control. All cultures were performed in duplicates. After the incubation period with the test compound, the cultures were examined microscopically, and cells were carefully trypsinized. The cell suspension was centrifuged at 1200 rpm for 7 min, and the cell pellet was re-suspended in 1 mL of fresh complete medium. 90 µL of the cell suspension was mixed with 10 µL of 0.4 % Trypan blue (HiMedia), incubated for about 5 min at room temperature and a manual cell count was performed using a haemocytometer.

Synthesis of itaconic anhydride

To a two-litre reaction kettle equipped with a mechanical stirrer and reflux condenser, ITA (0.75 mol) dissolved in one litre of chloroform was taken. To the solution, P_2O_5 (1.0 mol) was added. The reaction mixture was refluxed with stirring for 24 h. It was then decanted leaving a viscous brown residue at the bottom of the flask and the solution was concentrated to half by removing chloroform, using the rotary vacuum evaporator. On cooling the remaining solution to 0 °C, itaconic anhydride crystallizes out which was separated by filtration followed by drying in the oven for 2 h at 40 °C. The two crops of crystals were obtained giving white crystals of IA (yield, 90 %, m.p.: 69 °C), Scheme 1.

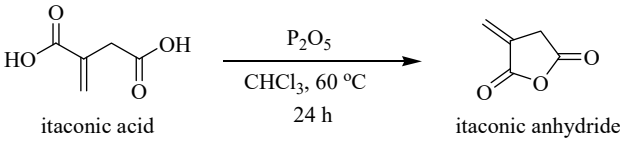

itaconic acid itaconic anhydride

Scheme 1. Synthesis of IA.

Synthesis of TAG

TAG was synthesized in a multistep reaction (Scheme 2). *α*-D-Glucose (0.33 mol) was added slowly to a mixture of acetic anhydride (1.96 mol) and 70 % perchloric acid (1.2 mL) at 35 °C, in a duration of 1 h with continuous stirring. After the addition of red phosphorus (0.48 mol) to the flask, it was cooled to 5 °C in an ice-salt mixture. Bromine (0.56 mol) was then added drop-wise, with continuous stirring at such a rate as to maintain the internal temperature below 20 °C. Subsequently, 15 mL of water was added during the course of 30 min with the careful control of temperature. The mixture was filtered, and the filter paper was washed with a little acetic acid. The filtrate so obtained contained tetra-*O*-acetyl-*α*-D-glucopyranose bromide. Meanwhile, a solution of sodium acetate (1.95 mol) in the water of 250 mL and glacial acetic acid 200 mL was prepared. To this solution, zinc dust (1.68 mol) along with $CuSO_4$ solution (0.04 mol in 40 mL water) was added at 5 °C. When the blue colour of $CuSO_4$ solution disappeared, the filtrate containing tetra-*O*-acetyl-*α*-D-glucopyranose bromide was added gradually in the time span of 1 h keeping the reaction temperature between –10 and –20 °C, and the stirring was continued for 3 h at the same temperature.

The obtained reaction mixture was filtered, and the filter paper was washed with 50 % acetic acid. The 500 mL water was added to the filtrate at 0 °C and the reaction mixture was extracted with chloroform. To remove the traces of water from the chloroform solution, it was

stored overnight on the bed of $CaCl_2$. The chloroform solution was decanted and evaporated under reduced pressure. The crude product was purified using column chromatography and recrystallized with petroleum ether and diethyl ether mixture (yield, 92 %, m.p.: 55 °C).

Synthesis of PSG

TAG (0.01 mol) was dissolved in 100 mL of water and the solution obtained was stirred at 80 °C for half an hour. It was then brought to room temperature and PSG was extracted with chloroform and concentrated using the rotary evaporator (yield, 85 %, m.p.: 125 °C), Scheme 2.

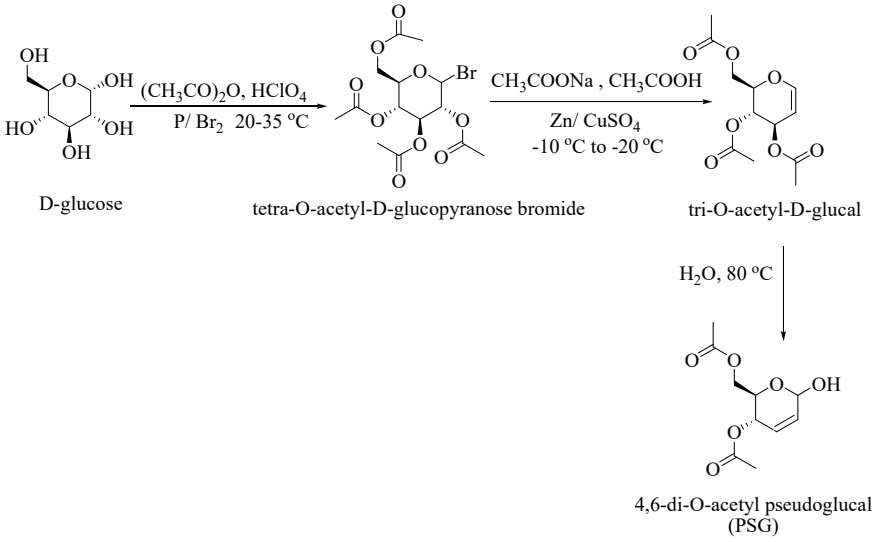

Scheme 2. Synthesis of TAG and PSG.

Synthesis of copolymers of IA–TAG

To the three-necked round bottom flasks equipped with mechanical stirrer and nitrogen atmosphere, IA and TAG were added with varying mole ratios such as 9:1, 8:2, 7:3, 6:4 and 5:5 and 1 % of AIBN. The temperature was maintained at about 60–65 °C and stirring was continued till the reaction mixture became viscous. The reaction mixture was washed with chloroform to remove the unreacted TAG and IA, and dried under vacuum at 80 °C. The copolymers so obtained are designated as IA–TAG, followed by a numerical suffix giving the moles of TAG in the monomer feed. For example, the copolymer prepared using one mole of TAG, and nine moles of IA is designated as IA–TAG1 (Scheme 3).

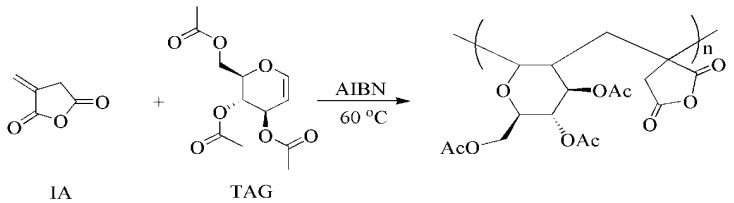

Scheme 3. Synthesis of IA-TAG copolymers via free radical polymerization.

Spectral data of the synthesized compounds are given in Supplementary material to this paper.

RESULTS AND DISCUSSION

TAG was obtained from D-glucose in a multistep reaction *via* acetylation and bromination, followed by reduction *in situ*, as shown in Scheme 2. TAG, upon treatment of with water at 80 °C, underwent Ferrier rearrangement to give PSG (Scheme 2). The copolymers of TAG and IA were obtained via bulk polymerization under free radical conditions. The homopolymer of IA was also prepared under similar conditions, but the homopolymer of TAG could not be obtained even after 96 h of continuous stirring.

The structural characterization of the obtained IA–TAG copolymers was done using ^{1}H-NMR spectroscopy. The ^{1}H-NMR spectrum of IA–TAG5 shown in Fig. S-5 of the Supplementary material, showed a sharp peak due to $–CH_2$ protons of IA in backbone at δ 1.8–1.9 ppm, and protons of $–CH_3$ of the acetyl group of TAG at δ 1.9–2.0 ppm, which confirmed the incorporation of the monomer of IA and TAG in the copolymer backbone. The succinic anhydride methylene group in the pendant is observed at δ 2.5 and 3.2 ppm. The presence of these peaks along with the peaks observed at δ 2.1–2.2 ppm and 3.6–3.7 ppm, due to CH bonds of TAG in the backbone, confirms the polymerization. The peaks in the region δ 4.9–5.5 ppm are due to CH groups in the pendant ring of TAG. The termination of the reaction can occur via disproportionation reaction generating vinylic groups which are observed in the region δ 5.8–6.1 ppm. The peaks are mostly broad due to the changes in the microstructure of the copolymers. This is a common phenomenon observed in ^{1}H-NMR spectra of polymers.[18]

Molecular and thermal characterization of IA–TAG copolymers

The molecular and thermal characterization of IA–TAG copolymers was done using GPC and DSC, respectively. The results are summarized in Table I. The molecular weight of IA–TAG copolymers was in the range of 5147 to 5469 g mol^{-1} and a slight increase in the molecular weight of copolymers was observed with the growth of the mole fraction of TAG in the feed, which is due to the higher molecular weight of TAG monomer. The polydispersity index of IA–TAG copolymers was found in the range of 1.7–2.1. The T_g of IA–TAG copolymers was found in the range of 133–148 °C. The DSC scans are shown in Fig. S-6 of the Supplementary material.

A marginal increase in T_g was observed with the rise of the TAG concentration in the feed and was in the order IA–TAG1 < IA–TAG2 < IA–TAG3 < < IA–TAG4 < IA–TAG5.

The rise of T_g with the increase in TAG in the feed ratio could be due to the incorporation of monomer with a bulky pendant group, but further growth of

TAG decreases the softening temperature, which may be due to lower melting point of TAG monomer.

TABLE I. Molecular weights (M_w), *PDI* and T_g of IA-TAG copolymers

Copolymer designation	Mole ratio of IA:TAG	M_w / g mol^{-1}	*PDI*	T_g / °C
IA–TAG1	9:1	5147	2.1	144
IA–TAG2	8:2	5200	2.0	202
IA–TAG3	7:3	5327	1.8	163
IA–TAG4	6:4	5436	1.8	139
IA–TAG5	5:5	5499	1.7	145

Antimicrobial and anticancer activity

The monomers (IA, TAG), PSG, poly(itaconic anhydride) (PIA) and copolymers of TAG and IA were tested for their potential as antimicrobial and anticancer agents. The *MMC* (concentration at which no cell growth was observed) of ITA, the monomers, IA and TAG, and the polymers derived from them were estimated using the broth dilution method. The *MMC* values for the 6 organisms tested against the corresponding polymers and monomers are shown in Fig. S-7 of the Supplementary material. The concentrations at which they exhibit anti--bacterial and anti-fungal activities are tabulated in Table II.

TABLE II. MMC (mg mL^{-1}) of ITA, IA, TAG and their copolymers *in vitro*

Sample designation	Microorganism				
	E. coli	*P. aeruginosa*	*S. aureus*	*S. pyogenes*	*C. albicans*
ITA	2	4	2	2.75	1
TAG	1.25	>5	1.25	3.75	1.25
IA	2.5	4.75	2.5	3	1
PIA	1.5	3.75	1.5	2	1.5
IA–TAG1	2.25	4.5	2.25	3	1
IA–TAG2	2	4	2	3	1.5
IA–TAG3	2	4.25	2	3	1.25
IA–TAG4	2	4.5	2	3.25	1.25
IA–TGA5	1.75	4.25	1.75	3.5	1.25
PSG	1.5	4	1.5	3	1.25

C. albicans was seen to be most sensitive (based on the number of polymers that inhibited its growth as well as the lower concentration of the polymers) while *P. aeruginosa* was seen to be most resistant. Of the test compounds ITA and IA the sensitivity of bacteria increases when a polar group, *i.e.*, anhydride in IA is changed to a more polar protic group, *i.e.*, COOH in ITA, thus increasing its hydrophilicity. A rise of sensitivity with the increase in number of polar groups was also observed for S. *Pyogenes* and C. *albicans*, which were more resistant towards TAG as compared to PSG, the latter having an OH functionality. The expansion of antibacterial properties by the introduction of hydroxyl groups

and the increased hydrophilicity have been reported for polyphosphoniums and phenolic compounds.[19–22] *E. coli* and *S. aureus* on the other hand were more sensitive towards TAG as compared to PSG, that may be due to the higher molecular weight of TAG, which negatively effects its diffusion through the bacterial cell membrane.[23]

TAG, PSG and ITA were seen to be most effective at low concentrations while IA was seen to be effective only at higher concentrations. For the given microorganisms, the antimicrobial activity of the IA–TAG copolymers was comparable to each other. The cytotoxicity of the polymers and monomers on A549 lung adenocarcinoma cell line was estimated by the Trypan blue viability assay. The viability of cells grown in the various polymers and monomers is given in Table III.

TABLE III. Viability (%) of different concentration of itaconic acid, anhydride and its polymers *in vitro*. The effect of itaconic acid, the monomers–IA and TAG and the polymers derived from them on A549 lung adenocarcinoma cell lines viability was estimated using the Tryphan blue viability assay. Data are shown as mean of three biological replicates. Statistical significance of the measurements was determined by Student's *t*-test ($^aP < 0.001$; $^bP < 0.01$ and $^cP < 0.05$). The effect of ITA, the monomers, IA and TAG, and the polymers derived from them on A549 lung adenocarcinoma cell lines viability was estimated using the Trypan blue viability assay

Sample designation	$c_{M/P}$ (concentration of monomers and polymers) / mg mL^{-1}					
	0.38		0.75		1.5	
	After 12 h	After 24 h	After 12 h	After 24 h	After 12 h	After 24 h
Itaconic acid	94.16	87.91	91.79	64.08[a]	6.12[a]	0[a]
TAG	76.76	52.95[a]	40.82[a]	36.64[a]	2.13[a]	2.7[a]
IA	96.45	91.67	92.86	88.28	83.07[c]	80.95[c]
Polyitaconic anhydride	91.49	83.83	21.25[a]	8.22[a]	9.46[a]	0[a]
IA–TAG1	93.88	82.79	93.80	78.79	68.11[a]	34.09[a]
IA–TAG2	95.24	92.28	88.79	87.11	87.5	76.5[b]
IA–TAG3	93.5	91.23	90.82	88.89	65.23[a]	28.78[a]
IA–TAG4	97.08	95.44	93.54	85.67	75[b]	20.37[a]
IA–TAG5	83.67	83.87	66.04[a]	50.67[a]	60.29[a]	22.86[a]
PSG	1.82[a]	0[a]	0[a]	0[a]	0[a]	0[a]

PSG was the most effective cytotoxic agent, whereas the monomer IA was the least effective even at higher concentrations as shown in Fig. S-8 of the Supplementary material.

These results were corroborated by the microscopic observation of the cells prior to trypsinizing them (Fig. 1). Microscopy revealed that, with increasing concentration of the test compound, the number of attached cells reduced as compared to the control wells. The amount of detachment was also seen to be different with different polymers. Further, the cultures with the most cytotoxic com-

pounds had distinct apoptotic morphology, such as discontinuous cell membrane and presence of apoptotic bodies within the cells. Panel A in Fig. 1 is illustrative of the effect of PSG after 12 and 24 h of incubation, at different concentrations, on the adhesive properties of the adherent cell line, A549 (10× objective). As can be seen, the number of cells that are detached from the culture surface increase with the concentration of the polymer. On closer observation (panel B), one can also see the cytotoxic effect of the polymer, as seen by the formation of apoptotic bodies (20× objective) on treating with IA. Similar observations were made with the other test compounds.

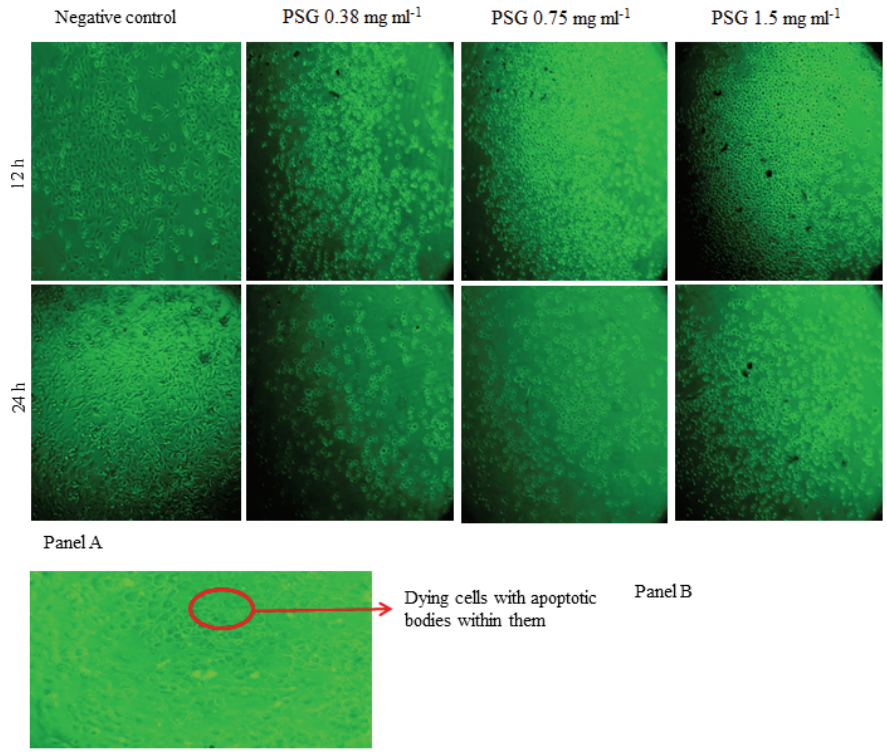

Fig. 1. Effect of ITA, IA and its copolymers with TAG on cell adhesion and morphology of A549 human lung adenocarcinoma cells.

CONCLUSIONS

In the current study, the monomers TAG and IA that were obtained from renewable resources, *i.e.*, sugar, were synthesized and characterized. The copolymers of IA and TAG were successfully synthesized using free radical polymerization conditions. Our studies reveal that the monomer, TAG, homopolymer of IA and copolymers of IA–PSG are excellent antimicrobial agents. The IA–TAG copolymers only work well as anti-fungal agents. However, at higher concen-

trations, they may be used as broad-spectrum antibiotics. Although the IA–TAG copolymers are significantly cytotoxic to A549 human lung adenocarcinoma cells, this effect is less profound than that of the base, TAG, and the homopolymer of IA. In this regard, PSG was seen to be the most cytotoxic, even at the lowest concentration tested. It can therefore be suggested that in addition to their possible use as antimicrobial agents, these sugar-based compounds may also be applied in the treatment of cancer. PSG is of particular interest and requires further studies to prove its proposed uses.

NOMENCLATURE

AIBN	Azobisisobutyronitrile
DMEM	Dulbecco's modified eagle medium
DSC	Differential scanning calorimeter
FBS	Foetal bovine serum
FT-IR	Fourier transform infrared spectroscopy
GPC	Gel permeation chromatography
IA	Itaconic anhydride
ITA	Itaconic acid
PIA	Poly(itaconic anhydride)
MMC	Minimum microbicidal concentration
NMR	Nuclear magnetic resonance
OD	Optical density
PSG	4,6-Di-*O*-acetyl pseudoglucal
TAG	Tri-*O*-acetyl-D-glucal
THF	Tetrahydrofuran
TMS	Trimethylsilyl

SUPPLEMENTARY MATERIAL

Additional data and information are available electronically at the pages of journal website: https://www.shd-pub.org.rs/index.php/JSCS/article/view/11108, or from the corresponding author on request.

Acknowledgements. CD, HS and RC are thankful to SICART-CVM Gujarat for GPC analysis, IISc Bangalore for ^{1}H NMR, and Department of Chemical Engineering, BITS Pilani K K Birla Goa Campus for DSC.

ИЗВОД

АНТИМИКРОБНА И АНТИКАНЦЕРОГЕНА АКТИВНОСТ КОПОЛИМЕРА ТРИ-*O*-АЦЕТИЛ-D-ГЛУКАЛА И АНХИДРИДА ИТАКОНСКЕ КИСЕЛИНЕ

CHETANA DEOGHARE[1], SHRUTI BALAJ[2], SAVITHA DHANDAPANI[3], HONEY SRIVASTAVA[4], ANASUYA GANGULY[5] И RASHMI CHAUHAN[4]

[1]Department of Chemistry, Institute of Sciences, Humanities and Liberal Studies, Indus University, Rancharda, via Silaj, Ahmedabad - 382115, Gujarat, India, [2]PlantaCorp GmbH, 20097 Hamburg, Germany, [3]Temasek Life Sciences Laboratory, National University of Singapore – 117604, Singapore, [4]Department of Chemistry, BITS-Pilani, K. K. Birla Goa Campus, Goa, India u [5]Department of Biological Sciences, BITS-Pilani, K. K. Birla Goa Campus, Goa, India

У раду је приказана синтеза и карактеризација мономера анхидрида итаконске киселине (IA) и три-*O*-ацетил-D-глукала (TAG) као и 4,6-ди-*O*-ацетил-D-глукала (PSG).

Хомополимери и кополимери IA и TAG синтетизовани су кополимеризацијом преко слободних радикала у маси коришћењем азо-бис-исобутиронитрила као иницијатора и са различитим односима мономера. Полимери су карактерисани у погледу структуре, грађе молекула и термичких својствава медодама ^{1}H-NMR спектроскопије, гел-пермеабилне хроматографије и диференцијалне скенирајуће калориметрије. Температура стакластог прелаза (T_g) кополимера је у опсегу од 139–145 °C. Највећи T_g су имали IA––TAG2 кополимери, док је IA–TAG4 кополимер показао најнижи T_g. Моларна маса кополимера била је у опсегу 5157–5499 g mol^{-1}. Мономер TAG подлеже Феријеовом преуређењу у води и даје PSG. Антимикробна активност IA, TAG, PSG и IA–TAG кополимера је проучавана методом разблаживања минималне микробицидне концентрације у хранљивом медијуму. TAG, IA и PSG, као и хомополимери и кополимери IA и TAG, одлични су антимикробни агенси.

(Примљено 28. августа, ревидирано и прихваћено 10. децембра 2021)

REFERENCES

1. C. Cesa-Luna, A. Baez, V. Quintero-Hernández, J. De La Cruz-Enríquez, M. D. Castañeda-Antonio, J. Muñoz-Rojas, *Acta Biol. Colomb.* **25** (2020) 140 (http://dx.doi.org/10.15446/abc.v25n1.76867)
2. P. K. Mantravadi, K. A. Kalesh, R. C. J. Dobson, A. O. Hudson, A. Parthasarathy, *Antibiotics* **8** (2019) 8 (http://doi.org/10.3390/antibiotics8010008)
3. P. K. Senthilkumar, D. Reetha, *Eur. Rev. Med. Pharmacol. Sci.* **15** (2011) 1034 (http://www.europeanreview.org/article/1031)
4. C. M. Franco, B. I. Vázquez, *Antibiotics* **9** (2020) 217 (http://dx.doi.org/10.3390/antibiotics9050217)
5. E. Chiellini, F. Chiellini, P. Cinelli, in *Degradable Polymers*, G. Scott, Ed., Springer, Dordrecht, 2002, p. 163 (http://doi.org/10.1007/978-94-017-1217-0_7)
6. Y. Zhu, C. Romain, C. K. Williams, *Nature* **540** (2016) 354 (http://dx.doi.org/10.1038/nature21001)
7. G. L. Gregory, E. M. Lopez-Vidal, A. Buchard, *Chem. Commun.* **53** (2017) 2198 (http://dx.doi.org/10.1039/c6cc09578j)
8. W. Priebe, I. Fokt, G. Grynkiewicz, in *Glycoscience*, B. Fraser-Reid, K. Tatsuta, J. Thiem, Eds., Springer-Verlag, Berlin, 2008, p. 699 (http://dx.doi.org/10.1007/978-3-540-30429-6_15)
9. T. Willke, K.-D. Vorlop, *Appl. Microbiol. Biotechnol.* **56** (2001) 289 (http://dx.doi.org/10.1007/s002530100685)
10. S. Shang, S. J. Huang, R. A. Weiss, *Polymer* **50** (2009) 3119 (http://dx.doi.org/10.1016/j.polymer.2009.05.012)
11. R. Chauhan, V. Choudhary, *J. Appl. Polym. Sci.* **109** (2008) 987 (http://doi.org/10.1002/app.28099)
12. L. Sollka, K. Lienkamp, *Macromol. Rapid Commun.* **42** (2021) 2000546 (http://dx.doi.org/10.1002/marc.202000546)
13. S. M. Osman, M. H. El-Newehy, S. S. Al-Deyab, A. El-Faham, *Chem. Cent. J.* **6** (2012) (http://dx.doi.org/10.1186/1752-153X-6-85)
14. P. S. Nayak, B. Narayana, B. K. Sarojini, S. Sheik, K. S. Shashidhara, K. R. Chandrashekar, *J. Taibah Univ. Sci.* **10** (2016) 823 (http://doi.org/10.1016/j.jtusci.2014.09.005)
15. R. Ashique, R. Chirakal, G. J. Schrobilgen, D. W. Hughes, T. Farncombe, K. Gulenchyn, R. Labiris, T. Truman, C. Saab, in *ACS Symp. Ser.* A, Vol. 1003, A. Gakh, K. L. Kirk,

Eds., American Chemical Society, Washington DC, , 2009, pp. 211–235 (http://dx.doi.org/10.1021/bk-2009-1003.ch010)
16. M.-J. Han, C.-W. Lee, K.-H. Kim, W.-Y. Lee, *Bull. Korean Chem. Soc*. **12** (1991) 85 (http://www.koreascience.or.kr/article/JAKO199113464455707.page)
17. C. Cottet, A. G. Salvay, M. A. Peltzer, M. Fernández-García, *Polymers* **13** (2021) 200 (https://doi.org/10.3390/polym13020200)
18. R. Chauhan, V. Choudhary, *J. Appl. Polym. Sci.* **115** (2010) 491 (https://doi.org/10.1002/app.30824)
19. K. Bae, S. H. Koo, W. Seo, *Arch. Pharm. Res.* **14** (1991) 41 (https://doi.org/10.1007/BF02857812)
20. Y. Xie, W. Yang, F. Tang F., X. Chen, L. Ren, *Curr. Med. Chem.* **22** (2015) 132 (https://doi.org/10.2174/0929867321666140916113443)
21. F. Farhadi, B. Khameneh, M. Iranshahi, M. Iranshahy, *Phytother. Res.* **33** (2019) 13 (https://doi.org/10.1002/ptr.6208)
22. T. J. Cuthbert, B. Hisey, T. D. Harrison, J. F. Trant, E. R. Gillies, P. J. Ragogna, *Angewandte Chemie* **57** (2018) 12707 (https://doi.org/10.1002/anie.201806412)
23. G. L. Y. Woo, M. W. Mittelman, J. P. Santerre *Biomaterials* **21** (2000) 1235 (https://doi.org/10.1016/s0142-9612(00)00003-x).

Journal of the Serbian Chemical Society
JSCS@tmf.bg.ac.rs • www.shd.org.rs/JSCS
J. Serb. Chem. Soc. 87 (5) S130–S134 (2022) *Supplementary material*

SUPPLEMENTARY MATERIAL TO

Antimicrobial and anticancer activities of copolymers of tri-*O*-acetyl-D-glucal and itaconic anhydride

CHETANA DEOGHARE[1], SHRUTI BALAJI[2], SAVITHA DHANDAPANI[3], HONEY SRIVASTAVA[4], ANASUYA GANGULY[5]* and RASHMI CHAUHAN[4]**

[1]*Department of Chemistry, Institute of Sciences, Humanities and Liberal Studies, Indus University, Rancharda, via Silaj, Ahmedabad - 382115, Gujarat, India,* [2]*PlantaCorp GmbH, 20097 Hamburg, Germany,* [3]*Temasek Life Sciences Laboratory, National University of Singapore – 117604, Singapore,* [4]*Department of Chemistry, BITS-Pilani, K. K. Birla Goa Campus, Goa, India and* [5]*Department of Biological Sciences, BITS-Pilani, K. K. Birla Goa Campus, Goa, India*

J. Serb. Chem. Soc. 87 (5) (2022) 629–640

SPECTRAL DATA

Itaconic anhydride

IR (KBr, cm^{-1}), Fig. S-1: 3599 (alkenyl C-H stretch), 1700 (>C=O of imide), 1621 (>C=C< of double bond of the ring), 731 (oop C-H bending). ^1H NMR (500 MHz, $CDCl_3$), δ / ppm, Fig. S-2: 6.5 ppm ($1H_a$, s); 5.9 ppm ($1H_b$, s); 3.6 ppm ($2H_c$, s).

*,** Corresponding authors. E-mail: (*)ganguly@goa.bits-pilani.ac.in; (**)rchauhan@goa.bits-pilani.ac.in

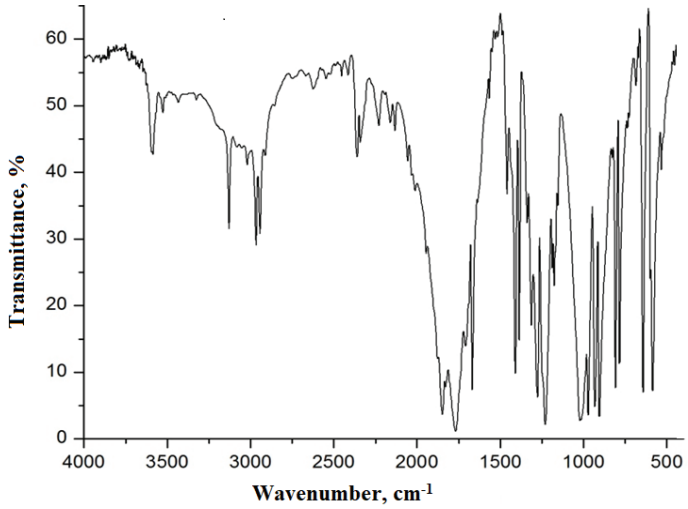

Fig. S-1. FT-IR Spectra of itaconic anhydride (IA).

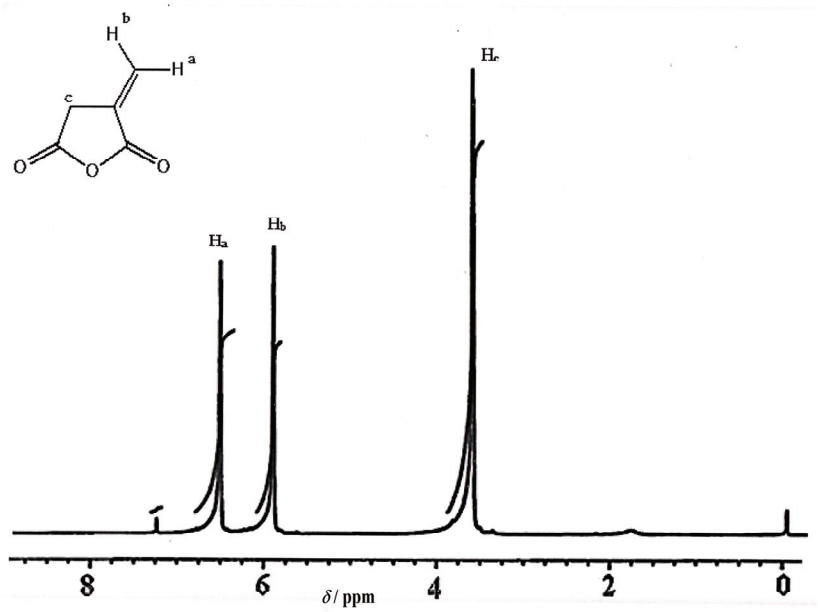

Fig. S-2. ^{1}H-NMR of IA.

TAG

^{1}H NMR (500 MHz, $CDCl_3$), δ / ppm, Fig. S-3: 2.0 ppm ($9H_a$, s); 4.0 ppm ($1H_c$, m); 4.2 ppm ($1H_d$, m); 4.3 ppm ($1H_b$, m); 4.8 ppm ($1H_g$, s); 5.2 ppm ($1H_e$, d); 5.3 ppm ($1H_f$, d); 6.4 ppm ($1H_h$, s).

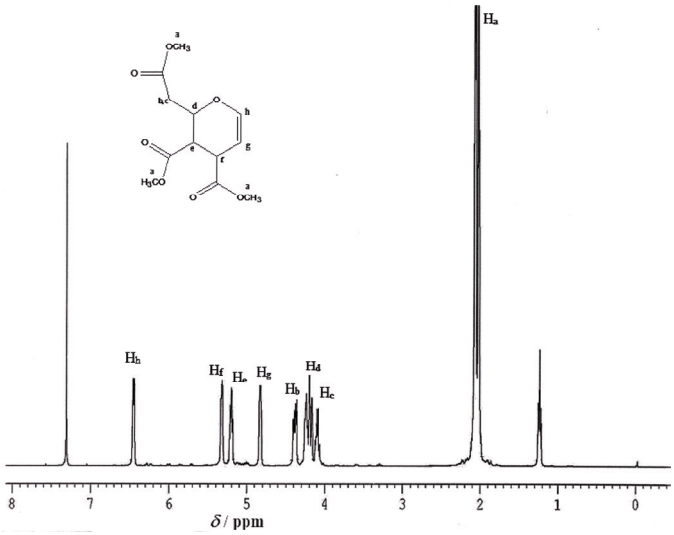

Fig. S-3. ^{1}H-NMR of TAG.

PSG

^{1}H-NMR (500 MHz, $CDCl_3$), δ / ppm, Fig. S-4: 2.0 ppm ($6H_a$, s); 2.2 ppm ($1H_h$, hump); 4.1 ppm ($1H_c$, m); 4.2 ppm ($1H_b$, m); 5.3 ppm ($1H_d$, m); 5.4 ppm ($1H_g$, d); 5.9 ppm ($1H_e$, $1H_f$, d).

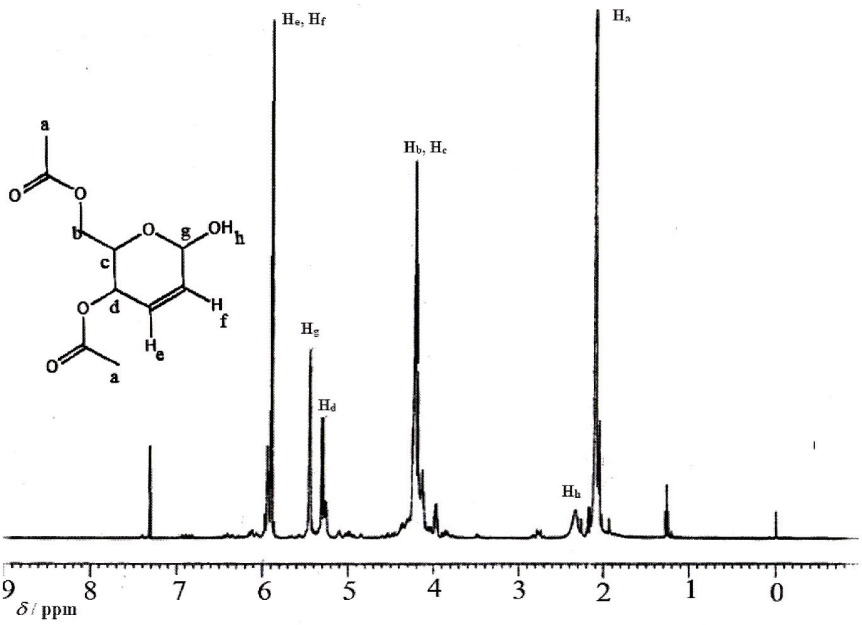

Fig S-4. ^{1}H-NMR of PSG.

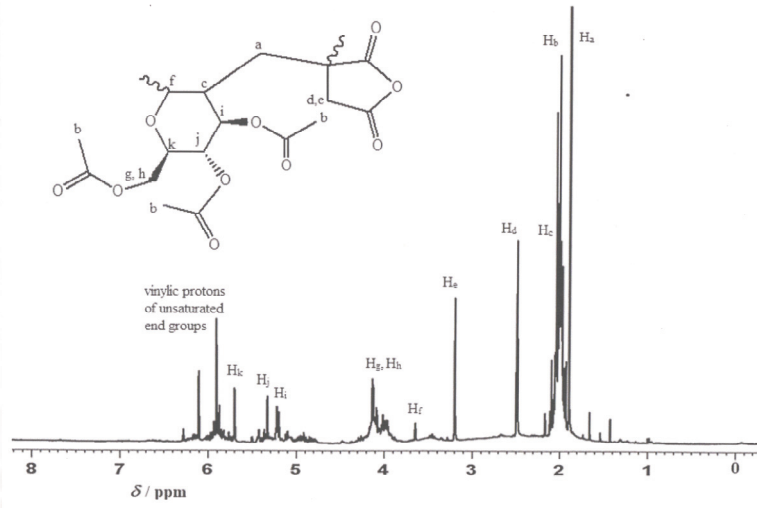

Fig. S-5. ^{1}H NMR spectrum of IA-TAG5.

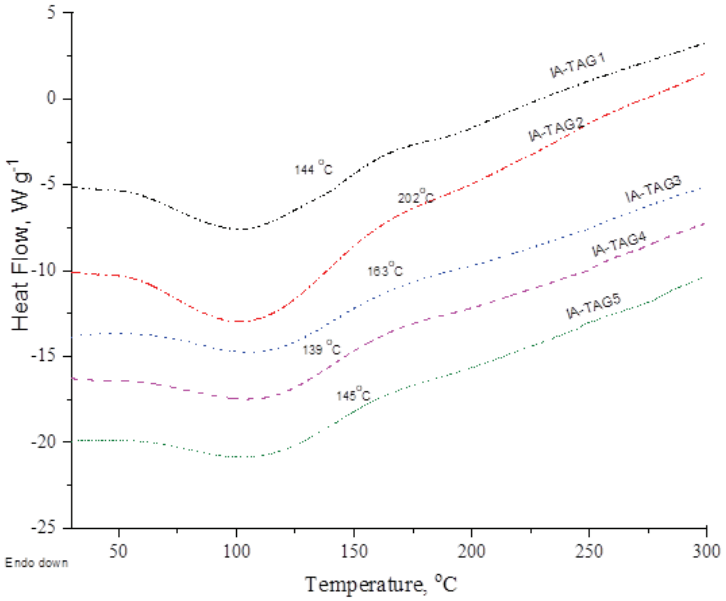

Fig S-6. DSC Scans of IA-TAG Copolymers

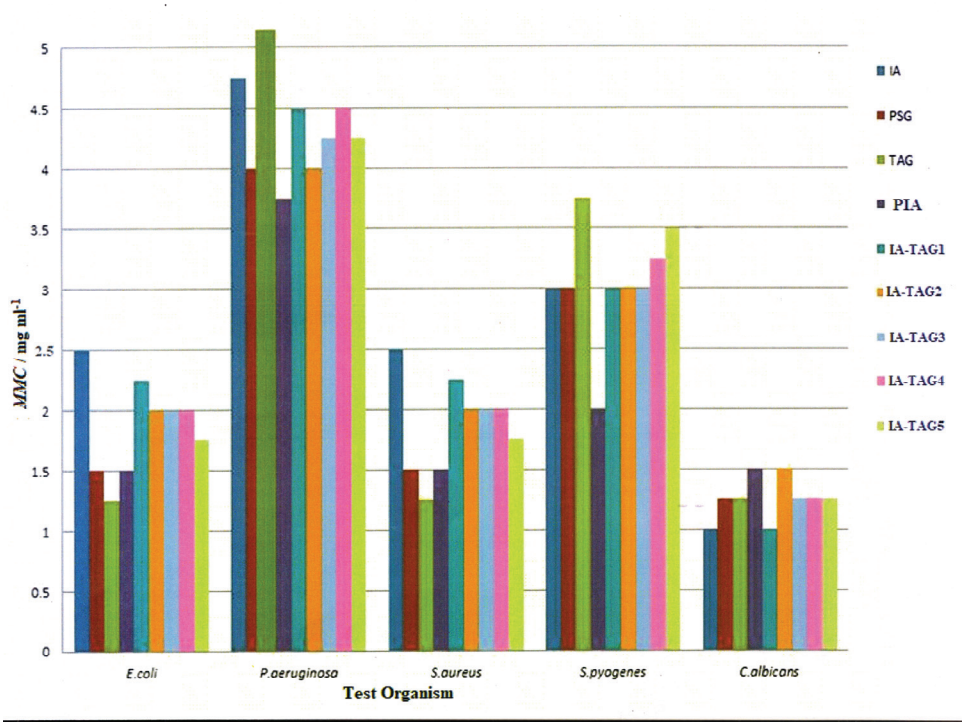

Fig S-7. Anti-microbial activity of Monomers and copolymers of IA and TAG.

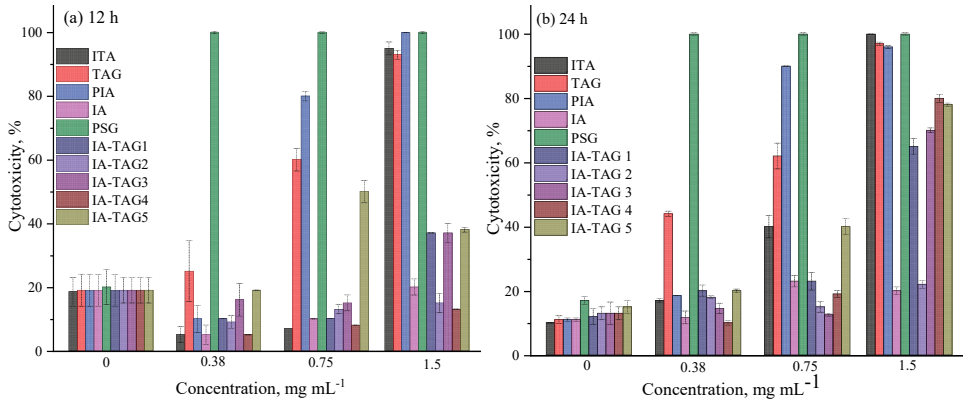

Fig S-8. The cytotoxic effect of the various test compounds after (a) 12h and (b) 24h on A549 human lung adenocarcinoma cells. The cytotoxicity of the test compounds was estimated using the trypan blue viability test. Error bars represent standard deviation.

Journal of the Serbian Chemical Society
JSCS-info@shd.org.rs • www.shd.org.rs/JSCS
J. Serb. Chem. Soc. *87* (5) 641–655 (2022)
JSCS–5547
Original scientific paper
Published 28 April 2022

Synthesis and physicochemical characterization of Arabic gum microgels modified with methacrylic acid as potential drug carriers

SANI M. IBRAHIM[1,2], MISNI MISRAN[1] and YIN YIN TEO[1]*

[1]*Department of Chemistry, Faculty of Sciences, University of Malaya, Kuala Lumpur, Malaysia and* [2]*Department of Chemistry, Faculty of Sciences, Federal College of Education, Zaria, Nigeria*

(Received 9 September 2021, revised 18 February, accepted 21 February 2022)

Abstract: Microgels of carbohydrate polymers are non-toxic and biocompatible that can readily be used in applications such as drug delivery, medicine, and pharmacy. In this work, Arabic gum (AG) microgels and methacrylic acid modified Arabic gum microgels (AGMAA) were synthesized *via* the water in oil emulsion polymerization technique using Tween 20 as the surfactant and hexane as the solvent. The microgels were characterized using various physicochemical methods such as Fourier transform infrared spectroscopy, thermal stability using differential scanning calorimetry, diffraction pattern analysis using X-Ray diffraction, morphology observation using field emission scanning electron microscopy and dynamic light scattering was used to analyze the size and zeta potential. The rate of deformation was higher in the AG microgels compared to the AGMAA microgels. The particle size and zeta potential of the AGMAA microgel were found to be larger and more negative than AG microgel, respectively. The particle size and zeta potentials of the microgels were found to be dependent on the amount of methacrylic acid as the modifying agent. The microgels were encapsulated with doxorubicin through the swelling method and the *in vitro* release was studied in mediums with pH values of 4.2 and 7.4. The results suggest the potentials of these microgels for drugs delivery.

Keywords: carbohydrate; encapsulation; drug delivery; doxorubicin; emulsion.

INTRODUCTION

Biopolymers of polysaccharide origin are currently used in different biomedical domains for applications such as drug delivery and tissue engineering due to their cytocompatibility and degradation possibility without causing damage to the systems.[1] Most of these biopolymers require additional modification to overcome

* Corresponding author. E-mail: yinyinteo@um.edu.my
https://doi.org/10.2298/JSC210909015D

the problem related to mechanical instability resulting from exposure to different media.[2,3]

Generally, microgels are targeted at increasing the drug loading, promote slow release and reduce the side effects of drugs during delivery for the application in the biomedicine and pharmaceutical fields. Microgel synthesis from natural polymers, such as carbohydrates, have shown an increasing trend due to their promising nature for drug delivery.[4] They are generally non-toxic, biodegradable, biocompatible and possess tuneable properties including shape, size and porosity.[5,6] The distinct properties of microgels include biocompatibility, permeability and water retention capacity have led to different applications of microgels in biomedical fields such as wound dressing, tissue engineering and blood vessel replacement, contact lenses and drug delivery systems.[7,8]

Arabic gum (AG) is among the class of carbohydrates that have found various uses in adhesive, food, cosmetics, medical and other industrial applications. The chemical and physical modification of AG provides new functionality for the desired application such as drug delivery devices and mimicking tissues for engineering. AG consists of molecules including arabinogalactan, amino acids and short chain arabinose side chains.[9] It has been used as emulsifier and for encapsulating flavours, especially unstable compounds,[10,11] binding agent in tablets processing[12] and also as a release modifier.[13]

AG microgels have been studied by many researchers for the development of delivery devices. Sarika and James synthesized nanogels using AG, gelatin, and aldehyde *via* the inverse-miniemulsion technique. The gelatin serves as a cross linking agent,[14] while Ganie *et al*. formulated nanogels of AG that were non-toxic using acetyl groups and iodine monochloride with the polysaccharide.[15] Farooq *et al*. prepared and modified AG microgels using diethylenetriamine and taurine that were found to be compatible and non-toxic.[6] Researchers have reported that microgels made from AG are degradable, non-toxic and compatible for drug delivery, but AG has poor mechanical strength, is highly soluble in water, and has low viscosity at high concentrations. It is possible to overcome these drawbacks through the modification of AG using a monomer with good mechanical strength, such as methacrylic acid (MAA).[16] Microgels formulated by combination of AG and MAA are hypothesized to improve their mechanical properties, swelling property and controllable viscosity. The present research was targeted on synthesizing MAA modified AG (AGMAA) microgels *via* water in oil emulsion system by cross linking and polymerization reactions. The emulsion technique was applied to promote the formation of spherical shapeed particles that are useful for many applications due to their large surface area. The capability of the AGMAA microgels as potential candidate as drug carriers was also evaluated through encapsulation of doxorubicin in the microgels.

EXPERIMENTAL

Arabic gum (AG) branched polysaccharide (*Mw*: 250,000 g mol^{-1}, Sigma–Aldrich), methacrylic acid (MAA) (*Mw*: 86.06 g mol^{-1}, 99 %, Merck), *N,N′*-methylenebisacrylamide (MBA, *Mw*: 154.17 g mol^{-1}, 99 %, Sigma–Aldrich), poly(ethylene glycol) sorbitan monolaurate (Tween 20), Sigma–Aldrich), ammonium persulfate (APS, *Mw*: 228.20 g mol^{-1}, Sigma–Aldrich), doxorubicin (Sigma–Aldrich), acetone (*Mw*: 58.08 g mol^{-1}, 99 %, Merck), hexane (*Mw*: 86.18 g mol^{-1}, 99 %, Sigma–Aldrich), ethanol (99 %, Sigma–Aldrich), and sodium hydroxide pellets (*Mw*: 40.0 g mol^{-1}, Schmidt) were used as received without modification.

Synthesis of Arabic gum microgel via *emulsion polymerization*

Microgels were synthesized according to a previously reported method using the inverse suspension method whereby oil in water emulsion systems was prepared.[8,17,18] A novel oil in water emulsion system consisting of surfactant Tween 20 (10 %) in hexane for the synthesis of AG microgels was applied in this study. A solution of 10 % AG in 0.5 M NaOH solution was prepared and stirred for one hour to form a homogenous solution. Thereafter, 10 ml of the prepared solution was transferred into 100 ml reaction bottle containing 50 ml of the emulsion system of Tween 20 in hexane. The mixture was mixed for 30 min at 1000 rpm using magnetic stirrer, 2 ml of 2.5 % ammonium persulphate solution was added, and stirred for 30 min at 60 °C, followed by the addition of 100 mg *N,N′*-methylene bisacrylamide (MBA) as the crosslinking agent of the polymerization reaction. The colour change of the mixture to whitish indicated the formation of particles through crosslinking. The stirring was continued for additional 30 min to ensure completeness of the reaction. The product was precipitated using excess acetone, the emulsion phase was decanted, and the solid residue of the microgel particles were washed twice with acetone and twice with ethanol:water solution in the ratio of (1:1) by volume. The AG microgels were incubated in an oven at 45 °C before analysis.

Synthesis of arabic gum cross-linked methacrylic acid microgel

Methacrylic acid modified Arabic gum microgels (AGMAA) were synthesized using a similar procedure to that given above with the addition of 2 ml solution of methacrylic acid and left stirring for 30 min before the final addition of 100 mg *N,N′*-methylene bisacrylamide (MBA) to crosslink AG and MAA in the emulsion reaction system. The colour of the mixture changed from colourless to whitish upon formation of the particles. The stirring was continued for an additional 30 min to allow complete crosslinking of the particles.

Physicochemical characterization

Fourier transform infrared spectroscopy (FTIR). AG, AGMAA microgels, AGMAA microgel entrapped doxorubicin, physical mixture of AGMAA microgels and doxorubicin, and all the starting materials were analysed using a Perkin Elmer Spectrum 400 at 25 °C. The wavenumber range of 4000–500 cm^{-1} at a resolution of 2 cm^{-1} was used for the analysis. The background was analysed to serve as a control. The microgels were dried in an oven before the analysis.

X-Ray diffraction analysis (XRD). The crystallinity and diffraction pattern of the microgels were analysed using an Empyrean X-ray diffractometer. The samples were exposed to CuKα radiation at an accelerating voltage of 40 kV and a current of 40 mA. The scan rate was set at 1°/min. The diffraction angle was varied within the range of 5 to 50° at 2θ. The analysis was performed at 25 °C.

Differential scanning calorimetry (DSC). The thermal properties of the microgels were analysed using differential scanning calorimeter (Perkin Elmer). About 7–10 mg of dried mic-

rogel samples was weighed in an aluminium pan while an empty pan was the reference pan. The sample was heated under an nitrogen atmosphere at a scanning rate of 10 °C/min. The measurements were performed within the temperature range of 20–350 °C.

Field emission scanning electron microscope (FESEM). The surface morphology of microgels was observed using a field emission scanning electron microscope. The microgels were initially swollen in water for 24 h, followed by freeze drying in liquid nitrogen for 48 h. The dried microgels samples were then coated with gold to prevent charging effect. The morphology was studied with a Quant FEG 450 instrument at a beam voltage of 5 kV. Surface images were captured at different magnifications and focus.

Hydrodynamic particle size and zeta potential measurement

The analysis of the mean particle size and zeta potential of AG and AGMAA microgels were measured using a Malvern Nano ZS Zetasizer Zen 3600 (Malvern Instruments Ltd., UK).[19] The samples were investigated at a backscattered angle of 173° using a scattering laser light 633 nm at 25 °C. The mean particle size and zeta potential were obtained from three replicates.

Degradation study of microgels

The microgels were swollen in phosphate buffer solution (PBS) of pH 7.4 for the degradation study at temperature 37 °C. The degradability of AG and AGMAA microgels were analysed. This enable assessing the effect of the cross-linked monomers on the rate of degradation of the microgels at pH 7. The microgels particles were first dried in oven to constant weight followed by immersion into 20 ml of aqueous buffer solutions at 37 °C for six weeks.[20] The weight of AG and AGMAA microgels particles were recorded every 24 h and the aqueous medium was replaced by fresh buffer solutions pre-equilibrated at 37 °C every 24 h throughout a period of six weeks.

The weight loss percentage or decrease in mass percentage was recorded as percentage degradation of the microgel materials as a function of time, as shown in Eq. (1):

$$\text{Degradation} = 100\frac{M_t}{M_{\max}} \tag{1}$$

where M_t is the weight at time t and M_{max} is the maximum swollen weight of the microgel.

Doxorubicin encapsulations and in vitro *drug release study*

The post-formation loading method was applied to entrap 3 mg doxorubicin in the formulated microgel. The encapsulation efficiency of the microgel was studied by measuring 300 mg of the dried microgel and added it into 30 ml doxorubicin solution of concentration 0.1 mg ml^{-1}. The mixture solution was placed on an orbital shaker at 25 °C under a constant shaking of 10 rpm for 24 h to ensure efficient encapsulation of the doxorubicin into the microgels. The entrapped doxorubicin in microgel was separated from the un-entrapped doxorubicin by centrifugation at 10,000 rpm for 10 min. The supernatant was collected for determination of the concentration of un-entrapped doxorubicin. The microgel samples were dried in an oven at 45 °C. The encapsulation efficiency of the doxorubicin was determined according to Eq. (2), where c_{TDS} represented the concentration of doxorubicin that was initially introduced into the preparation, c_{DS} is the concentration of drugs left in the supernatant after the centrifugation. A series of doxorubicin in deionized water varying in concentration were prepared as standards for the calibration curve and measured at 485 nm using a UV–Vis spectrophotometer:

$$EE = 100\frac{c_{TDS} - c_{DS}}{c_{TDS}} \tag{2}$$

The *in vitro* drugs release from the microgels with different loading capacity was investigated in mediums of pH 4.2 and pH 7.4. The study of drug release at pH 4.2 was performed to assess the drug release and kinetics in acidic medium while pH 7.4 represent a neutral pH. All the studies were performed at a temperature of 37 °C.

The kinetic of drug released was studied using the Ritger–Peppas model[21] as one of the most appropriate models used for hydrogels and microgel drug release study, where the ratio of drug release is directly proportional to time as shown in Eq. (3):

$$F_D = \frac{m_t}{m_\infty} = kt^n \quad (3)$$

where F_D is the ratio of drug release at time t, to the equilibrium swollen state. m_t and m_∞ are the amount of drugs released at time t and at equilibrium state, respectively. n is the diffusion exponent of the release mechanism and k is the proportionality constant that measures the speed of release and geometrical parameters comparable to the drug-polymer system.

RESULTS AND DISCUSSION

Synthesis of AG microgels via *emulsion polymerization*

The emulsion system consisting of 10 % of aqueous Tween 20 in hexane enabled the formation of reversed micelle to accommodate Arabic gum molecules in the core of reversed micelle that are hydrophilic.[8,17] Addition of APS generated free radical during heating at temperature ≈60 °C to create active sites on the Arabic gum molecules. Addition of MBA into the emulsion system under constant stirring allowed the diffusion of the MBA molecules into the core of the reversed micelles. Subsequently, MBA cross-linked with the molecular radical active site of the hydroxyl group in Arabic gum molecules to terminate the reaction. Tween 20 as a surfactant remained in the structure to provide a template for the formation of microgels.[22]

Formulation of Arabic gum-grafted-poly(methacrylic acid) microgels

A similar reaction occurred between AG and MAA as in the formation of AG microgel, except that MAA was introduced into the reaction after the generation of AG radicals. The AG radical abstracted a proton from the ethylene group of methacrylic acid leading to propagation of the polymer chains [23–25] through graft polymerization to form the Arabic gum–grafted-poly(methacrylic acid). Then, the cross-linking agent (MBA) was added into the emulsion system to terminate the chain propagation. In the termination reaction, MBA cross-linked the molecules of AG with radical active hydroxyl group and the radical active ethylene group of poly(methacrylic acid). The proposed scheme is shown in the graphical abstract while the digital images of the products are shown in Fig. 1.

FTIR spectroscopy

The FTIR spectrum of starting materials and the synthesized microgels are shown in Fig. 2. The AG spectrum indicates the presence of peaks at 3279 (OH), 2928 (CH stretch), 1601 (C=O group), 1410 (CH_2 group) and 1026 cm^{-1} (CO

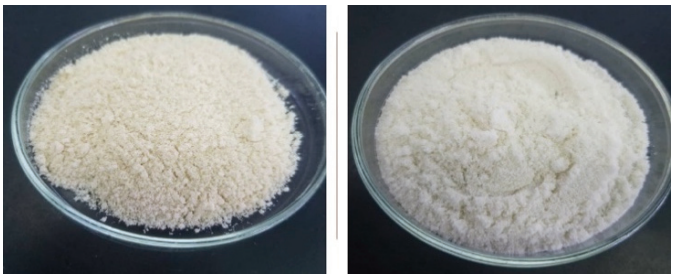

a b

Fig. 1. Digital images of :a) AG microgels and b) AGMAA microgels.

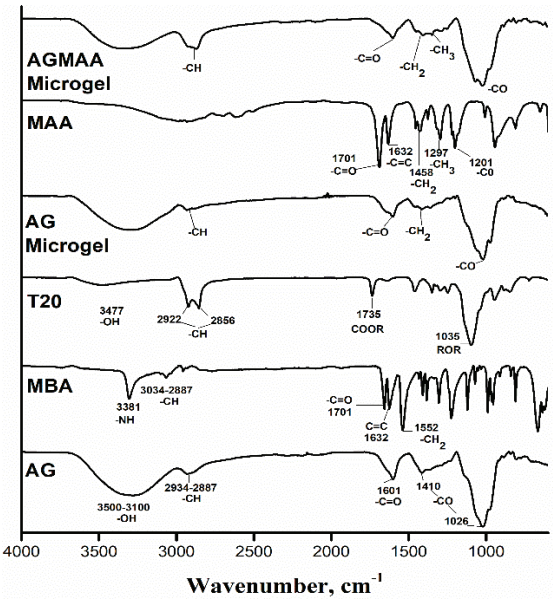

Fig. 2. FTIR Spectra of AG, MBA, T20, AG microgel, MAA and AGMAA microgel.

group). The Tween 20 spectrum shows the presence of hydrogen bonded O–H stretching at 3477 cm^{-1}, asymmetric and symmetric methylene stretching vibration at 2922 and 2856 cm^{-1}, carbonyl group from R–CO–O–R at 1734 cm^{-1} and ether linkages of polyethylene glycol ($–CH_2–O–CH_2–$) as a sharp peak at 1092 cm^{-1}. The AG microgel spectrum indicates a broad peak at 3302 cm^{-1} of NH and OH stretching due to their overlapping and the peaks at 2928, 1605 and 1026 cm^{-1} correspond to C–H stretching, C=O group and CO stretch, respectively. The low intensity but visible peaks in the range of 900–1150 cm^{-1} correspond to the ethylene group indicates the presence of Tween 20 in the microgel.

The spectrum of the AGMAA microgels shows peaks at 3302 (OH/NH stretch), 2928 (CH stretch), 1601 (C=O), 1434 ($–CH_2$ group), 1303 ($–CH_3$ group) and 1026 cm^{-1} (C–O stretch). The disappearance of the peak at 1632 cm^{-1} (C=C group) indicated the successful grafting of AG and MAA molecules in the mic-

rogel. The presence of Tween 20 in the microgel was identified by the band at 1100 cm^{-1}, correspond to $–CH_2–O–CH_2–$ group.

The interaction between doxorubicin and AGMAA microgels at the level of functional groups was evaluated using the FTIR spectrum as shown in Fig. 3. The spectrum of doxorubicin showed characteristic absorption bands at 3309 (N–H asymmetric stretching), 2920 (C–H stretching), 1731 (C=O symmetric stretching), 1617 and 1578 (amide I and amide II, respectively), 1285 (O–H···O), and 991 cm^{-1} (=C–H bending).[26,27] AGMAA microgel entrapped doxorubicin showed characteristic bands at 3280 (OH/NH stretch), 2935 (CH stretch), broadening band at 1624 (C=O) an–$^{-1}$ (C–O stretch) that can be attributed to AGMAA microgel. On the other hand, the presence of bands at 1539 cm^{-1} (amide II), and the characteristic band for doxorubicin at 1286 cm^{-1} also noticed, this indicated the presence of doxorubicin molecules in the AGMAA microgels. The spectra of AGMAA microgel entrapped doxorubicin was found approximately similar to that of the physical mixture. The absence of a new peak in the physical mixture suggested that there was no chemical interaction between doxorubicin and the AGMAA microgel. This demonstrated the integrity and stability of DOX within the AGMAA microgel.

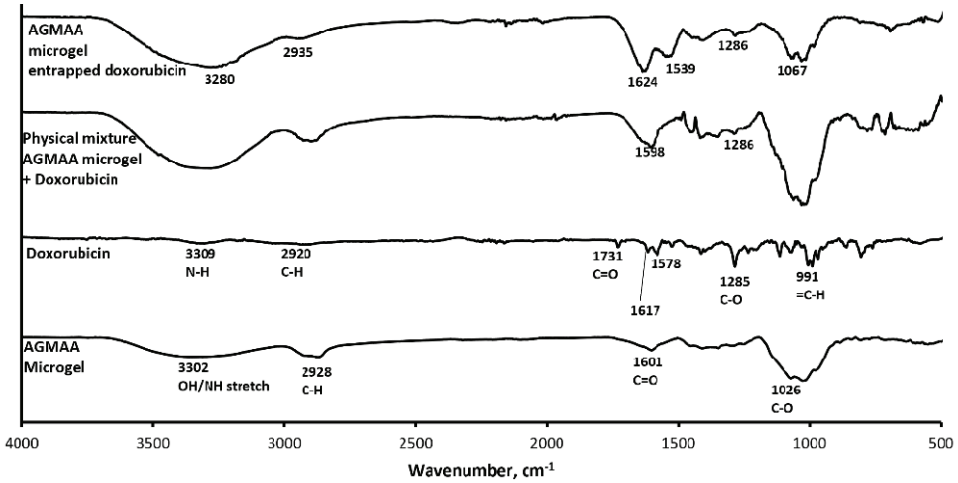

Fig. 3. FTIR Spectra of AGMAA microgel, Doxorubicin, physical mixture of AGMAAmicrogel + doxorubicin, and AGMAA microgel entrapped doxorubicin.

Differential scanning calorimetry (DSC)

The thermograms of AG and AGMAA microgels are shown in Fig. 4. Two major curves were observed in the thermogram, one endothermic and one exothermic. The endothermic curves correspond to the melting temperature of microgels that appeared at 183 and 171 °C for AG and AGMAA, respectively. The

microgels changed phase from solid to liquid state. These data were found similar to AG microgels by Farooq *et al*. and AGMAA hydrogels by Mamman *et al*.[6,16] The melting enthalpy of the Arabic gum microgel was higher (152 J g^{-1}) than that of the AGMAA microgel (139 J g^{-1}). The lower melting peak and melting enthalpy for AGMAA microgels could be attributed to the formation of branches by MAA in the AG molecules. The ordered arrangement of the AG was disrupted by grafting with MAA molecules, this relaxed the stiffness of the molecular arrangements in the AG molecules. The exothermic curves at 277 and 290 °C for AG and AGMAA microgels, respectively, indicate decomposition of the microgels. The decomposition enthalpy for AG and AGMAA microgels were –25.4 and –149 J g^{-1}, respectively. The difference in temperature and enthalpies of decomposition suggests the grafting of MAA on AG stabilized the formulated microgels.

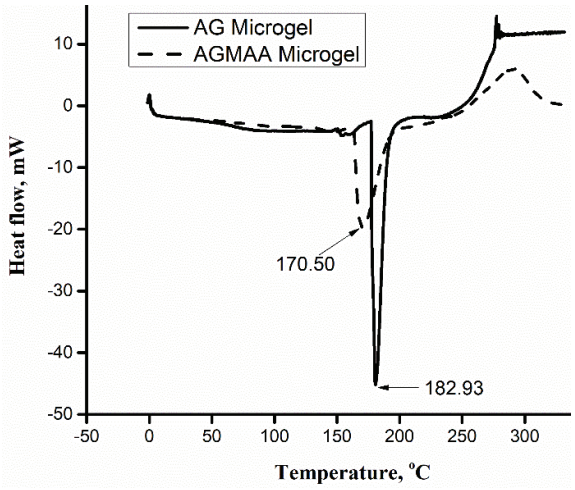

Fig. 4. DSC thermograms of AG and AGMAA microgels.

X-Ray diffraction

The XRD plots of the AG and AGMAA microgels are presented in Fig. 5. The XRD of the AG microgel showed the presence of two characteristics peaks at 2θ 14 and 20°. The first peak was sharp with a low peak area confirming the unique structural reformation due to cross-linking of the AG particles while the latter peak was broad with a low intensity is usually found as a characteristic peak of Arabic gum but with high intensity as amorphous polymer.[16] The distinctive sharp peak of the AG microgel indicates the absence of modifying agents and regularity in the newly formed semi-crystalline structure with a characteristic sharp peak at 2θ = 14°. The AGMAA microgels showed a reflection peak at 2θ = = 20°. The semi-crystal nature of the gum was reduced due to the introduction of MAA monomers into the main structure.

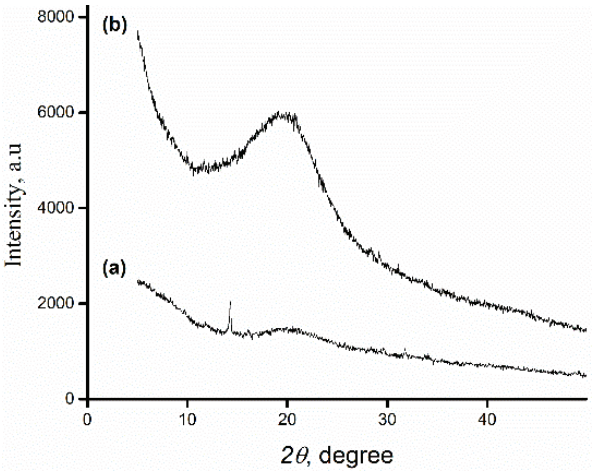

Fig. 5. XRD Spectrum of the microgels: a) Arabic gum microgel and b) AGMAA microgel.

Field emission scanning electron microscopy (FESEM)

The micrographs of the AG microgel and AGMAA microgel are shown in Fig. 6. The particles are spherical because the microgels were formed within the spherical shape micelles during polymerization, the system where the processes of grafting and cross-linking occured.[6,26] The micrograph of AG microgels is shown in Fig. 6a. It shows the presence of uniform and closely packed spherical microgels from the inner point of view. While Fig. 6b shows the micrograph of AGMAA microgel, the morphology shows the presence of many spherical structures that are not as closely packed as the AG microgels.

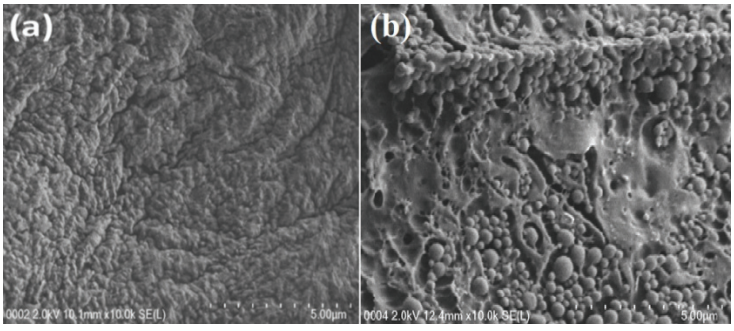

Fig. 6. FESEM micrographs of: a) AG microgel and b) AGMAA microgel.

Particle size and potential analysis

The average range of the particle size distribution by number of the AG microgel was smaller than the size of the methacrylic acid modified AGMAA microgels. The AG and AGMAA microgels have particle size ranges of 1.0–7.0

and 0.7–7.5 μm, respectively. The particles size depends on the amount of surfactant introduced in the emulsion system and agrees with AG microgels synthesized by other researchers.[6,18] A subsequent study was conducted by reducing the amount of surfactant from 10 % as stated in the synthesis procedure to 5 % in order to determine the effect of the surfactant on the size of the microgel particles and it was found that the size of the microgels has a direct relation with the emulsion system. This is shown in Fig. 7a and b where the size is shown to increase as the surfactant concentration is increased.

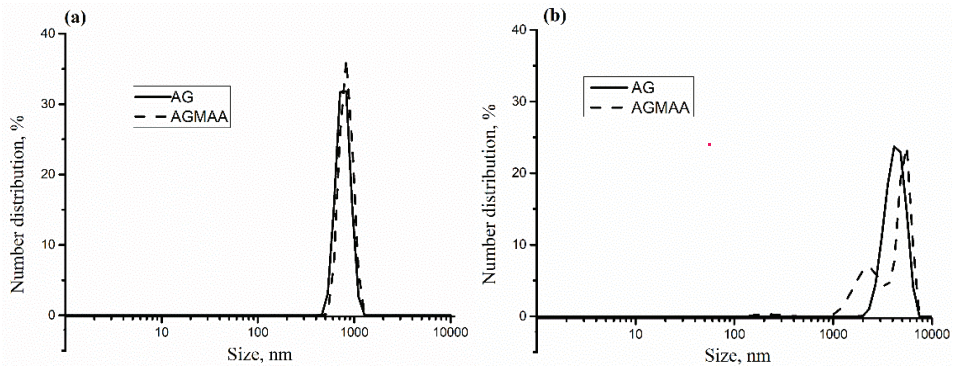

Fig. 7. Microgel particles sizes of AG and AGMAA microgels at: a) 5 and b) 10 % surfactant.

The zeta potential, conductivity, and electrophoretic mobility (velocity per field strength) of the microgels are given in Table I. The magnitude of zeta potential for AGMAA microgels are significantly more negative as compared to the AG microgels. AG microgels displayed a lower magnitude of the zeta potential (–21.5 mV) compared to AGMAA microgels (–48.5 mV). AGMAA microgels showed the highest magnitude of the zeta potential, possibly attributed to ionization[28] of the methacrylic acid monomers in the polymer chain resulting in the presence of anions surrounding the surface.[28]

TABLE I. Zeta potential, conductivity and electrophoretic mobility of the microgels

Microgel	Zeta potential, mV	Conductivity, mS cm^{-1}	Electrophoretic mobility, μm cm V s^{-1}
AG	–21.5	3.9	–1.7
AGMAA	–48.5	1.9	–3.8

Degradation study of the microgels

The degradation study of the microgels was only performed in phosphate buffer solution pH 7.4, the microgel samples were immersed in the medium and the AG microgel swelled to maximum size in three days. There was a significant loss of weight/degradation of the AG microgel to 88 % after four days immersion in the medium. It continued to degrade until only 36 % of its weight remained

after thirteen days. On the following day, there was a drastic decrease of weight from 36 to 18 % and subsequently to 4 % after fifteen days and further reduced to 0.01 % on the subsequent day. Complete 100 % degradation of the Arabic gum crosslinked microgel had occurred after the seventeenth days. On the contrary, for the AGMAA microgels, the maximum swelling in the phosphate buffer solution pH 7.4 was achieved in two days. The microgels started to degrade after three days and down to 51 % in twenty-eight days. The modified microgel particles continued to degrade and only 2 % of the initial microgel weight was left after 36 days immersed in the medium. In conclusion, about 98 % of the AGMAA microgel was degraded in 36 days. Degradation depended solely on the structural composition of each microgel sample, AG microgel which degrade faster and has highest percentage degradation is as the result of the availability of carboxylic group and lack of synthetic materials such as the monomers and cross-linking agents while the slow degradation rate observed in AGMAA microgels could be attributed to the presence of synthetic monomers of methacrylic acid and high cross-linking between the carboxylic group of AG molecules and ethylene group of the methacrylic acid.[16] The degradation is shown graphically in Fig. 8.

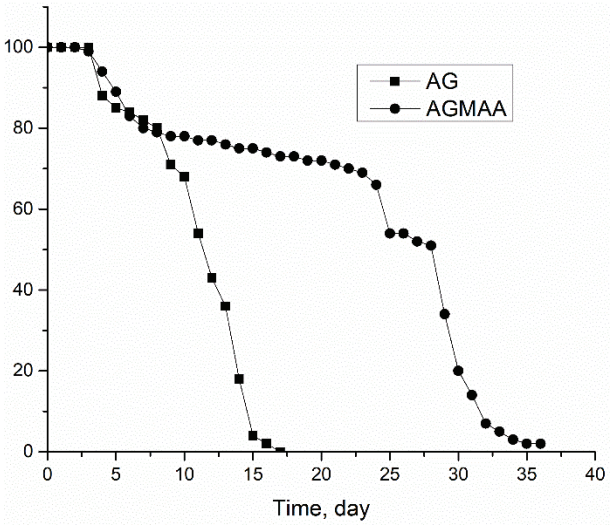

Fig. 8. Degradation of AG microgels and AGMAA microgels in phosphate buffer pH 7.4; the values at *y*-axis relate to content of residuals in %.

Drug encapsulation

The post-formation loading method was used to entrap doxorubicin in microgels to study the potential of formulated microgels as drug carrier. The concentration of doxorubicin entrapped in the microgels were determined from the calibration curve. The encapsulation efficiency of the AG microgel was 61.3±0.3 %

that was lower than AGMAA microgel 73.4±0.3 %. Drug encapsulation on microgels depends on the swelling capacity on absorption. The high percentage encapsulation by AGMAA microgel is ascribed to the high swelling rate of the microgels compare the AG microgels.

In vitro *drug release study*

The *in vitro* release profile of doxorubicin drug from the AG microgels and AGMAA microgels in buffer solutions of pH 4.2 and pH 7.4 at 37 ℃ are shown in Fig. 9. The *in vitro* drug release from the microgel formulations is dependent on the medium of release and the microgel formulation. The percentage release in acidic medium (pH 4.2) for all the formulations was higher as compared to the release in pH 7.4.

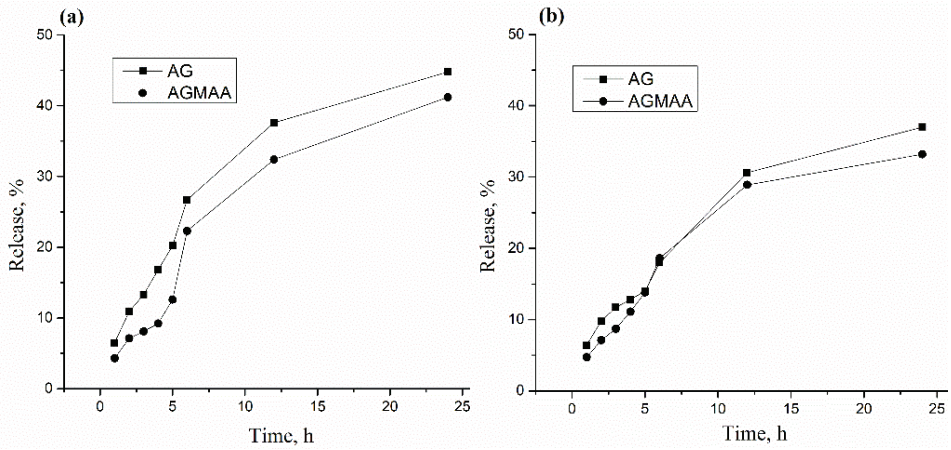

Fig. 9. Release of doxocubicin from microgels at pH: 4.2 (a) and 7.4 (b).

A high rate of release was recorded in all the media within the first 5 h, and this could be credited to the presence of doxorubicin drugs that are loosely attached to the microgel particles after the centrifugation process. AG and AGMAA have a percentage release of 44.8 and 41.3 % in pH 4.2 and 37.0 and 33.2 % in pH 7.4, respectively. The lower release at high pH is attributable to the restriction of protonation of the carboxylic group at higher pH by the presence of the surfactant molecules on the microgels surfaces leading to a low rate of network expansion.

The *in vitro* release kinetics of the microgels were investigated using the Ritger–Peppas model and the data generated for the kinetics were fitted and the kinetics data such as diffusion exponent (n) for the mechanism of drug release and the geometry parameter constant (k) for the velocity of drug release that is analogous to a polymer-drug system were calculated and the results are given in Table II. The kinetics data at pH 4.2 and pH 7.4 were different that is due to the

swelling and interaction of the microgels molecules at the different pH values. The value of n for AG and AGMAA microgels were 0.58 and 0.71 at pH 4.2 and 0.53 and 0.60 at pH 7.4, respectively.

TABLE II. Release kinetics of doxorubicin from microgels at pH 4.2 and 7.4 (values separated by /)

Microgel	n	$k \times 10^{-4}$, h^{-n}	R^2	r
AG	0.58/0.53	6.1/6.0	0.87/0.85	0.93/0.92
AGMAA	0.71/0.60	6.8/6.4	0.89/0.87	0.94/0.93

The observed n values that are greater than 0.43 but less than 0.85 indicate non-Fickian diffusion mechanism controlled by swelling and diffusion drug release mechanism. The value of the geometry parameter k for the release velocity was lowered at the high pH indicating a slower rate of drug release at pH 7.4 for the microgel formulations. The values of the statistical parameters such as R^2 and Pearson (r) indicate good fitting of the generated data to the Ritger–Peppas model.

CONCLUSIONS

The concentration of the surfactant plays an important role on the microgel formation process and affects the size (hydrodynamic diameter) distribution by number of the synthesized microgels. The synthesis of Arabic gum methacrylic acid modified microgel showed a significant improvement in terms of the size, zeta potential and the mechanical strength. Swelling and degradation study indicate a higher rate of degradation for the AG microgels as compared to the AGMAA microgels. These results demonstrated the possibility of microgel formation with improved strength and functionality using microemulsion polymerization method, and the microgel could be used for biomedical and pharmaceutical applications, especially in drug delivery, due to their tunable properties with the required size and surface area for catalytic reactions.

Acknowledgement. The research work was supported by University of Malaya, Malaysia. It was financially supported by RU Grant (ST042-2020).

ИЗВОД

СИНТЕЗА И ФИЗИЧКО–ХЕМИЈСКА КАРАКТЕРИЗАЦИЈА МИКРОГЕЛА ГУМАРАБИКЕ МОДИФИКОВАНЕ МЕТАКРИЛНОМ КИСЕЛИНОМ КАО ПОТЕНЦИЈАЛНОГ НОСАЧА ЛЕКОВА

SANI M. IBRAHIM[1,2], MISNI MISRAN[1] и YIN YIN TEO[1]

[1]*Department of Chemistry, Faculty of Sciences, University of Malaya, Kuala Lumpur, Malaysia и* [2]*Department of Chemistry, Faculty of Sciences, Federal College of Education, Zaria, Nigeria*

Микрогелови полимера угљених хидрата су нетоксични и биокомпатибилни и могу се лако користити у примени за су испоруку лекова, медицини и фармацији. Овај рад је показао синтезу микрогела гумарабике (AG) и микрогел гумарабике модификоване метакрилном киселином (AGMAA) користећи технику емулзионе полимеризације вода

у уљу са Tween 20 као површински активним средством и хексаном као растварачем. Микрогелови су окарактерисани коришћењем различитих физичко–хемијских анализа, као што је инфрацрвена спектроскопија са Фуријеовом трансформацијом, термичка стабилност диференцијалном скенирајућом калориметријом, дифракцијом рендгенских зрака, морфологија помоћу скенирајућег електронског микроскопа, док је динамичко расипање светлости коришћено за анализу величине и зета потенцијала. Степен деформације је био већи у микрогелу гумарабике у поређењу са микрогелом гумарабике модификованом метакрилном киселином. Утврђено је да су величина честица и зета потенцијал микрогела гумарабике модификоване метакрилном киселином већи и негативнији од микрогела гумарабике. Утврђено је да величина честица микрогела и зета потенцијали зависе од количине метакрилне киселине као агенса за модификовање. Микрогелови су инкапсулирани са доксорубицином методом бубрења и *in vitro* ослобађање је проучавано у медијуму са pH 4,2 и 7,4. Резултати указују на могућност примене ових микрогелова за испоруку лекова.

(Примљено 9. септембра 2021, ревидирано 18. фебруара, прихваћено 21. фебруара 2022)

REFERENCES

1. G. Ciofani, S. Del Turco, A. Rocca, G. De Vito, V. Cappello, M. Yamaguchi, X. Li, B. Mazzolai, G. Basta, M. Gemmi, *Nanomedicine* **9** (2014) 773 (https://www.futuremedicine.com/doi/pdfplus/10.2217/nnm.14.25)
2. J. K. Oh, D. I. Lee, J. M. Park, *Prog. Polymer Sci.* **34** (2009) 1261 (https://doi.org/10.1016/j.progpolymsci.2009.08.001)
3. H. Jing, J. Shi, P. Guoab, S. Guan, H. Fu, W. Cui, *Colloids Surfaces,. A* **611** (2021) 125805 (https://doi.org/10.1016/j.colsurfa.2020.125805)
4. P. M. Outuki, L. M. B. de Francisco, J. Hoscheid, K. L. Bonifácio, D. S. Barbosa, M. L. C. Cardoso, *Colloids Surfaces, A* **499** (2016) 103 (https://doi.org/10.1016/j.colsurfa.2016.04.006)
5. T. S. Anirudhan, J. Parvathy, A. S . Nair, *Carbohyd. Polym.* **136** (2016) 1118 (https://doi.org/10.1016/j.carbpol.2015.10.019)
6. M. Farooq, S. Sagbas, M. Sahiner, M. Siddiq, M. Turk, N. Aktas, N. Sahiner, *Carbohyd. Polym.* **156** (2017) 380 (https://doi.org/10.1016/j.carbpol.2016.09.052)
7. J. Jacob, J.T. Haponiuk, S. Thomas, S. Gopi, *Mat. Today Chem.* **9** (2018) 43 (https://doi.org/10.1016/j.mtchem.2018.05.002)
8. S. Sagbas, N. Sahiner, *Carbohyd. Polym.* **200** (2018) 128 (https://doi.org/10.1016/j.carbpol.2018.07.085)
9. A. S. Hoffman, *Adv. Drug Deliv. Rev.* **64** (2012) 18 (https://doi.org/10.1016/j.addr.2012.09.010)
10. A. Romo-Hualde, A. I. Yetano-Cunchillos, C. González-Ferrero, M. J. Sáiz-Abajo, C. J. González-Navarro, *Food Chem.* **133** (2012) 1045 (https://doi.org/10.1016/j.foodchem.2012.01.062)
11. D. Verbeken, S. Dierckx, K. Dewettinck, *App. Microbiol. Biotech.* **63** (2003) 10 (https://doi.org/10.1007/s00253-003-1354-z)
12. T. R. Bhardwaj, M. Kanwar, R. Lal, A. Gupta, *Drug Dev. Ind. Pharm.* **26** (2000) 1025 (https://doi.org/10.1081/DDC-100100266)
13. N. Malviya, S. Jain, S. Malviya, *Acta Pol. Pharm.* **67** (2010) 113 (https://ptfarm.pl/pub/File/acta_pol_2010/2_2010/113-118.pdf)

14. P. R. Sarika, N.R. James, *Int. J. Biol. Macromol.* **76** (2015) 181 (https://doi.org/10.1016/j.ijbiomac.2015.02.038)
15. S. A. Ganie, A. Ali, N. Mazumdar, *Carbohyd. Polym.* **129** (2015) 224 (https://doi.org/10.1016/j.carbpol.2015.04.044)
16. I. S. Mamman, Y. Y. Teo, M. Misran, *Polym. Bull.* **78** (2021) 3399 (https://doi.org/10.1007/s00289-020-03267-4)
17. S. Sagbas, S. Butun, N. Sahiner, *Carbohyd. Polym.* **87** (2012) 2718 (https://doi.org/10.1016/j.carbpol.2011.11.064)
18. P. Ilgin, G. Avci, C. Silan, S. Ekici, N. Aktas, R. S. Ayyala, V. T. John, N. Sahiner, *Carbohyd. Polym.* **82** (2010) 997 (https://doi.org/10.1016/j.carbpol.2010.06.033)
19. Y. Y. Teo, M. Misran, K. H. Low, *J. Chem.* **9** (2012) 421286 (https://doi.org/10.1155/2012/421286)
20. R. A. McBath, D. A. Shipp, *Polym. Chem.* **1** (2010) 860 (https://doi.org/10.1039/C0PY00074D)
21. P. L. Ritger, N.A. Peppas, *J. Control. Rel.* **5** (1987) 23 (https://doi.org/10.1016/0168-3659(87)90034-4)
22. B. Wedel, T. Brändel, J. Bookhold, T. Hellweg, *ACS Omega* **2** (2017) 84 (https://doi.org/10.1021/acsomega.6b00424)
23. W. Gao, C. Li, J. Li, Q. Zhang, N. Wang, B. Abdel-Magid, X. Qu, *J. Adh. Sci. Tech.* **33** (2019) 2031 (https://doi.org/10.1080/01694243.2019.1625852)
24. N. A. Harun, S. Kassim, S. T. Muhammad, F. E. Rohi, N. N. Norzam, N. S. M. Tahier, *AIP Conf. Proc.* **1885** (2017) 020032 (https://doi.org/10.1063/1.5002226)
25. J. X. Zhong, J. R. Clegg, E. W. Ander, N. A. Peppas, *J. Biomed. Mat. Res., A* **106** (2018) 1677 (https://doi.org/10.1002/jbm.a.36371)
26. S. Kayal, R. V. Ramanujan, *Mater. Sci. Eng.* **30** (2010) 484 (https://doi.org/10.1016/j.msec.2010.01.006)
27. D. Matyszewska, E. Napora, K. Żelechowska, J. F. Biernat, R. Bilewicz, *J. Nanopart. Res.* **20** (2018) 143 (https://doi.org/10.1007/s11051-018-4239-x)
28. L. Chang, J. Liu, J. Zhang, L. Deng, A. Dong, *Polym. Chem.* **4** (2013) 1430 (https://doi.org/10.1039/C2PY20686B)
29. S. M. North, S. P. Armes, *Polym. Chem.* **11** (2020) 2147 (https://doi.org/10.1039/D0PY00061B).

Journal of the Serbian Chemical Society
JSCS-info@shd.org.rs • www.shd.org.rs/JSCS
J. Serb. Chem. Soc. *87* (5) 657–667 (2022)
JSCS–5548
Original scientific paper
Published 2 February 2022

A study of the effects of sodium alginate and sodium carboxymethyl cellulose on the growth of common duckweed (*Lemna minor* L.)

BIANCA V. BOROS[1], NATHALIE I. GRAU[2], ADRIANA ISVORAN[1]*
ADINA D. DATCU[3], NICOLETA IANOVICI[3] and VASILE OSTAFE[1]

[1]*West University of Timisoara, Faculty of Chemistry, Biology, Geography, Department of Biology–Chemistry, Pestalozzi 16, Timisoara, 300115, Romania & Advanced Environmental Research Laboratories, Oituz 4A, Timisoara, 300086, Romania,* [2]*RWTH Aachen University, Institute for Environmental Research, Worringerweg 1, 52074 Aachen, Germany and* [3]*West University of Timisoara, Faculty of Chemistry, Biology, Geography, Department of Biology–Chemistry, Pestalozzi 16, Timisoara, 300315, Romania*

(Received 5 August, revised 7 October, accepted 20 October 2021)

Abstract: Sodium alginate (ALG) and sodium carboxymethyl cellulose (CMC) are two polysaccharides that have a wide range of applications, which could lead to accidental pollution of the environment, making the assessment of their potential ecotoxicity imperative. The present study assesses the effects of ALG and CMC on the growth response of common duckweed (*Lemna minor* L.). The results emphasize that both polysaccharides can be classified as practically nontoxic based on their EC_{50} values, with ALG having a relatively higher toxicity compared to CMC. It was also observed that high doses of 1, 5 and 10 mg mL^{-1} of the two polysaccharides produced growth inhibitory effects against common duckweed. The toxicity of biopolymers against common duckweed, measured as EC_{50} values, seems to be correlated to the hydrophobicity of the monomers building the polymer. The EC_{50} values increase linearly with increasing water solubility (log *S*) values and decrease linearly with the lipophilicity (log *P*) values.

Keywords: ecotoxicity; growth inhibition; biopolymer, EC_{50}.

INTRODUCTION

Sodium alginate (ALG) and sodium carboxymethyl cellulose (CMC) are two polysaccharides. Alginates are natural polysaccharides that mainly occur in the cell walls of brown algae. The main biological source of sodium alginate is represented by brown algae species, such as *Macrocystis pyrifera*, *Ascophyllum nodosum* and *Laminaria* sp., but bacterial species, such as *Pseudomonas* sp. and

* Corresponding author. E-mail: adriana.isvoran@e-uvt.ro
https://doi.org/10.2298/JSC210805082B

Azotobacter sp., can also produce alginates.[1,2] Alginates are salt equivalents of alginic acid, an anionic polysaccharide composed of two repeating units. These units, D-mannuronate and L-guluronate, form homopolymeric blocks of either D-mannuronate, or L-guluronate, interspersed with alternating monomers. This structure makes alginic acid a linear binary copolymer.[3,4] Alginates have a wide range of applications, especially in the pharmaceutical and biomedical industries. Alginates can be used as drug and protein delivery systems, wound dressings, in cell culture and tissue regeneration, as 3D bioprinting bioink, adsorbents for the removal of different compounds from aqueous solutions, *etc*.[4–6]

Carboxymethyl cellulose is an anionic water-soluble cellulose ether, one of the most important cellulose derivatives. CMC is produced by the reaction of chloroacetic acid, or its sodium salt, with alkali cellulose swollen in aqueous NaOH.[7–9] Sodium carboxymethyl cellulose is a copolymer. *β*-D-glucose and *β*-D--glucopyranose 2-*O*-(carboxymethyl)-monosodium salt are the two monomers of CMC, these being linked *via* *β*-1,4-glycosidic bonds. The two monomers are not randomly distributed along the macromolecule, the substitution of the –OH groups with −COOH groups taking place slightly predominantly at the C-2 of glucose.[4,5] CMC has applications in industries such as pharmaceutical (as a suspending agent or tablet excipient), medical (in infection control or wound healing), cosmetic (as suspending agent or for the increase of viscosity), food (acting as water-binder and thickener), textile industry (as coatings), detergents (acting as a suspending agent), paper (in coating colours that improve the surface properties of paper), *etc*.[7,8,10,11]

All the applications of ALG and CMC could lead to accidental pollution of the environment with these two polysaccharides, the assessment of their potential ecotoxicity therefore being imperative.

There are a multitude of standardized ecotoxicity tests for both terrestrial and aquatic environments. The duckweed growth inhibition assay is one of these tests, in which duckweed colonies are exposed for 7 days to the test substance and several parameters can be analysed, such as number of green fronds, percent inhibition of growth rate and half maximal effective concentration.[12]

A simple search regarding the words “alginate”, “carboxymethyl cellulose”, “ecotoxicity” and “duckweed” in the Web of Science Core Collection (Web of Science, Clarivate Analytics) for the period 2000–2021 revealed that the number of published scientific articles regarding each of these terms is constantly increasing (Fig. 1).

Due to the wide range of applications of ALG and CMC, as well as the increased importance of protecting the environment and analysing the ecotoxicity of potential pollutants, investigating the potential ecotoxicological effects of sodium alginate and carboxymethyl cellulose is essential. The available data in the Web of Science Core Collection on these subjects are scarce, only a few art-

icles being published about ALG or CMC and duckweed, but they do not describe the potential ecotoxicological effects of these polysaccharides towards duckweed. To the best of our knowledge, the current study is the only one that addresses the effects of sodium alginate and sodium carboxymethyl cellulose on the growth of *Lemna minor*.

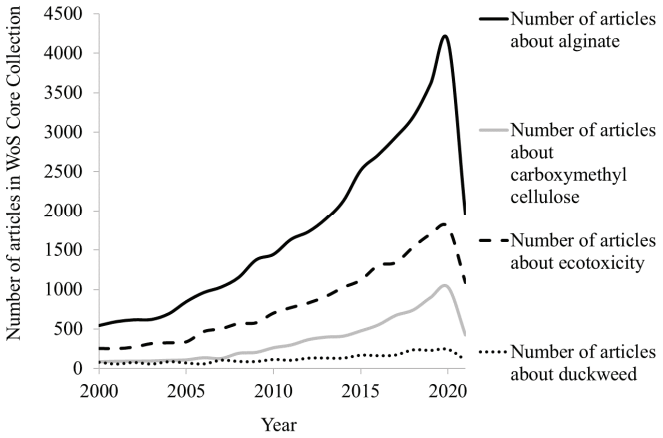

Fig. 1. Bibliometric analysis of research in 2000–2021 from the Web of Science Core Collection (Web of Science, Clarivate Analytics) on alginate, carboxymethyl cellulose, ecotoxicity and duckweed.

The aim of this research was to study the effects of sodium alginate and carboxymethyl cellulose on the growth response of common duckweed (*Lemna minor* L.), highlighting the potential ecotoxic effects of these two biopolymers.

EXPERIMENTAL

Materials

Sodium alginate from brown algae (Cat. No. W201502) and medium viscosity sodium carboxymethyl cellulose (Cat. No. C4888) were purchased from Sigma–Aldrich and used as supplied. Zinc chloride ($ZnCl_2$, Cat. No. 3533) was purchased from Carl Roth.

Tested polysaccharides

Ten concentrations of ALG and CMC were tested: 10, 5, 1, 0.5, 0.1, 0.05, 0.01, 0.005, 0.001 and 0.0005 mg mL^{-1}.

Duckweed culture

Common duckweed, *Lemna minor* L., was used as the test organism for the assessment of growth response to ALG and CMC. The duckweed was collected from a natural habitat and was surface sterilised and cultured in the laboratory for several months before being used in the ecotoxicity tests. The duckweed culture was maintained under standard conditions, as described in the OECD[13] and EPA guidelines,[14] under continuous cool white fluorescent lighting at a temperature of 24±2 °C.

Duckweed growth inhibition test

The growth response of duckweed to ALG and CMC was assessed through a growth inhibition assay conducted in accordance with an OECD guideline,[13] the chosen positive control being 0.5 % $ZnCl_2$. The exposure conditions were the same as the culture conditions, in accordance with the OECD[13] and EPA guidelines.[14] All experiments were performed in triplicate and the data are presented as mean values.

A number of 35 fronds per test vessel for each tested concentration, negative and positive control, were used to assess the effects of ALG and CMC. After an exposure period of 7 days, the effects of ALG and CMC on the total number of fronds and on the number of green fronds were analysed. The total number of fronds and the number of green fronds were determined by manual counting.

Ecotoxicity data analysis

The data regarding the total number of fronds was used for the calculation of the average specific growth rate (μ) as described in the OECD[13] guideline. μ was calculated based on the measurement variable in the test or control vessel at time i (N_i, the beginning of the test) and at time j (N_j, the end of the test), and on the entire test period (t) from i to j, using Eq. (1):

$$\mu_{i\text{-}j} = \frac{\ln N_j - \ln N_i}{t} \quad (1)$$

Dose-response curves were plotted, and the half maximal effective concentration was calculated based on the total number of fronds (EC_{50}) and on the average specific growth rate (E_rC_{50}) using Microsoft Office Excel 365 with Solver Add-in. Based on the calculated EC_{50} values, the tested polysaccharides were classified into one of the aquatic ecotoxicity categories (Table I) according to U.S. EPA.[15]

TABLE I. Toxicity categories for aquatic ecotoxicity according to U.S. EPA[15]

Categories according to U.S. EPA	EC_{50} / mg L^{-1}
Very highly toxic	<0.1
Highly toxic	0.1–1
Moderately toxic	>1–10
Slightly toxic	>10–100
Practically nontoxic	>100

Computation of physicochemical parameters

The SwissADME[16] web tool was used for the computation of some physicochemical parameters, such molecular weight, lipophilicity as log P values and water solubility as log S values, based on the simplified molecular-input line-entry system (SMILES) formulas of the analysed compounds. These parameters were determined for the monomers of the two tested polysaccharides, as well as monomers of two other polymers, carboxymethyl chitosan and polyacrylamide, in order to assess the influence of the physicochemical properties on the ecotoxicity of these compounds. The SMILES of the monomers and all chemical structures were built using ACD/ChemSketch freeware.[17]

Statistical analysis

For the statistical analysis of the data, the PAST[18] software was used. The normality of the data was tested using the Shapiro–Wilk W test. The distribution analysis was followed by an ANOVA analysis which included Levene's, Tukey's posthoc, Kruskall–Wallis and Mann–

–Whitney U tests. If the data were normally distributed, the homogeneity of variance among treatments was determined through Levene's test and an analysis of variances was determined through Tukey's posthoc test. Otherwise, non-parametric tests were performed (Kruskall–Wallis and Mann–Whitney U tests). The difference was considered significant only if the p value was smaller than 0.05 ($p < 0.05$). All correlation analysis were done through Pearson Linear r correlation test.

RESULTS AND DISCUSSION

The percentage of green fronds in the samples treated with the two polysaccharides, compared to the negative control, was approximately 90 %, except for the three highest tested concentrations: 1, 5 and 10 mg mL^{-1}. The percentages of the three highest concentrations of ALG were 83, 56 and 33 %, respectively, and for CMC they were 88, 57 and 2 %, respectively (Fig. 2).

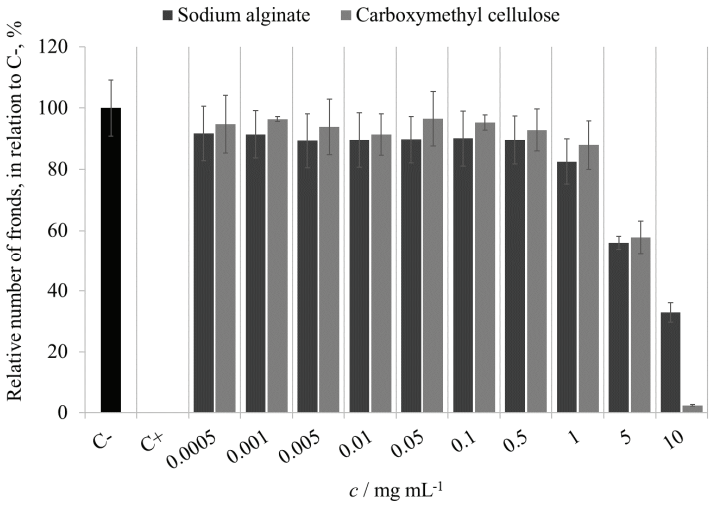

Fig. 2. Percentage of green fronds compared to the negative control for ALG and CMC, as well as the negative and positive controls.

The statistical analysis of normality of the data regarding the number of green fronds showed that the data for ALG were normally distributed, while the data for CMC were not normally distributed. Thus, the ALG data was analysed by parametric tests, while the CMC data was analysed by non-parametric tests.

The Levene's test of homogeneity of variance among treatments had a p value of 0.03 (<0.05) for ALG, and the Kruskall–Wallis test had a p value of 0.01 (<0.05) for CMC, the variances being significantly different. Thus, Tukey's posthoc test was performed for ALG, and the Mann-Whitney U tests for CMC (Table II).

The total number of fronds decreases in a relatively linear manner with the concentrations of both ALG ($R^2 = 0.89$) and CMC ($R^2 = 0.92$), Fig. 3. ALG pro-

duces a stronger decrease in the number of fronds compared to CMC, which highlights the higher toxic effect of ALG on common duckweed.

TABLE II. Results of Tukey's posthoc test for ALG (above diagonal) and of Mann–Whitney U tests for CMC (below diagonal). Statistically significant data ($p < 0.05$) are written in bold

c / mg mL^{-1}	c / mg mL^{-1}									
	10	5	1	0.5	0.1	0.05	0.01	0.005	0.001	0.0005
	p values									
10		0.2333	**0.0001**	**0.0022**	**0.0000**	**0.0007**	**0.0022**	**0.0008**	**0.0004**	**0.0055**
5	**0.0324**		0.2032	**0.0243**	**0.0216**	**0.0155**	**0.0243**	**0.0171**	**0.0093**	**0.0253**
1	**0.0111**	**0.0369**		0.9984	0.9975	0.9976	0.9984	0.9983	0.9883	0.9930
0.5	**0.0111**	**0.0369**	0.6742		1	1	1	1	1	1
0.1	**0.0174**	**0.0498**	0.3169	0.4529		1	1	1	1	1
0.05	**0.0179**	0.0518	0.2187	0.7133	0.8845		1	1	1	1
0.01	**0.0174**	**0.0498**	0.6213	1	0.6552	0.3807		1	1	1
0.005	**0.0109**	**0.0358**	0.6752	1	0.7110	1	0.8041		1	1
0.001	**0.0314**	0.0765	0.2909	0.2909	0.5784	0.8584	0.4673	0.7628		1
0.0005	**0.0179**	0.0518	0.5403	1	0.8845	0.7715	1	0.8049	0.8584	

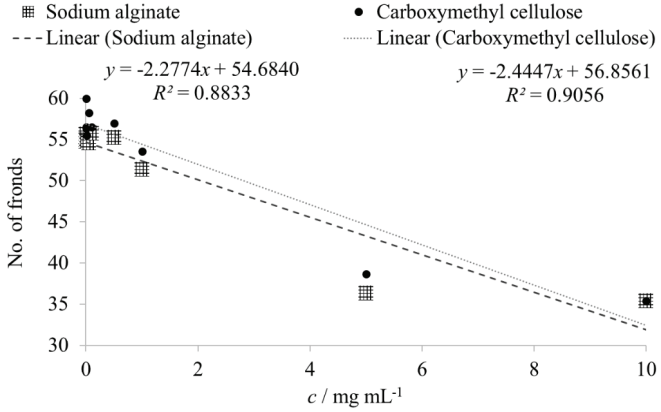

Fig. 3. The effect of the ALG and CMC concentration on the total number of fronds.

The Pearson Linear r correlation test showed a strong negative correlation between the total number of fronds and the concentration of ALG (–0.94) and CMC (–0.95), with a high probability of correlation for both ALG ($p = 5.4\times10^{-5}$) and CMC ($p = 2.3\times10^{-5}$).

Dose-response curves were plotted for both ALG (Fig. 4) and CMC (Fig. 5) based on the total number of fronds and on the average specific growth rate. The half median effective concentrations were calculated based on the total number of fronds (EC_{50}, Figs. 4 and 5) and on the average specific growth rate (E_rC_{50}) (Table III).

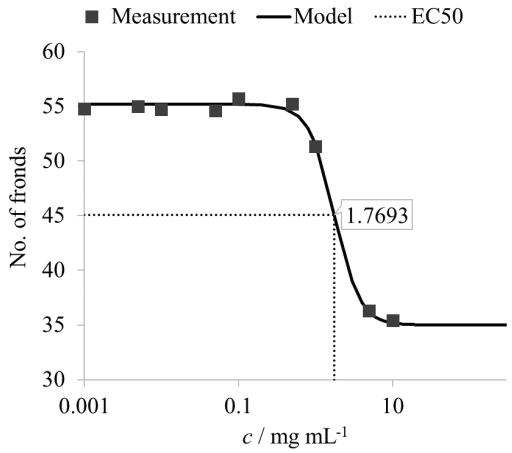

Fig. 4. Dose-response curve of total number of fronds and the concentration of ALG.

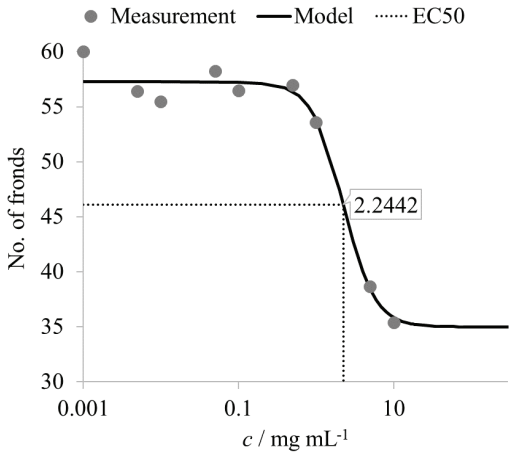

Fig. 5. Dose-response curve of the total number of fronds and the concentration of CMC.

According to the U.S. EPA15 toxicity categories for aquatic ecotoxicity, ALG and CMC can be classified as practically nontoxic based on the obtained EC_{50} values, ALG being slightly more toxic than CMC, having lower EC_{50} and ErC_{50} values.

TABLE III. EC_{50} and E_rC_{50} values for ALG and CMC

Polysaccharide	EC_{50} / mg L^{-1}	E_rC_{50} / mg L^{-1}
ALG	1769.3	1786.8
CMC	2244.2	2532.7

In order to assess the possible correlation between some physicochemical parameters of the polysaccharides and their toxicity against common duckweed, specific literature for ecotoxicity data obtained for other biopolymers was searched. This proved difficult due to the lack of information on the ecotoxicity

of other polysaccharides towards duckweed or even polymers. Thus, data from two identified articles: the effect of carboxymethyl chitosan (CMCS) on *L. minor* L.[19] and the effect of polyacrylamide (PAM) on *Lemna aequinoctialis* Welw[20] were included in this study.

The SMILES formulas necessary for the computation of the physicochemical properties were generated for the monomers of the four polymers: sodium *β*-D-mannuronate (Fig. 6, **a**) and sodium *α*-L-guluronate (Fig. 6, **b**) for ALG;

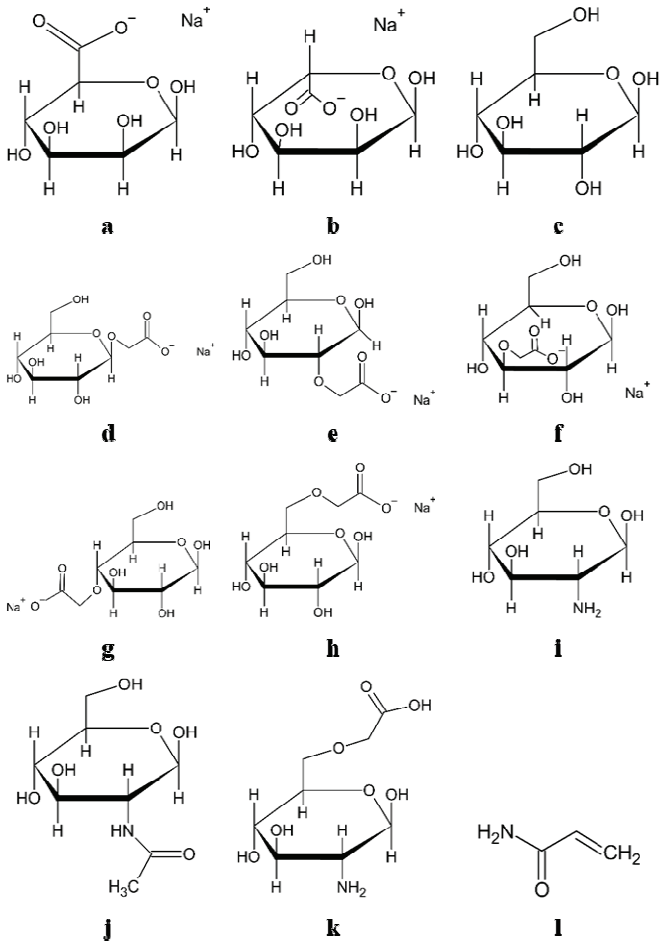

Fig. 6. Chemical structures of the monomers used for the computation of the physicochemical parameters using SwissADME: **a**) sodium *β*-D-mannuronate and **b**) sodium *α*-L-guluronate for ALG; **c**) D-glucose, **d**) sodium 1-*O*-carboxymethyl-D-glucose, **e**) sodium 2-*O*-carboxymethyl-D-glucose, **f**) sodium 3-*O*-carboxymethyl-D-glucose, **g**) sodium 4-*O*-carboxymethyl-D-glucose and **h**) sodium 5-*O*-carboxymethyl-D-glucose for CMC; **i**) D-glucosamine, **j**) *N*-acetyl-D-glucosamine and **k**) *O*-carboxymethyl-D-glucosamine for CMCS; **l**) acrylamide for PAM.

D-glucose (Fig. 6, **c**) and sodium carboxymethyl-D-glucose (Fig. 6, **d**–**h**) for CMC; D-glucosamine (Fig. 6, **i**), *N*-acetyl-D-glucosamine (Fig. 6, **j**), *O*-carboxymethyl--D-glucosamine (Fig. 6, **k**) for CMCS; acrylamide (Fig. 6, **l**) for PAM.

Starting from the SMILES formulas, the values of molecular weight, log *P* and log *S* for the monomers of the investigated biopolymers were computed. Besides these parameters, log *P* and log *S* strongly affect the EC_{50} value. The EC_{50} values increased linearly (R^2 = 0.82) with increasing log *S* value (Fig. 7) and linearly decreased (R^2 = 0.96) with the log *P* values (Fig. 8).

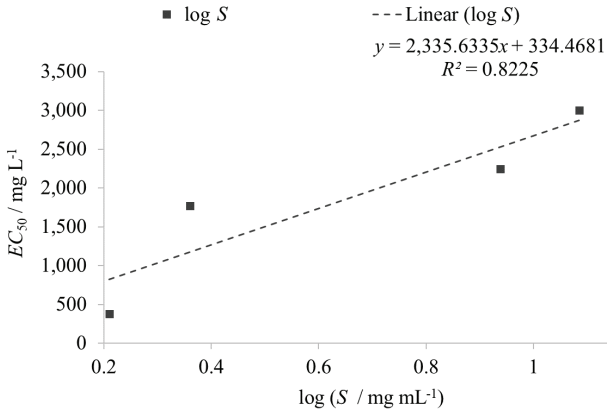

Fig. 7. The effect of log *S* values on the EC_{50} values.

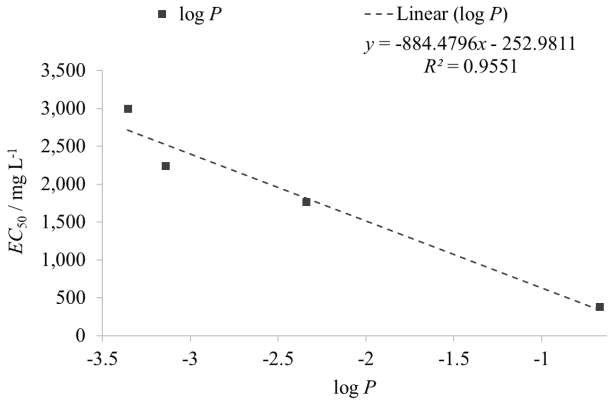

Fig. 8. The effect of log *P* values on the EC_{50} values.

Statistical analysis revealed that only log *P* showed a statistically significant (p = 0.0227) correlation (–0.97) with the EC_{50} values.

CONCLUSIONS

Based on the EPA toxicity categories for aquatic ecotoxicity and taking into account the EC_{50} values, this study shows that both sodium alginate and carboxymethyl cellulose can be classified as practically nontoxic. However, it was observed that the high concentrations (1, 5 and 10 mg mL^{-1}) of the two polysaccharides had some growth inhibitory effects on duckweed. It was also observed that sodium alginate had a relatively higher toxicity compared to carboxymethyl cellulose. The computational data reveals that the physicochemical parameters log *S* and log *P* influence the EC_{50} values. The EC_{50} values increased linearly with increasing log *S* value and decreased linearly increasing log *P* values, only the correlation between EC_{50} and the log *P* values being statistically significant. Although both polysaccharides can be classified as being practically non-toxic, these had concentration-dependent adverse effects on duckweed. These effects could pose a risk to the environment in the event of accidental pollution due to the widespread use of ALG and CMC. These effects must be taken into consideration in the processing of waste containing these polysaccharides in significant concentrations, which highlights the importance of the present results.

И З В О Д

ПРОУЧАВАЊЕ УТИЦАЈА НАТРИЈУМ-АЛГИНАТА И НАТРИЈУМ-КАРБОКСИМЕТИЛ ЦЕЛУЛОЗЕ НА РАСТ ОБИЧНЕ СОЧИВИЦЕ (*Lemna minor* L.)

BIANCA V. BOROS[1], NATHALIE I. GRAU[2], ADRIANA ISVORAN[1], ADINA D. DATCU[3], NICOLETA IANOVICI[3] и VASILE OSTAFE[1]

[1]*West University of Timisoara, Faculty of Chemistry, Biology, Geography, Department of Biology–Chemistry, Pestalozzi 16, Timisoara, 300315, Romania & Advanced Environmental Research Laboratories, Oituz 4, Timisoara, 300086, Romania,* [2]*RWTH Aachen University, Institute for Environmental Research, Worringerweg 1, 52074 Aachen, Germany и* [3]*West University of Timisoara, Faculty of Chemistry, Biology, Geography, Department of Biology–Chemistry, Pestalozzi 16, Timisoara, 300315, Romania*

Натријум-алгинат (ALG) и натријум-карбоксиметил целулоза (CMC) су два полисахарида са широким спектром примене, који може довести до случајног загађења животне средине, па је процена њихове потенцијалне екотоксичности императив. Ова студија процењује ефекте ALG и CMC на раст обичне сочивице (*Lemna minor* L.). Резултати указују да се оба полисахарида могу класификовати као практично нетоксична на основу вредности EC_{50}, при чему ALG има релативно већу токсичност у односу на CMC. Такође је примећено да високе дозе ова два полисахарида, од 1,5 и 10 mg mL^{-1}, производе инхибиторне ефекте на раст обичне сочивице. Чини се да је токсичност биополимера против обичне сочивице, мерена као EC_{50} вредност, у корелацији са хидрофобношћу мономера који граде полимер. Вредности EC_{50} линеарно расту са повећањем вредности log *S* и линеарно се смањују са вредностима log *P*.

(Примљено 5. августа, ревидирано 7. октобра, прихваћено 20. октобра 2021)

REFERENCES

1. M. Fertah, A. Belfkira, M. Taourirte, F. Brouillette, *Arab. J. Chem.* **10** (2017) S3707 (https://doi.org/10.1016/j.arabjc.2014.05.003)

2. I. W. Sutherland, in *Biomaterials*, D. Byrom, Ed., Palgrave Macmillan, London, 1991, p. 307 (https://doi.org/10.1007/978-1-349-11167-1_7)
3. K. I. Draget, G. S. Bræk, O. Smidsrød, *Carbohydr. Polym.* **25** (1994) 31 (https://doi.org/10.1016/0144-8617(94)90159-7)
4. K. Y. Lee, D. J. Mooney, *Prog. Polym. Sci.* **37** (2012) 106 (https://doi.org/10.1016/j.progpolymsci.2011.06.003)
5. E. Axpe, M. L. Oyen, *Int. J. Mol. Sci.* **17** (2016) 1976 (https://doi.org/10.3390/ijms17121976)
6. B. Wang, Y. Wan, Y. Zheng, X. Lee, T. Liu, Z. Yu, J. Huang, Y. S. Ok, J. Chen, B. Gao, *Crit. Rev. Environ. Sci. Technol*. **49** (2019) 318 (https://doi.org/10.1080/10643389.2018.1547621)
7. A. Casaburi, Ú. Montoya Rojo, P. Cerrutti, A. Vázquez, M. L. Foresti, *Food Hydrocoll*. **75** (2018) 147 (https://doi.org/10.1016/j.foodhyd.2017.09.002)
8. F. Yaşar, H. Toğrul, N. Arslan, *J. Food Eng*. **81** (2007) 187 (https://doi.org/10.1016/j.jfoodeng.2006.10.022)
9. H. Toğrul, N. Arslan, *Carbohydr. Polym*. **54** (2003) 73 (https://doi.org/10.1016/S0144-8617(03)00147-4)
10. M. T. Ghannam, M. N. Esmail, *J. Appl. Polym. Sci*. **64** (1997) 289 (https://doi.org/10.1002/(SICI)1097-4628(19970411)64:2<289::AID-APP9>3.0.CO;2-N)
11. V. Kanikireddy, K. Varaprasad, T. Jayaramudu, C. Karthikeyan, R. Sadiku, *Int. J. Biol. Macromol*. **164** (2020) 963 (https://doi.org/10.1016/j.ijbiomac.2020.07.160)
12. B. V. Boros, V. Ostafe, *Nanomaterials* **10** (2020) 610 (https://doi.org/10.3390/nano10040610)
13. OECD 221, *Lemna sp. Growth Inhibition Test* (2006)
14. US EPA 850.4400, *Aquatic Plant Toxicity Test Using Lemna spp* (2012)
15. U.S. Environmental Protection Agency, *Analysis Phase: Ecological Effects Characterization, In Technical Overview of Ecological Risk Assessment*, EPA, Washington DC, 2017 (https://www.epa.gov/pesticide-science-and-assessing-pesticide-risks/technical-overview-ecological-risk-assessment-0)
16. A. Daina, O. Michielin, V. Zoete, *Sci. Rep*. **7** (2017) 42717 (https://doi.org/10.1038/srep42717)
17. *ACD/ChemSketch Freeware*, version 2020.2.0, Advanced Chemistry Development, Inc., Toronto, www.acdlabs.com (accessed 10.06.2021)
18. Ø. Hammer, D. A. Harper, P. D. Ryan, *Palaeontol. Electron*. **4** (2001) 9 (https://paleo.carleton.ca/2001_1/past/past.pdf)
19. B. V. Boros, N. I. Grau, V. Ostafe, *Res. J. Agric. Sci*. **51** (2019) 14 (https://www.rjas.ro/paper_detail/3065)
20. A. J. Harford, A. C. Hogan, D. R. Jones, R. A. van Dam, *Water Res*. **45** (2011) 6393 (https://doi.org/10.1016/j.watres.2011.09.032).